University of Alberta

Analysis of an Open-Cathode Fuel Cell Stack in an Enclosure for Varying Operating Conditions

by

Samantha Marie Miller

A thesis submitted to the Faculty of Graduate Studies and Research in partial fulfillment of the requirements for the degree of

Master of Science

Department of Mechanical Engineering

Spring 2013
Edmonton, Alberta

To my family

Abstract

Open-cathode polymer electrolyte fuel cell (PEFC) stacks use hydrogen as fuel, are a high efficiency power source, and do not produce CO_2, NO_x, SO_x, or particulate matter. When used as a remote power source, the PEFC stack must be protected from adverse environmental conditions. To provide optimal operating conditions to the PEFC stack, an actively controlled enclosure is proposed. A mathematical model of a transient, non-isothermal, lumped parameter, open-cathode fuel cell stack is developed and coupled with an enclosure model. The open-cathode fuel cell stack mathematical model includes characterization of the cathode channel, the anode channel and the membrane electrode assembly (MEA). The transient mass and energy transport equations for the coupled system are solved to determine the optimal operating conditions for the PEFC stack within the enclosure. A Horizon H-12 Fuel Cell Stack and two enclosure designs are tested, characterized and fitted to the mathematical model.

Acknowledgements

I would like to thank my supervisor Dr. Marc Secanell for offering me the opportunity to work on this research project. His spirit and enthusiasm for developing environmentally responsible energy systems is refreshing and inspiring. In addition, his patience, guidance and understanding have been invaluble during this work.

Thank you to the department electronics technician, Rick Conrad, for designing and building the RH sensor - computer interface for the experiments.

Thank you to my colleagues in the Energy Systems Design Lab for the interesting discussions about fuel cells and life. In particular, thank you Michael Moore for sitting across from me for 2 years and listening, and Pedro Mateo for being a night owl like me. Thank you Frederik Wunder for running some of the experiments.

Thank you Amanda Kotchon for coffee breaks.

I would like to thank my parents for supporting me through out my life, always encouraging me to take on a challenge, and to do my best. Finally, I thank my husband, Jason Keuling, for his patience, support and love.

Table of Contents

List of Tables

List of Figures

Nomenclature

English Letters

a_i^{ν} Activity of species i

A_{fan} Cross-sectional area of fan, $[m^2]$

A_k Cross-sectional area of location k, $[m^2]$

A_{mem} Cell active area, $[m^2]$

$A_{o,ca}$ Ratio of platinum to catalyst layer in cathode $[m^2Pt/m^2CL]$

$A_{s,encl}$ Heat exchange area between stack & enclosure, $[m^2]$

$c_{p,i}$ Specific heat capacity of species i, $[J/(kg \cdot K)]$

$c_{q,i}$ Molar concentration of species i in location q, $[mol/m^3]$

$c_{O_2}^0$ Bulk concentration in flow channel, $[mol/m^3]$

$c_{O_2}^*$ Catalyst layer reactant concentration, $[mol/m^3]$

$c_{O_2}^{0*}$ Reference O_2 concentration, $[mol/m^3]$

d_k Diameter of location k, $[m^2]$

D^{eff} Effective diffusivity, $[m^2/s]$

D_{m,H_2O} Diffusion coefficient for water in PEM, $[m^2/s]$

D_{m,H_2O}^{ref} Reference diffusion coefficient for water in PEM, $[m^2/s]$

$\mathcal{D}_{A,B}$ Diffusion coefficient for species A in B, $[m^2/s]$

E_{OCV} Open circuit voltage, $[V]$

EW_{mem} Equivalent weight of membrane, $[g/equi]$

F Faraday constant, $[C/mol]$

Δg_f° Gibb's free energy of reaction, $[J/kg]$

h_i Enthalpy of species i, $[J/kg]$

h_q Height of channel q, $[m]$

$(hA)_q$ Convective heat transfer and area of q, $[W/K]$

$(hA)_{amb}$ Convective heat transfer and area of stack, $[W/K]$

ΔH_{vap} Heat of vaporization of water, $[J/kg]$

I Current, $[A]$

j Current density, $[A/m^2]$

j_L Limiting current density, $[A/m^2]$

$j_{o,q}$ Reference exchange current density, $[A/m^2_{CL}]$

$k_{m,p}$ Permeability of water in membrane, $[m^2]$

k_c Condensation rate constant, $[s^{-1}]$

k_v Evaporation rate constant, $[s^{-1}]$

L_q Channel length, $[m]$

m_{encl} Mass of air in enclosure, $[kg]$

$m_s c_{p,s}$ Stack mass and specific heat (empirical), $[J/K]$

M_i Molecular weight of species i, $[g/mol]$

$\dot{m}^z_{i,k}$ Mass flow rate of in location k with direction z, $[kg/s]$

$\dot{m}_{q,i}$ Mass flow rate of species i in channel q, $[kg/s]$

$\dot{m}_{q,phase}$ Rate of phase change in channel q, $[kg/s]$

$\dot{m}_{trans}$ Water transport through membrane q, $[kg/s]$

n Number of electrons transferred, $[e^-/mol$ reactant$]$

n_{cell} Number of cells in stack

$n_{q,chan}$ Number of channels q per cell

$\dot{n}_{q,i}$ Molar flow rate of species i in channel q, $[mol/s]$

P_{q,H_2O^v} Partial pressure of water vapour in channel q, $[Pa]$

$P_{q,sat}$ Saturation pressure in channel q, $[Pa]$

$\dot{Q}_k$ Energy losses at location k, $[W]$

R Universal Gas Constant, $[J/mol.K]$

R_{comps} Resistivity of stack components, $[\Omega]$

R_{ionic} Ionic membrane resistance, $[\Omega]$

R_{ins} Wall resistance, $[m^2K/W]$

S_q Source terms in channel q, $[kg/s]$

S_x Standard deviation

ΔS° Entropy of reaction, $[J/(kg \cdot K)]$

T_k Temperature at location k, $[W]$

t_m Membrane thickness, $[m]$

$t_{\alpha,\nu}$ Student's t-test probability

U_{wall} Enclosure heat transfer coefficient, $[W/(m^2 \cdot K)]$

u_q Flow velocity in channel q, [m/s]

u_{avg} Average flow velocity [m/s]

u_{max} Maximum flow velocity [m/s]

V_{cell} Cell voltage, $[V]$

V_k Volume of location k, $[V]$

$\dot{W}_k$ Power at location k, [W]

w_q Channel width, $[m]$

$x_{q,i}$ Mole fraction of species i in channel q

$y_{q,i}$ Mass fraction of species i in channel q

Greek Letters

α Confidence level

α_c Cathodic transfer coefficient

β_q Condensation/Evaporation switching term

η_{act} Activation energy losses, $[V]$

η_{conc} Concentration energy losses, [V]

η_{ohmic} Ohmic energy losses, $[V]$

λ Stoichiometric ratio

λ_q Water content of membrane at interface q

μ_i Dynamic viscosity species i, $[Pa \cdot s]$

ν Number of degrees of freedom

ρ_q Air density in channel q, $[kg/m^3]$

ρ_{mem} Membrane density,$[kg/m^3]$

ϕ_q Relative humidity in channel q, [%]

σ_{303K} Membrane conductivity at 303K, $[S/m]$

$\sigma_{a,T}$ Variable membrane conductivity, $[S/m]$

$\sigma_{A,B}$ Average Lennard Jones parameter for species A and B

ω_u Error and uncertainty

$\Omega_{A,B}$ Average Lennard Jones parameter for species A and B

Subscripts and Superscripts

amb Ambient

an Anode channel

ca Cathode channel

eff	Effective parameter
$encl$	Enclosure
i	Species index
k	Location
o	Reference
q	Anode or cathode channel
s	Stack
z	Direction of mass flow I (in) or O (out)
ν_i	Species stoichiometry

Abbreviations

ASTM American Society for Testing and Materials

CL Catalyst Layer

DMFC Direct Methanol Fuel Cell

EPS Extruded Polystyrene

FCTS Fuel Cell Test Station

GDL Gas diffusion layer

MEA Membrane Electrode Assembly

PEM Polymer electrolyte membrane

PEFC Polymer electrolyte fuel cell

PFSI Perfluorosulfonated Ionomer

RH Relative Humidity

STP Standard Atmospheric Temperature and Pressure

TEG Thermoelectric Generator

Chapter 1

Introduction

1.1 Motivation

Northern Canada and the Arctic present a power supply challenge as remote power delivery is required for systems as diverse as wildlife surveillance, telecommunication towers, exploration expeditions, and oil and gas extraction and pumping stations. Unlike existing technology for power supply, such as thermoelectric generators (TEG) and engine-generator sets, polymer electrolyte fuel cells (PEFC) are a high efficiency power source which do not produce pollutants such as CO_2, NO_x and SO_x, when operated with H_2 produced from renewable sources. An electrochemical reaction of hydrogen and oxygen from atmospheric air occurs in a PEFC, generating electricity and water. With an efficiency of 50%, the PEFC has a reduced fuel requirement for a given power output. Additionally, hydrogen can be produced by alternative power sources such as wind turbines and solar cells, in which case the PEFC system would produce zero emissions.

A PEFC system will therefore be studied in this thesis as a novel, energy efficient power source for remote power supply. In order to keep the system cost effective, an open-cathode stack is selected because it uses air at ambient pressure to supply oxygen to the cathode. The air is forced through the stack by a fan. This allows control of the amount of reactant available to the cathode. Conventional fuel cell stacks use compressors to pressurize the air in the cathode channels [1]. The compressor has a higher power requirement than the fan, therefore the fan is more efficient and causes less parasitic losses to the stack power. Another advantage of the open-cathode fuel cell stack is that it is air-cooled by the same fan that supplies the reactant. Conventional fuel cell stacks use cooling systems to maintain acceptable operating temperatures

which require additional components. These components, such as a coolant pump, increase both the cost and parasitic power losses associated with conventional stack design. Therefore the open-cathode fuel cell stack design was selected for this research because it is cost effective and efficient. [2]

Santa Rosa et al. [3] studied a commercial 10W SRE 10SR4-A air cooled fuel cell stack system. Their experimental results showed that the air flow rate, which controls cathode oxygen delivery, water vapour and liquid water distribution, and cell temperature, has a significant effect on the performance of the fuel cell stack. The effect of the air flow rate on cell performance was also studied by Wu et al. [4]. It was shown that at high air flow rates, dehydration of the membrane caused a decrease in the cell performance.

Recently, Sasmito et al. [5] developed a comprehensive mathematical model of an open-cathode fuel cell stack with a forced air fan. This steady state model was solved in FLUENT with the fan characterized as an interface. Simulation results showed the fan power and cathode channel height affects the stack performance [5]. Further development of their model revealed natural convection is ineffective for cooling stacks with 12 or more cells and liquid coolant flow is most effective [6]. Forced air convection is shown to be effective at cooling a stack [6] and as the fan has reduced parasitic losses, it is preferred. Sasmito et al. also reported that fan selection and stack channel design affect the performance of the stack based on how well the stack is cooled [7].

The main concern with open-cathode polymer electrolyte fuel cells is that their performance varies widely with operating conditions. In the Arctic environment where temperature and relative humidity variations are extreme, an open-cathode fuel cell stack might show limited reliability. Additionally, at temperatures below 0℃, a major concern is freezing of the product water. Freezing and ice formation in the PEFC is to be avoided as the volume expansion during ice formation may cause damage to the stack in the forms of delamination, crack formation, broken carbon-fibre electrodes and pore size distribution changes [8].

A portable power source design developed by the US Army was tested by Chu et al. [9] at low temperatures. The fuel cell stack showed good performance in the temperature range of 2℃ to 50℃, but the performance at -10℃ was limited. Ice formation in the hydrogen output line led to performance drops, but this was remedied by removing the ice from the line [9].

The solution proposed in this research is to place an open-cathode polymer electrolyte fuel cell (PEFC) stack in an insulated enclosure which can

control the conditions in which the stack operates, thereby permitting optimal performance of the fuel cell stack. An enclosure is proposed to keep the fuel cell stack warm during operation. At temperatures below freezing, the fuel cell stack will no longer operate well [9]. Therefore by placing the stack in an insulated enclosure, it can be kept above freezing conditions. The waste heat energy produced by the fuel cell stack during operation will be contained within the insulated enclosure and used to heat the air inside the enclosure. This will keep the fuel cell stack within the range of desired operating temperatures. A properly designed enclosure is required to ensure that the fuel cell has acceptable operating conditions available inside the enclosure.

The focus of this work is primarily the development and experimental validation of a coupled transient, non-isothermal, lumped parameter mathematical model of the fuel cell stack and enclosure which will predict the effect of varying enclosure designs on the performance of the fuel cell stack. This model can be used for new enclosure design and enclosure design optimization by fuel cell producing companies such as Dantherm [10] and Ballard [11], or SFC Energy [12] and Ensol [13] who are developing an enclosure design for their portable direct methanol fuel cell (DMFC), the EFOY [14].

1.2 Literature Review

To study the performance of the open-cathode PEFC stack in an enclosure at varying conditions, a transient, non-isothermal, lumped parameter model is to be developed. The following sections consist of a detailed literature review of existing research on each of the aspects of the mathematical model: enclosures, lumped parameter modelling style, open-cathode fuel cells, transient fuel cells, non-isothermal fuel cells, and cold temperature operation.

1.2.1 Enclosures

The fuel cell system proposed in this work controls the conditions in which the stack operates by placing it in an enclosure. This insulated enclosure can be used to control the temperature of the stack and the composition of the inlet gas available to the open-cathode. While many articles highlight the importance of insulating the stack in cold operating conditions, [15–21], there is very little literature which details analysis of the effect of the enclosure on the operating conditions and stack performance.

The purpose of the insulation around the fuel cell is to prevent the loss of thermal energy generated by the fuel cell in order to maintain the temperature of the fuel cell above freezing. In a thermal analysis by Giddey et al. [22], it was shown that nearly half of the heat lost by the fuel cell stack to the environment was recoverable through proper insulation of the fuel cell. For outdoor applications where the ambient temperatures are below freezing, an insulated enclosure is a necessary system component.

Some fuel cell stack systems with enclosures for cold temperature use have been patented and tested experimentally in literature. An insulated enclosure around a fuel cell and water circulation system was recently patented by United Technologies Corporation (UTC) [20]. A catalytic burner and the circulation of heated convection air are used to maintain the temperature of the enclosure in this design.

Ward et al. [15] designed a portable fuel cell system in an insulated enclosure which was to be used for cold start operation at temperatures from -40℃ to 40℃. The system employed the use of a start up heater and exothermic heat energy from a hydride reaction to heat the alkaline fuel cell stack. A movable separator was placed between the fuel cell and the hydrogen storage unit where the hydride reaction occurred to stop the heat transfer when the fuel cell was sufficiently heated.

A portable fuel cell system was designed by Oszcipok et al. [16] to determine the ability of a conventional, pressurized fuel cell system to operate in outdoor conditions between -20℃ to 40℃. This thermally insulated enclosure system was used to test the cold start-up ability of the fuel cell using passive and active heating. Passive heating of the fuel cell stack uses the excess thermal energy produced by stack operation to heat the stack. Oszcipok et al [16] determined that the auxiliary components and end plates were too significant of a source of heat loss for passive heating to be viable during cold starts. An active cold start of the fuel cell stack uses an additional heat source to heat the stack to 0℃ prior to start up. Oszcipok et al. tested a catalytic burner plate and an electric heating foil and determined that the electric heating foil was preferable due to its increased efficiency. They also showed that active heating with an efficient heating system was preferable to passive heating as the power draw of the auxiliary components during stack operation was inefficient. The insulated enclosure used to contain the heat around the fuel cell stack during the cold start was not studied in this work.

A fuel cell system designed and patented by Intelligent Energy Ltd [21]

proposes the use of the irreversible heat energy produced by the fuel cell stack to heat the incoming air through recirculation of the air exiting the stack. Baffles are placed at the enclosure outlet and used to regulate the quantity of cathode outlet air which is recirculated within the enclosure and rejected from the enclosure. This permits temperature control through the recirculation of air warmed by the stack during cold temperature operation and the expulsion of hot air if the stack requires cooling.

Based on the current literature review, it appears that enclosure design for fuel cell stacks has been mainly performed empirically [15, 16, 23, 24]. There was no literature found which included any analysis of gas composition and temperature in an enclosure. Further, there is no analysis for controlling the gas composition in the enclosure. Nor did these studies include an analysis of the enclosure parameters such as insulation, volume and inlet flow rate on the performance of the stack. Therefore, a coupled fuel cell and enclosure model is necessary to improve the current design of enclosures for fuel cell stacks.

1.2.2 Fuel Cell Stack Systems

A polymer electrolyte fuel cell stack consists of a number of cells stacked together. One cell consists of several components: a hydrogen delivery system, an anode gas diffusion layer (GDL), an anode catalyst layer, a Nafion© membrane, a cathode catalyst layer, a cathode GDL and an oxygen delivery system, as shown in Figure 1.1. The operation of a fuel cell is thus: hydrogen flows through channels in the bipolar plates, and passes through the anode GDL where it reacts at the anode catalyst layer forming hydrogen protons

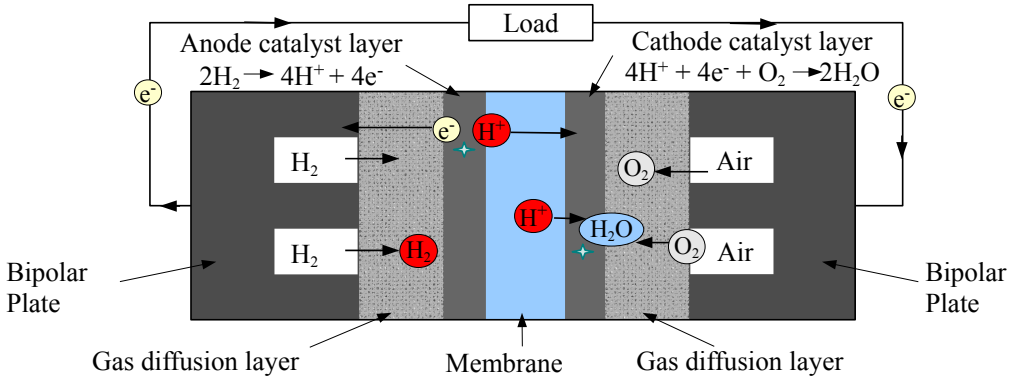

Figure 1.1 – Fuel Cell Structure and Operation

and electrons:

$$2H_2 \rightleftharpoons 4H^+ + 4e^- \tag{1.1}$$

The hydrogen protons pass through the Nafion© membrane to the cathode catalyst layer and the electrons are collected by the bipolar plate and the current is passed through a load.

On the cathode side, air flows through channels in the bipolar plates and passes through the cathode GDL where the oxygen reacts at the cathode catalyst layer with the hydrogen protons which passed through the membrane forming water:

$$O_2 + 4H^+ + 4e^- \rightleftharpoons 2H_2O \tag{1.2}$$

In this model, the GDLs, catalyst layers and membrane will be referred to as the membrane electrode assembly (MEA). To simplify the model, the GDLs and catalyst layers will be assumed of negligible thickness and modelled as interfaces between the bipolar plate channels and the membrane [25–30].

Conventional Fuel Cell Stacks

The conventional fuel cell stack usually has pressurized inlet flow streams to both the anode and the cathode channels. A compressor is used to supply the pressurized air and the hydrogen is supplied from a compressed air cylinder. The compressor can take up to 20% of the power delivered by a fuel cell stack to compress the inlet air [1]. The advantage of a pressurized stack is that it aides with reactant delivery through the entire channel which will increase stack power. The disadvantage is that it has a high parasitic power draw.

Additional auxiliary systems typically used with convectional fuel cell stacks include humidifiers for the anode and cathode gas supply and a liquid water cooling system. These auxiliary systems use some of the power supplied by the stack and therefore reduce its efficiency.

Open-Cathode Fuel Cell Stacks

The open-cathode fuel cell stack differs from the conventional stack as it is not pressurized. Therefore, rather than using a pump to deliver air to the cathode, the air will be delivered passively or by a fan. In the passive open-cathode design, the stack simply uses the ambient air which passes over the cathode channels by natural convection [31]. In the forced open-cathode design, a fan is used to blow air through the cathode channels.

The advantage of the passive cathode reactant delivery system is that no auxiliary components are required. Therefore, passive delivery systems have higher efficiency because there power is not required to run the reactant delivery system. The disadvantage of a passive reactant delivery system is that there the delivery of reactant cannot be controlled. This limits the amount of oxygen available to the stack at a given time and therefore limits the power available from the stack [31].

The advantage of the fan forced cathode reactant delivery system is that a fan has less parasitic power draw than a pump [5]. In comparison with the passive reactant delivery method, the fan delivery system is an auxiliary system with some power draw and a reduced efficiency. The fan system is preferred, however, because it allows control of the quantity of reactant delivered to the fuel cell stack channels.

1.2.3 Fuel Cell Stack Mathematical Modelling

Fuel cell stack mathematical models that analyze system performance under various operating conditions have been developed. Empirical models have also been derived to represent the components in the fuel cell stack [32]. Considerable literature exists detailing the intricacies of a single fuel cell in mathematical models, however for the project under consideration, detailed analysis of the fuel cell is not feasible due to computational limitations since the focus is on a transient stack model.

The conventional, pressurized, single fuel cell was the initial focus for the development of fuel cell models. Steady-state, isothermal mechanistic models of the fuel cell have been developed by numerous researchers [33–37] and used for optimization of fuel cell stack conditions [38, 39]. These models characterize the electrochemical reaction, mass transport effects and membrane hydration. Empirical results have been incorporated into some of the models [35, 40]. Thermal and water management have been incorporated into others [36, 37].

The main components of fuel cell stack models are:

- mass transport analysis
- electrochemical model
- thermal energy analysis
- water management

- transient

These components will be expanded in the following sections. Further, stack models are classified as lumped or layered models depending on complexity.

Mass Transport Analysis

During operation of the fuel cell stack, an oxidation reaction occurs at the anode catalyst layer, producing hydrogen protons and electrons from hydrogen gas. At the cathode side of the membrane, the oxygen in air reacts at the cathode catalyst layer with the protons and electrons to form water. Bipolar plates with channels are used to deliver the reactants to the catalyst layer on the anode and cathode sides of the stack.

The anode and cathode of the cell are composed of numerous channels and the anode and cathode channels will be defined as one of the channels in the bipolar plate and one rib of the bipolar plate land as shown in Figure 1.2.

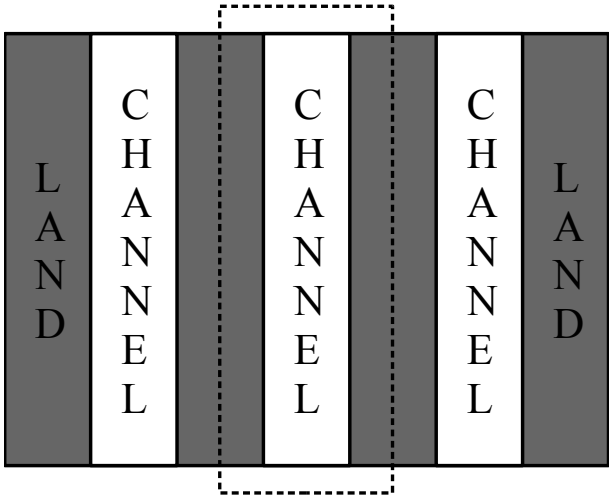

Figure 1.2 – Area of Channel and Land to be Modelled

The mass transport through the channels is modelled by a general mass balance which includes, for each species of gas, all mass entering the channel, all mass leaving the channel, and all mass sources and sinks. The rate of change of mass in the channel volume is equal to the rate of change of mass due to the convective flux into and out of the channel and the rate of increase due to sources. In mathematical form, the mass balance is given from Reynolds

Transport Theorem [41]:

$$\frac{d}{dt}\int_V \rho_q dV = -\int_A \left[\vec{n}\cdot(\rho_q\vec{u})\right] dA + \int_V S_q dV \tag{1.3}$$

where ρ_q is the density of the gases in channel q, V is the volume of the channel, A is the cross-sectional area of the channel that is perpendicular to the flow, $\vec{n}$ is the vector normal to the cross-section of the channel, u is the flow velocity in the channel, and S_q represents source terms.

Hydrogen gas, and occasionally water vapour, are delivered to the anode catalyst layer through the anode channels in the bipolar plate. To humidify the hydrogen auxiliary equipment, such as a bubbler humidifier, is used to increase the relative humidity of the gas. Air is supplied to the cathode catalyst layer through the cathode channels. In conventional, pressurized fuel cell stacks, a pump is used to increase the pressure of the air taken from the atmosphere. A bubbler humidifier might also be used to increase the relative humidity of the cathode reactant air [38]. Pumps have a high parasitic power draw and therefore reduce the efficiency of the fuel cell stack. The advantage of pressurized fuel cell stacks is that they can reach higher power levels due to the quantity of reactant delivered in a time period.

For the cathode reactant delivery, a fan forced open-cathode stack will be modelled. A passive, one-dimensional, steady-state, semi-empirical, open-cathode fuel cell model was developed by Litster and Djilali [31], which included a detailed catalyst layer model and semi-analytical models of the ionic, heat and mass transfer. This model was to be used for small, portable applications such as a cellular phone [31]. A non-isothermal, one-dimensional, open-cathode model that coupled the heat and mass transfer through theoretical analysis was developed by O'Hayre et al. [42]. Yalcinoz and Alam [43] further improved this model by adding a dynamic component to the thermal model.

Electrochemical Model

Fuel cell electrochemical models are usually comprised of four components: a) open cell voltage, b) activation overpotential losses c) ohmic losses and d) concentration losses [44]. A general semi-empirical expression for the cell voltage is:

$$V_{cell} = E_{OCV} + \eta_{act} + \eta_{ohmic} + \eta_{conc} \tag{1.4}$$

The open cell voltage, E_{OCV} is obtained by using the Nernst equation.

This is the maximum electro-motive force (EMF) of the cell reaction with correction factors for its operating temperature and pressure [1]. Thus, the Nernst equation represents the reversible cell voltage for the operating conditions. The activation overpotential, η_{act}, is the energy required to surpass the activation barrier and allow the electrochemical reaction to proceed. It will control the speed of reaction at the electrode. The ohmic losses, η_{ohmic}, are a representation of losses due to the resistance in the electrodes and membrane to the electron and ion flows. The concentration losses, η_{conc}, are due to the use of reactants at the electrodes causing concentration changes[1]. The overpotential losses have been theoretically derived [35] and empirically derived [32] for various particular fuel cells.

Thermal Model

Most steady-state thermal models consist of the energy balance of the fuel cell stack. The energy equations are derived from theoretical thermodynamics. The energy terms that can be included can vary depending on the requirements of particular analyses.

Typical energy terms include [45]:

- sensible heat of the electrochemical reaction
- thermal changes due to mass transport
- heat loss from the stack to the surroundings through conduction and convection
- latent heat of water

The sensible heat produced by the fuel cell stack is the irreversible heat losses from the electrochemical reaction [1]. These losses are a function of the cell voltage and current. Mass transport in the system brings energy in and takes energy out. The thermal energy changes due to mass transport depend on the temperature of the gases being transported into and out of the area of the fuel cell stack under consideration.

The heat losses from the stack to the environment can be considered as uniform heat sinks, and can be separated into three forms [16]:

- conduction losses
- convection losses

- radiation losses

The conduction losses occur anywhere the stack is in direct contact with another solid object. The forced convective losses occur at all locations where the stack is in contact with a fluid. For cases with forced air flow from a pump or a fan blowing on an exposed surface of the stack, it is generally assumed that forced convection losses will dominate over free convection losses. Radiation losses are minor due to the low operating temperature of the PEMFC and therefore are usually neglected [25–27, 43, 46].

The latent heat is a function of the heat of vaporization of water in the gas channels [45]. The latent heat of water term only needs to be considered if the model includes condensation and evaporation of water [36, 37]. Some models [26] simply assume the water to be in the form of vapour, therefore ignoring the latent heat term.

Water Management Model

PEFCs use a Nafion© membrane as the proton conductor which is placed between the electrodes of the fuel cell. It, therefore, acts as a barrier between the electrodes separating the reactants. The conductivity and resistivity of the Nafion membrane depend on its water content [47]. If the membrane water content is too low, the membrane will dry out and it will have high resistivity and low conductivity [47]. Low conductivity leads to poor fuel cell performance due to an increase in the ohmic losses. Conversely, if the membrane contains too much water, it can cause the electrodes to flood which prevents the reaction from occurring. Therefore, management of the distribution of water in the membrane is an important aspect of fuel cell operation [35].

Water transport through the membrane is a function of three processes: electro-osmotic drag, diffusion and convection. Based on the processes that are included, there are two methods of modelling the membrane that have been reported in literature, a diffusion based model and a hydraulic based model [47]. The diffusion based model is a macroscopic, single phase model which provides a good characterization of the membrane at low water content and includes diffusion and electro-osmotic drag as the water transport mechanisms [48]. The hydraulic model is a good approximation for membranes with high water content and it includes liquid water pressure, convection and electro-osmotic drag as the primary transport mechanisms [48].

Springer et al. [35] presented an empirically determined diffusion based

membrane model which included electro-osmotic drag and diffusion. Electro-osmotic drag is the process by which water molecules are dragged through the membrane by the protons passing from the anode to the cathode [35]. The diffusive flux across the membrane is a function of the water concentration gradient between the electrodes.

By adding the convective flux of water across the membrane, as developed in the hydraulic model, to the diffusion based model developed by Springer et al. [35], a model for the net transport of water across the membrane is obtained [47, 49]. This leads to equilibrium of water content through out the membrane.

Proton transport through the membrane occurs in the form of hydronium ions, which are composed of the proton and water from the membrane. Therefore, the transport of protons across the membrane, which is necessary for the reaction to occur, depends on the water content of the membrane. Springer et al. [35] and Sone et al. [50] used empirical data to fit a correlation function between the conductivity of the membrane and the water content.

Transient Thermo-Electric Model

There are a limited number of transient models of a fuel cell system because the dynamic equations require complex solutions [51]. The transient models of fuel cell stacks couple mass transport, thermal and electrochemical models with accumulative transient terms where applicable. Further improving their mechanistic model [33, 40], Amphlett et al. [46] developed a fuel cell stack model with a transient energy balance. Their empirical electrochemical model and the mass transport were assumed to be at steady-state.

Transient fuel cell stack models were also developed by Xue et al. [27], Pathapati et al.[29], Xue et al. [26], Chu et al. [30], Philipps and Ziegler [25], and Sharifi et al. [51]. Xue et al. [27] developed a transient fuel cell stack model in 2004 which included dynamic variation of the mass transport and thermal energy, and used a semi-empirical, steady state electrochemical model. This model served as a basis for further development by numerous researchers [25, 26, 29, 30, 51]. In particular, Xue et al. [26] continued development of their model by adding a characterization of the water phase change in the gas channels in 2005. Pathapati et al. [29] added the effect of channel pressure.

Recently, a transient lumped parameter model was developed by Chu et al. [30], which features transient liquid water cooling and instantaneous phase change for a conventional fuel cell stack. This mathematical model included

a transient characterization of the mass transport and the thermal. Empirical equations were used to characterize the electrochemical model. Philipps and Ziegler [25] developed a transient, non-isothermal fuel cell stack model, which incorporates a transient mass transport, thermal and electrochemical models for a zero-dimension stack. It also include a transient characterization of water phase change.

The fuel cell stack for this research will be a transient zero-dimension stack model which includes mass transport, thermal energy, water phase change and a theoretical electrochemical model. A lumped parameter approach similar to that taken by Xue et al. [27], Xue and Tang [26], Chu et al. [30] and Philipps and Ziegler [25] will be used to characterize the stack.

The significant differences with the model being developed for this research, with respect to the previously developed lumped parameter models are:

1. theoretically developed electrochemical model with concentration losses included
2. water vapour phase change will be characterized as developed by He et al. [52]
3. open-cathode fuel cell stack design
4. only air cooling of the stack (i.e. no liquid coolant)

This will provide an improved model which is necessary in order to analyze an open-cathode, air-cooled stack.

Lumped and Layered Models

Two modelling techniques are used for modelling the fuel cell stack, the lumped method and the layered method. Lumped models assume that there is a constant temperature through-out the stack [53]. Some lumped models consider only the stack as a single unit; others assume the stack to be composed of multiple identical cells. The lumped thermal model does not take into account the temperature distribution for each of the individual cells, nor the effects of the end plates [53].

A lumped parameter model of the fuel cell stack was developed by Kolodziej to model the thermal dynamics [54]. This model treated the fuel cell stack as a single unit via a nonlinear continuous stirred-tank reactor model, and studied the effect of coolant flow rate through the stack.

Some lumped parameter models which study the detailed mass transport, thermal energy, and electrochemistry of one cell and solve for the stack using a number of identical cells have been presented in literature by Xue et al. [27], Pathapati et al.[29], Xue et al. [26], Chu et al. [30], Philipps and Ziegler [25], and Sharifi et al. [51].

The layered model takes into account the temperature variations in the fuel cells within the stack. A stack layered model therefore consists of several cell models coupled together. The cell models that are layered into stacks can vary considerably in terms of complexity based on the purpose of the stack model. Sundaresan and Moore determined that the varying temperature effects within a fuel cell stack are important to consider during transient operation of the fuel cell, particularly for cold starts [53].

In this work, a lumped stack model will be developed for simplicity, therefore the temperature variation between cells in the stack will not be characterized.

1.2.4 Cold Temperature Stack Operation

Cold start-up and operation at sub-zero temperatures negatively affects the performance of the stack. In cases where the stack temperature drops below freezing, ice formation can permanently damage the stack [8]. Therefore, the main concern with cold temperature fuel cell start-up and operation is the state of the water in the cell. Additionally, during low temperature starts, the power output of the fuel cell is less than at the optimal operating temperatures. Datta et al.[55] tested a fuel cell system in Antarctica which showed only 33% of rated power capacity at -25℃. The fuel cell performance is impeded at low temperatures by the slower kinetic reactions and the membrane resistance.

For good start up and operating performance of the fuel cell stack, the effect of the cold temperature needs to be delicately balanced between the perspective of heat generation (and therefore time to reach optimal operating temperature), electrical current generation (or power output) and protecting the fuel cell from degradation.

During cold temperature operation, the waste heat generated due to poor cell performance is available to heat the cell. Unfortunately, the stack does not generate sufficient heat to maintain an operating temperature high enough to prevent ice formation when the stack is in an environment below -10℃ for long term operation [9], [56]. Active heating of the fuel cell prior to the start

of the fuel cell permits the fuel cell to start operating at a higher temperature thus producing a higher power output [16]. If an efficient method of heating the fuel cell is used, the limited hydrogen can be conserved.

Heating Methods

To address the concerns with fuel cell use at freezing temperatures, various solutions have been proposed. Keep warm systems, nitrogen purge systems and heating systems have been detailed in literature and patents to deal with heat and water management of a fuel cell stack in freezing conditions. The keep warm systems propose that the fuel cell stack should be insulated from the external environment and if necessary, heating systems are to be used to keep the fuel cell stack at an acceptable temperature to prevent freezing. For cold start conditions, it is proposed that the stack be purged of nitrogen prior to shut down [57] and then heated prior to start up, or recommended that the stack is kept above freezing while it is not operating. In cases where the stack is to be kept above 0°C, external heating methods must be used when the stack is not operating. There are numerous patents concerning the management of the fuel cell temperature for cold temperature start up and operation, mainly dealing with automotive fuel cell requirements [19, 20, 58–60].

For example, a UTC Fuel Cells LLC patent[20] details a system that prevents the fuel cell from freezing by running a catalytic burner with a hydrogen and oxygen combustion reaction. Within a thermally insulated enclosure, the hot combustion gases will heat the fuel cell and water management system by air convection.

Passive heating methods have been studied where the waste heat produced by the fuel cell stack is used to heat up the fuel cell stack when it is being operated in cold temperatures. Oszcipok et al. [57] reported that it is desirable to run the stack at a less efficient electrochemical reaction to generate heat. A lower voltage output of the fuel cell allows for a higher current to pass through the cell, which results in faster cell heating[18, 57].

Other methods of managing the temperature of the stack during cold temperature operation include: using preheated gases to introduce heat to the fuel cell stack and circulating warmed coolant through the stack. A system for heating and circulating coolant was patented by GMC[60], where coolant is heated via combustion or an electrical heat source, and a heat storage unit which stores waste heat produced during fuel cell operation.

Based on the literature available at the time of this research, it is proposed

to used an active heating system for cold start. An enclosure that uses an active heating method to heat the air inside is proposed. Using the mathematical model developed in this research, the amount of energy required to heat the air to an acceptable operating temperature can be obtained. These results will not be rigorously experimentally validated in this work.

Stack Heat Management

During operation of a fuel cell system, electrical energy and irreversible heat energy are generated. A variety of sources of the generated heat include the electrochemical reactions, system irreversibilities, ohmic resistance of the fuel cell membrane and water condensation [61]. In order to ensure that the fuel cell stack is operating at the optimal temperature, the stack heat generation must be managed. During operation of a fuel cell stack in cold temperature conditions, additional heating or cooling of the stack may be required depending on how much heat the stack generates.

A study by Koh et al. [62] showed that single fuel cells do not have the ability to maintain their operating temperature through their own heat generation, thus external heating is used. When fuel cells are connected in stacks, however, they have the ability to generate sufficient heat energy to increase their operating temperature beyond acceptable operating conditions. At cold ambient temperatures, the heat losses to the environment will determine whether additional heating is required during operation. If so, the heating methods outlined in Section 1.2.4 can be employed. In cases where the stack is capable of over heating, external cooling methods need to be applied, as a thermal analysis of a fuel cell stack by Giddey et al. revealed that very little heat leaves the stack through the exhaust air [22].

In this thesis, the fuel cell system which is being designed intends to conserve the irreversible heat being produced by the cell in an enclosure to heat incoming ambient air. Therefore, the composition and form of the irreversible heat leaving the fuel cell stack is important. If the cell is being exposed to subzero temperatures, the coolant in the cell must be able to withstand those temperatures. Even if the coolant will be used to heat the cell during a start up operation, it can fall to temperatures below freezing when the cell is not operational. Therefore, a forced air-cooled, open-cathode fuel cell stack is recommended.

1.3 Contributions

The novel aspect of this research is the study of the effect of an enclosure on fuel cell stack performance, particularly for cold climate conditions. The main contributions are:

- the development of a coupled mathematical model of an enclosure coupled with a fuel cell stack
- the development of an experimental setup for testing fuel cell stacks and enclosure/fuel cell stack systems at varying temperature and relative humidity conditions
- experimental testing of a fuel cell stack in an enclosure
- development and experimental validation of a transient, non-isothermal, open-cathode fuel cell stack mathematical model

1.4 Structure of the Thesis

The work presented in this thesis describes a mathematical model of an open-cathode fuel cell stack coupled with an enclosure for protection from unfavourable climates. An introduction to fuel cell stack and enclosure models is presented in Chapter 1, with particular emphasis on the energy and water management concerns associated with low temperature operation. Chapter 2 develops the transient, non-isothermal mathematical model of the fuel cell stack and validates it through existing work and experimental results. Chapter 3 presents the enclosure design and mathematical model, which is validated through experimental results. Chapter 4 details the experimental set ups used for testing the fuel cell stack fan, the fuel cell stack, and the stack inside the enclosure. The fuel cell stack model is coupled with the enclosure model and compared to experimental results in Chapter 5, where the effect of the enclosure on fuel cell stack performance is evident. The conclusions of this work and areas of further development are outlined in Chapter 6.

Chapter 2

Fuel Cell Stack

A transient, non-isothermal, lumped parameter, mathematical model of the fuel cell stack is developed to study the operation of the fuel cell stack in varying conditions. It will be later coupled with an enclosure model to simulate the effects of the enclosure during operation.

The mathematical model of the fuel cell stack is developed based on the premise that the stack consists of three control volumes: the anode gas channel, the cathode gas channel and the remaining cell volume. A similar approach has been taken by several researchers [25, 26], with the assumption of plug flow and negligible liquid water in the gas channels.

2.1 Mass Transport

The channels in the anode and cathode of a fuel cell stack are used to delivery reactant gases to the electrodes where reactions occur generating electrical power. These channels can be generally modelled as straight, square channels with one inlet and one outlet, as shown in Figure 2.1

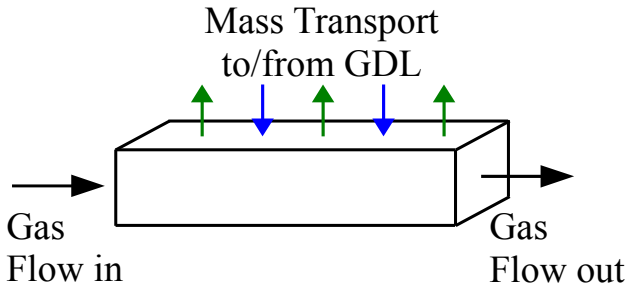

Figure 2.1 – Gas Transport Through Channel

Reactant gases are delivered to the fuel cell through a series of channels for both the anode and cathode. A general mass balance is developed for each channel to characterize the flow through the channels. The mass transport occurring in these channels includes: flow into and out of the channels, reactant consumption, production of water, water transport from across the membrane, and evaporation and condensation of water.

As the gases flow along the channel, they will diffuse into the GDL to the catalyst layer where they react. Any gaseous product formed at the catalyst layer is also diffused back through the GDL. To simplify the model, the diffusion from the catalyst layer to the channel will be treated as a bulk mass flow source in the quantities consumed or produced.

Any water entering or leaving the membrane, and produced by the hydrogen-oxygen reaction, will be treated as vapour in the fuel cell channels. Once in the channel in gaseous form, the water vapour may condense if the channel has already reached saturation. The transport of water vapour from the membrane through the GDL will be treated as a source or sink term in the channel mass balance. The condensation and evaporation in the channel is treated as a bulk source term.

The mass transport in a channel is therefore derived from the Reynolds Transport Theorem and characterized by a general mass balance of the gases. The rate of change of mass in a control volume (i.e. the channel volume) is equal to the rate of decrease of mass due to the convective flux into and out of the channel and the rate of increase due to sources. The diffusive flux is negligible as the gases are assumed well mixed and composition changes are driven by changes to the bulk convective flux.

In mathematical form, the mass balance is given by [41]:

$$\frac{d}{dt}\int_V (\rho_q)\, dV = -\int_A [\vec{n}\cdot(\rho_q\vec{u})]\, dA + \int_V S_q dV \tag{2.1}$$

where ρ_q is the density of the gases in channel q, V is the volume of the channel, A is the cross-sectional area of the channel that is perpendicular to the flow, $\vec{n}$ is the vector normal to the cross-section of the channel, $\vec{u}$ is the flow velocity in the channel, and S_q represents source terms.

In equation (2.1), the term on the left hand side represents the rate of change of mass in the channel volume. The first term on the right hand side represents the convective flux into and out of the channel along a vector $\vec{n}$ which is perpendicular to the cross-section of the channel (i.e. along the channel). This first right hand side term will account for the bulk flow into

and out of the channel. The second term on the right hand side is the change in mass due to sources. This term accounts for all sources of mass in the channel volume, including use of reactants, addition of product, water transport, and water phase change. This general mass balance will be used to solve for the density, ρ_q of the gas in a channel during operation of the fuel cell.

It is also important to study the gas composition in the channels to ensure that there if adequate reactant delivery. A mass balance will therefore be solved for each of the gas species to study the change in mass fraction of each species within the channel.

Using a mass balance similar to equation (2.1) for each species in the mixture, a species mass balance is obtained as:

$$\int_V \frac{\partial}{\partial t} \left(y_{q,i} \rho_q \right) dV = - \int_A \left[\vec{n} \cdot \left(\rho_q \vec{u} \right) \right] dA + \int_V S_q dV \tag{2.2}$$

where $y_{q,i}$ is the mass fraction of the species i in the channel q.

The term on the left hand side represents the change in the mass of one species in the channel volume. The first term on the right hand side represents the convective mass flow into and out of the channel of the same species. The source term accounts for any reactants used, products generated, water transport and phase change, depending on the species. This species mass balance will be solved for the mass fraction $y_{q,i}$ of each species i in the channel q.

The fuel cell stack will be operating at low temperatures, so the quantity of water vapour required to reach saturation will be low. Therefore, it is reasonable to assume the presence of liquid water in the channels. There are many mathematical models of fuel cells [31, 42, 43] which have assumed the absence of liquid water and/or neglected water accumulation effects. A few researchers, however have accounted for liquid water in the channels and water phase change [25, 26, 30].

This mathematical model of the fuel cell stack will account for the presence of liquid water in the channels through a mass balance in the channel volume. The change in mass of liquid water $m_{q,l}$ must be equal to the change in mass entering and exiting the channel through inlet and outlet flow and the source terms for liquid water.

The mass balance for liquid water to be solved for each of the channels is:

$$\frac{\partial m_{q,l}}{\partial t} = - \left[\sum_i \dot{m}_{q,l} \right] + \dot{S}_q \tag{2.3}$$

Equations (2.1), (2.2) for N-1 species, and (2.3) will be solved simultaneously to obtain the gas mixture density, the mass fraction of N-1 species, and the quantity of liquid water in the anode and cathode channels of the fuel cell.

To obtain the mass fraction of the remaining species, the following equation is used:

$$y_{q,N} = 1 - \sum_{i=1}^{N-1} y_{q,i} \tag{2.4}$$

2.1.1 Discretization

The differential mass transport equations to be solved for the channels are discretized by solving the integration terms over their respective values. Discretization is important for this mathematical model to simplify the partial differential equations depending on time and space to ordinary differential equations which depend only on time.

There are several channel designs for transporting the reactants: pin-type, straight, serpentine, integrated, and interdigitated flow fields [63]. This fuel cell stack model can be applied to straight channels, or serpentine channels if an effective length is used.

The straight channel design consists of straight, parallel flow channels which are connected to the gas inlet and outlet. The conventional design has one inlet flow which is divided among the many parallel channels. This can lead to unstable voltages because water can accumulate in the flow channels and obstruct gas flow [63]. The open-cathode design has a fan which draws air through all the open channels. This can help reduce reactants from flowing preferentially through the less blocked channels because the flow into each channel is independent. An advantage of the straight channel design is that it is simple to manufacture.

The serpentine channel design consists of several serpentine channels that run parallel to each other. This design may improve the distribution of the reactant, but causes pressure and concentration losses due to channel length [63].

This model will use a straight channel design with the conventional single inlet to many straight channels to single outlet design for the anode. The open-cathode straight channel design will be applied for the cathode.

For mass transport in the channels, the convective flow through the channels corresponds to the mass flux into and out of the channel volume passing perpendicular to the cross sectional area. Therefore, the first term on the right

hand side of the convective fluxes is integrated over the cross sectional area of the channel and is thus represented by the sum of the mass flux into the channel, $\sum_i \dot{m}^I_{q,i}$ minus the sum of the mass flux out of the channel,$\sum_i \dot{m}^O_{q,i}$.

As the model is zero-dimensional in the space domain, the change in the density within the channel volume and the mass source terms are assumed consistent at a given time through out the channel. Therefore, there is no location dependency for the term on the left hand side and the second term on the right hand side. The mass balance is therefore integrated as follows:

$$\frac{d\rho_q}{dt}V = \sum_i \dot{m}^I_{q,i} - \sum_i \dot{m}^O_{q,i} + \sum_i \dot{m}_{q,i,source} \tag{2.5}$$

where $\sum_i \dot{m}_{q,i,source}$ is the sum of the mass consumption, production, or phase change of all source terms of all the species.

For the species composition of the gases within the channel, the model is treated in the same way as for the density within the channel volume. Therefore, the change in mass fraction of the species will not depend on location within the volume and complete mixing at a given time step will be assumed through out the channel. The convective fluxes will again be integrated over the cross sectional area to give a sum of mass fluxes of the species into the channel less the mass fluxes of the species out of the channel. The species source term is again independent of location.

$$\frac{\partial \rho_{q,i}}{\partial t}V = \frac{\partial}{\partial t}\left[y_{q,i}\rho_q V\right] = \sum_i \dot{m}^I_{q,i} - \sum_i \dot{m}^O_{q,i} + \sum_i \dot{m}_{q,i,source} \tag{2.6}$$

The change in mass fraction term has two time dependent parameters, mass fraction y_i and the density in the channel ρ_q. Therefore, the chain rule is applied to differential the terms:

$$\frac{\partial y_{q,i}}{\partial t}\left[\rho_q V\right] + \frac{\partial \rho_q}{\partial t}\left[y_{q,i}V\right] = \sum_i \dot{m}^I_{q,i} - \sum_i \dot{m}^O_{q,i} + \sum_i \dot{m}_{q,i,source} \tag{2.7}$$

As liquid water does not fill the channel volume in the same way gases do, it is treated from a mass accumulation perspective. Equation (2.3) is already in the discretized form.

2.1.2 Cathode Mass Transport

The cathode channel in the fuel cell delivers oxygen to the catalyst layer via the gas diffusion layer where it is reacted with hydrogen protons and produces

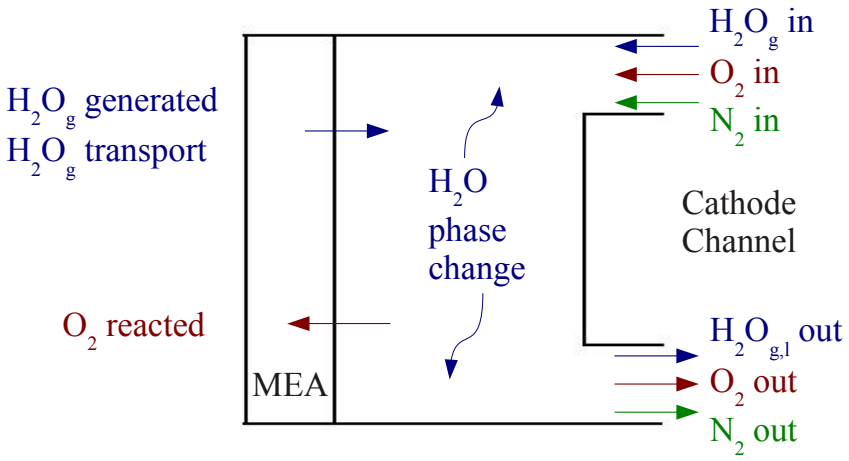

Figure 2.2 – Cathode Channel Mass Transport

water. To deliver oxygen to the channel, the open-cathode fuel cell stack uses a fan which draws air from the environment into the channels. Atmospheric air contains mainly oxygen, nitrogen and water vapour, and it is assumed that all other species are of negligible quantities.

As the fuel cell stack operates, the changes in the gas composition and temperature of the gases in the channel will affect the density of the gases. Due to the coupled nature of these properties, it is therefore necessary to determine the density of the gases in the channel at a given time. A mass balance of the species in the cathode channel is developed from equation (2.1) to solve for the density of the gases in the channel.

Figure 2.2 shows that within the control volume of the cathode channel, a gas mixture composed of oxygen, nitrogen and water vapour enters the channel from the environment, $\sum_i \dot{m}^I_{ca,i}$, and leaves through the outlet, $\sum_i \dot{m}^O_{ca,i}$. Oxygen is consumed by the reaction, $\dot{m}_{O_2,used}$, water vapour is generated by the reaction, $\dot{m}_{H_2O,gen}$, water vapour is transported across the membrane, $\dot{m}_{trans}$, and some water may undergo phase change, $\dot{m}_{phase}$.

The general mass balance for the density in the cathode channel is thereby:

$$\frac{\partial \rho_{ca}}{\partial t} V_{ca} = \sum_i \dot{m}^I_{ca,i} - \sum_i \dot{m}^O_{ca,i} - \dot{m}_{O_2,used} + \dot{m}_{H_2O,gen} - \dot{m}_{phase} + \dot{m}_{trans} \quad (2.8)$$

where a negative $\dot{m}_{phase}$ term indicates evaporation. Water transport through the membrane is assumed to be positive in the direction from anode to cathode, thus it is added to the cathode.

During operation of the fuel cell stack, the reaction is limited by the quan-

tity of oxygen available. At low oxygen concentrations, the fuel cell stack will have poor performance. Therefore, it is necessary to determine the fraction of mass of oxygen in the channel. Using equation (2.6), the mass fraction of oxygen can be determined at a given time as a function of the mass flow of oxygen into and out of the system, and oxygen consumed:

$$\frac{\partial \rho_{ca,O_2}}{\partial t} V_{ca} = \frac{\partial y_{ca,O_2}}{\partial t} \rho_{ca} V_{ca} + \frac{\partial \rho_{ca}}{\partial t} y_{ca,O_2} V_{ca} = \dot{m}^{I}_{ca,O_2} - \dot{m}^{O}_{ca,O_2} - \dot{m}_{O_2,used} \quad (2.9)$$

where y_{ca,O_2} is the mass fraction of oxygen.

To reduce the resistivity of the membrane in the fuel cell stack, proper humidification of the membrane is required. The cathode provides three sources of water to the membrane. Water vapour coming into the channel with the air from the environment can pass through the GDL to the cathode catalyst layer and the membrane. It is assumed that this water will condense in the membrane electrode assembly (MEA). Liquid water is produced by the reaction of hydrogen protons and oxygen. Finally, water is transported between the anode and the cathode channels through the membrane. The hydration of the membrane therefore depends in part on the concentration of water in the cathode channel. To determine the mass fraction of water vapour in the cathode channel, a mass balance is developed. The water vapour mass fraction is a function of the water vapour entering and leaving, phase change, reaction product water and water migration at the membrane interface [25].

$$\begin{aligned} \frac{\partial \rho_{ca,H_2O^v}}{\partial t} V_{ca} &= \frac{\partial y_{ca,H_2O^v}}{\partial t} \rho_{ca} V_{ca} + \frac{\partial \rho_{ca}}{\partial t} y_{ca,H_2O^v} V_{ca} \\ &= \dot{m}^{I}_{ca,H_2O^v} - \dot{m}^{O}_{ca,H_2O^v} + \dot{m}_{H_2O,gen} - \dot{m}_{ca,phase} + \dot{m}_{trans} \end{aligned} \quad (2.10)$$

The remaining gas species, nitrogen, will be solved as the difference of the total of the mass fractions, one, less the mass fractions of oxygen and water vapour. Therefore the mass fraction of nitrogen is:

$$y_{ca,N_2} = 1 - y_{ca,H_2O^v} - y_{ca,O_2} \quad (2.11)$$

The mass transport terms for the inlet mass flow, outlet mass flow, oxygen consumption, water production, water phase change and water transport are developed in the following sections.

Cathode Inlet Mass Flow, $\dot{m}^I_{ca,i}$

The gas entering the cathode channel through the inlet consists of air from the environment with a given relative humidity and the remaining gas is at the standard 21% oxygen, 79% nitrogen concentration. The open-cathode fuel cell stack fan is set at a constant flow rate for the simulations. This constant flow rate is selected based on a stoichiometric ratio and the maximum current achieved by the stack. The molar flow rate of air, $\dot{n}^I_{ca,stack}$, in mol/s, is given by:

$$\dot{n}^I_{ca,stack} = \frac{1}{1 - x^I_{ca,H_2O^v}} \left[\frac{\lambda_{ca}(I_{max})}{4(0.21)F} n_{cell} \right] \tag{2.12}$$

where λ_{ca} is the stoichiometric ratio, I_{max} is the maximum current, in A, at which the stack will be tested, F is Faraday's constant in C/mol, n_{cell} is the number of cells in the stack, and x^I_{ca,H_2O^v} is the molar fraction of water vapour entering the cathode determined by:

$$x^I_{q,H_2O^v} = \frac{P^I_{q,H_2O^v}}{P_{amb}} \tag{2.13}$$

where P^I_{q,H_2O^v} is the partial pressure of water vapour entering the cathode channel and P_{amb} is the ambient pressure. The partial pressure of water vapour is determined based on the relative humidity, ϕ_q in the channel q and saturation pressure, $P_{q,sat}$:

$$P^I_{q,H_2O^v} = \phi_q P_{q,sat} \tag{2.14}$$

For one channel in one fuel cell, the molar flow rate of gas delivered to the cell is divided among the channels in the cell. The total flow rate available to the stack is first divided by the number of cells and then by the number of channels $n_{ca,chan}$ in each cell. Therefore, to determine the molar flow gas into the cathode channel, the following equation is developed:

$$\dot{n}^I_{ca,chan} = \frac{\dot{n}_{ca,stack}}{n_{cell} n_{ca,chan}} = \frac{1}{1 - x^I_{H_2O^v}} \left[\frac{\lambda_{ca}(I_{max})}{4(0.21)F n_{ca,chan}} \right] \tag{2.15}$$

Therefore, the species mass transport terms to be used in equation (2.8) are developed from this channel inlet molar flow rate, taking into account their specific molar fraction and molar mass. The species mass flow rates in the inlet

gas are therefore:

$$\dot{m}^I_{ca,O_2} = (0.21) M_{O_2} \dot{n}^I_{ca,chan} = \frac{0.21}{1 - x^I_{H_2O^v}} \left[\frac{\lambda_{ca}(I_{max}) M_{O_2}}{4F n_{ca,chan}} \right] \tag{2.16}$$

$$\dot{m}^I_{ca,N_2} = (0.79) M_{N_2} \dot{n}^I_{ca,chan} = \frac{0.79}{1 - x^I_{H_2O^v}} \left[\frac{\lambda_{ca}(I_{max}) M_{N_2}}{4F n_{ca,chan}} \right] \tag{2.17}$$

$$\dot{m}^I_{ca,H_2O^v} = (x^I_{H_2O^v}) M_{H_2O} \dot{n}^I_{ca,chan} = \left(\frac{x^{in}_{H_2O}}{1 - x^{in}_{H_2O}} \right) \left[\frac{\lambda_{ca}(I_{max}) M_{H_2O}}{4F n_{ca,chan}} \right] \tag{2.18}$$

Cathode Outlet Mass Flow, $\dot{m}^O_{ca,i}$

The outlet mass flow of the cathode channels is assumed to be driven by the species pressure differential between the channel and the external environment. This pressure differential in the channel is characterized as Poiseuille flow in a channel for a laminar regime [41]. The average outlet velocity for the cathode channel u_{ca} is thus a function of the pressure differential:

$$u_{ca} = \frac{d^2_{ca} \Delta P_{ca}}{32 \mu_{ca} L_{ca}} \tag{2.19}$$

where d_{ca} is the effective diameter of the channel, in m, ΔP is the difference in pressure, in Pa between the channel and the environment, μ_{ca} is the viscosity of the gas, in $Pa * s$, based on species composition, and L_{ca} is the length of the cathode channel, in m.

The viscosity of the gas is obtained as a function of the gas composition:

$$\mu_{ca} = \sum_{i=1}^{N} x_{ca,i} \mu_i \tag{2.20}$$

where $x_{ca,i}$ is the molar fraction of the species, i, of gas in the cathode channel and μ_i is the density of that gas at the channel temperature.

The mass flow rate of each species out of the channel is given by:

$$\dot{m}^O_{ca,i} = \rho_{ca} y_{ca,i} u_{ca} A_{ca} \tag{2.21}$$

where A_{ca}, in m^2, is the cross-sectional area of the cathode channel.

Cathode Oxygen Consumption, $\dot{m}_{O2,used}$

The reaction which occurs at the cathode catalyst layer consumes oxygen. Oxygen in the air in the cathode channel passes through the gas diffusion layer to the cathode catalyst layer where it reacts. The oxygen consumed by the reaction, in kg/s, for one channel in the fuel cell is given by Faraday's law of electrolysis [1]:

$$\dot{m}_{O_2,used} = \frac{M_{O_2} I}{4 F n_{ca,chan}} \tag{2.22}$$

where I is the current of the cell in A, the molar mass of oxygen, M_{O_2} is in kg/mol, and Faraday's constant is in C/mol.

Cathode Water Production, $\dot{m}_{H_2O,gen}$

The reduction of oxygen at the cathode catalyst layer forms water. The product water is assumed to be in vapour form once it reaches the cathode channel. The amount of water vapour generated by the reaction in one channel in a cell, in kg/s, is:

$$\dot{m}_{H_2O,gen} = \frac{M_{H_2O} I}{2 F n_{ca,chan}} \tag{2.23}$$

Cathode Water Phase Change, $\dot{m}_{q,phase}$

If the fuel cell channel exceeds water saturation, water will condense in the channel. It is assumed that the liquid water in the channel exists as small droplets in the gas phase. With the transient model, changing conditions can also cause evaporation of liquid water which is present in the channel. Water phase change in the channel is treated as a source term, $\dot{m}_{q,phase}$, and the rate of change is different depending on whether condensation or evaporation occurs.

For condensation, the amount of water which changes phase depends on the quantity of excess water vapour in the channel for the given saturation conditions and the condensation rate. Evaporation is a function of the evaporation rate and the remaining space available for water vapour in the air before saturation is reached. The phase change rate of water in the cathode channel,

$\dot{m}_{ca,phase}$, in kg/s, is [52]:

$$\begin{aligned}\dot{m}_{ca,phase} =& \frac{k_c V_{ca}\left(1-s_{ca}\right) M_{H_2O}}{RT_{ca}(x,t)}\left(P_{ca,H_2O^v}-P_{ca,sat}\right)\beta_{ca} \\ &+ k_v V_{ca} s_{ca}\rho_{H_2O,l}\left(P_{ca,H_2O^v}-P_{ca,sat}\right)\left(1-\beta_{ca}\right)\end{aligned} \tag{2.24}$$

where the first term on the right hand side represents the condensation rate and the second term represents the evaporation rate. In equation (2.24), k_c, in s^{-1}, is the rate of condensation of water and k_v, in $kPa^{-1}s^{-1}$ is the evaporation rate of water, V_{ca} is the channel volume in m^3, s_{ca} is the saturation of the channel, R is the universal gas constant in $\frac{kPa*m^3}{mol*K}$, M_{H_2O} is the molar mass of water in kg/mol, P_{ca,H_2O^v} is the partial pressure of water vapour in the channel in kPa, $P_{ca,sat}$ is the saturation vapour pressure in the channel in kPa at the channel temperature, and β_{ca} is a switching term which activates either the condensation or evaporation term and negates the other [52].

The switching term β_{ca} is a function of the difference between the partial pressure of water vapour in the channel and the saturation pressure of the channel.

$$\beta_{ca} = \frac{1}{2} + \frac{\left|P_{ca,H_2O^v} - P_{ca,sat}(T_{ca}(x,t))\right|}{2\left(P_{ca,H_2O^v} - P_{ca,sat}(T_{ca}(x,t))\right)} \tag{2.25}$$

Therefore, if the difference between the partial pressure of water vapour in the channel and the saturation pressure is positive, there is more water in the channel than the gas can hold as vapour so condensation will occur. In this case, the switching term β_{ca} will be 1, which activates the condensation term in equation (2.24). When the difference between the partial pressure of water vapour in the channel and the saturation pressure is negative, there is space available for any liquid water to evaporate. The switching term β_{ca} is therefore 0, which activates the evaporation term of equation (2.24).

The saturation term s_{ca} controls whether evaporation occurs and its rate. If there is no liquid water in the channel to evaporate, the saturation term will be zero as it is a function of the mass of liquid water in the channel $m_{ca,H_2O,l}$, and expressed as:

$$s_{ca} = \frac{m_{ca,H_2O,l}}{\rho_{H_2O,l} V_{ca}} \tag{2.26}$$

where $\rho_{H_2O,l}$ is the density of liquid water in kg/m^3.

Cathode Water Transport through Membrane, $\dot{m}_{trans}$

Water is transported through the membrane in the fuel cell stack by three mechanisms: electro-osmotic drag, back diffusion and convective flux. The membrane water transport model is developed in Section 2.2. For the water transport through the membrane term for the mass balance, it is important to identify that transport is set as positive in the direction from the anode to the cathode. Therefore, it appears as an addition to the cathode. The water transported through the membrane will be assumed to be in vapour form when it enters the cathode channel as it is evaporated while passing through the GDL.

Cathode Channel Liquid Water

If the conditions in the channel are such that water exceeds saturation, there will be liquid water present in the channel. It is assumed no liquid water enters the channel; the only source of liquid water is through phase change in the channel. As the relative humidity of the air entering the channel is less than 100%, it is reasonable to assume all the water is in vapour form. Any liquid water either transported through the membrane or generated by the reaction is assumed to have reached a vapour state during diffusion through the GDL and therefore enters the channel in vapour form. The liquid water is assumed to leave the channel in the form of droplets. Therefore, the liquid water mass balance for the cathode channel is:

$$\frac{\partial m_{ca,H_2O^l}}{\partial t} = -\dot{m}^{O}_{ca,H_2O^l} + \dot{m}_{ca,phase} \tag{2.27}$$

The liquid water leaving the $1mm^3$ cathode channel is characterized as $1mm^3$ droplets which are released once sufficient liquid water volume has built up to form a droplet of this size. Therefore, if the mass of liquid water in the channel has reached the size of a $1mm^3$ droplet, this droplet will be forced out of the cathode channel. If there is insufficient liquid water to form a full $1mm^3$ droplet, no liquid water leaves the cathode channel. Mathematically, this is expressed as:

$$\dot{m}_{ca,H_2O^l} = \begin{cases} \rho_{H_2O^l} V_{droplet} & \text{if } x \geq \rho_{H_2O^l} V_{droplet}, \\ 0 & \text{if } x < \rho_{H_2O^l} V_{droplet}. \end{cases} \tag{2.28}$$

where $V_{droplet} = 1mm^3$.

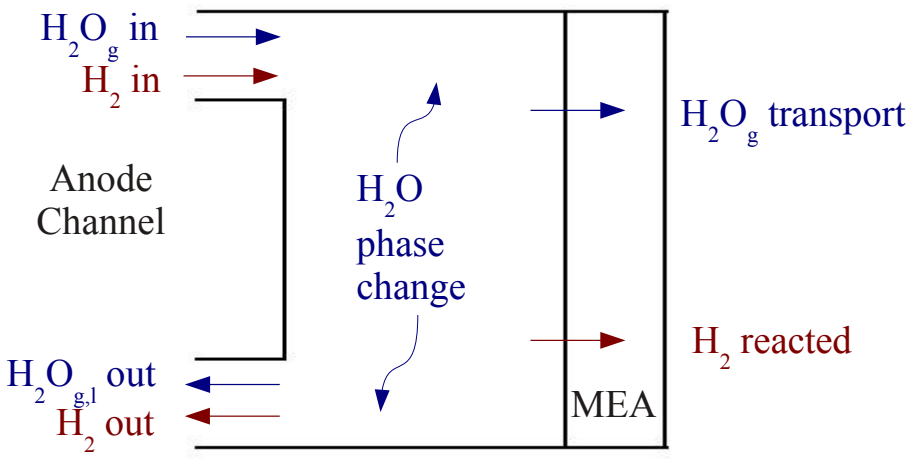

Figure 2.3 – Anode Channel Mass Transport

The cathode mass balance will be solved for the ODE equations (2.8), (2.10), (2.9) and (2.27) for ρ_{ca}, y_{ca,H_2O^v}, y_{ca,O_2}, and m_{ca,H_2O^l} respectively.

2.1.3 Anode Mass Transport

The anode channel contains flow of two species of gas: hydrogen and water vapour, and liquid water. The hydrogen is diffused through the gas diffusion layer (GDL) to the anode catalyst layer where it reacts to produce electrons and hydrogen protons. These hydrogen protons pass through the membrane and react with oxygen at the cathode catalyst layer. Hydrogen is delivered to the anode catalyst layer as it flows through a series of channels which abut the GDL.

During operation of the fuel cell stack, it is necessary to ensure that sufficient hydrogen is reaching the anode catalyst layer to maintain the reaction. Additionally, there is the possibility of formation of liquid water in the anode channel which must be characterized. Dry hydrogen is often used as the anode reactant supply in air-breathing fuel cells, therefore there is the potential for membrane dry out on the anode side of the membrane.

Figure 2.3 shows a schematic of the mass transport mechanisms in the anode channel, which consists of gas entering and leaving the channel, hydrogen consumed by the reaction, water vapour transported through the membrane, and water phase change.

A general mass balance is solved for the gas density ρ_{an} in the anode channel, which considers all inlet $\sum_i \dot{m}^I_{an,i}$ and outlet flow $\sum_i \dot{m}^O_{an,i}$, reactant

used,$\dot{m}_{H_2,used}$, phase change, $\dot{m}_{an,phase}$ and water transport, $\dot{m}_{trans}$ through the membrane.

$$\frac{\partial \rho_{an}}{\partial t} V_{an} = \sum_i \dot{m}^I_{an,i} - \sum_i \dot{m}^O_{an,i} - \dot{m}_{H_2,used} - \dot{m}_{an,phase} - \dot{m}_{trans} \tag{2.29}$$

where the phase change term, $\dot{m}_{an,phase}$, is negative during evaporation and therefore subtracted to result in an increase in water vapour. Water transport through the membrane is assumed to be positive in the direction from anode to cathode, thus it is subtracted from the anode.

The composition of gas in the anode channel indicates whether the fuel cell is receiving sufficient reactant hydrogen. If humidified, it can also be used to analyze if the membrane is receiving adequate water to prevent membrane dry-out. To characterize the gas composition in the anode channel, the change in the mass fraction of hydrogen in the channel is determined as a function of the mass flow of hydrogen into the channel $\dot{m}^I_{an,H_2}$, the mass flow of hydrogen out of the channel $\dot{m}^O_{an,H_2}$, and the rate at which hydrogen is consumed by the fuel cell reaction $\dot{m}_{H_2,used}$.

$$\frac{\partial \rho_{an,H_2}}{\partial t} V_{an} = \frac{\partial y_{an,H_2}}{\partial t} \rho_{an} V_{an} + \frac{\partial \rho_{an}}{\partial t} y_{an,H_2} V_{an} = \dot{m}^I_{an,H_2} - \dot{m}^O_{an,H_2} - \dot{m}_{H_2,used} \tag{2.30}$$

where y_{an,H_2} is the mass fraction of hydrogen, ρ_{an} is the gas density in the anode channel, V_{an} is the anode channel volume.

There are only two species of gas present in the anode channel: hydrogen and water vapour. Therefore, as the sum of the mass fractions will always be equal to one, the mass fraction of water vapour y_{an,H_2O^v} in the anode channel is:

$$y_{an,H_2O^v} = 1 - y_{an,H_2} \tag{2.31}$$

Anode Inlet Mass Flow, $\dot{m}^I_{an,i}$

A cylinder of compressed hydrogen supplies hydrogen gas to the anode at atmospheric pressure. The hydrogen gas contains no water vapour, but water vapour may be added through the use of a humidifier. To develop a general set of equations, the possibility of water vapour being added will be included.

The flow rate of hydrogen in the anode is variable and controlled based on the load draw from the fuel cell stack. The variable hydrogen flow is set

at a stoichiometry with respect to the current draw required by the stack. Therefore, the molar flow rate of hydrogen and water vapour into the system is:

$$\dot{n}^{I}_{an,stack} = \left(\frac{1}{1 - x^{I}_{an,H_2O^v}}\right)\frac{\lambda_{an}(I)}{2F}n_{cell} \tag{2.32}$$

where I is the current produced by the stack in A, λ_{an} is the stoichiometric ratio, F is Faraday's constant, and n_{cell} is the number of cells in the stack. The molar flow rate is also a function of composition of water vapour x^{I}_{an,H_2O^v} and hydrogen in the gas which is characterized in the first part of the term. The molar fraction of water vapour is determined based on the anode relative humidity, ϕ_{an}, as in equation (2.13) in the cathode.

The flow rate supplied to the anode is divided evenly among the channels $n_{an,chan}$ in the cells n_{cell}, therefore:

$$\dot{n}^{I}_{an,chan} = \frac{\dot{n}_{an,stack}}{n_{cell}n_{an,chan}} = \left(\frac{1}{1 - x^{I}_{an,H_2O^v}}\right)\frac{\lambda_{an}(I)}{2Fn_{an,chan}} \tag{2.33}$$

The mass flow rates of these two species in the anode supply flow can be determined based on the molar flow rate, the molar mass of the species and molar fraction of the gas which is composed of the specific species. Therefore, the mass flow rate of hydrogen into the anode is:

$$\dot{m}^{I}_{an,H_2} = \frac{\lambda_{an}(I)}{2Fn_{an,chan}} \tag{2.34}$$

and the mass flow rate of water vapour into the anode is:

$$\dot{m}^{I}_{an,H_2O^v} = \left(\frac{x^{I}_{an,H_2O}}{1 - x^{I}_{an,H_2O}}\right)\frac{\lambda_{an}(I)}{2Fn_{an,chan}} \tag{2.35}$$

Anode Outlet Mass Flow, $\dot{m}^{O}_{an,i}$

The outlet mass flow in the anode channels is developed using the same pressure differential method as for the cathode channels as detailed in Section 2.1.2 for the cathode channel

Anode Hydrogen Consumption, $\dot{m}_{H_2,used}$

The hydrogen in the anode channel passes through the gas diffusion layer to the anode catalyst layer where it reacts. The consumption of hydrogen is characterized as a sink in the anode channel. The amount of hydrogen reacted in one cell depends on the amount of current the stack is producing:

$$\dot{m}_{H_2,used} = \frac{M_{H_2} I}{2F} \tag{2.36}$$

where I is the current produced in A, M_{H_2} is the molar mass of hydrogen in kg/mol, and F is Faraday's constant in C/mol.

Anode Water Phase Change, $\dot{m}_{an,phase}$

The phase change term for water in the anode channel is developed in the same way as for the cathode channel.

Anode Water Transport through Membrane, $\dot{m}_{trans}$

The membrane water transport phenomena are detailed in Section 2.2

Anode Channel Liquid Water, $\dot{m}_{an,H_2O^l}$

The liquid water in the anode channel is treated the same as in the cathode channel.

2.2 Membrane Model

Polymer electrolyte fuel cells (PEFCs) use a perfluorosulfonated ionomer (PFSI), also known as Nafion, membrane because of their high proton conductivity [42]. During the operation of a fuel cell, the membrane transports hydrogen protons, in the form of hydronium ions, from the anode catalyst layer to the cathode catalyst layer where they react with oxygen to form water. The membranes need to be hydrated with liquid water to allow for the proton transport. If the membrane is too dry, its higher proton resistance to conductivity will prevent the proton transport from occurring [42]. The membrane will also transport liquid water between the two electrodes by three mechanisms: electro-osmotic

drag, diffusion and convection.

Water Transport Across Membrane

The semi-empirical model developed by Springer et al [35] is widely used and will serve as a basis for the model developed for this work. Models have also been developed by Bernardi et al [34], Nguyen and White [36] and Weber et al. [48], [47], [64]. The model by Springer et al. only accounts for electro-osmotic drag and diffusion. Weber et al. [47] indicated that convection should be included in cases where the liquid pressure between the anode and the cathode is not equilibrated, as is the case for this model.

Therefore, the water transport across the membrane in the fuel cell is:

$$\dot{m}_{trans} = (\dot{n}_{drag} - \dot{n}_{diff} - \dot{n}_{conv})\, A_{chan} M_{H_2O} \tag{2.37}$$

where $\dot{n}_{drag}$ is the molar electro-osmotic drag, $\dot{n}_{diff}$ is the molar diffusion, and $\dot{n}_{conv}$ is the molar convection, and A_{chan} is the active area of the channel.

Electro-osmotic drag is the phenomenon where the protons being transported across the membrane cause water molecules to be dragged across the membrane [42]. As the motion of the protons is from the anode to cathode, electro-osmotic drag is expressed in this direction. From the model developed by Springer et al. [35], the electro-osmotic drag was defined as a function of a drag coefficient n_d, and the proton flux across the membrane (i.e. the current flux).

$$\dot{n}_{drag} = n_d \frac{j}{F} \tag{2.38}$$

where j is the current per area in A/cm^2.

The drag coefficient n_d is a function of the hydration of the membrane λ and expressed as:

$$n_d = \frac{2.5}{22}\lambda \tag{2.39}$$

where λ is the water content of the membrane.

For this model, the membrane water content is taken to be the minimum of the content at the anode interface and the cathode interface. It is assumed that the interface with less water content will limit the quantity of water transported from the anode to the cathode. The water content of the membrane at the interface between the membrane and the channel, q, can be expressed by empirical fitting polynomials developed by Springer et al. [35]:

$$\lambda_q = \begin{cases} 0.0043 + 17.81 a_q - 39.85 a_q^2 + 36.0 a_q^3, & 0 < a_q \leq 1 \\ 14 + 1.4\,(a_q - 1)\,, & 1 < a_q \end{cases} \tag{2.40}$$

where a_q is the activity of water vapour in the channel q. In this model, it is assumed that the conditions in the channels are the conditions at the boundaries of the membrane, therefore the activity of water is:

$$a_q = \frac{P_{q,H_2O^v}}{P_{sat}} \tag{2.41}$$

The second water transport mechanism is diffusion across the membrane which is driven by the concentration gradient between the anode and the cathode [42]. The diffusion frequently occurs in the direction of the cathode toward the anode as the cathode is likely to have a higher water concentration. Electro-osmotic drag brings water to the cathode and the cathode produces water, so diffusion acts to counterbalance these mechanisms. The molar flux of water across the membrane by diffusion is given by:

$$\dot{n}_{diff} = D_{m,H_2O}\frac{c_{ca,H_2O^v} - c_{an,H_2O^v}}{t_m} \tag{2.42}$$

where D_{m,H_2O} is the diffusivity of water in the membrane, c_{q,H_2O^v} is the concentration of water at the interface of the membrane and the channel q, and t_m is the membrane thickness.

The membrane diffusion coefficient, D_{m,H_2O} is determined by an empirical fit function based on the temperature and water content of the membrane, as well as a reference diffusion coefficient, D^{ref}_{m,H_2O} [49].

$$D_{m,H_2O} = n_{drag}D^{ref}_{m,H_2O}exp\left(2416\left(\frac{1}{303} - \frac{1}{T_s}\right)\right) \tag{2.43}$$

where 303K is the reference temperature at which D^{ref}_{m,H_2O} was determined.

The reference membrane diffusion coefficient is an empirical function fit at 303K by Springer et al. [35]:

$$D^{ref}_{m,H_2O} = 2.563 - 0.33\lambda_{mem} + 0.0264\lambda^2_{mem} - 0.000671\lambda^3_{mem} \tag{2.44}$$

for $\lambda > 4$. For $\lambda < 4$ the following empirical functions were developed by Pukrushpan et al. [65]

$$\lambda_q = \begin{cases} D^{ref}_{m,H_2O} = 10^{-6} & \lambda_{mem} < 2 \\ D^{ref}_{m,H_2O} = 10^{-6}\left(1 + 2\left(\lambda_{mem} - 2\right)\right) & 2 \leq \lambda_{mem} < 3 \\ D^{ref}_{m,H_2O} = 10^{-6}\left(3 - 1.67\left(\lambda_{mem} - 3\right)\right) & 3 \leq \lambda_{mem} < 4 \end{cases} \tag{2.45}$$

The water vapour concentration in channel q, which is assumed the concentration at the interface boundary of the membrane is calculated as a function of the membrane properties [49]:

$$c_q = \frac{\rho_{mem}}{EW_{mem}}\lambda_q \tag{2.46}$$

where λ_q is the membrane water content in channel q, ρ_{mem} is the dry membrane density, and EW_{mem} is the membrane equivalent weight.

The third transport mechanism is convective flux which occurs across the membrane as a function of the pressure differential between the anode and cathode sides of the membrane [47]. As the cathode side often has a higher partial pressure than the anode, the convective flux is assumed to act in the direction from cathode to anode.

$$\dot{n}_{conv} = \frac{c_{ca,H_2O^v} + c_{an,H_2O^v}}{2} \frac{k_{m,p}}{\mu_{H_2O^l}} \frac{P_{ca} - P_{an}}{t_m} \tag{2.47}$$

where $k_{m,p}$ is the permeability of the membrane, $\mu_{H_2O^l}$ is the dynamic viscosity of water, and P_q is the liquid pressure of water in the channel q; assumed to be the same as the channel pressure [25].

Membrane Conductivity

The conductivity of the membrane depends on the hydration of the membrane, λ as water in the membrane is necessary to create hydronium ions, the main method by which hydrogen protons are transported across the membrane. The ionic conductivity of the membrane was determined empirically and also depends on the temperature of the membrane and the water activity. At 303K, Springer et al. [35] measured the membrane conductivity to be:

$$\sigma_{303K} = 0.005139\lambda - 0.00326 \tag{2.48}$$

where λ is the average membrane water content, taken as the average of the water content on the anode and cathode sides.

Springer et al. developed a modifier for this membrane to account for the influence of the temperature on membrane conductivity [35]:

$$\sigma_{a,T} = \sigma_{303K} exp\left(1268\left(\frac{1}{303} - \frac{1}{T_s}\right)\right) \tag{2.49}$$

2.3 Electrochemical Model

The reactions in the fuel cell stack are the hydrogen oxidation reaction and oxygen reduction reaction:

$$2H_2 \rightarrow 4H^+ + 4e^- \tag{2.50}$$

$$\underline{O_2 + 4H^+ 4e^- \rightarrow H_2O} \tag{2.51}$$

$$2H_2 + O_2 \rightarrow 2H_2O \tag{2.52}$$

These electrochemical reactions produce potentials in each electrode. At standard conditions, the hydrogen-oxygen fuel cell has a potential E° of 1.229V [42], which is derived from the Gibb's free energy of the reaction:

$$E^\circ = \frac{-\Delta g_f^\circ}{4F} \tag{2.53}$$

where Δg_f°, in J/kg is the Gibb's free energy of the reaction at STP.

As the fuel cell stack is not operating at standard conditions, it is necessary to apply correction factors to determine the reversible voltage of the fuel cell for its operating conditions. As the fuel cell stack will be operating at near ambient pressure, only a temperature correction factor will be applied. The temperature correction factor depends on the change in entropy of the reaction, Δs in J/kgK and the temperature of operation, T in K, such that:

$$E_T = \frac{\Delta s}{2F}(T - T_0) \tag{2.54}$$

where F is Faraday's constant, in C/mol, and T_0 is the standard reference temperature, which is 273K at STP.

The reversible voltage also depends on the concentration of the reactants available to the system. The activity correction is used to account for changes in the cell potential as a function of the changes in concentration. Thus, the cell voltage is: [42].

$$E_N = \frac{RT}{2F} ln \frac{a_{H_2O}^2}{a_{O_2} a_{H_2}^2} \tag{2.55}$$

where a_i is the activity of the species. The activity for ideal gases, oxygen and hydrogen, is the ratio of the partial pressure of the gas to the standard pressure: $a_i = P_i/P_0$. The activity for liquid water is one.

Therefore, the open circuit reversible voltage for the fuel cell stack with corrections for temperature and activity is:

$$E_{OCV} = E^\circ + E_T - E_N \tag{2.56}$$

The fuel cell stack reaction experiences potential losses during the reaction due to irreversible processes, in particular: activation energy, ohmic losses and concentration losses. The cell voltage can be expressed as [43]:

$$V_{cell} = E_{OCV} - \eta_{act} - \eta_{conc} - \eta_{ohmic} \tag{2.57}$$

where E_{OCV} is the open circuit voltage defined in Equation (2.56), η_{act} is the activation overpotential, η_{ohmic} is the ohmic resistance loss and η_{conc} is the concentration loss.

The activation overpotential is the energy losses necessary to overcome the energy barrier that prevents spontaneous reactions in the fuel cell. Based on electrochemical principles, the rate of a reaction is given by a Butler-Volmer equation. Including both the forward and reverse barriers to activation, the Butler-Volmer equation for the electrochemical reaction in the fuel cell stack is [66]:

$$j = j_0 \left(e^{\alpha n F \eta / (RT)} - e^{-(1-\alpha) n F \eta / (RT)} \right) \tag{2.58}$$

where j is the current density in the cell in A/cm^2, j_0 is the reference exchange current density in A/cm^2, α is the transfer coefficient, n is the number of electrons transferred in the reaction, F is Faraday's constant in C/mol, η is the overpotential in V, R is the universal gas constant in $J/(mol * K)$, and T is the stack temperature in K.

The overpotential will be derived from the Butler-Volmer equation for each the anode and the cathode.

In the anode, a small overpotential is assumed and a Taylor series expansion of the Butler-Volmer equation can be used as an approximation [66]. The higher order terms greater than 1 of the Taylor series expansion are ignored. Therefore, the overpotential for the anode is calculated as:

$$j = j_0 \frac{n F \eta_{an,act}}{RT} \tag{2.59}$$

and rearranged to solve for the anode activation overpotential as:

$$\eta_{an,act} = \frac{RT_{an}}{F} \left(\frac{j}{j_{0,an}} \right) \tag{2.60}$$

where $\eta_{an,act}$ is the activation overpotential for the anode reaction.

In the cathode, the overpotential is large so the reverse barrier to activation is ignored, such that it is assumed that the cathode overpotential is solely an irreversible process. This simplification is known as the Tafel equation [66]:

$$j = j_{0,ca} e^{\alpha_c n F \eta_{act} / (RT)} \tag{2.61}$$

which is rearranged to solve for the cathode activation overpotential:

$$\eta_{ca,act} = \frac{RT_{ca}}{\alpha_c F} ln \left(\frac{j}{j_{0,ca}} \right) \tag{2.62}$$

where $\eta_{an,act}$ is the activation overpotential for the cathode reaction.

The total loss due to the activation overpotentials is the sum of the activation overpotential losses in the anode and the cathode:

$$\eta_{act} = \frac{RT_{an}}{F} \left(\frac{j}{j_{o,an}} \right) + \frac{RT_{ca}}{\alpha_c F} ln \left(\frac{j}{j_{o,ca}} \right) \tag{2.63}$$

where α_c is the cathodic transfer coefficient [46], and $j_{o,an}$ and $j_{o,ca}$ are the reference exchange current densities, in A/cm^2, in the anode and cathode respectively.

The reference exchange current density in the anode is assumed to be constant. The reference exchange current density in the cathode $j_{o,ca}$ in A/cm^2, however, depends on temperature [2], and is expressed by the empirical equation:

$$j_{o,ca} = A_{o,ca} 10^{3.271 - 3826/T_s} \tag{2.64}$$

where $A_{o,ca}$ is the ratio of platinum to catalyst layer area in $cm^2 Pt/cm^2 CL$, and T_s is the stack temperature in K.

The concentration losses are derived from the reaction kinetic losses from the oxygen depletion in the cathode and the effect of oxygen depletion on the Nernst voltage. The Nernst voltage loss, caused by oxygen depletion in the channels, is derived as a function of the concentration of oxygen on the catalyst layer, $c^*_{O_2}$, and the bulk oxygen concentration, $c^0_{O_2}$. From the Nernst equation (2.55)

$$\begin{aligned}
\eta_{conc} &= E^0_N - E^*_N \\
\eta_{conc} &= \left(E^0 - \frac{RT}{nF} ln \frac{1}{c^0_{O_2}} \right) - \left(E^0 - \frac{RT}{nF} ln \frac{1}{c^*_{O_2}} \right) \\
\eta_{conc} &= \frac{RT}{nF} ln \left(\frac{c^0_{O_2}}{c^*_{O_2}} \right)
\end{aligned} \tag{2.65}$$

Concentration losses also affect the rate of the reaction in the fuel cell, causing a voltage loss in the activation overpotential particularly in the case of high overpotential in the cathode. From the Tafel equation for high overvoltages:

$$j = j^0_0 \left(\frac{c^*_{O_2}}{c^0_{O_2}} e^{\alpha n F \eta / (RT)} \right) \tag{2.66}$$

Therefore, the effect of the concentration of the reactant on the activation overpotential is:

$$\begin{aligned}
\eta_{conc} &= E^*_{act} - E^0_{act} \\
\eta_{conc} &= \left(\frac{RT}{\alpha_c nF} ln \frac{j c^{0*}_{O_2}}{j^0_{ca,0} c^*_{O_2}} \right) - \left(\frac{RT}{\alpha_c nF} ln \frac{j c^{0*}_{O_2}}{j^0_{ca,0} c^0_{O_2}} \right) \\
\eta_{conc} &= \frac{RT}{\alpha_c nF} ln \left(\frac{c^0_{O_2}}{c^*_{O_2}} \right)
\end{aligned} \tag{2.67}$$

The limiting current density is the maximum current density possible due to mass transport limitations and is derived as a function of the consumption rate of the reactant:

$$j_L = nFD^{eff}\frac{c^0_{O_2}}{t_m} \tag{2.68}$$

where j_L is the limiting current density, D^{eff} is the effective diffusivity of oxygen in the catalyst layer, and t_m is the electrode thickness. This equation can be rearranged in terms of the bulk reactant concentration:

$$c^0_{O_2} = \frac{j_L t_m}{nFD^{eff}} \tag{2.69}$$

and the catalyst layer oxygen concentration can be described as:

$$c^*_{O_2} = c^0_{O_2} - \frac{jt_m}{nFD^{eff}} \tag{2.70}$$

Therefore, the ratio of bulk oxygen concentration to catalyst layer concentration is:

$$\frac{c^0_{O_2}}{c^*_{O_2}} = \frac{j_L}{j_L - j} \tag{2.71}$$

This relationship can be substituted into the two sources of losses due to concentration effects, and these two sources are summed to obtain:

$$\eta_{conc} = \frac{RT_{ca}}{nF}\left(1 + \frac{1}{\alpha_c}\right) ln\left(\frac{j_L}{j_L - j}\right) \tag{2.72}$$

where j_L is the limiting current density in A/cm^2. Equation (2.72) is the total concentration losses in the fuel cell reaction.

The ohmic losses are calculated from the resistance of the fuel cell membrane. As the resistance of the membrane depends on its humidification, the empirical fuel cell membrane model used by Paquin and Fréchette, which focuses on water management of the air-breathing fuel cell, was selected [67]. This model was originally presented by Sone et al. [50] for relating Nafion© membrane ionic conductivity with relative humidity:

$$\eta_{ohmic} = j(\sum (R_{comps} * A_{mem}) + R_{ionic}) \tag{2.73}$$

where R_{comps} is the resistance of the stack components, in Ω, which is measured empirically, A_{mem} is the active area of the membrane in A/cm^2 and R_{ionic} is represented by [67]:

$$R_{ionic} = \frac{t_m}{\sigma_{a,T}} \tag{2.74}$$

where t_m is the membrane thickness, and $\sigma_{a,T}$, the empirical relation of ionic conductivity of the membrane is developed in Section 2.2 and depends on the temperature of the membrane and the membrane water content.

2.4 Energy Balance

During the operation of a PEFC stack, the temperature of the stack must remain within an acceptable operating range of approximately 0℃ and 95℃. At higher temperatures, the reaction kinetic losses are reduced so the stack has better performance [66]. However, if the temperature is too high the membrane in the stack can dry out which prevents proton transport across the membrane. Conversely, at sub-zero operating temperatures, the fuel cell stack risks freezing. If the fuel cell stack freezes, the water expansion can damage the membrane and the electrodes by crack formation and delamination [8]. Therefore, it is important to monitor the temperature of the fuel cell stack.

The temperature of the open-cathode fuel cell stack is affected by several sources and losses of thermal energy. The electrochemical reaction which occurs during fuel cell stack operation generates thermal heat which is dissipated through out the fuel cell stack. The stack temperature is also affected by the thermal energy associated with the transport of gases into and out of the stack. Additionally, water evaporation or condensation within the fuel cell stack channels will affect the temperature of the channels and consequently the overall temperature of the stack. Finally, heat convection occurs between the stack and the surrounding air.

The mathematical model of the fuel cell stack is developed by dividing the stack into a number of identical cells. Each cell has been divided into a number of anode channels and cathode channels. It has been assumed that all anode channels have identical operation, as do all cathode channels. Therefore, only one anode channel and one cathode channel will be solved. These will be multiplied by the number of channels in a cell to characterize one cell.

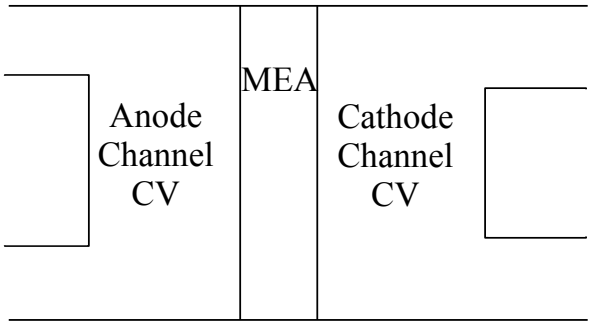

Figure 2.4 – Anode and Cathode Control Volumes

Additionally, it is assumed that the temperature of the gases in the anode and cathode channels is the same as the temperature of the outlet gases. Therefore, the three control volumes considered are: the anode channel, cathode channel, and the stack volume minus the channels, as shown in Figure 2.4.

To solve for the overall stack temperature, it is assumed that all the cells within the stack behave identically.

2.4.1 Gas Channel Energy Balance

The anode and cathode channels will have different temperatures because they have unique reactions occurring at the catalyst layer interface and different gases passing through the channels. Therefore, it is necessary to develop an energy balance to solve for the temperature in the anode and cathode channels separately. Heat energy is also transferred between the channels and the overall cell volume through convection. Therefore, a complete analysis of the energy condition within the channels is required to obtain an accurate cell temperature.

The energy balance for a gas channel takes into account the heat sources and sinks, and energy transported with mass into and out of the channel. As only the overall channel temperature is required, the model will have no spatial dimensions and be solved only for the change in temperature with time.

The fuel cell stack generates heat, electrical power and water during operation. The open-cathode fuel cell stack uses rapid air flow through the cathode channels to cool the fuel cell by carrying away some of the heat by forced convection. Therefore, the temperature of the cathode channel is necessary to characterize the forced convection cooling through the fuel cell stack cathode channels. The water vapour produced by the fuel cell stack leaves through the cathode channel. Depending on the conditions in the channel, this water may be condensed, which will also affect the cooling of the fuel cell stack.

The anode channel supplies hydrogen to the anode catalyst layer. It may supply water to the membrane in the case of humidified hydrogen gas input, or remove water from the membrane if the membrane is well saturated. The gas passing through the anode channel also removes heat through convection.

To determine the temperature of a channel in the fuel cell, an energy balance of the channel is developed. Using the first law of thermodynamics, the change in energy in the system is calculated as the difference of the energy entering and leaving the system [68]. Therefore, the change in the energy in

the channel gases is equal to the sum of the heat sources, $\dot{Q}_{q,in}$ and energy transported by mass into the channel $\sum_i \dot{m}^I_{q,i} c_{p,i} T_q$, less the heat sinks $\dot{Q}_{q,out}$ and energy transported by mass out of the channel $\sum_i \dot{m}^O_{q,i} c_{p,i} T_q$, such that:

$$\frac{\partial E_q}{\partial t} = \dot{Q}_{q,in} - \dot{Q}_{q,out} + \sum_i \dot{m}^I_{q,i} c_{p,i} T_q - \sum_i \dot{m}^O_{q,i} c_{p,i} T_q \tag{2.75}$$

where the mass transport of each species i of gas is considered for the respective anode, an, or cathode, ca, channel denoted by q.

The change in energy in the system is the sum of the change in energy of each species of gas in the channel volume V_q. The change in energy of the gas is given, for an ideal gas, as a function of its specific heat capacity $c_{p,i}$ and temperature T_q. Therefore, the change in energy is given by:

$$\frac{\partial E_q}{\partial t} = \sum_i \frac{\partial y_{q,i}}{\partial t} \Big(\rho_q V_q c_{p,i} T_q \Big) + \frac{\partial \rho_q}{\partial t} \left(\sum_i y_{q,i} V_q c_{p,i} T_q \right) + \left(\sum_i y_{q,i} \rho_q V_q c_{p,i} \right) \frac{\partial T_q}{\partial t} \tag{2.76}$$

The first term on the right hand side expresses the change in species mass fraction, $y_{q,i}$ with time; the second term, the change in gas density, ρ_q with time; and the third, the change in temperature T_q with time.

Cathode Channel

For the cathode channel, the heat sources and sinks are:

a) convective heat transfer between the gases in the channel and the MEA

b) energy from water phase change in the channel

c) energy transported into and out of the channel through gas transport

Figure 2.5 shows the energy balance of the cathode channel. This energy balance is given in mathematical terms from equations (2.75) and (2.76):

$$\begin{aligned} \frac{\partial T_{ca}}{\partial t} = \left(\sum_i y_{ca,i} \rho_{ca} V_{ca} c_{p,i} \right)^{-1} \Bigg[& \dot{Q}_{conv,ca} + \dot{Q}_{ca,phase} + \sum_i \dot{m}^I_{ca,i} c_{p,i} T_{ca} \\ & - \sum_i \dot{m}^O_{ca,i} c_{p,i} T_{ca} - \sum_i \frac{\partial y_{ca,i}}{\partial t} \Big(\rho_{ca} V_{ca} c_{p,i} T_{ca} \Big) \\ & - \frac{\partial \rho_{ca}}{\partial t} \left(\sum_i y_{ca,i} V_{ca} c_{p,i} T_{ca} \right) \Bigg] \end{aligned} \tag{2.77}$$

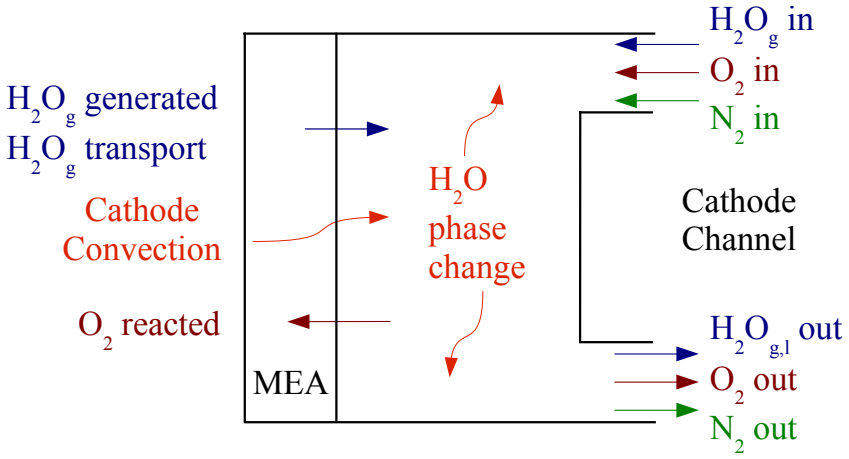

Figure 2.5 – Cathode Channel Energy Balance

where T_{ca}, in K, is the cathode temperature, $y_{ca,i}$, in kg_i/kg is the mass fraction of a gas species in the cathode channel, ρ_{ca}, in kg/m^3 is the cathode gas density, V_{ca}, in m^3, is the cathode volume, $c_{p,i}$ is the specific heat capacity of the species i in the channel, $\dot{Q}_{conv,ca}$, in W, represents the change in heat due to convective heat transfer, $\dot{Q}_{ca,phase}$, in W, represents the change in heat due to water phase change, $\dot{m}^I_{ca,i}$, in kg/s is the species gas flow into the cathode channel, and $\dot{m}^O_{ca,i}$, in kg/s is the species gas flow out of the cathode channel. In the cathode channel, the gas species are: oxygen, nitrogen and water vapour.

The convective heat transfer between the gas and the cell is a source or sink of energy in the cathode channel depending on the temperature difference between the gas in the channel, T_{ca}, and the cell, T_s. It is also a function of the contact surface area, $A_{s,ca}$, in m^2, and the convective heat transfer coefficient, h_{ca} in W/m^2K [68]. Expressed by Newton's law of cooling:

$$\dot{Q}_{conv,ca} = h_{ca} A_{s,ca} \left(T_{ca} - T_s\right) \tag{2.78}$$

the convective heat transfer term will be treated as a heat source in equation (2.77). The temperature difference term will account for a condition where convection is removing heat. The convective heat transfer coefficient, h_{ca}, is a function of the properties of the fluid, fluid flow type and velocity, and surface geometry [68], and it will be experimentally determined in Chapter 5.

The phase change in the cathode channel depends on the heat of evaporation, the quantity of water changing phase and whether evaporation or

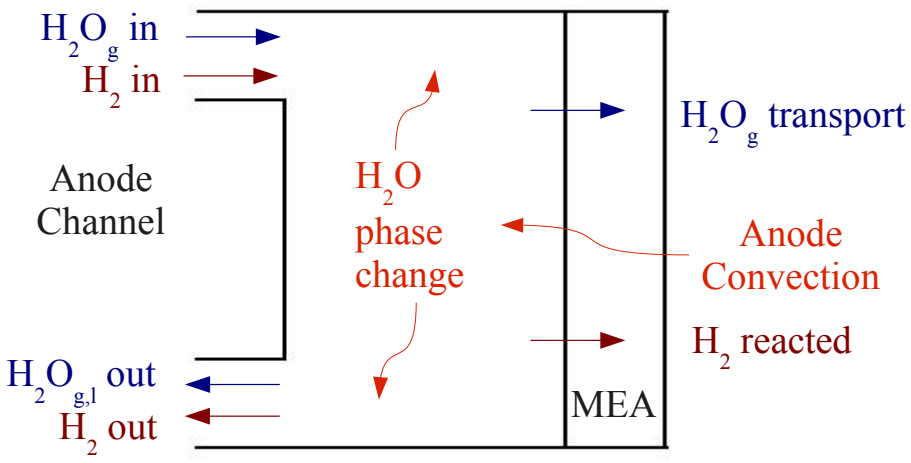

Figure 2.6 – Anode Channel Energy Balance

condensation is occurring. The mass of water changing phase, $\dot{m}_{ca,phase}$, in kg/s was obtained in the Cathode Mass Transport Section 2.1.2.

The heat released or absorbed during the water phase change is [25]:

$$\dot{Q}_{ca,phase} = \Delta H_{vap} \dot{m}_{ca,phase} \tag{2.79}$$

where ΔH_{vap}, in J/kg is the heat of vaporization of water.

Anode Channel

The anode channel undergoes heat energy changes based on the transport of gas species through the channel, convective heat transfer between the channel and the stack, and water phase change. The heat energy transport in the anode channel is shown in Figure 2.6.

As with the cathode channel, the energy balance in the anode channel is expressed in mathematical terms from equations (2.75) and (2.76), and solved for the anode channel temperature. The governing equation is:

$$\begin{aligned}\frac{\partial T_{an}}{\partial t} = \left(\sum_i y_{an,i}\rho_{an}V_{an}c_{p,i}\right)^{-1}\Bigg[&\dot{Q}_{conv,an} + \dot{Q}_{an,phase} + \sum_i \dot{m}^I_{an,i}c_{p,i}T_{an} \\ &- \sum_i \dot{m}^O_{an,i}c_{p,i}T_{an} - \sum_i \frac{\partial y_{an,i}}{\partial t}\left(\rho_{an}V_{an}c_{p,i}T_{an}\right) \\ &- \frac{\partial \rho_{an}}{\partial t}\left(\sum_i y_{an,i}V_{an}c_{p,i}T_{an}\right)\Bigg]\end{aligned} \tag{2.80}$$

where T_{an} is the anode temperature, $y_{an,i}$ is the mass fraction of a gas species in the anode channel, ρ_{an} is the anode gas density, V_{an} is the anode gas volume, $c_{p,i}$ is the specific heat capacity of the species i in the channel, $\dot{Q}_{conv,an}$ represents the convective heat change, $\dot{Q}_{an,phase}$ represents the change in energy due to water phase change, $\dot{m}^{I}_{an,i}$ is the species gas flow into the anode channel, and $\dot{m}^{O}_{an,i}$ is the species gas flow out of the anode channel. The gas species in the anode channel are hydrogen and water vapour.

The two heat sources in the anode channel are the convective heat transfer between the channel and the MEA/stack, and the water phase change in the channel. The convective heat transfer $\dot{Q}_{conv,an}$ is expressed using Newton's law of cooling [68]:

$$\dot{Q}_{conv,an} = h_{an} A_{s,an} \left(T_{an} - T_s\right) \tag{2.81}$$

where $A_{s,an}$ is the surface area between the anode channel and the MEA/stack. The difference between the anode channel temperature and stack temperature drives the direction of heat transfer. The anode channel convective heat transfer coefficient h_{an} depends on the properties of the fluid, flow type, fluid velocity and surface geometry of the anode channel, and is determined experimentally [68].

The water phase change in the anode channel is a function of the mass of water changing phase, as expressed by equation (2.24), and the heat of vaporization of water ΔH_{vap}. When condensation occurs, heat energy is released into the anode channel by the mass of water changing from vapour to liquid. The mass phase change term $\dot{m}_{an,phase}$ is positive for condensation to liquid water, therefore the phase change term will be treated as a heat source. In the case of evaporation, heat energy is removed from the anode channel to produce water vapour from the liquid water. The mass phase change term $\dot{m}_{an,phase}$ is negative in this case, expressing the heat removal. Therefore, the anode channel phase change term is [25]:

$$\dot{Q}_{an,phase} = \Delta H_{vap} \dot{m}_{an,phase} \tag{2.82}$$

2.4.2 Stack/MEA Energy Balance

The fuel cell stack is modelled as a combination of a number of identical cells, where each cell consists of a number of identical anode and cathode channels. To determine the stack temperature, an energy balance of the fuel cell stack is developed. The following outlines the energy sources in the fuel cell stack. The electrochemical reaction in the fuel cell stack produces energy in the form

of thermal heat and electrical power. The gases in the cathode and anode channels experience convective heat transfer with the fuel cell stack, and the stack experiences convective heat transfer due to its temperature differential with the surrounding environment. Heat is also absorbed during evaporation of the liquid water produced by the fuel cell stack electrochemical reaction at the membrane/catalyst layer interface. Therefore, the water produced can be assumed in vapour form and the heat of formation for water vapour is used. Water that is transported through the membrane condenses at the membrane/catalyst interface on one side of the membrane and evaporates at the membrane/catalyst interface at the other side. As both membrane/catalyst interfaces are included in the stack control volume, the net energy of these phase changes is zero.

The energy balance for the fuel cell stack is:

$$m_s c_{p,s} \frac{\partial T_s}{\partial t} = \dot{Q}_{rxn} + \dot{Q}_{phase} - \dot{W}_{elec} - \dot{Q}_{amb} - \dot{Q}_{conv,ca} n_{ca,chan} n_{cell} - \dot{Q}_{conv,an} n_{an,chan} n_{cell} \tag{2.83}$$

where m_s is the mass of the stack in kg/s, $c_{p,s}$ is the specific heat capacity of the stack in J/kgK, T_s is the stack temperature in K, $\dot{Q}_{rxn}$ is the total energy produced by the fuel (i.e. Δh_{rxn}) reaction in the fuel cell stack in W, $\dot{Q}_{phase}$ is the energy from evaporation of the water produced by the reaction in W, $\dot{W}_{elec}$ is the energy produced as electrical power in W, $\dot{Q}_{amb}$ is the convective heat transfer between the stack and the surroundings in W, and $\dot{Q}_{conv,ca}$ and $\dot{Q}_{conv,an}$, in W, represent the convective heat transfer from the stack to the cathode and anode gas channels, respectively. The latter are multiplied by the number of anode, $n_{an,chan}$, and cathode channels, $n_{an,chan}$ respectively, and number of cells n_{cell} in a stack.

The total energy produced by the chemical reaction $\dot{Q}_{rxn}$ of hydrogen and oxygen to form water (2.52) depends on the heat of formation of water and the amount of water produced.

$$\dot{Q}_{rxn} = \Delta H_f \dot{m}_{H_2O,prod} \tag{2.84}$$

where the heat of formation of water ΔH_f is for liquid water, and $\dot{m}_{H_2O,prod}$ is the amount of water vapour produced.

It is assumed that the liquid water produced by the reaction is evaporated while in the GDL before reaching the gas channels. The energy used for to evaporate the water will be represented as a loss from the system as that

energy is used to bring the water to a higher energy state in vapour form.

$$\dot{Q}_{phase} = -\dot{m}_{H_2O,prod}\Delta H_{vap} \tag{2.85}$$

where ΔH_{vap} is the heat of vaporatization of water at the stack temperature.

The total energy produced by the electrochemical reaction is in two forms, waste heat energy and electrical power. The electrical energy is removed through the current collectors and produces the current in the stack. Therefore, only the waste heat is available to heat the stack, so the electrical power $\dot{W}_{elec}$ is removed. The electrical power produced by the electrochemical reaction is:

$$\dot{W}_{elec} = IV_{cell}n_{cell} \tag{2.86}$$

where I is the current produced by the stack in A, V_{cell} is the voltage in V of one cell, as determined by Equation (2.57), and n_{cell} is the number of cells in the stack.

Convective heat transfer between the fuel cell stack and the surrounding ambient air occurs through all stack surface areas $A_{s,st}$ which are exposed. To simplify the model, the overall geometry will be considered for this surface area. As will be shown in the enclosure model in Chapter 3, one side of the fuel cell stack undergoes conductive transport with the surface on which it is installed. From Newton's law of cooling [68]:

$$\dot{Q}_{amb} = h_{amb}A_{s,st}\left(T_s - T_{amb}\right) \tag{2.87}$$

where h_{amb} is an experimentally determined convective heat transfer coefficient, and T_{amb} is the ambient temperature.

The cathode convective transport, $\dot{Q}_{conv,ca}$, is given by equation (2.78), but it is multiplied by the number of cathode channels in one cell $n_{ca,chan}$ and again by the number of cells in the stack n_{cell} to account for the heat removed from all the cathode channels. The anode channel convective transport, $\dot{Q}_{conv,an}$, obtained in equation (2.81), and it is also multiplied by the number of anode channels in one cell $n_{an,chan}$ and the number of cells in the stack.

$$\dot{Q}_{conv,q} = h_q A_{s,q}\left(T_q - T_s\right) n_{q,chan}n_{cell} \tag{2.88}$$

Model Summary

The transient temperatures of the fuel cell stack, and the anode and cathode channels, are therefore obtained using equations (2.83), (2.80), (2.77). This

gives a characterization of the fuel cell stack which permits studies of the temperature during changing ambient conditions and fuel cell stack power production to prevent freezing and overheating of the stack.

Table 2.1 – Stack mathematical model

Variable	*Governing Equation*
Cathode channel density, ρ_{ca}	2.8
Oxygen mass fraction in cathode, y_{ca,O_2}	2.9
Water vapour mass fraction in cathode, y_{ca,H_2O^v}	2.10
Mass of liquid water in cathode, m_{ca,H_2O^l}	2.27
Anode channel density, ρ_{an}	2.29
Hydrogen mass fraction in anode, y_{an,H_2}	2.30
Mass of liquid water in cathode, m_{an,H_2O^l}	2.27
Cathode temperature, T_{ca}	2.77
Anode temperature, T_{an}	2.80
Stack temperature, T_s	2.83

In summary, the mathematical model of the open-cathode stack is solved simultaneously for 10 unknowns defined by 10 governing ordinary differential equations, as detailed in Table 2.1

2.5 Validation

There are very few models reported in literature which give sufficient model parameters and results to permit validation. The fuel cell stack model developed in this work is validated by qualitative comparison with experimental data presented in literature by Philipps and Ziegler[25]. This work developed a mathematical model to predict fuel cell performance and compared it to experimental data. It was selected as it gave sufficient parameters to build a complete model. Philipps and Ziegler [25] have, however, published limited results from their simulations therefore, only a qualitative comparison of the models is possible.

The fuel cell stack model developed by Philipps and Ziegler [25] is transient, non-isothermal, and accounts for liquid and vapour water. This model served as the basis for the development of the model in this work. It relies solely on convective heat transfer with the ambient air for cooling, and solves for a single cell which is multiplied to obtain a full stack model. The improvements applied for this research model are: a theoretically developed electrochemical model, a phase change term that accounts for the difference between evaporation and

Table 2.2 – Philipps and Zeigler Model Parameters

Parameter	*Value*	*Reference*
Physical		
Number of Cells	6	[25]
Cell Active Area (cm^2)	30.2	[25]
Length of Anode Channel (m)	0.465	[25]
Length of Cathode Channel (m)	0.465	[25]
Width of Anode Channel (m)	0.0015	[25]
Width of Cathode Channel (m)	0.0015	[25]
Height of Anode Channel (m)	0.0006	[25]
Height of Cathode Channel (m)	0.0008	[25]
Membrane Thickness (μm)	25	estimated
Membrane Equivalent Weight (g/equi)	1100	[65],[47]
Anode Channel Volume (m^3)	5.58×10^{-7}	[25]
Cathode Channel Volume (m^3)	4.2×10^{-7}	[25]
Number of Anode Channels	2	[25]
Number of Cathode Channels	2	[25]
Empirical		
Anode Heat Transfer Coefficient (W/K)	0.105	fitted [25]
Cathode Heat Transfer Coefficient (W/K)	0.115	fitted [25]
Ambient Heat Transfer Coefficient (W/K)	0.07	fitted [25]
Mass of the Stack (kg)	51	fitted [25]
Heat Capacity of Stack (J/kgK)	770	[25]
Component Resistance (Ω)	0.0	fitted
Membrane Diffusivity Coefficient (m^2/s)	5.5×10^{-11}	[25]
Membrane Effective Permeability (m^2)	1.58×10^{-18}	[25]
Evaporation Rate Coefficient $\left(\frac{cm^2 LV}{(cm^2 ch)kPa*s}\right)$	1	fitted
Condensation Rate Coefficient $\left(\frac{cm^2 LV}{(cm^2 ch)s}\right)$	10	fitted
Environmental		
Environment Pressure (kPa)	101	
Enivronment Temperature (K)	298	
Electrochemical		
Anode Reference Current Density (A)	1	[69]
Cathode Reference Area ($cm^2 Pt/cm^C L$)	200	[2]
Cathodic Coefficient	1	[33]
Limiting Current (A/cm^2))	0.3	fitted

Table 2.3 – Operating Conditions for Validation Model

Parameter	*Value*	*Reference*
Operating Conditions		
Anode Channel Pressure (kPa)	101	
Cathode Channel Pressure (kPa)	101	
Anode Channel Inlet Flow Rate	$\lambda_{AN} = 2$, at 6A	[25]
Cathode Channel Inlet Flow Rate	$\lambda_{CA} = 2$, at 6A	[25]
Anode Channel Inlet RH (%)	0	
Cathode Channel Inlet RH (%)	50	
Anode Channel Inlet Temperature (K)	298	
Cathode Channel Inlet Temperature (K)	298	
Current (A)	1A, 3A, 6A, 3A, 1A	[25]

condensation, and changes were made to the formulation of the stack energy balance.

The specific parameters used for this validation are listed in Table 2.2, and

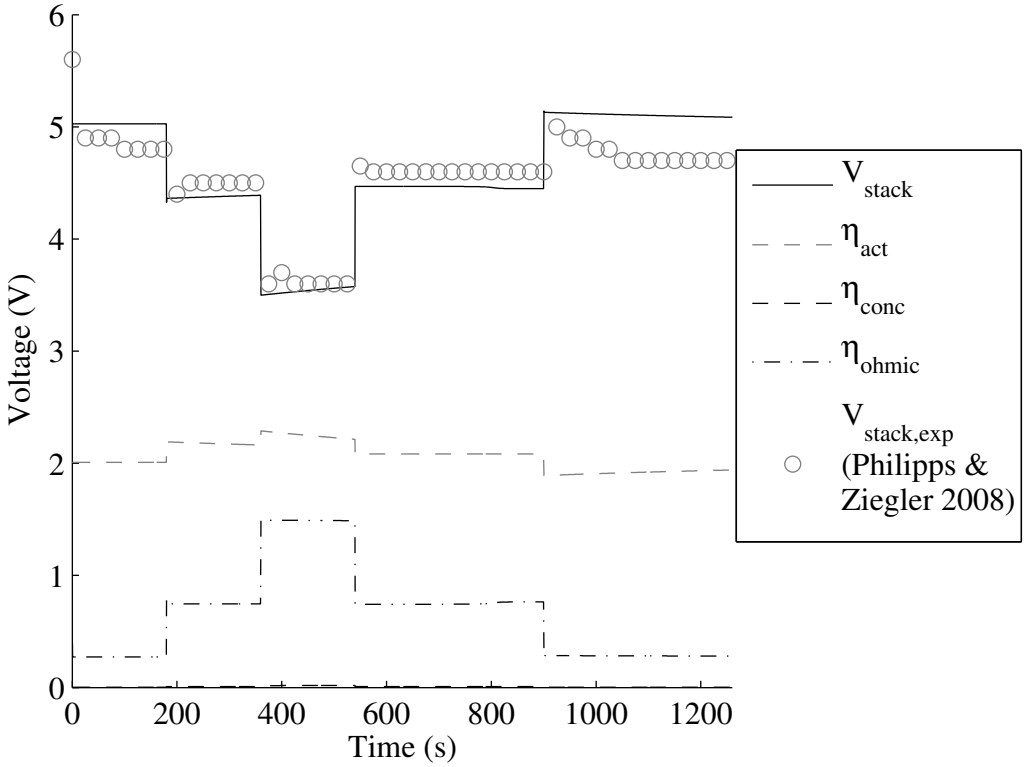

Figure 2.7 – Validation of Electrochemical Model

the operating conditions are listed in Table 2.3. All parameters are taken from the article by Philipps and Ziegler [25], except for those indicated. The phase change rate, limiting current density, and stack mass were not reported in the original article and were adjusted by parameter estimation.

Experimental tests of the conventional fuel cell stack developed at the Fraunhofer Institute for Solar Energy Systems (ISE) are reported in the article by Philipps and Ziegler [25]. These experiments are executed with ascending steps of 1A, 3A and 6A at 3 minutes each, followed by 6 minute descending steps to 3A and 1A. The mathematical model developed in this work is compared to these results.

The fuel cell stack model developed by Philipps and Ziegler [25] takes a semi-empirical approach to the electrochemical model. Their model does not include concentration losses or activation losses from the anode. Additionally, a constant change in entropy, which does not depend on the temperature of the cell, is applied for the temperature correction factor to the Nernst equation.

The fuel cell stack model developed in this work can be fitted to the experimental data reported by Philipps and Ziegler [25] by fitting the limiting current density and the component resistance. Figure 2.7 shows the agreement

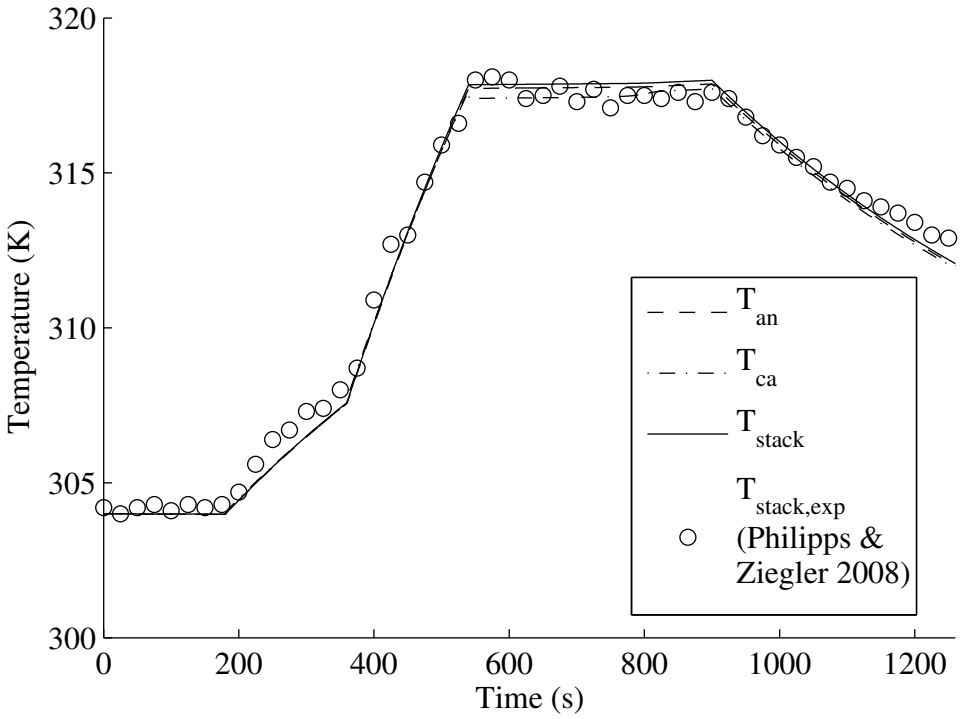

Figure 2.8 – Validation of Energy Model

between the experimental data and mathematical model simulation. In this case, it is fitted to $1A/cm^2$, which is often cited in literature as the limiting current density for a fuel cell [2]. The majority of the ohmic losses are due to the resistance of the cell. The cell resistance is predicted by scaling a measured cell resistance reported by O'Hayre et al. [42] of 0.012Ω for a $9cm^2$ cell to 0.04Ω for the $30.2cm^2$ ISE cell.

Figure 2.8 shows the temperature of the stack measured experimentally by Philipps and Ziegler [25], in comparison with the simulation results of the fuel cell stack model developed in this work. The fitted mathematical model approximates the experimental results well, and the model accurately predicts the changes in the stack temperature during current steps. The convective heat transfer coefficient and area for the anode, hA_{an}, cathode, hA_{ca}, and stack, hA_{amb}, were fitted as reported by Philipps and Ziegler [25], as was the mass of the stack, m_s. The evaporation and condensation phase change rates were fitted to minimize fluctuations in the simulation predictions.

2.6 Parametric Studies

Two sets of parametric studies were performed using the fuel cell stack model. The first studies the effect of varying the estimated parameters for the Horizon H-12 Fuel Cell Stack on the fuel cell stack results. The knowledge obtained from this study is used to fit the estimated parameters to the results from experiments, detailed in Chapter 5.3. The second study examines the sensitivity of the model to the input conditions: ambient temperature, relative humidity and fan flow rate.

2.6.1 Estimated Parameters

The fuel cell stack model developed was used to predict the performance of a Horizon H-12 Fuel Cell Stack. Experimental data was obtained from testing the Horizon H-12 Fuel Cell Stack and the model parameters were fitted, as detailed in Chapter 5. The parameters were fitted based on theoretically calculated and measured values for similar stacks from literature. The parameters were manipulated within the order of magnitude of the initial estimate to obtain the best visual fit. Several parametric studies of the fuel cell stack model were undertaken prior to fitting to the experimental data to determine effect of varying the parameters which will be empirically fitted in Chapter 5.

Table 2.4 – Horizon H-12 Fuel Cell Stack Model Parameters

Parameter	*Value*	*Reference*
Physical		
Number of Cells	13	[70]
Cell Active Area (cm^2)	13.1	[70]
Length of Anode Channel (m)	0.05	measured
Length of Cathode Channel (m)	0.02	measured
Width of Anode Channel (m)	8×10^{-4}	measured
Width of Cathode Channel (m)	1.2×10^{-3}	measured
Height of Anode Channel (m)	1×10^{-4}	measured
Height of Cathode Channel (m)	1.6×10^{-3}	measured
Membrane Thickness (μm)	50	estimated
Membrane Equivalent Weight (g/equi)	1100	[47, 65]
Anode Channel Volume (m^3)	1.28×10^{-6}	calculated
Cathode Channel Volume (m^3)	1.92×10^{-6}	calculated
Number of Anode Channels	5	measured
Number of Cathode Channels	34	measured
Empirical		
Membrane Diffusivity Coefficient (m^2/s)	5.5×10^{-11}	[25]
Membrane Effective Permeability (m^2)	1.58×10^{-18}	[25, 47]
Environmental		
Environment Pressure (kPa)	101	
Enivronment Temperature (K)	298	
Electrochemical		
Anode Reference Current Density (A)	1	[69]
Cathode Reference Area ($cm^2 Pt/cm^C L$)	200	[2]
Cathodic Coefficient	1	[33]

Table 2.5 – Test Conditions

Parameter	*Value*
Operating Conditions	
Anode Channel Pressure (kPa)	101 (Approx. room conditions)
Cathode Channel Pressure (kPa)	101 (Approx. room conditions)
Anode Channel Inlet Flow Rate	$\lambda_{AN} = 2$, minimum 0.1L/min
Cathode Channel Inlet Flow Rate (kg/s)	2.2×10^{-6}
Anode Channel Inlet RH (%)	0
Cathode Channel Inlet RH (%)	20 (Approx. room conditions)
Anode Channel Inlet Temperature (K)	303
Cathode Channel Inlet Temperature (K)	295 (Approx. room conditions)
Current (A)	Steps of 0.4A from 0A to 2A to 0A

Table 2.6 – Empirically Estimated Paramters

Parameter	*Nomenclature*	*Estimated Value*
Ambient Heat Transfer Coefficient and Area	$h_{amb}A_{s,st} = hA_{amb}$	0.002 W/K
Cathode Heat Transfer Coefficient and Area	$h_{ca}A_{s,ca} = hA_{ca}$	0.003 W/K
Anode Heat Transfer Coefficient and Area	$h_{an}A_{s,an} = hA_{an}$	0.2 W/K
Mass and Specific Heat Capacity of Stack	$m_s c_{p,s}$	90 J/K
Limiting Current Density	i_L	0.16 A/cm^2
Cell Component Resistance	R_{comps}	0.02 Ω
Evaporation Rate Coefficient	k_v	$10\left(\frac{cm^2 LV}{(cm^2 ch)kPa*s}\right)$
Condensation Rate Coefficient	k_c	$10\left(\frac{cm^2 LV}{(cm^2 ch)s}\right)$

The physical, environmental and electrochemical parameters of the Horizon H-12 Fuel Cell Stack are listed in Table 2.4, and the test operating conditions are listed in Table 2.5.

The parameters to be fitted based on the experimental data from the Horizon H-12 Fuel Cell Stack are listed in Table 2.6

For this parametric study, the current is increased in steps of 0.4A, each lasting 5 minutes, from 0A to 2A, and then decreased in 8 minute steps of

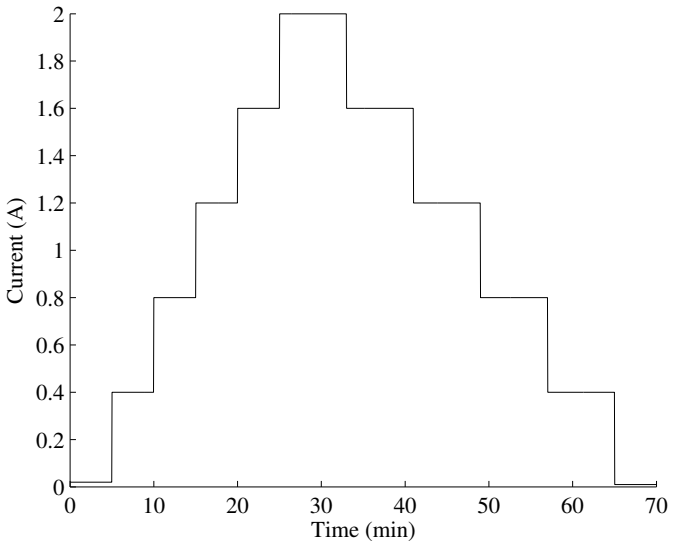

Figure 2.9 – Current Steps for Parametric Study

0.4A from 2A to 0A, as shown in Figure 2.9

Cathode Heat Transfer Coefficient, hA_{ca}

The heat transfer from the stack to the surroundings is governed by the convective heat transfer coefficient between the stack and the air. The area where this occurs is difficult to measure because there is a case around the stack. Additionally, the heat transfer area for the anode and cathode channels is difficult to measure. Therefore, a lumped convective heat transfer coefficient and area will be determined empirically for the stack, hA_{amb}, anode channel, hA_{an}, and cathode channel, hA_{ca}.

Figure 2.10 shows the effect of changing the cathode heat transfer coefficient. The cathode heat transfer coefficient and area, hA_{ca} was set to 0.001W/K, 0.003W/K and 0.005W/K to show the sensitivity of the temperature of the stack and stack gases, where 0.003W/K is the fitted heat transfer

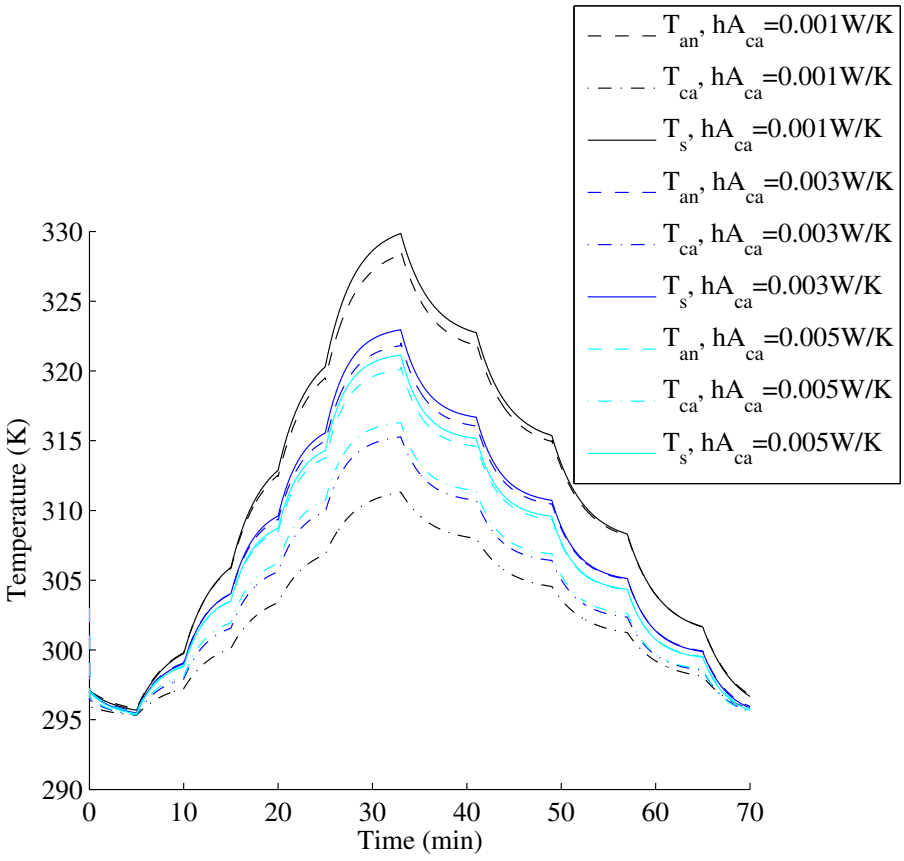

Figure 2.10 – Effect of Varying Cathode Heat Transfer Coefficient on Temperature

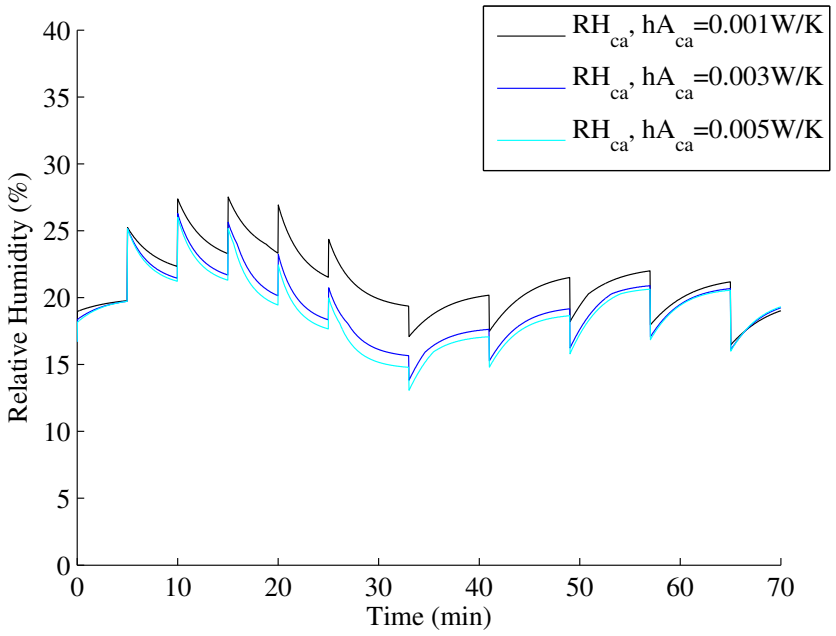

Figure 2.11 – Effect of Varying Cathode Heat Transfer Coefficient on Cathode Relative Humidity

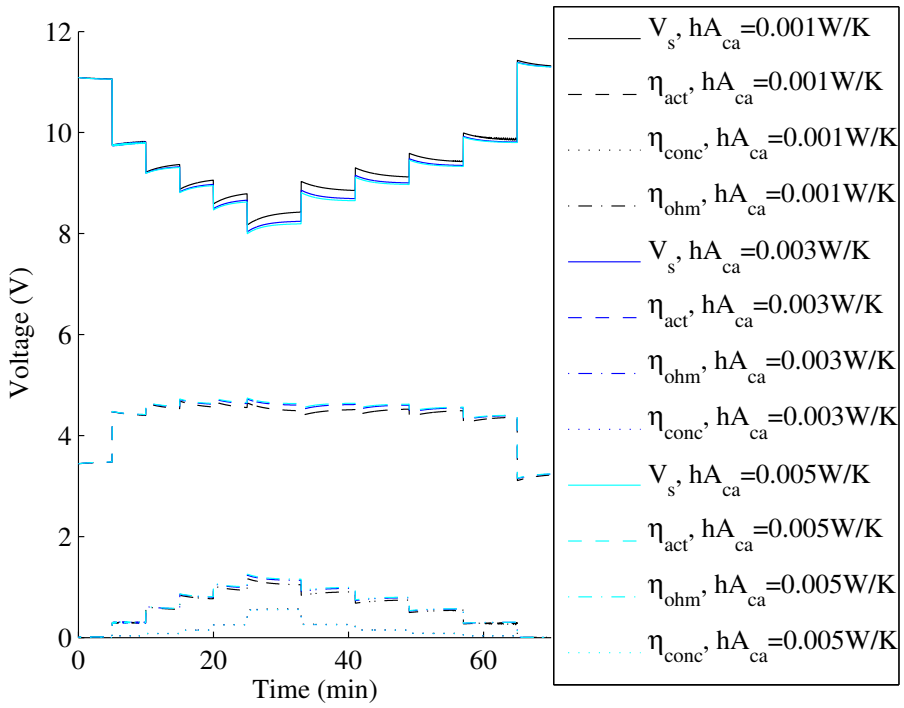

Figure 2.12 – Effect of Varying Cathode Heat Transfer Coefficient on Stack Performance

coefficient reported in Chapter 5. This parameter was estimated using theoretical calculations to be 0.006W/K [71], and was fitted to the experimental data as 0.003W/K.

When the cathode heat transfer coefficient is increased, the temperature of the cathode increases, and the temperature of the stack decreases because the amount of heat transferred to the cathode from the MEA/stack increases. There is a negligible effect to the relationship between the anode temperature and the stack temperature. A comparison of the change in temperature from $hA_{ca} = 0.005W/K$ to $hA_{ca} = 0.003W/K$, and $hA_{ca} = 0.003W/K$ to $hA_{ca} = 0.001W/K$ shows that as hA_{ca} increases, the sensitivity of the change in the stack temperature to a change in the parameter hA_{ca} decreases. A decrease in hA_{ca} also increases the time to reach equilibrium.

Figure 2.11 shows the effect of a change in the cathode heat transfer coefficient on the relative humidity at the outlet of the cathode. The relative humidity is affected by the change in temperature in the cathode, shown in Figure 2.10. As the temperature increases, the relative humidity decreases.

Figure 2.12 shows the effect of the change in the cathode heat transfer coefficient on the stack voltage. The increase in stack temperature leads to a decrease in the activation losses and a decrease in the ohmic losses, thus higher stack performance.

Anode Heat Transfer Coefficient, hA_{an}

Figure 2.13 shows the effect of changing the anode heat transfer coefficient. For this parametric study, the anode heat transfer coefficient and area, hA_{an}, was set to 0.0002W/K, 0.002W/K and 0.02W/K, which show the effect of varying the parameter, where 0.002W/K is the fitted heat transfer coefficient reported in Chapter 5 using the same method as for hA_{ca}.

Note that this range of values is larger than for the cathode because the stack temperature is less sensitive to changes to the value of hA_{an} A decrease in the anode heat transfer coefficient causes a decrease in the anode temperature because the heat transfer between the MEA/stack and the anode decreases. The cathode and stack experience minimal temperature change. As the anode heat transfer coefficient increases, the sensitivity of the stack temperature to a change in the parameter hA_{an} decreases as the anode gases reach the same temperature as the stack.

The anode heat transfer coefficient and area, hA_{an}, has a smaller value and is less sensitive than the cathode heat transfer coefficient and area, hA_{ca}.

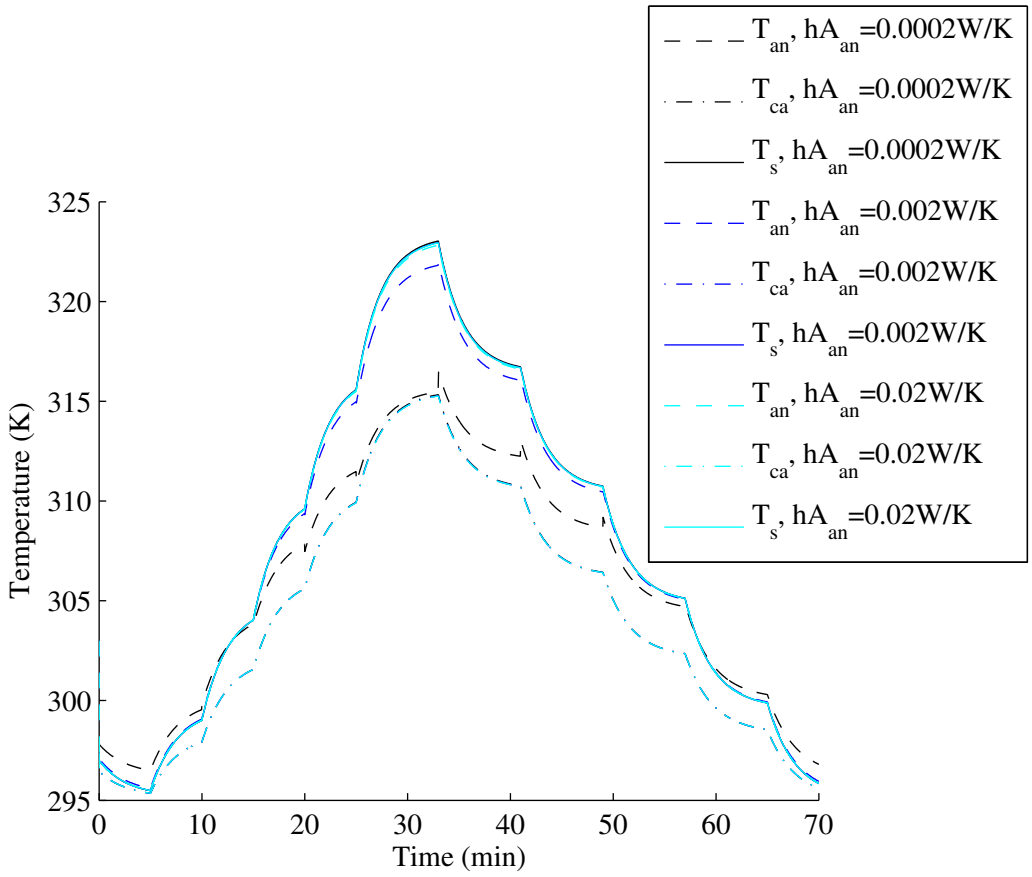

Figure 2.13 – Effect of Varying Anode Heat Transfer Coefficient on Temperature

This occurs for two reasons, one related to the heat transfer coefficient and one related to the area. The anode channel flow is significantly slower than the flow in the cathode channel, which leads to a lower heat transfer coefficient for the anode channel. Since the area does not change, it stands to reason that the combined term for the anode channel will be less sensitive because a change in the term is a function of only the heat transfer coefficient, which is less sensitive in the anode channel. As for the area, the total cell area is divided over 5 anode channel and 34 cathode channels. So for one channel, the area in the anode channel is significantly larger than for one cathode channel. Therefore, it is reasonable that the combined heat transfer coefficient and area for the anode and cathode channels are of the same order.

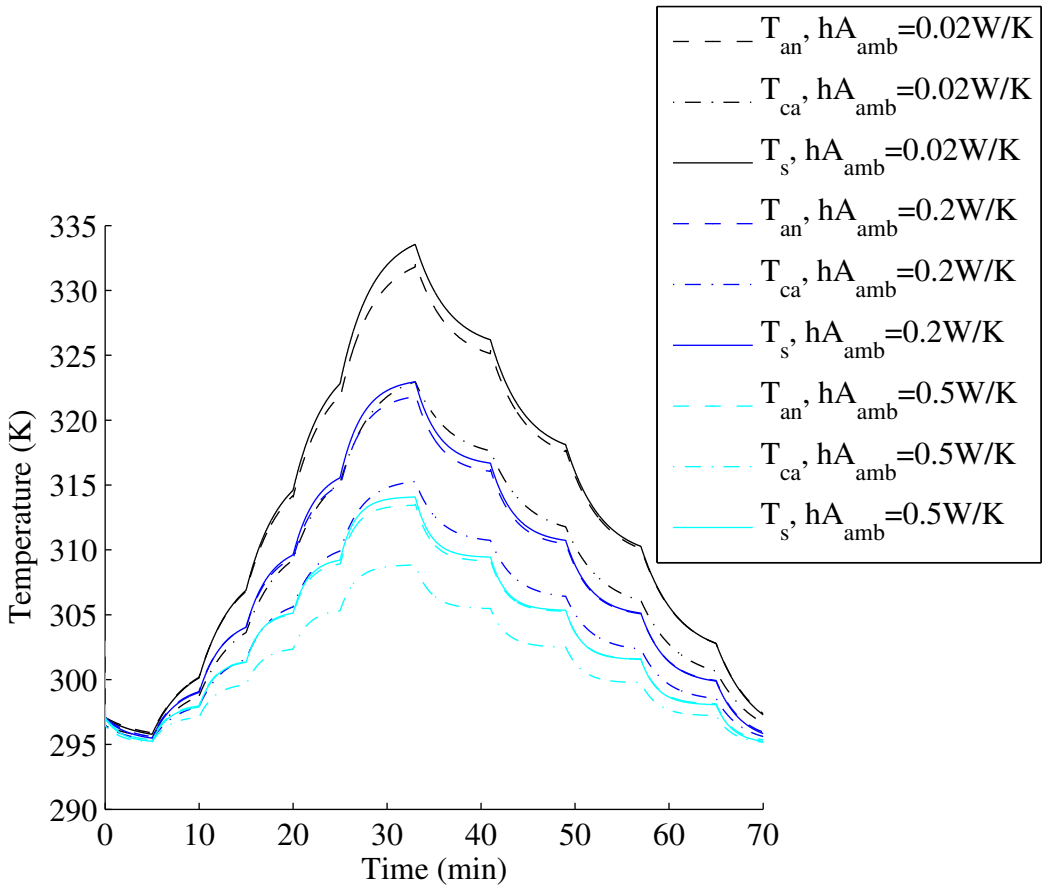

Figure 2.14 – Effect of Varying Ambient Heat Transfer Coefficient on Temperature

Ambient Heat Transfer Coefficient, hA_{amb}

The effect of varying the ambient heat transfer coefficient on the performance of the fuel cell stack is shown in Figure 2.14. The ambient heat transfer coefficient and area, hA_{amb} was set to 0.02W/K, 0.2W/K and 0.5W/K as these values show the sensitivity of the temperature output from the simulations. Chapter 5 reports that 0.2W/K is the fitted heat transfer coefficient. As the ambient convective heat transfer coefficient increases, the temperature of the stack decreases. The difference between the stack and anode temperatures is maintained, but cathode temperature is less sensitive to changes in hA_{amb}. As hA_{amb} decreases, the sensitivity of the system decreases, as shown when comparing the effect of the tenfold change in hA_{amb} from 0.2W/K to 0.02W/K in comparison with the change in hA_{amb} from 0.5W/K to 0.2W/K.

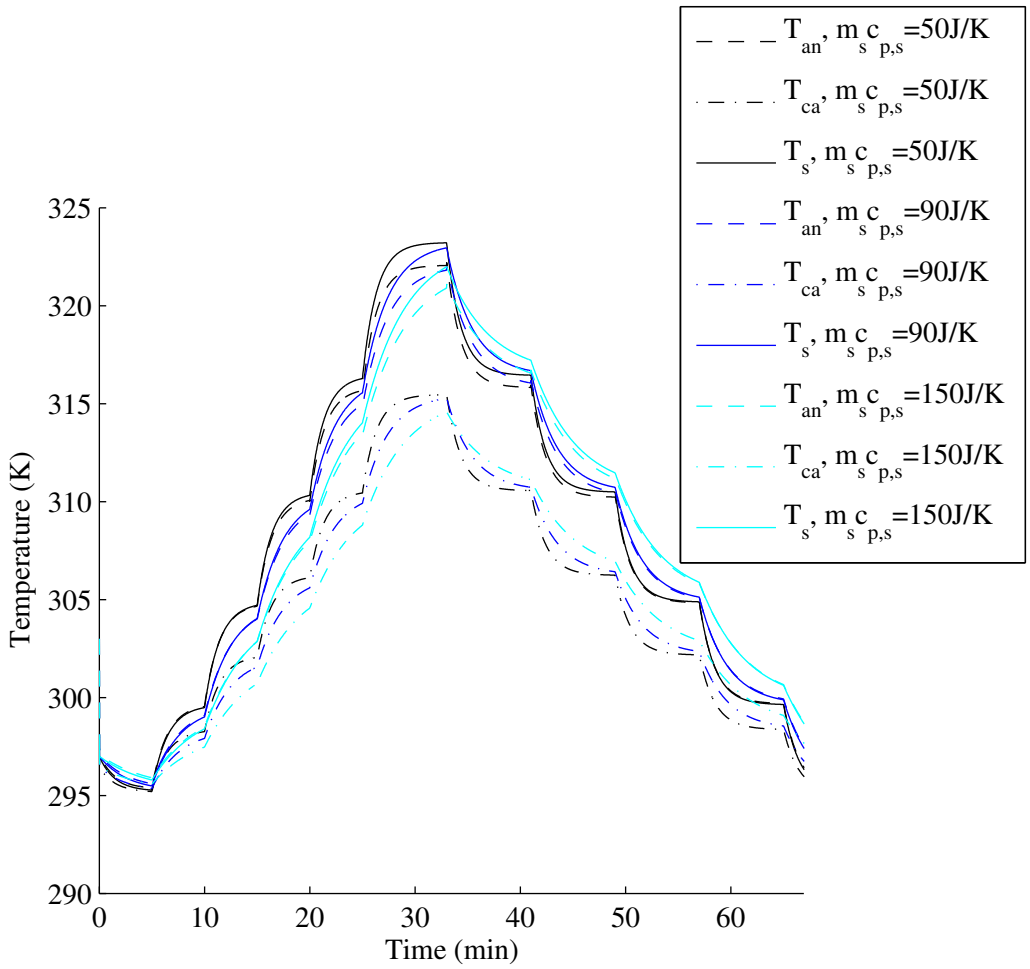

Figure 2.15 – Effect of Varying Stack Mass and Specific Heat Capacity Coefficient on Temperature

Stack Mass and Specific Heat Capacity, $m_s c_{p,s}$

The stack mass and specific heat capacity are combined into one term as both will be fitted. The mass of the stack can be estimated by assuming it is entirely composed of graphite and then the specific heat capacity of graphite is applied. Assuming graphite at a density of $2.5 g/cm^3$ and specific heat capacity of $0.711 J/(g \cdot K)$ [72], for the stack volume of $5cm \times 2cm \times 6.5cm$, this gives a mass and specific heat capacity term of 115J/K. However, the stack is not entirely composed of graphite, and there is some variability in data reported for graphite density and specific heat capacity, therefore this term is fitted. The fitted mass and specific heat capacity is shown in Chapter 5 to be 90J/K, thus 50J/K and 150J/K are selected for the parametric study to show the sensitivity of the parameter. Figure 2.15 shows the effect of changing the

stack mass and specific heat capacity. Increasing this parameter causes an increase in the time to reach equilibrium. The observed trends suggest that the same equilibrium point will be reached for all cases.

Limiting Current Density, i_L

The limiting current density depends on the properties of the stack and its ability to reach a high current density. The parameters selected for this study are $0.16A/cm^2$, $0.5A/cm^2$, and $1A/cm^2$. The typically reported limiting current density for a cell is $1A/cm^2$ [2], and Chapter 5 reports that the fitted limiting current density for this stack is $0.16A/cm^2$. Experiments showed a maximum operating stack current of 2A for the $13.1cm^2$ active area, so $0.16A/cm^2$ is

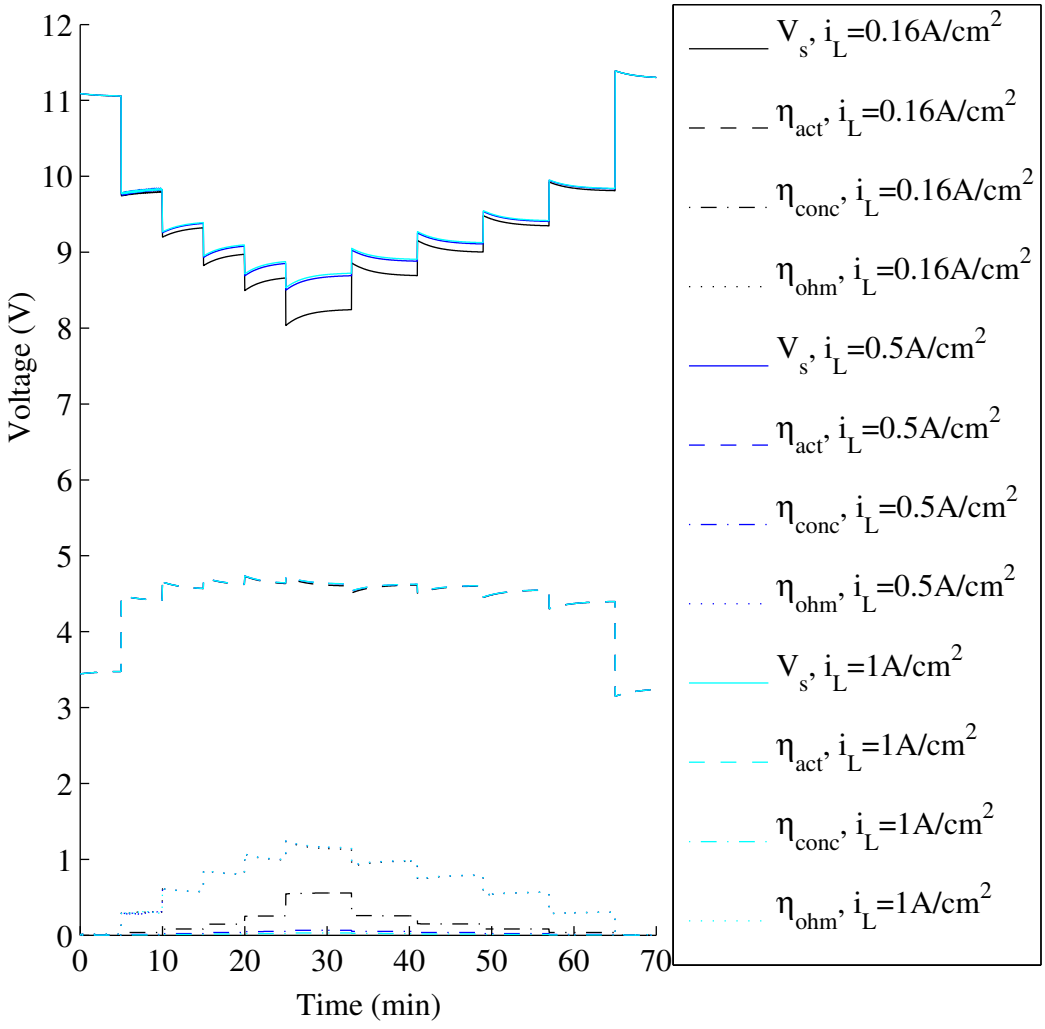

Figure 2.16 – Effect of Varying Limiting Current Density on Stack Performance

just slightly greater than $2A/13.1cm^2$. Therefore, $0.5A/cm^2$ was selected to show the sensitivity of the parameter. Figure 2.16 shows that an increase in the limiting current density leads to a decrease in the concentration losses. As the limiting current density approaches the current density of the test, there is a significant increase in the concentration losses. When the current density that can be achieved increases, the concentration losses at a given current will decrease as the stack is operating further away from its maximum current condition.

Stack Component Resistance, R_{comps}

The electrical resistivity of all the stack components, excluding the membranes, will influence the ohmic losses of the stack performance. The values selected for this parametric study are $R_{comps} = 0.002\Omega$, $R_{comps} = 0.02\Omega$, and $R_{comps} = 0.2\Omega$, which show the sensitivity of the stack resistance, and $R_{comps} = 0.02\Omega$ is

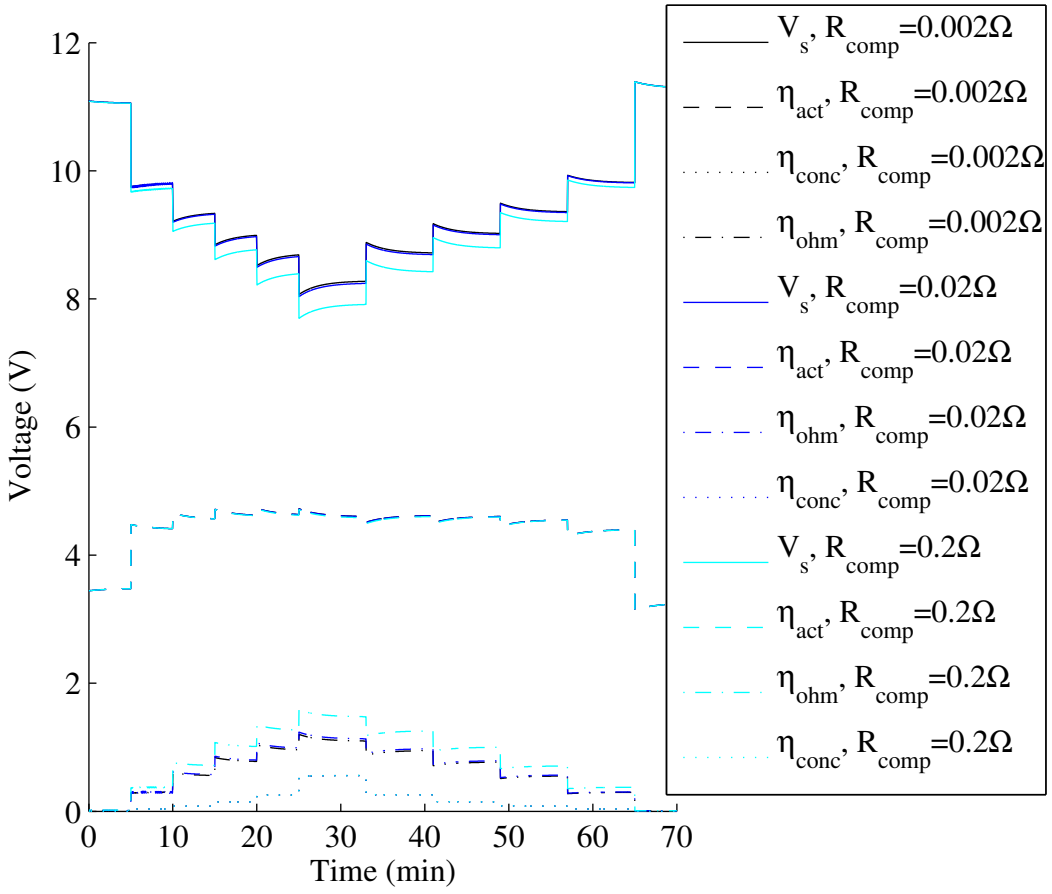

Figure 2.17 – Effect of Varying Stack Component Resistance on Stack Performance

the fitted stack resistance reported in Chapter 5. The fitted term is calculated as a function of the cell resistance measured by O'Hayre et al. [42] for their cell, which was 0.012Ω for a $9cm^2$ active area, whereas the cells in this stack have an active area of $13.1cm^2$. Therefore, the scaled initial guess for the component resistance was 0.017Ω and this was fitted to the experimental data in Chapter 5 to be 0.02Ω.

Figure 2.17 illustrates that when the component resistance increases, the ohmic losses increase. The ohmic losses consist of both the stack resistance and membrane resistance, therefore as the stack membrane resistance decreases, the ohmic losses will be dominated by the membrane resistance. For low stack resistance, $R_{comps} = 0.002\Omega$, the ohmic losses are dominated by membrane resistance, and for high stack resistance, $R_{comps} = 0.2\Omega$, the ohmic losses are dominated by the stack resistance.

Summary

In summary, when fitting the estimated parameters the effects on the outputs shown in Table 2.7 are observed. The estimated parameters that are examined are: the ambient heat transfer coefficient and area, hA_{amb}; cathode channel heat transfer coefficient and area, hA_{ca}; anode channel heat transfer coefficient and area, hA_{an}; mass and specific heat capacity of the stack, $m_s c_{p,s}$; limiting current density, i_L; and component resistance, R_{comps}. The effects shown in Table 2.7 are a summary of the effects shown in Figures 2.10 - 2.17.

The output parameters that are examined are: the stack temperature, T_s; the anode outlet temperature, T_{an}; the cathode outlet temperature, T_{ca}; the cathode outlet relative humidity, RH_{ca}; the time for the response to reach steady state, τ; and the stack voltage, V_s.

To increase the stack temperature, the cathode heat transfer coefficient and area can be decreased, and/or the ambient heat transfer coefficient and area can be decreased. To increase the cathode temperature, the cathode heat transfer coefficient and area can be decreased, and/or ambient heat transfer coefficient can be decreased. To increase the anode temperature with minimal effect on the stack temperature, the anode heat transfer coefficient should be decreased. Otherwise, the anode temperature will increase when the stack temperature increases. To increase the time until the stack reaches steady state, the stack mass and heat transfer coefficient should be increased. Finally, the limiting current density and component resistance will affect the stack voltage. An increase in the limiting current density leads to a decrease in

Table 2.7 – Effect of Varying Parameters on Energy Balance

Variable Parameter	T_s	T_{an}	T_{ca}	RH_{ca}	τ	V_s
Ambient Heat Transfer						
Coefficient and Area, $hA_{amb} \uparrow$	$\downarrow\downarrow$	$\downarrow\downarrow$	$\downarrow$	$\uparrow$	$\downarrow$	$\downarrow$
Cathode Heat Transfer						
Coefficient and Area, $hA_{ca} \uparrow$	$\downarrow$	$\downarrow$	$\uparrow$	$\downarrow$	$\downarrow$	$\downarrow$
Anode Heat Transfer						
Coefficient and Area, $hA_{an} \uparrow$	$\times$	$\uparrow$	$\times$	$\times$	$\uparrow$	$\times$
Mass and Specific Heat						
Capacity of Stack, $m_s c_{p,s} \uparrow$	$\downarrow^\star$	$\downarrow^\star$	$\downarrow^\star$	$\downarrow^\star$	$\uparrow$	$\downarrow^\star$
Limiting Current Density, $i_L \uparrow$	$\downarrow$	$\downarrow$	$\downarrow$	$\uparrow$	$\times$	$\uparrow$
Cell Component Resistance, $R_{comps} \uparrow$	$\uparrow$	$\uparrow$	$\uparrow$	$\downarrow$	$\times$	$\downarrow$

$\times$ no change

$\star$ steady state temperature reached is the same for all cases but as the time constant increases, it takes longer to reach steady state, so in the transient region, there is a decrease in the temperature relative to a case with a shorter time to steady state

the concentration losses, thus the stack votlage increases. An increase in the component resistance leads to an increase in the ohmic losses, thus the stack voltage decreases.

2.6.2 Model Sensitivity to Input Conditions

The fuel cell stack model is used to study the performance of the stack with varying input conditions, specifically: ambient temperature, ambient relative humidity and inlet fan speed. The purpose of this sensitivity study is to examine the effect of changing ambient and inlet conditions on the performance of the stack. The results of this sensitivity study can be used to determine the optimal operating conditions for the stack.

The following studies report the steady state conditions of the stack after 20 minutes of operation at the given set of operating conditions.

Ambient Temperature

The effect of changing the ambient temperature surrounding the stack is studied to examine whether the stack is adequately cooled. Simulations at 5 applied currents: 0.4A, 0.8A, 1.2A, 1.6A, and 2A are computed for 5 ambient temperatures: -10℃, 0℃, 10℃, 20℃, and 30℃. The dots reported indicate the conditions achieved at approximately steady state, after 20 minutes of operation at the given conditions.

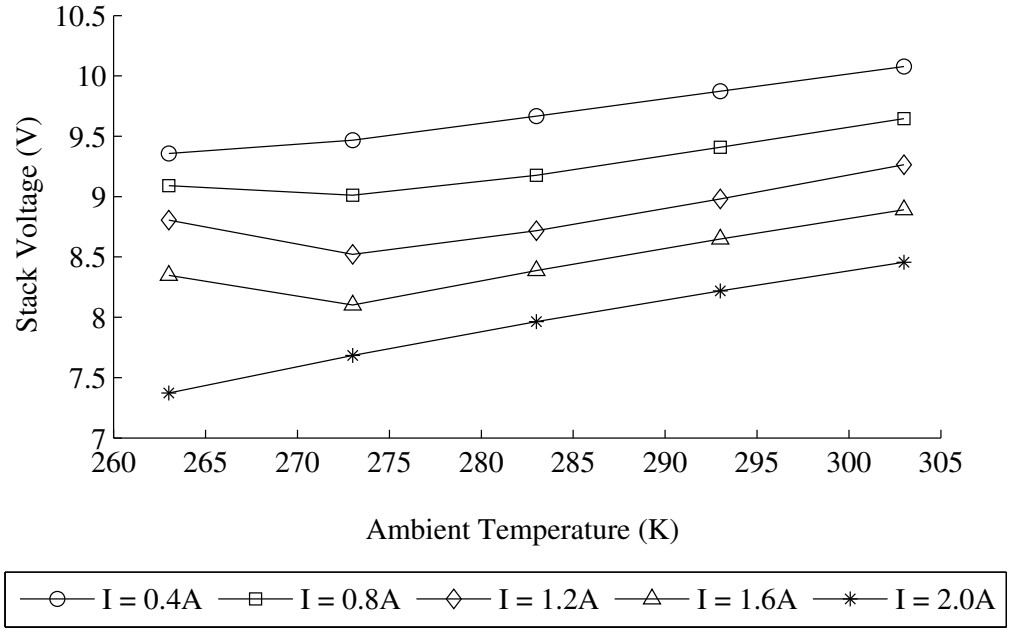

Figure 2.18 – Effect of Ambient Temperature on Stack Performance

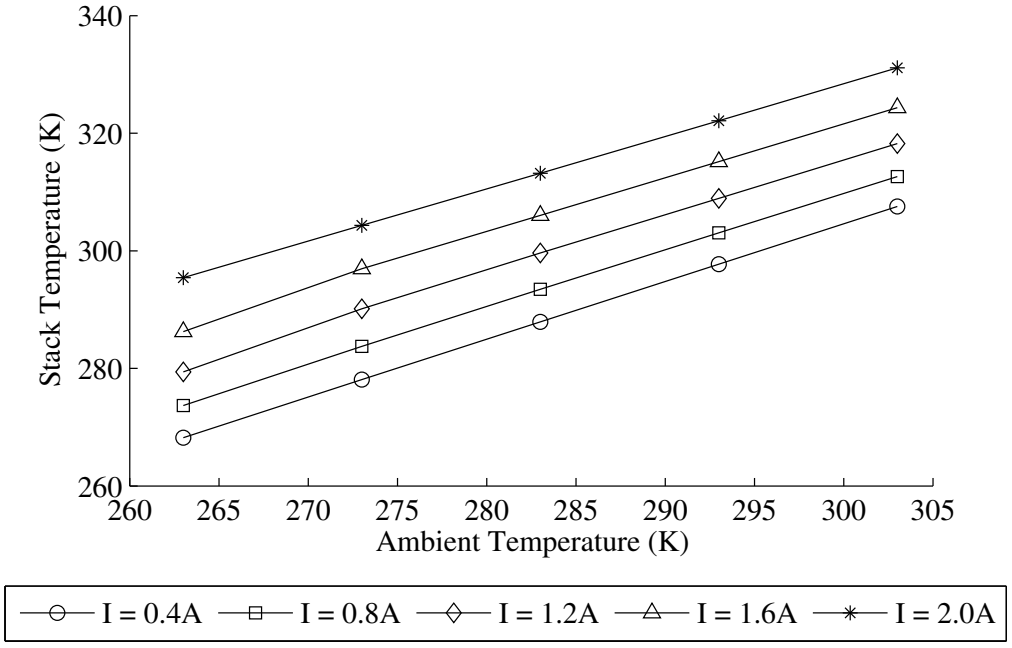

Figure 2.19 – Effect of Ambient Temperature on Stack Temperature

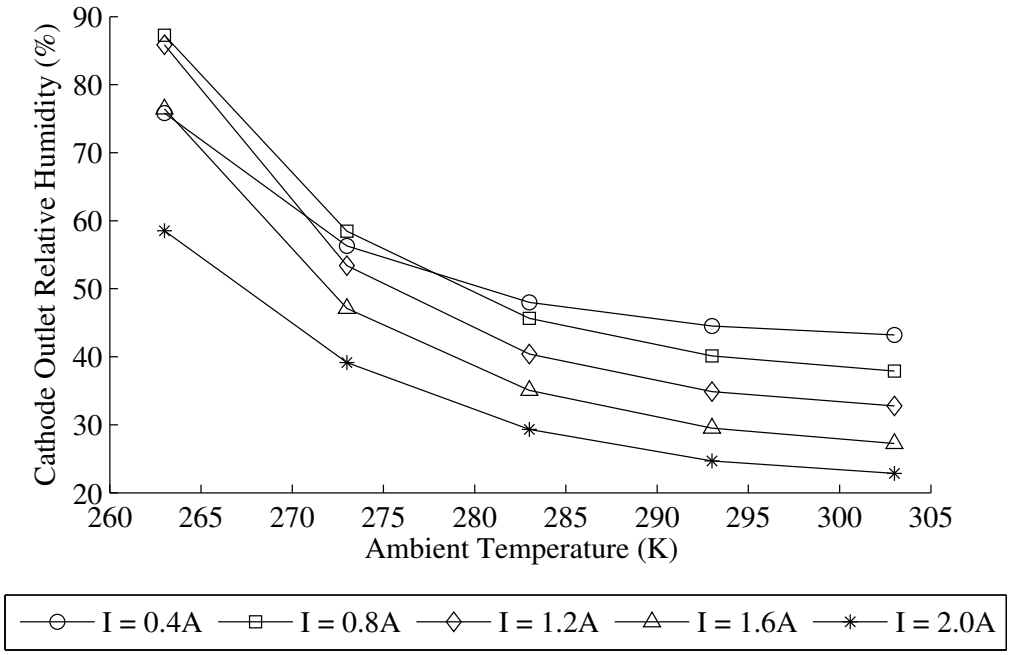

Figure 2.20 – Effect of Ambient Temperature on Cathode Outlet Relative Humidity

Figure 2.18 shows the performance of the fuel cell stack at varying temperatures for the 5 applied currents. Figure 2.19 shows the temperature of the stack and Figure 2.20 shows the relative humidity of the cathode outlet.

For a constant ambient temperature, the stack voltage, shown in Figure 2.18 decreases as the imposed current increases. This is expected because the increase in imposed current leads to a drop in the stack voltage. Figure 2.19 shows that the increase in imposed current at a constant ambient temperature leads to an increase in the stack temperature. To produce a higher current, the reaction also releases more energy than for a lower current, which causes the stack temperature to rise.

In Figure 2.20, for a constant temperature, the cathode outlet relative humidity will generally be lower for a higher imposed current. This occurs because the cathode outlet relative humidity is a function of the stack temperature. An increase in applied current leads to a higher stack temperature, and a lower cathode outlet relative humidity. An exception to this is noted at low temperature (0℃ and below). The cathode outlet relative humidity is also a function of the amount of water produced by the reaction. Comparing the cases at 0.4A and 0.8A at 0℃ and below, it is observed that the case at 0.4A has a lower cathode outlet relative humidity than the case at 0.8A,

despite having a lower temperature, as shown in Figure 2.19. This occurs because there is less water produced by the reaction at 0.4A, so despite the lower temperature, the quantity of water is also reduced and therefore the cathode outlet relative humidity is lower.

For a given current, the performance of the stack, shown in Figure 2.18 increases as the ambient temperature increases. This occurs because as the ambient temperature increases, the stack temperature also increases, shown in Figure 2.19, and the increase in stack temperature leads to a decrease in the activation overpotential.

For the lowest temperature case at -10℃, it is observed that the performance of the stack is better for the 0.8A, 1.2A, and 1.6A cases than at 0℃. This occurs because the relative humidity is high, so the membrane is well humidified and the stack gives better performance than at a lower humidity condition. The low current case at 0.4A does not have better performance at the low temperature because the low stack temperature causes high activation overpotential. The high current case at 2A does not show this effect either because the relative humidity is too low, as shown in Figure 2.22.

Ambient Relative Humidity

The effect of changing the ambient relative humidity of the air surrounding the stack, which enters the cathode channels, is examined to determine if the stack membranes are adequately humidified. Simulations are applied at 5 currents: 0.4A, 0.8A, 1.2A, 1.6A and 2A, and at 5 different ambient relative humidity conditions: 10%, 30%, 50%, 70% and 90%. Each simulation reports the performance of the stack at the steady state achieved after 20 minutes.

Figure 2.21 shows the performance of the fuel cell stack with varying ambient relative humidity for the 5 applied currents. Figures 2.22 and 2.23 show the stack temperature and relative humidity of the cathode outlet respectively.

Figure 2.20 shows that an increase in the ambient relative humidity has a negligible effect on the stack temperature. This is expected because unless condensation or evaporation occurs, the quantity of water vapour in the gas causes little energy change in the stack. It is observed that the increase in imposed current leads to an increase in the stack temperature.

The cathode outlet relative humidity increases as the ambient relative humidity increase, as shown in Figure 2.23. The slope for this increase changes for different applied currents because the stack temperature, and thus the cathode temperature, increases with increasing current. Therefore, for the same

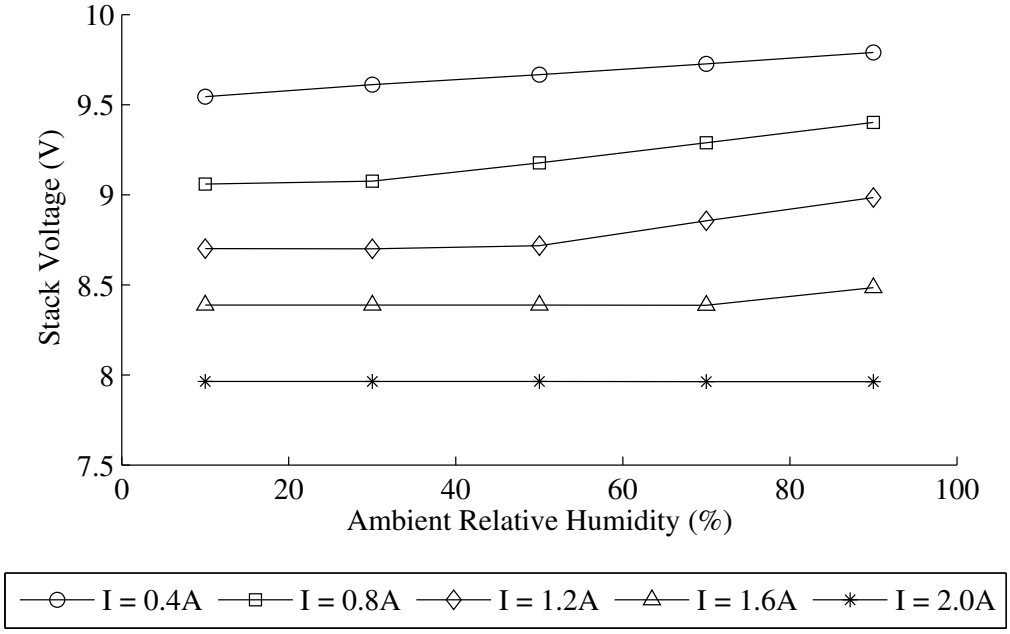

Figure 2.21 – Effect of Ambient Relative Humidity on Stack Performance

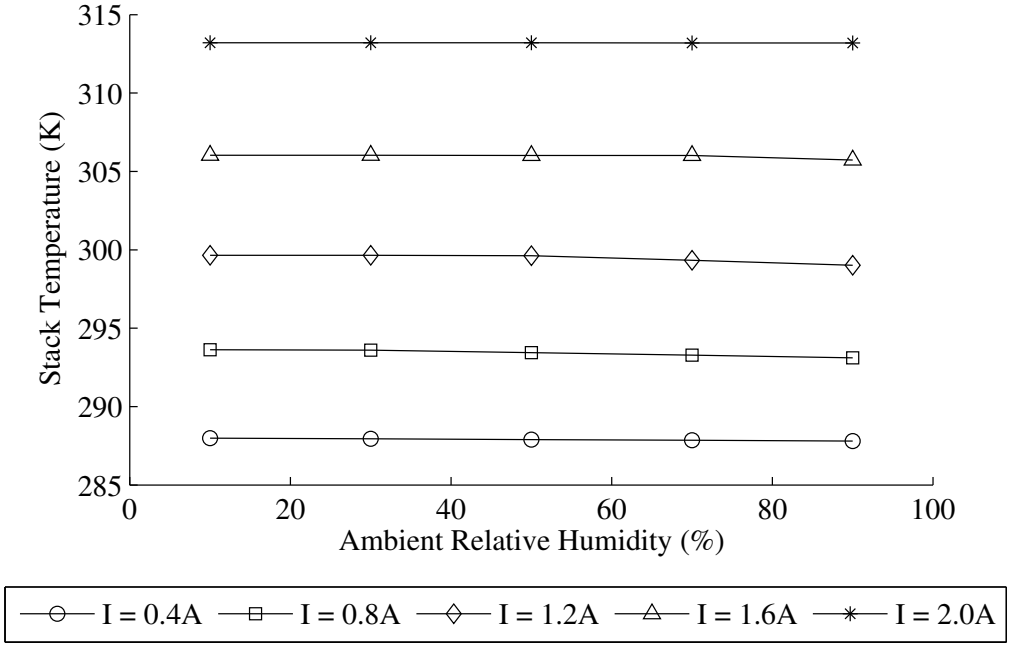

Figure 2.22 – Effect of Ambient Relative Humidity on Stack Temperature

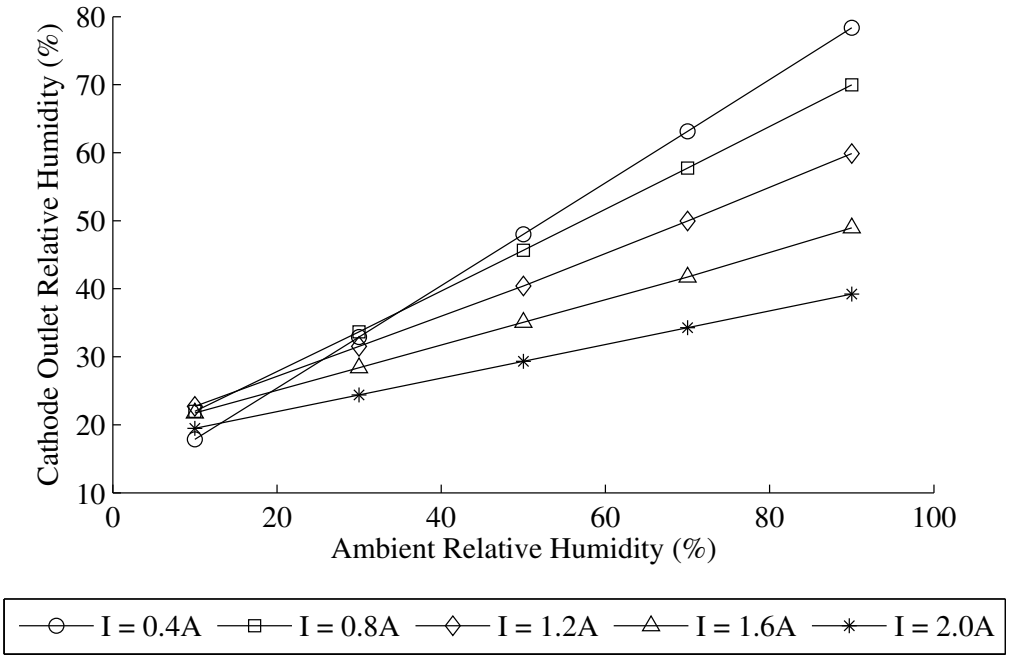

Figure 2.23 – Effect of Ambient Relative Humidity on Cathode Outlet Relative Humidity

ambient relative humidity, at higher current and thus stack temperature, the cathode outlet relative humidity is lower.

For high current (2A), an increase in the ambient relative humidity has no effect on the performance of the stack, as shown in Figure 2.21. For lower currents, however, there appears to be a point at which the ambient relative humidity does affect the stack performance. This point occurs when the increase in ambient relative humidity overcomes the effect of the stack temperature.

Cathode Inlet Fan Speed

The cathode inlet fan delivers air to the cathode channels, which provides oxygen for the reaction, and water vapour to humidify the membranes. The effect of changing the fan speed is studied at 5 applied currents: 0.4A, 0.8A, 1.2A, 1.6A and 2A. The fan is set at a constant flow rate based on Equation 2.12, where I_{max} is set to 2A and the stoichiometric ratio is varied to obtain 5 different inlet flow rates set at stoichiometric ratios of 2, 20, 50, 100, and 200, at 2A. The simulation for each case is run for 20 minutes and the steady state condition after this time is reported.

Figure 2.24 shows the performance of the fuel cell stack with varying inlet flow rates for the 5 applied currents. The stack temperature and relative

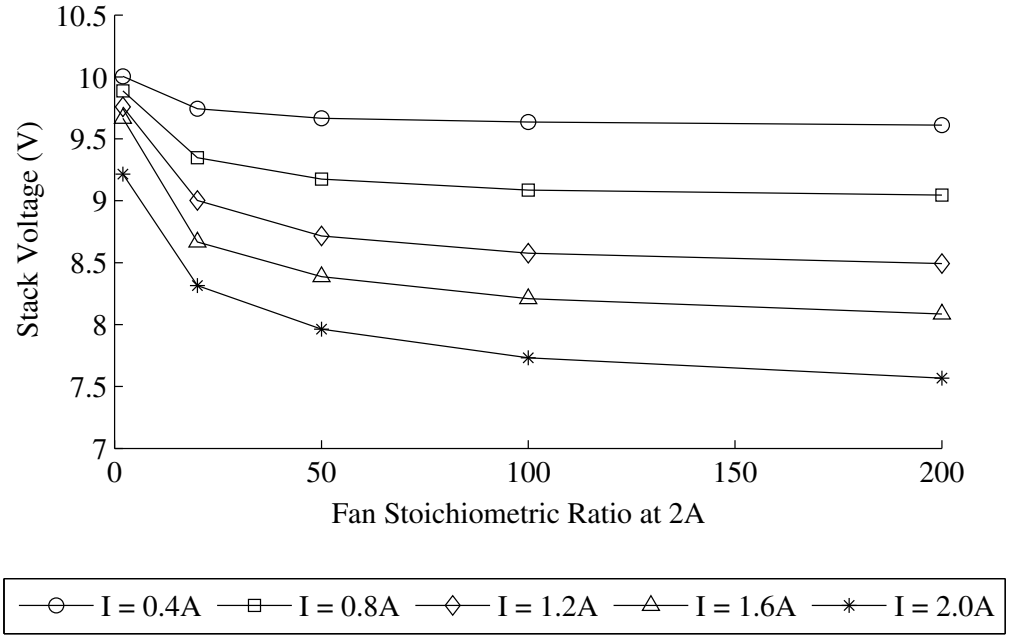

Figure 2.24 – Effect of Inlet Fan Flow Rate on Stack Performance

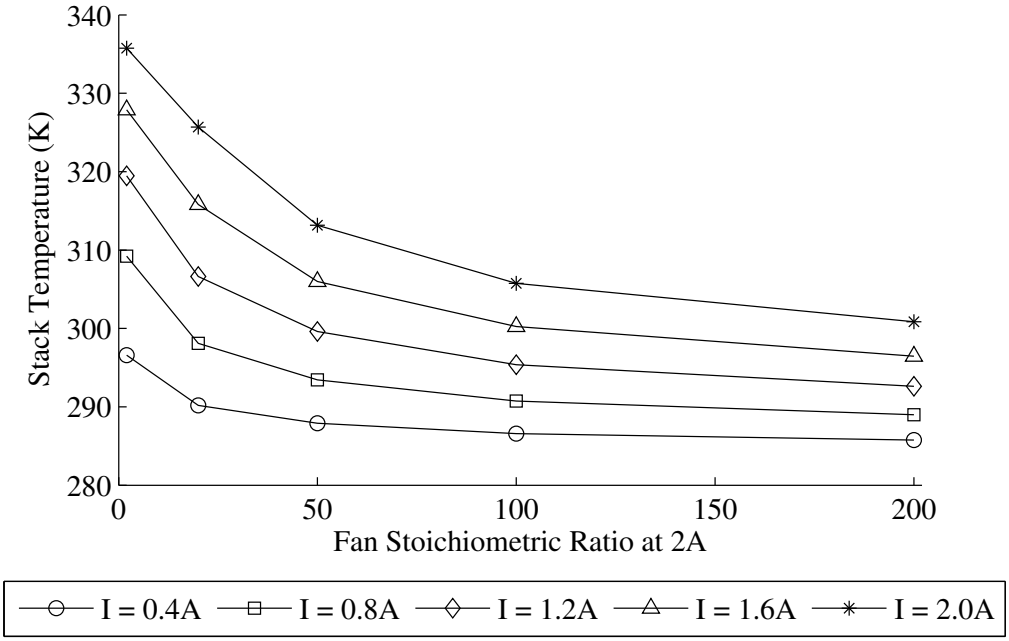

Figure 2.25 – Effect of Inlet Fan Flow Rate on Stack Temperature

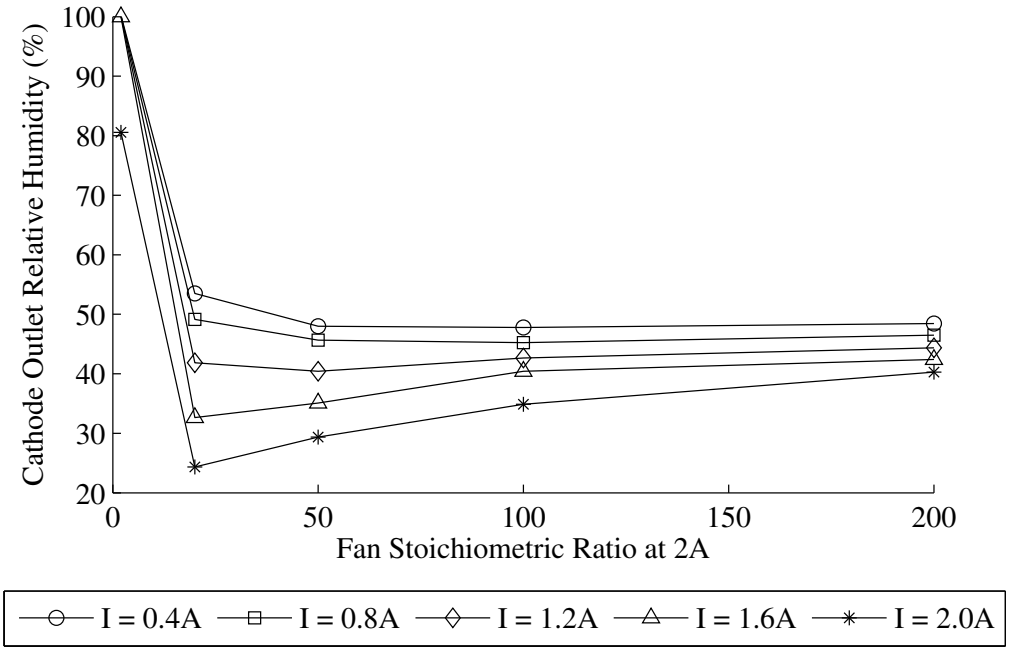

Figure 2.26 – Effect of Inlet Fan Flow Rate on Cathode Outlet Relative Humidity

humidity of the cathode outlet are shown in Figures 2.25 and 2.26 respectively.

The stack temperature, shown in Figure 2.25, decreases for a given imposed current as the fan flow rate increases. This occurs because at higher fan flow rates, the stack cooling rate increases. The air flowing through the cathode channels, driven by the inlet fan, can remove more heat at a higher flow rate.

Figure 2.26 shows that the cathode outlet relative humidity is very high for all the cases at lowest flow rate. This occurs because the inlet air is not fast enough to remove the product water from the reaction, so this water accumulates, despite the higher temperatures. However, by the case at a stoichiometric ratio of 20 at 2A, it is observed that the fan is removing most of the product water and the effect of the temperature dominates the outlet relative humidity. At very high flow rates, the outlet relative humidity approaches the ambient relative humidity.

The performance of the fuel cell stack, shown in Figure 2.24, indicates that at low flow rates, the performance of the stack for a given imposed current is higher than for high flow rates. This occurs because the membranes are well humidified and the stack is still receiving sufficient oxygen at stoichiometric ratio of 2 at 2A. As the stack temperature drops with increasing fan speed, shown in Figure 2.25, the stack voltage also drops because the activation over-

potential increases.

Summary

A summary of the results from the sensitivity studies on the effects of the input conditions on stack performance is detailed in Table 2.8. The variable parameters are: the ambient temperature, T_{amb}; the ambient relative humidity, RH_{amb}; and the cathode inlet fan speed, $\dot{m}_{fan}$. The effect of changing these parameters was detailed in Figures 2.18 - 2.26. The output parameters which were responding to these parameter changes are: the stack temperature, T_s; the cathode outlet relative humidity, RH_{ca}; and the cathode inlet fan speed, $\dot{m}_{fan}$.

Table 2.8 – Effect of Varying Parameters on Energy Balance

Variable Parameter	T_s	RH_{ca}	V_s
Ambient Temperature $T_{amb} \uparrow$	$\uparrow$	$\downarrow$	$\uparrow$
Ambient Relative Humidity $RH_{amb} \uparrow$	$\times$	$\uparrow^{\dagger}$	$\uparrow$
Cathode Inlet Fan Speed $\dot{m}_{fan} \uparrow$	$\downarrow$	$\star$	$\downarrow$

$\times$ no change
† minimal increase, depends on applied current and temperature
$\star$ approaches ambient conditions, depends on applied current and temperature.

Chapter 3

Enclosure Model

An insulated enclosure is proposed to protect the fuel cell stack during operation in cold climates. The purpose of the enclosure is threefold. First, the fuel cell stack must stay within acceptable operating temperatures of 0℃ to 80℃. Second, there must be adequate oxygen available in the enclosure to supply the open-cathode fuel cell stack with sufficient reactant. Finally, the fuel cell stack requires that the membrane remain humidified, therefore the relative humidity of the air in the enclosure must also be monitored and controlled.

To address the first concern that the temperature remains within specific limits, the walls of the enclosure will be insulated to keep the enclosure temperature above 0℃. To keep the enclosure temperature below 80℃, cooling will be provided by fans installed in the enclosure walls. These same fans will be used to control the gas composition within the enclosure. By varying the fan speed, the amount of air entering the enclosure from the external environment can be managed to obtain specific conditions within the enclosure. The outlet of the enclosure is a simple hole that is controlled by back pressure in the enclosure.

Therefore, the enclosure design consists of one or more inlet fans, insulated walls, and an outlet opening, as shown in Figure 3.1. A mathematical model of the enclosure is developed to study its effect on the performance of the fuel cell stack. For simplicity, the enclosure walls are modelled as insulation which traps the heat produced by the fuel cell stack within the enclosure. The insulated enclosure will keep the stack warm and insulate the inside of the enclosure from the cold ambient temperatures. In the mathematical model, the inlet fan can be independently controlled to bring in ambient air when required to control the composition of the gases in the enclosure. The gases in the enclosure are the reactant supply for the fuel cell cathode, and are used

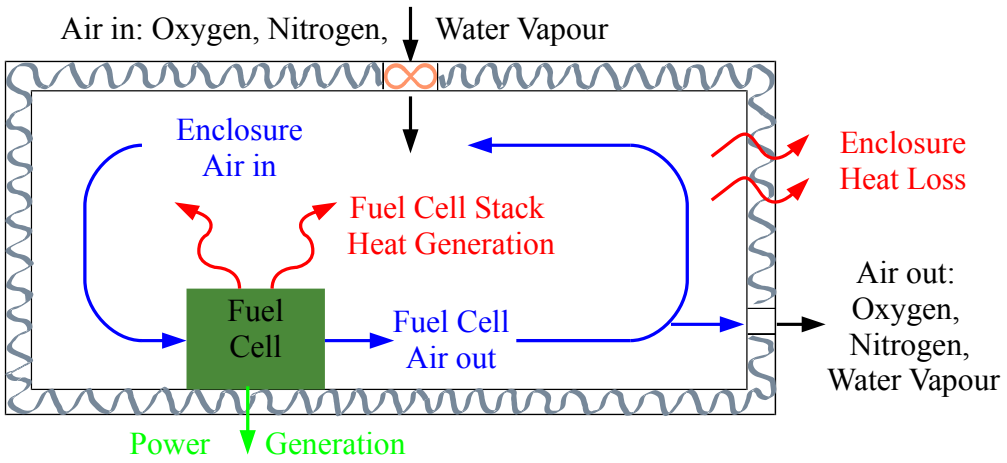

Figure 3.1 – Enclosure Design

for cooling the stack. The outlet opening is modelled as a simple hole in the side of the insulated enclosure for this research, but it could be a controlled exit with a mechanism for opening and closing the outlet to increase control of the conditions inside the enclosure.

This enclosure design is very similar to a fuel cell enclosure system patented by Intelligent Energy Ltd [21]. Their design heats the air that enters the enclosure by two means: recirculation of air leaving the stack and irreversible heat energy produced by the stack. To regulate the enclosure temperature, baffles are used to recirculate with the enclosure or reject to the environment the air leaving the stack [21]. The propsed enclosure design for this research does not include the use of baffles to control the stack outlet air. The stack outlet air is output directly to the stack for recirculation in all cases.

A fuel cell stack is installed in the enclosure where it uses air from the enclosure for its reaction and expels the outlet gas from the fuel cell stack into the enclosure. The air expelled from the fuel cell stack mixes with the air inside the enclosure through recirculation rather than being expelled directly out of the enclosure.

In the following sections, the mathematical model to analyze gas composition and temperature in the enclosure is presented and validated.

3.1 Gas Mass Balance

When the fuel cell stack is installed in the enclosure, it is necessary to study the composition of the gas in the enclosure. The gas in the enclosure supplies oxygen, a reactant, to the cathode. It also supplies water to the membrane to prevent the membrane from drying out. This is of primary importance; if insufficient reactant is available to the cathode, the fuel cell stack will not operate and might degrade. The membrane has 3 ways of obtaining water: cathode inlet, anode inlet and water generated by the reaction. As the anode is often run with dry hydrogen, it is important to provide adequately humidified air to the cathode. If the membrane dries out, its resistivity will be too high for the fuel cell stack to operate. Therefore, the gas composition in the enclosure is studied through a mathematical model.

The presence of an operating fuel cell stack in the enclosure will affect the enclosure conditions. Therefore, the mathematical model of gas composition in the enclosure is developed with the consideration that it will be coupled with the fuel cell stack model.

The mass transport mathematical model predicts the gas composition of the enclosure by first determining the density of the gas in the enclosure. This requires consideration of the composition of all air flow into and out of the enclosure. The mass transport within the enclosure includes two inlets and two outlets, as shown in Figure 3.2. The inlet fan installed in the side of the enclosure wall provides air to the enclosure from the external environment. The first outlet for the enclosure is the fuel cell cathode inlet fan. Air drawn into the fuel cell stack to be reacted at the cathode is considered to have left the enclosure as the gas which leaves the fuel cell stack will not be of the same composition. This gas leaving the fuel cell stack is the other air supply to the enclosure. The gas leaving the the fuel cell stack cathode is added to the enclosure gas and therefore an air supply to the enclosure. The outlet port installed in the enclosure wall serves as an outlet for the enclosure and its out flow is regulated by back pressure in the enclosure.

As shown in Figure 3.2, it is possible for the gases leaving the fuel cell stack to be recirculated within the enclosure. The gases leaving the fuel cell stack are low in oxygen content, but will have a higher humidity than the gas which entered the fuel cell stack. The fuel cell stack outlet gas is recirculated into the enclosure air, so that the water produced by the fuel cell stack will help to humidify the inlet air to the stack. Additional oxygen is supplied to the

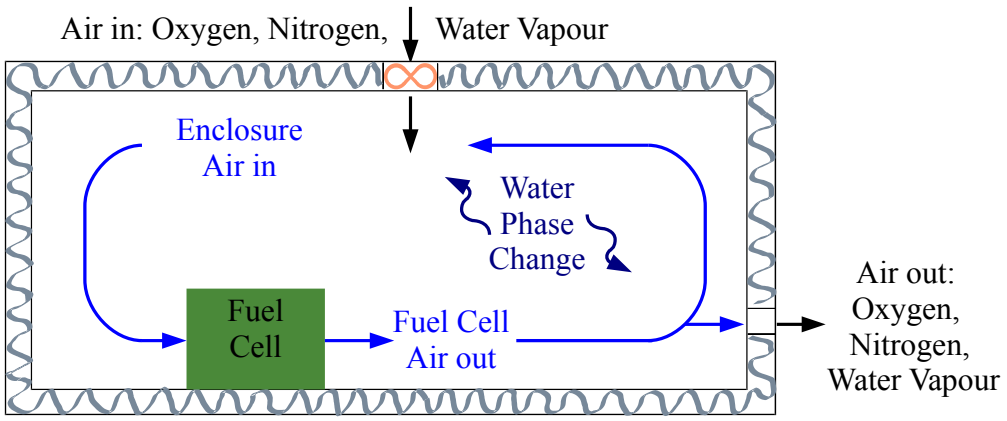

Figure 3.2 – Mass Flow in Enclosure

enclosure by the enclosure inlet fan to prevent oxygen depletion.

A mathematical model of the enclosure is developed assuming complete mixing of all the gases. A mass balance of the gases is used to charactize the density of gas in the enclosure. The rate of change of mass in the control volume (i.e. the enclosure) is equal to the rate of convective flux into and out of the enclosure. In this case, the diffusive flux is negligible and there are no sources of gas. Water evaporation may occur if liquid water exists in the enclosure and condensation may occur if the gas is saturated.

Using a mass balance for the air-water vapour mixture, and taking into account the inlet and outlet conditions previously specified, leads to:

$$\frac{\partial \rho_{encl}}{\partial t} V_{encl} = \sum_i \dot{m}^I_{i,encl} - \sum_i \dot{m}^I_{i,FC} + \sum_i \dot{m}^O_{i,FC} - \sum_i \dot{m}^O_{i,encl} - \dot{m}_{e,phase} \tag{3.1}$$

The term on the left hand side represents the rate of change of mass in the enclosure. The convective flux on the right hand side is represented by the sum of the mass flow rates into and out of the enclosure. The convective terms are: $\sum_i \dot{m}^I_{i,encl}$, the sum of the mass flow rates of each species entering the enclosure at ambient conditions, $\sum_i \dot{m}^I_{i,FC}$, the sum of the mass flow rates of each species leaving the enclosure to enter the fuel cell stack cathode channel at enclosure conditions, $\sum_i \dot{m}^O_{i,FC}$, the sum of the mass flow rates of each species entering the enclosure from the outlet of the fuel cell stack cathode channel at cathode channel conditions, and $\sum_i \dot{m}^O_{i,encl}$, the sum of the mass

flow rates of the species leaving the enclosure to the external environment at enclosure conditions. Finally, $\dot{m}_{e,phase}$ is the water phase change term which is negative to indicate gas loss when condensation occurs. Equation (3.1) is solved for the density, ρ_{encl} in kg/m^3, of the air in the enclosure. V_{encl}, in m^3 is the volume of air in the enclosure.

Enclosure Inlet Mass Flow, $\sum_i \dot{m}^I_{i,encl}$

The inlet mass flow rate of each species to the enclosure, $\dot{m}^I_{i,encl}$ in kg/s, is determined based on ambient air composition. The mechanisms for inlet flow are a prescibed, forced flow rate generated by the fan, shown in the first term, and diffusion, represented by the second term. The forced flow rate is a function of the velocity of the air once it passes through the fan and the size of the fan. The diffusion is assumed to occur over the wall thickness and is a function of the difference between the density of air in the environment and the density of air in the enclosure. Air is assumed to be a dilute mixture of oxygen in nitrogen.

$$\dot{m}^I_{i,encl} = y_{i,amb}\left(\rho_{amb}u_{fan}A_{fan} + \mathcal{D}_{O_2N_2}A_{fan}\frac{\rho_{amb}-\rho_{encl}}{t_{wall}}\right) \tag{3.2}$$

The density, ρ_{amb} in kg/m^3, of the ambient air depends on ambient temperature and pressure, ρ_{encl} is the density of the air in the enclosure, $\mathcal{D}_{O_2N_2}$ in m^2/s is the oxygen-nitrogen diffusion coefficient, and t_{wall} in m is the wall thickness. The fan cross-sectional area, A_{fan} in m^2, is measured for the specific experiment fan, and the flow velocity, u_{fan} in m/s, is determined from data obtained by testing the specific fan being used, as detailed in Chapter 4. The species composition of the gas is determined by first determining the fraction of water vapour in the air via the relative humidity. The remaining air is assumed to be at the standard Earth ambient gas composition of 21% oxygen and 79% nitrogen.

Air is assume to be a dilute mixture of oxygen in nitrogen. The diffusion coefficient for dilute oxygen in nitrogen is temperature dependent, and is therefore defined as [73]:

$$\mathcal{D}_{O_2N_2} = 1.8583\times10^{-5}\frac{\sqrt{T^3_{avg}\left(\frac{1}{M_{O_2}}+\frac{1}{M_{N_2}}\right)}}{P_{avg}\sigma^2_{O_2N_2}\Omega_{\mathcal{D}_{O_2N_2}}} \tag{3.3}$$

which is in m^2/s, T_{avg} and P_{avg} are is the average of the environment and enclosure temperatures and pressures, M_{O_2} and M_{N_2} are the molar masses of

oxygen and nitrogen, and $\sigma_{O_2N_2}$ and $\Omega_{\mathcal{D}_{O_2N_2}}$ are functions of the Lennard-Jones parameters [73].

Enclosure Outlet Mass Flow, $\sum_i \dot{m}^O_{i,encl}$

The outlet gas mass flow rate from the enclosure, $\sum_i \dot{m}^O_{i,encl}$, is controlled by the pressure differential between the enclosure and the ambient conditions. The outlet flow is charactized as a pipe outlet where the average volume flow rate through the pipe can be determined using Poiseuille's Law [41]. Assuming laminar flow through the outlet hole in the insulated enclosure wall, the pressure differential between the enclosure and the ambient environment drives the mass flow rate out of the enclosure through the outlet hole. Equation (3.4) is derived from Poiseuille's law to solve for the average outlet flow velocity, u_{out}, as a function of the pressure difference, hole diameter and length of the outlet hole (i.e. width of the enclosure wall).

$$u_{out} = \frac{d^2_{out}\Delta P}{32\mu_i L_{out}} \tag{3.4}$$

ΔP, in Pa, is the difference in pressure between the enclosure and the ambient environment, d_{out}, in m, is the diameter of the outlet hole in the enclosure wall, μ_q, in $Pa*s$, is the viscosity of the gas based on species composition, and L_{out}, in m, is the width of the enclosure wall.

The outlet gas mass flow rate for each species, $\dot{m}^O_{i,encl}$, can be determined as the product of the average flow velocity, u_{out}, in m/s; the mass fraction of the species, $y_{i,encl}$, in kg_i/kg; gas density, rho_encl, in kg/m^3; and the cross-sectional area,$A_{out,encl}$, in m^2, of the outlet. Equation (3.5) is used to calculate the outlet mass flow rate, $\dot{m}^O_{i,encl}$, assuming that the density of the air is uniform at the outlet [72].

$$\dot{m}^O_{i,encl} = y_{i,encl}\rho_{encl}u_{out}A_{encl,out} \tag{3.5}$$

The fuel cell stack inlet mass flow rate $\sum_i \dot{m}^I_{i,FC}$ and outlet mass flow rate $\sum_i \dot{m}^O_{i,FC}$ are discussed in the fuel cell stack model Chapter 2. These variables are used to couple the stack and enclosure models.

Water Phase Change, $\dot{m}_{e,phase}$

Water will condense in the enclosure if saturation is exceeded and evaporate if the gas is not saturated and there is liquid water in the enclosure. It is

assumed that liquid water in the enclosure is in the form of small droplets attached to the walls. The transient water phase change term, $\dot{m}_{e,phase}$, is positive if condensation occurs and negative if evaporation occurs.

The amount of water which condenses depends on the quantity of excess water vapour in the channel and the condensation rate. The amount of water evaporated depends on the remaining space available in the air for water vapour and the evaporation rate. The phase change rate of water in the enclosure, $\dot{m}_{e,phase}$, in kg/s, is modelled as [52]:

$$\begin{aligned}\dot{m}_{e,phase} =& \frac{k_c V_{encl}\left(1-s_{encl}\right) M_{H_2O}}{RT_{encl}}\left(P_{encl,H_2O^v}-P_{encl,sat}\right)\beta_{encl} \\ &+ k_v V_{encl} s_{encl} \rho_{H_2O,l}\left(P_{encl,H_2O^v}-P_{encl,sat}\right)\left(1-\beta_{encl}\right)\end{aligned} \tag{3.6}$$

where the first term on the right hand side represents the condensation rate and the second term represents the evaporation rate. In equation (3.6), k_c, in s^{-1}, is the rate of condensation of water and k_v, in $kPa^{-1}s^{-1}$ is the evaporation rate of water, V_{encl} is the enclosure volume in m^3, s_{encl} is the saturation of the enclosure, R is the universal gas constant in $\frac{kPa*m^3}{mol*K}$, M_{H_2O} is the molar mass of water in kg/mol, P_{encl,H_2O^v} is the partial pressure of water vapour in the enclosure in kPa, $P_{encl,sat}$ is the saturation vapour pressure in the enclosure in kPa,, and β_{encl} is a switching term which activates either the condensation or evaporation term and negates the other [52].

The switching term β_{encl} is a function of the difference between the partial pressure of water vapour in the channel and the saturation pressure of the channel.

$$\beta_{ca} = \frac{1}{2} + \frac{\left|P_{ca,H_2O^v} - P_{ca,sat}(T_{ca}(x,t))\right|}{2\left(P_{ca,H_2O^v} - P_{ca,sat}(T_{ca}(x,t))\right)} \tag{3.7}$$

If the difference between the partial pressure of water vapour in the enclosure and the saturation pressure is positive, condensation will occur because there is more water in the enclosure than the gas can hold as vapour. Thus, the switching term β_{encl} will be 1, which activates the condensation term in equation (3.6). If the difference between the partial pressure of water vapour in the enclosure and the saturation pressure is negative, evaporation will occurs because there is space available for additional water vapour in the gas, assuming liquid water exists. The switching term β_{encl} is thus 0, which activates the evaporation term of equation (3.6).

The saturation term s_{encl} controls whether evaporation occurs and its rate. If there is no liquid water in the enclosure to evaporate, the saturation term

will be zero because it is a function of the mass of liquid water in the enclosure $m_{encl,H_2O,l}$, and expressed as:

$$s_{ca} = \frac{m_{encl,H_2O,l}}{\rho_{H_2O,l} V_{encl}} \tag{3.8}$$

where $\rho_{H_2O,l}$ is the density of liquid water in kg/m^3.

Species Mass Balance

The next step to determine the gas composition in the enclosure is to solve for the mass fractions of the species in the moist air. To prevent oxygen depletion and membrane dry-out, it is necessary to analyze the oxygen and water vapour content of the air in the enclosure.

Using the same mass balance method, the mass fraction of each species can be determined. The rate of change of mass of each species within the enclosure is equal to the rate of convective flux of each species into and out of the enclosure. Again, diffusive flux is neglected and there are no gas sources.

Each of the mass fluxes into and out of the enclosure may contain any of the species: oxygen, nitrogen and water vapour. It is assumed that any other gas species which may be present are in negligible quantities. The sum of the mass fractions of the species will always be one. Therefore, only 2 of the 3 species mass fractions are solved using the mass balance equation. The third is solved as the remaining mass fraction to obtain the total of one.

Oxygen is brought into the enclosure through the ambient inlet mass flow, $\dot{m}^I_{O_2,encl}$, and enters the fuel cell stack cathode channels for reaction at the fuel cell stack inlet mass flow rate, $\dot{m}^I_{O_2,FC}$. The fuel cell stack uses in the air for reaction, but as the stoichiometry of the inlet mass flow rate is generally greater than one, some oxygen remains in the gas flow out of the fuel cell stack, $\dot{m}^O_{O_2,FC}$. This excess oxygen from the fuel cell stack outlet is recirculated within the enclosure. Finally, oxygen leaves the enclosure through a pressure controlled outlet at a mass flow rate, $\dot{m}^O_{O_2,encl}$, calculated by Equation (3.5). Therefore, a mass balance in oxygen results in:

$$\begin{aligned} \frac{\partial \rho_{O_2}}{\partial t} \rho_{encl} V_{encl} &= \frac{\partial y_{O_2,encl}}{\partial t} \rho_{encl} V_{encl} + \frac{\partial \rho_{encl}}{\partial t} y_{O_2,encl} V_{encl} \\ &= \dot{m}^I_{O_2,encl} - \dot{m}^I_{O_2,FC} + \dot{m}^O_{O_2,FC} - \dot{m}^O_{O_2,encl} \end{aligned} \tag{3.9}$$

Equation (3.9) is solved for the mass fraction of oxygen in the enclosure, y_{O_2}, to analyze the oxygen concentration in the enclosure and prevent oxygen de-

pletion. If there is insufficient oxygen in the enclosure, the fuel cell stack will not operate.

Water vapour enters the enclosure with the moist environment air, $\dot{m}^I_{H_2O,encl}$. This water vapour is circulated and mixed with water vapour in the enclosure. Enclosure water vapour enters the fuel cell stack with an inlet mass flow rate, $\dot{m}^I_{H_2O,FC}$, as specified by the fuel cell stack model in Section 2.1.2. The outlet mass flow, $\dot{m}^O_{H_2O,FC}$, from the fuel cell stack also contains water vapour, usually at a higher concentration as water is produced by the fuel cell stack. This water vapour leaving the fuel cell stack is recirculated in the enclosure. Water vapour exits the enclosure at a mass flow rate of $\dot{m}^O_{H_2O,encl}$, which is controlled by the pressure difference between the enclosure and the ambient environment as calculated by Equation (3.5). Therefore, the final water vapour mass balance in the enclosure is:

$$\begin{aligned}\frac{\partial \rho_{H_2O}}{\partial t}\rho_{encl}V_{encl} &= \frac{\partial y_{H_2O,encl}}{\partial t}\rho_{encl}V_{encl} + \frac{\partial \rho_{encl}}{\partial t}y_{H_2O,encl}V_{encl} \\ &= \dot{m}^I_{H_2O,encl} - \dot{m}^I_{H_2O,FC} + \dot{m}^O_{H_2O,FC} - \dot{m}^O_{H_2O,encl} \end{aligned} \tag{3.10}$$

Equation (3.10) is solved for the mass fraction of water vapour in the enclosure, y_{H_2O}. The humidfication of the enclosure will thus be studied to ensure the fuel cell stack maintains acceptable membrane hydration.

As the sum of the mass fractions will always be one, nitrogen can be solved as one minus the sum of the mass fractions of the other species, i.e.:

$$y_{N_2,encl} = 1 - y_{H_2O,encl} - y_{O_2,encl} \tag{3.11}$$

Equations (3.1), (3.9) and (3.10) are the ODEs that are solved to obtain the composition of the gas in the enclosure at varying operating conditions. Equations (3.2), (3.4), (3.5) and (3.11) are used as closure equations for the mass transport model.

3.2 Liquid Mass Balance

The enclosure can experience a wide range of temperatures which may lead to condensation of water vapour, or evaporation of liquid water in the enclosure. If the enclosure gas is saturated, water vapour may condense in the enclosure. It is assumed that no liquid water enters the enclosure. Sources of liquid water in the enclosure are: condensation, and possible fuel cell stack cathode output into the enclosure. Liquid water is assumed to accumulate in the enclosure

and does not leave through the enclosure outlet. Evaporation may occur if some liquid water accumulates in the enclosure.

The liquid water mass balance for the enclosure is:

$$\frac{\partial m_{encl,H_2O^l}}{\partial t} = -\dot{m}^O_{FC,H_2O^l} + \dot{m}_{e,phase} \tag{3.12}$$

where $\dot{m}^O_{FC,H_2O^l}$, in kg/s, is the liquid water leaving the cathode channel in droplet form as described by equation (2.27), and $\dot{m}_{e,phase}$ is added as condensation leads to an increase in the liquid water in the enclosure.

3.3 Energy Balance

The operation of the fuel cell stack depends on the stack being maintained at temperatures high enough that it does not freeze. The purpose of the insulated walls of the enclosure is to keep the air in the enclosure at an acceptable temperature for operation of the fuel cell stack. The inlet fan is used to provide ambient air to cool the enclosure. It can generally be assumed that the enclosure air will be warmer or at least the same temperature as the surroundings during operation of the fuel cell stack. This occurs because the operating fuel cell stack generates heat which will warm up the air in the enclosure. The heat generated by the fuel cell stack can have a significant impact on the enclosure air temperature. The temperature of the enclosure also affects the performance of the fuel cell stack. Therefore, the heat energy in the enclosure must be coupled with the fuel cell stack. These effects on the heat transfer within the enclosure will be considered while analyzing the effect of the enclosure on the fuel cell stack operation.

The mathematical model of the enclosure is developed using an energy balance of all sources and sinks of heat energy in the enclosure. As shown in Figure 3.3, the heat energy sources are: heat energy generated by the fuel cell stack operation, heat energy carried with the two inlet mass flows, and condensation. The heat energy sinks are: heat lost through the enclosure walls to the external environment, the heat energy carried with the two outlet mass flows, and evaporation. The two inlet mass flows which bring energy into the enclosure are the inlet fan in the enclosure wall and the air which leaves the fuel cell stack and enters the enclosure. The two outlet mass flows that take energy out of the enclosure are the back-pressure outlet in the enclosure wall and the air which leaves the enclosure when entering the fuel cell stack. The mass flows in the enclosure are detailed in Section 3.1.

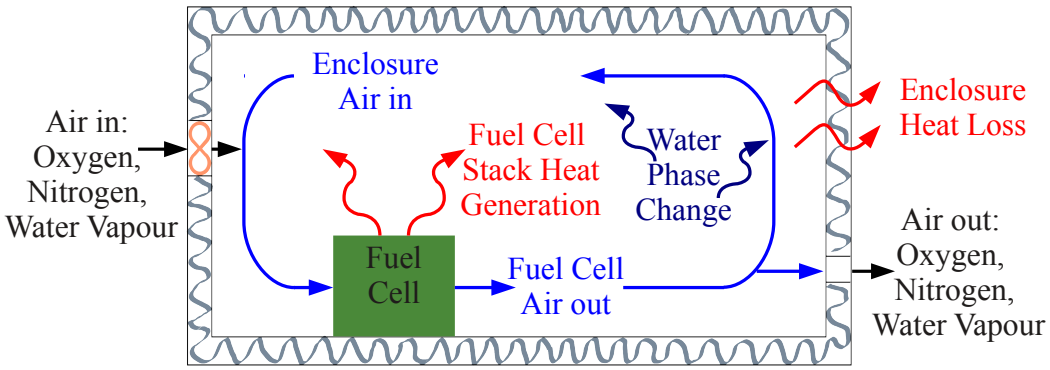

Figure 3.3 – Thermal Model of Enclosure

It is assumed that there are no other contents in the enclosure aside from the fuel cell stack. Therefore, the control volume for the energy balance will include only the air inside the enclosure and the enclosure walls. If other significant items are added to the enclosure they would need to be modelled as heat sinks taking into account their heat transfer properties.

To determine the temperature in the enclosure, a mathematical model of the thermal energy balance of the enclosure is developed. The rate of change of the thermal energy in the enclosure is equal to the difference between the thermal energy entering the enclosure and the thermal energy leaving the enclosure. Based on the aforementioned heat sources and sinks, the energy balance for the enclosure is given by:

$$\frac{\partial E_{encl}}{\partial t} = \dot{Q}_{conv,FC} - \dot{Q}_{cond,FC} - \dot{Q}_{wall} + \dot{Q}_{e,phase} + \sum_{in} \dot{m}^{I}_{i,amb} h_i - \sum_{in} \dot{m}^{I}_{i,FC} h_i + \sum_{out} \dot{m}^{O}_{i,FC} h_i - \sum_{out} \dot{m}^{O}_{i,encl} h_i \tag{3.13}$$

where the left hand term is the rate of change of thermal energy in the enclosure. The first term on the right hand side is the energy generated by the fuel cell stack, $\dot{Q}_{conv,FC}$ which is diffused into the enclosure by natural heat convection, and modelled as a source term into the enclosure. The second term, $\dot{Q}_{cond,FC}$ accounts for the conduction through the enclosure wall where the fuel cell stack is installed touching the wall. The third term, $\dot{Q}_{wall}$ is thermal conduction between the enclosure and the ambient environment through the

enclosure wall. The change in energy caused by phase change, $\dot{Q}_{e,phase}$, is the fourth term. The fifth through eighth terms on the right hand side are heat transferred by mass flow into and out of the system.

The heat transfer due to mass flow is considered for each species in the mass flow stream to account for the varying gas composition. It is assumed that the velocity of the mass flows is slow enough to neglect kinetic energy and that there is no significant potential energy. Therefore, only the enthalpy, h_i, of the gases in the enclosure are included. The gases in the enclosure are treated as ideal gases, therefore the enthalpy is approximated as the specific heat capacity of the gas at constant pressure times the temperature, T_{encl} of the gas in the enclosure [72].

$$h_i = c_{p,i} T_{encl} \tag{3.14}$$

The specific heat capacities, $c_{p,i}$ in J/kgK, of the species i of the gas is assumed constant.

The change in energy in the enclosure, $\frac{\partial E_{encl}}{\partial t}$, is rewritten using the chain rule in terms of the time dependent variables: temperature, T_{encl} in K; species composition, $y_{i,encl}$ in kg_i/kg; and gas density, ρ_{encl} in kg/m^3, as shown in Equation (3.15).

$$\begin{aligned}
\frac{\partial E_{encl}}{\partial t} &= \frac{\partial}{\partial t}\left[\left(\sum_i \rho_{i,encl} V_{encl} c_{p,i} + m_{iw} c_{p,iw}\right) T_{encl}\right] \\
&= \sum_i \frac{\partial y_{i,encl}}{\partial t}\left(\rho_{encl} V_{encl} c_{p,i} T_{encl}\right) + \frac{\partial \rho_{encl}}{\partial t}\left(\sum_i y_{i,encl} V_{encl} c_{p,i} T_{encl}\right) \\
&\quad + \left(\sum_i y_{i,encl} \rho_{encl} V_{encl} c_{p,i} + m_{iw} c_{p,iw}\right) \frac{\partial T_{encl}}{\partial t}
\end{aligned} \tag{3.15}$$

where m_{iw}, in kg, is the mass of the insulating walls of the enclosure which is calculated based on the density of the insulation and wall volume, and $c_{p,iw}$, in J/kgK, is the specific heat capacity of the insulating enclosure walls.

The energy in the enclosure gas is equal to the sum of the energy in each species, where the energy in each species is the product of its mass fraction, the enclosure air density, the volume of the enclosure, the specific heat capacity of the species and the enclosure temperature. Again, the kinetic and potential energy in the gas in the enclosure is assumed negligible. The volume of the enclosure is constant and the gas specific heat capacity is assumed constant. Thus the chain rule expansion of the change in energy of the gas

in the enclosure expands to three terms for the transient properties. The first term on the right hand side accounts for the change in the species mass fraction in the enclosure, the second for the change in the the density of the air in the enclosure, and the third for the change in the enclosure temperature.

Stack to Enclosure Convection, $\dot{Q}_{conv,FC}$

The fuel cell stack is hotter than the enclosure because it generates heat during operation. Therefore, a temperature differential between the fuel cell stack and the enclosure will develop. Thermal enegy is transferred from the fuel cell stack to the enclosure air by convective heat transfer. Newton's law of cooling states that the rate of convective heat transfer varies with the temperature differential between the surface and the fluid [68]. The fuel cell stack is treated as a lumped model where the entire stack is at the same temperature, T_s in K, at a given time, as determined by the fuel cell stack model developed in Section 2.4. Using Newton's law of cooling as applied to the fuel cell stack convection between the fuel cell stack surface area which is in contact with the enclosure air, $A_{s,encl}$ in m^2, gives an expression for the heat transfer from the stack to the air in the enclosure.

$$\dot{Q}_{conv,FC} = h_s A_{s,encl} \left(T_s - T_{encl}\right) \tag{3.16}$$

The heat transfer coefficient for the fuel cell stack, h_s in W/m^2K, is an experimentally determined which depends on the fluid properties, fluid velocity, type of fluid motion and surface properties [68].

Stack to Enclosure Conduction, $\dot{Q}_{cond,FC}$

The area where the fuel cell stack is installed touching the enclosure wall is treated as a conduction zone through the enclosure wall. Using Fourier's law of heat conduction, the rate of heat conduction through the walls can be determined. The rate of heat conduction is a function of the conductivity of the walls, the temperature differential between the two sides of the wall and the surface area of the wall [68]. The conductive heat transfer through the wall where the fuel cell stack is installed is expressed as:

$$\dot{Q}_{cond,FC} = U_{wa} A_{surf,FC} \left(T_s - T_{amb}\right) \tag{3.17}$$

where the coefficient of conductivity of the walls, U_{wa} in W/m^2K, is a function of the wall resistance R-value and the air film developed where the wall is

exposed to the ambient air. The surface area, $A_{surf,FC}$ in m^2, includes only the area where the fuel cell stack is in direct contact with the enclosure wall. T_{amb}, in K, is the ambient external environment temperature.

For the case of heat conduction from the stack through the wall, the coefficient of conductivity U_{wa} is treated as a thermal resistance network [68]. Therefore, the resistivity of the insulation R_{ins} and the air film at the outside wall of the enclosure $R_{air,amb}$ are connected in series to get the total heat transfer coefficient:

$$U_{wa} = \frac{1}{R_{ins}} + \frac{1}{R_{air,amb}} \tag{3.18}$$

Enclosure to Ambient Convection, $\dot{Q}_{wall}$

The energy lost by conduction through the walls of the enclosure depends on the properties of the insulation that is used, as well as the temperature differential between the enclosure and its surroundings, as expressed as:

$$\dot{Q}_{wall} = U_{awa} A_{surf,encl} \left(T_{encl} - T_{amb}\right) \tag{3.19}$$

where $A_{surf,encl}$ is the surface area of the enclosure walls which are in contact with the enclosure gas.

The heat transfer coefficient U_{awa} for the case where the wall is in contact with the enclosure air on the inside and ambient air on the outside is modelled as a thermal resistance network [68]. The resistivity of the insulation R_{ins} and the air films on both sides of the wall of the enclosure $R_{air,encl}$ and $R_{air,amb}$ are connected in series to get the total heat transfer coefficient:

$$U_{awa} = \frac{1}{R_{air,encl}} + \frac{1}{R_{ins}} + \frac{1}{R_{air,amb}} \tag{3.20}$$

Phase Change Energy, $\dot{Q}_{e,phase}$

If condensation occurs in the enclosure because water saturation is exceeded, liquid water will be produced so $\dot{m}_{e,phase}$ will be positive and the energy released by the condensation is expressed by $\dot{Q}_{e,phase}$. If evaporation occurs in the enclosure because there is liquid water in the enclosure and the

gas is not satuated, $\dot{m}_{e,phase}$ will be negative and the energy, $\dot{Q}_{e,phase}$, used to evaporate the water is removed.

$$\dot{Q}_{e,phase} = \dot{m}_{e,phase}\Delta H_{vap} \tag{3.21}$$

where ΔH_{vap} is the heat of vaporatization of water at the stack temperature.

Using Equations (3.13) and substituting Equations (3.15)-(3.20), the energy balance of the enclosure is solved for the temperature of the gas in the enclosure. Gas compositions are obtained using the equations detailed in Section 3.1. The mathematical model couples the enclosure model with the fuel cell stack model such that the effect of the fuel cell stack on the enclosure conditions is analyzed. Additionally, this allows the study of the effect of varying enclosure conditions on the performance of the fuel cell stack.

Model Summary

In summary, the enclosure model uses 5 governing equations to solve for 5 unknowns, as outlined in Table 3.1

Table 3.1 – Enclosure mathematical model

Variable	*Governing Equation*
Enclosure air density, ρ_{encl}	3.1
Oxygen mass fraction in enclosure, y_{encl,O_2}	3.9
Water vapour mass fraction in enclosure, y_{encl,H_2O^v}	3.10
Mass of liquid water in cathode, m_{encl,H_2O^l}	3.12
Enclosure temperature, T_{encl}	3.15

3.4 Validation

The transient mathematical model of the enclosure was validated by comparing the steady state temperatures achieved by the transient model to the expected steady state determined by a steady state model. The steady state model was developed using the equations identified in the previous section Equations (3.1) - (3.20), but without the transient terms. In particular, the phase change term was omitted because of its time dependency.

Both the steady state enclosure model and transient enclosure model were solved for the same enclosure design and the temperature inside the enclosure was compared. The general parameters for the validation and parametric studies of the enclosure model are listed in Table 3.2.

Table 3.2 – Enclosure and Fuel Cell Stack Model Parameters

Parameter	*Value*	*Reference*
Enclosure height (m)	0.26	
Enclosure width (m)	0.26	
Enclosure length (m)	0.26	
Enclosure volume (m^3)	0.0175	
Outlet cross-sectional area (m^2)	0.004	
Ambient Pressure (kPa)	101	
Enclosure wall (W/m^2K)	1	
External air film (W/m^2K)	0.03	[74]
Internal vertical air film (W/m^2K)	0.12	[74]
Internal horizontal air film (W/m^2K)	0.107	[74]
Plastispan density (kg/m^3)	22 [75]	22 [75]
Plastispan specific heat capacity (J/kgK)	1500 [76]	1500 [76]
Fuel cell - Enclosure contact area (m^2)	0.0035	[70]
Evaporation Rate Coefficient $\left(\frac{cm^2LV}{(cm^2ch)s}\right)$	10	estimated
Condensation Rate Coefficient $\left(\frac{cm^2LV}{(cm^2ch)s}\right)$	10	estimated
Number of cells in Stack	13	[70]
Fan flow stoichiometry at 1A for stack	4	
Ambient Temperature (K)	253	
Ground Temperature (K)	253	
Ambient relative humidity	40%	
Stack current (A)	0, 0.4, 1.2, 1.6, 0.8	

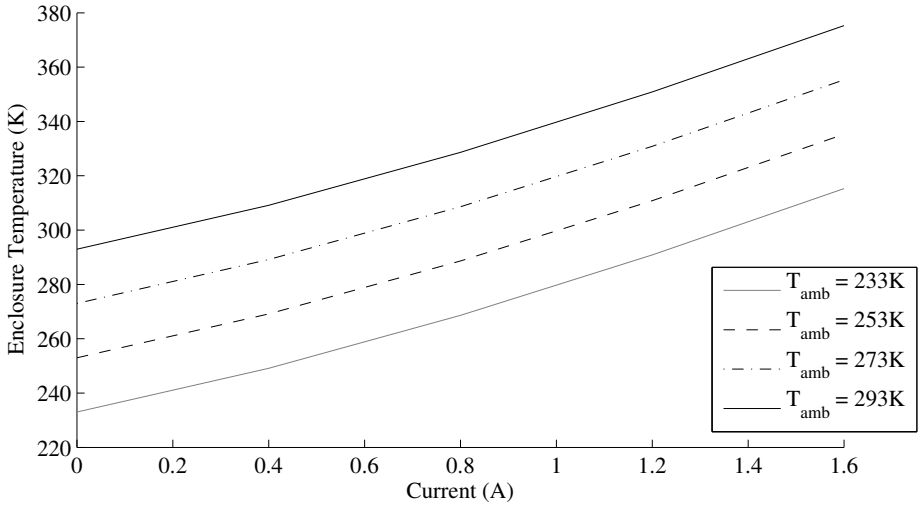

Figure 3.4 – Steady-State Enclosure Temperature at Varying External Temperatures

The inlet flow rate to the enclosure is set by a fan running at a constant velocity. The mass flow rate associated with this velocity is related to the density of the air and size of the fan, as well as diffusion into the enclosure, and is calculated by (3.2). The experiments reported in Chapter 5 were run with the enclosure fan at 0.34m/s, which is low on its operating range. This equates to a stoichiometric ratio of 124 at 1A, which is very high for the fuel cell stack. At this high flow speed, many of the effects of changing the design parameters, particularly to the gas composition are no longer visible. To illustrate the effects of changing parameters, the validation and parametric studies were run at a stoichiometric ratio of 4 for all the tests (aside from the specific fan air speed parametric study cases).

The steady state enclosure model in Figure 3.4 shows that when the current output of the stack increases, the temperature in the enclosure also increases. This is expected as the stack produced more heat as the current increases. Additionally, when the ambient temperature increases, the temperature in the enclosure increases, which is also expected as the losses through the enclosure walls decrease.

Figure 3.5 shows the temperature of the enclosure for the transient model for current jumps of 0A for 5 minutes, 0.4A for 20 minutes, 1.2A for 20 minutes, 1.6A for 20 minutes and 0.8A for 20 minutes. In all cases the steady operating temperature of the enclosure is rapidly reached as this model assumes that the

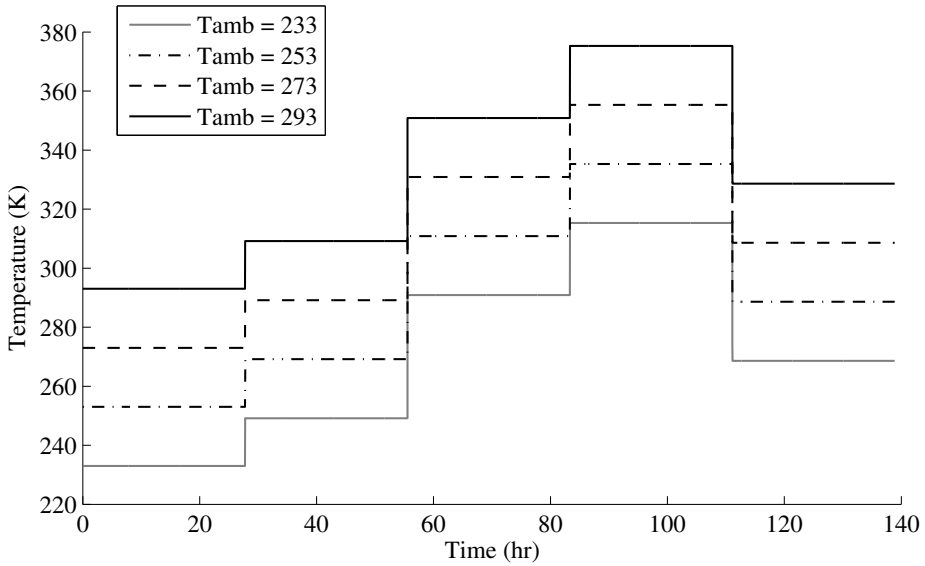

Figure 3.5 – Steady-State Enclosure Temperature at Varying External Temperatures

change in heat produced by the fuel cell stack is instantaneous and that all of the heat produced by the stack is emitted directly into the enclosure.

The temperature of the steady state model at a given fuel cell stack current output and ambient temperature is identical to that of the transient model once steady conditions have been achieved for the same operating conditions, as shown in Appendix A. This indicates that the transient model has been developed correctly, and also that the effect of the transient gas composition on the temperature of the enclosure is negligible.

The mass transport model was also validated by comparing the transient model to the steady state simulations. The results were also identical for the two models, and therefore are not shown.

3.5 Enclosure Parametric Studies

A parametric study is carried out using the transient model of the enclosure to study how design changes affect the temperature, gas composition and relative humidity in the enclosure. A base case with the properties listed in Table 3.2 is simulated with a Horizon H-12 Fuel Cell Stack installed. Further

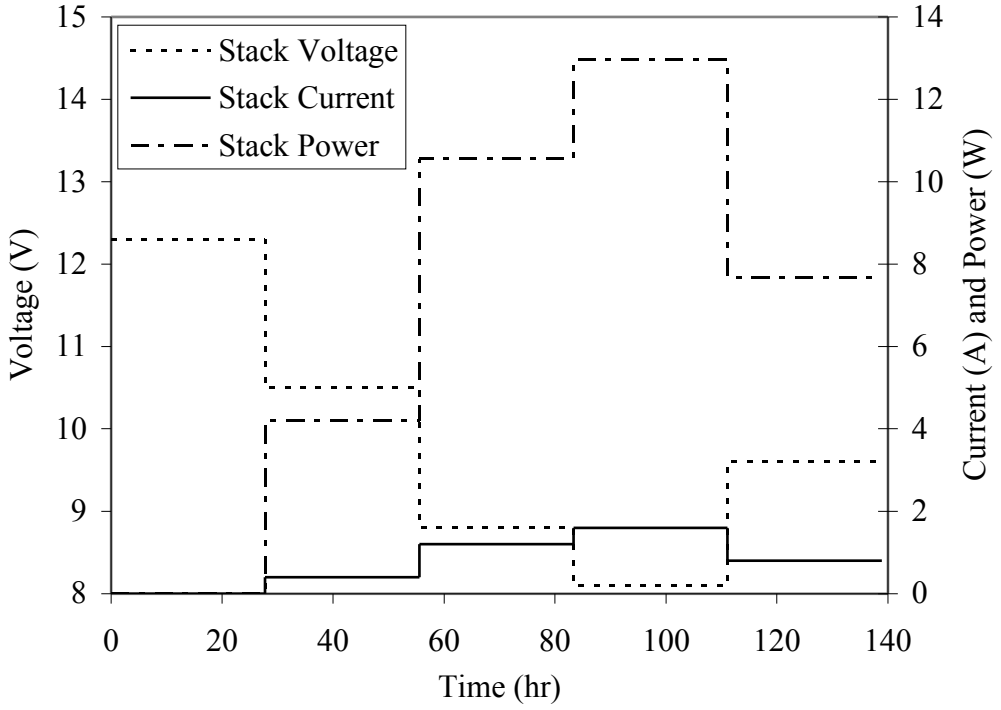

Figure 3.6 – Fuel Cell Stack Performance for Testing Enclosure

simulations are then completed by varying one parameter and comparing to the base case. Parameters to be tested include: wall insulation R-value, enclosure size, inlet mass flow rate and the size of the outlet hole which affects outlet mass flow rate. Additionally, the effect of varying ambient environment conditions, temperature and relative humidity, will be studied in order to find the optimal parameters for building the enclosures for the experimental study in Chapter 5.

The parametric study simulations are effectuated with an imposed current in steps of 2.8 hours for 0A, 0.4A, 1.2A, 1.6A and 0.8A, as shown in Figure 3.6. The associated voltage and power produced by the stack indicated in Figure 3.6 are reported by Horizon Fuel Cell Technologies for their H-12 Fuel Cell Stack [70].

The parameters to be studied are:

a) the enclosure size

b) enclosure insulation

c) enclosure inlet mass flow rate

d) ambient temperature

e) ambient relative humidity

3.5.1 Enclosure Walls

Insulation

The purpose of the insulated enclosure walls is to create a barrier that reduces the heat loss from the fuel cell stack to the ambient environment by trapping the heat inside the enclosure. The thermal resistance of the wall insulation determines how well the enclosure will keep heat inside and how much heat energy will pass through the wall to the ambient environment. In Equations (3.17) and (3.19), the thermal resistance is directly related to the heat transfer through the enclosure walls. Three RSI values a) 1 RSI, b) 1.4 RSI and c) 2.1 RSI are studied. These values are selected because they are the RSI-values of the extruded polystyrene (EPS) that will be used during the experiments in Chapter 5 for wall thicknesses of 1 inch (2.5cm), 2 inches (5.1cm), and 3 inches (7.6cm) respectively.

Figure 3.7 shows that if the thermal resistance of the enclosure wall decreases, the enclosure temperature decreases. This occurs because a decrease

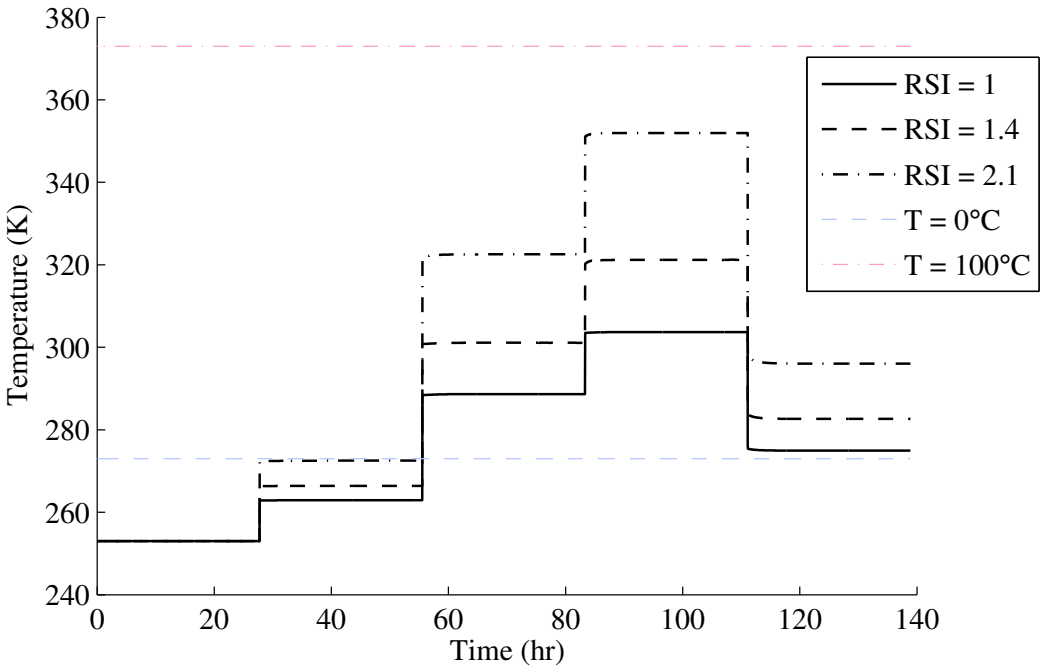

Figure 3.7 – Effect of Changing Wall Insulation on Enclosure Temperature

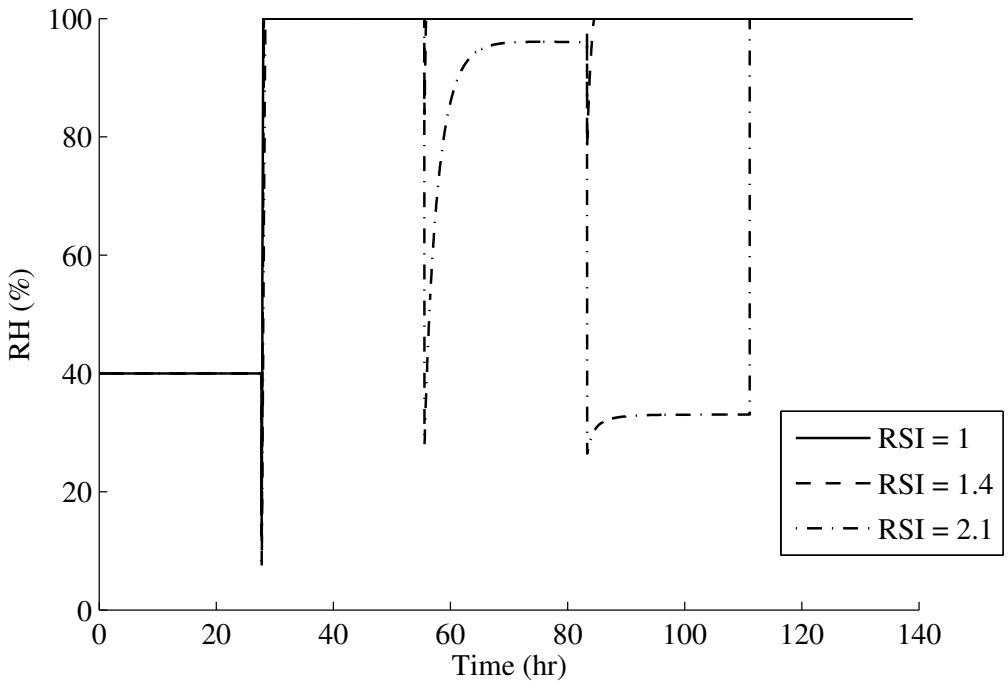

Figure 3.8 – Effect of Changing Wall Insulation on Enclosure Relative Humidity

in the thermal resistance leads to an increase in the heat transfer through the walls of the enclosure, and thus a lower temperature.

Figure 3.8 shows that increasing the insulation thermal resistance results in a lower relative humidity. At higher temperatures, the saturation pressure of water increases, so the gas can hold more water vapour. Therefore, with an increase in temperature, the relative humidity decreases. This occurs because the definition of the relative humidity is the partial pressure of water over the saturation pressure: $RH = P_{H_2O}/P_{sat}$, where the partial pressure of water vapour remains constant and the saturation pressure increases.

The gas reaches fully saturated conditions once the fuel cell stack starts operating because the fuel cell stack generates water, and at low temperatures, the saturation pressure is very low. Only a small amount of water is required to reach fully saturated conditions at these low temperatures and the amount of water generated by the stack is sufficient for this to occur. The small oscillations observed in the temperature and relative humidity when the enclosure is at fully saturated conditions are a function of the time dependency of the phase change.

Figure 3.9 shows the density of the gases in enclosure. Gas density is affected by the temperature changes. An increase in temperature in the en-

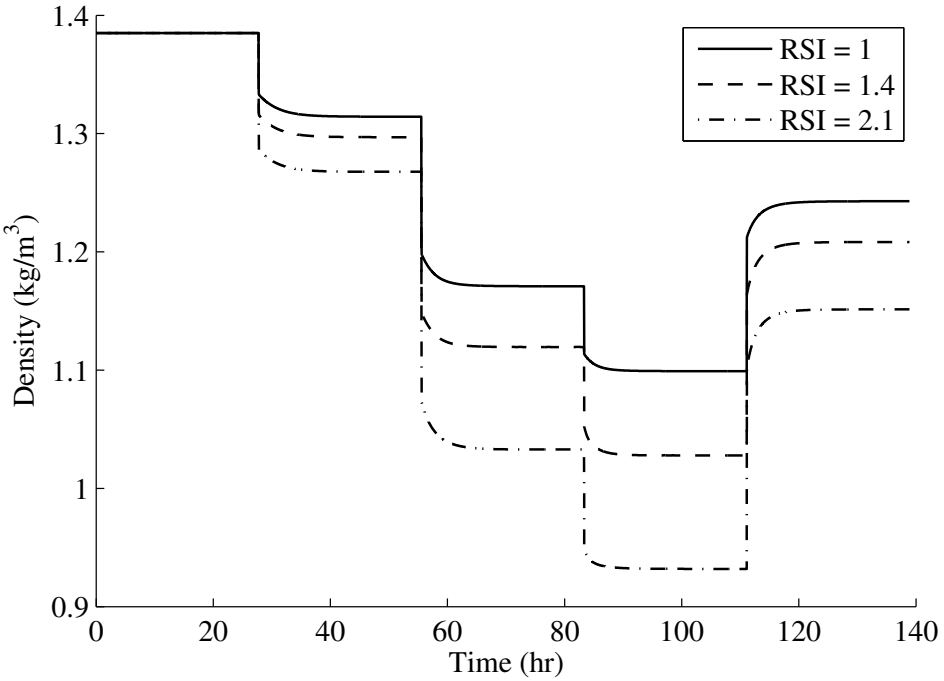

Figure 3.9 – Effect of Changing Wall Insulation on Enclosure Gas Density

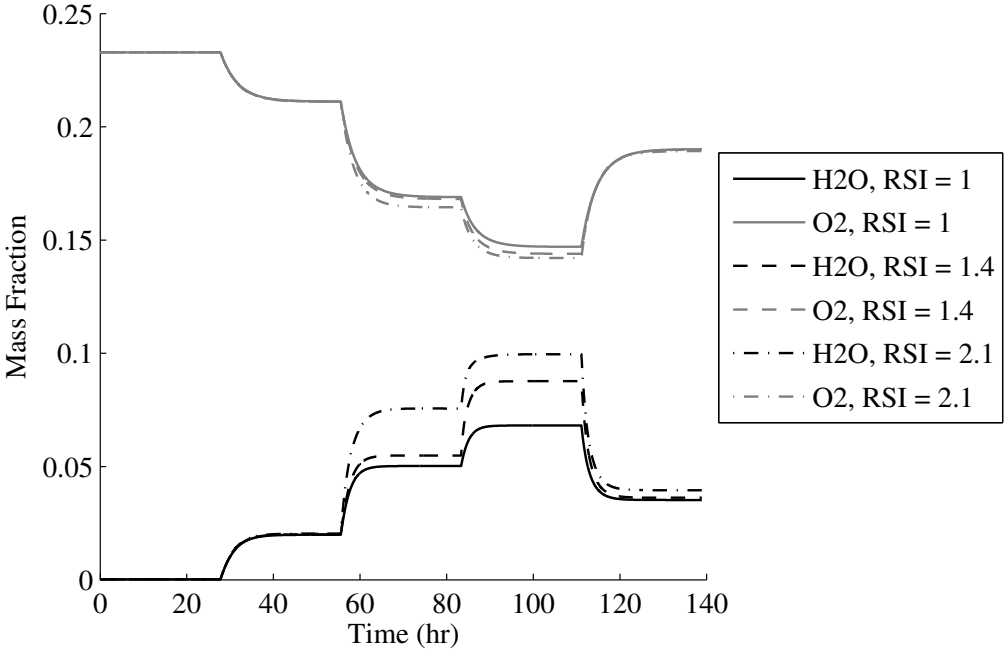

Figure 3.10 – Effect of Changing Wall Insulation on Enclosure Gas Composition

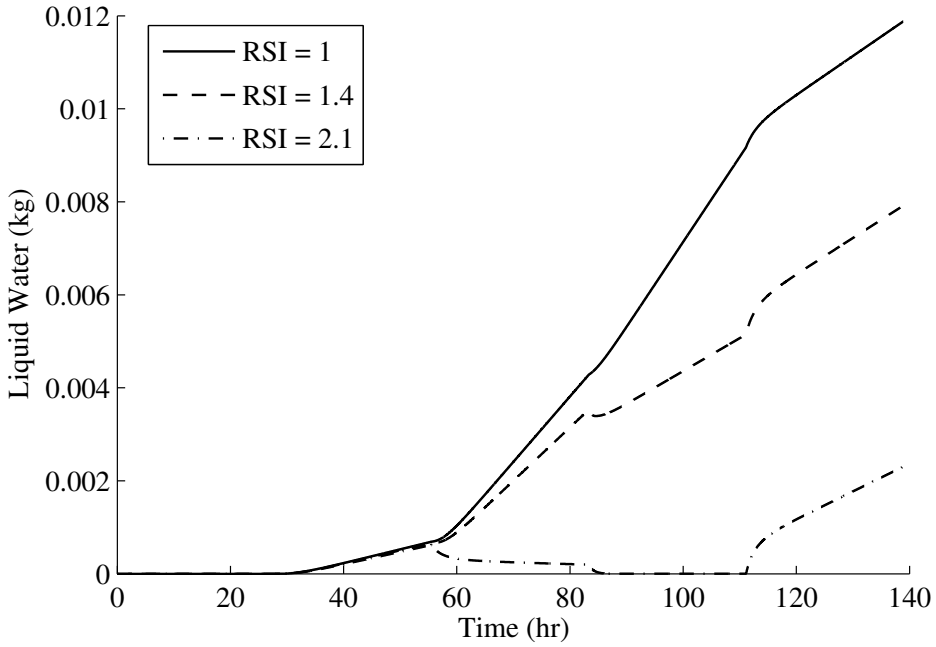

Figure 3.11 – Effect of Changing Wall Insulation on Enclosure Liquid Water Content

closure leads to a lower gas density. Figure 3.10 shows the changes in the gas composition for the different levels of insulation. An increase in stack power leads to an increased water generation, and the increase in temperature means the saturation pressure increases so the air can hold more water. The change in the oxygen mass fraction is caused by the change in density in the enclosure. When the gas in the enclosure is at a higher temperature, its density is lower and this causes a decrease in the enclosure pressure.

Figure 3.11 shows the quantity of water in the enclosure. For the cases with a thermal resistance of 1 RSI and 1.4 RSI, water condensation occurs in the second to fifth current steps. This condensation occurs because the temperature is lower in the enclosure, as shown in Figure 3.7. Therefore the saturation pressure is low and the mass fraction of water that can be held by the air decreases.

These changes in mass fraction are also evident in the relative humidity, as shown in Figure 3.8, where the case at 2.1 RSI shows relative humidity less than 100% in the fourth current step, which corresponds to Figure 3.11 where there is no liquid water to evaporate and bring up the relative humidity. This case will therefore reach equilibrium at a lower relative humidity condition because the water vapour pressure is less than the saturation pressure.

Enclosure Size

The enclosure consists of a cuboid geometry of insulated walls. The size of the enclosure was studied because of its effect on the heat retaining properties of the enclosure. Three enclosure sizes of a) 24cm x 24cm x 24cm, b) 26cm x 26cm x 26cm and c) 28cm x 28cm x 28cm, were selected because these small changes in enclosure size lead to significant changes in the enclosure temperature. Additionally, considering cubes of increasing size is easy to visualize and conceptualize.

Figure 3.12 shows the change of gas temperature with changes in the enclosure size. An increase in enclosure size results in a decrease in the enclosure temperature. This occurs because increasing the enclosure size increases the surface area through which energy from inside the enclosure can be lost to the environment.

A change in the size of the enclosure changes the amount of time required to reach steady state. With an increased enclosure size, the time required to reach steady state increases. This occurs because the enclosure holds more air and therefore requires more time for the gases recirculating within it to reach

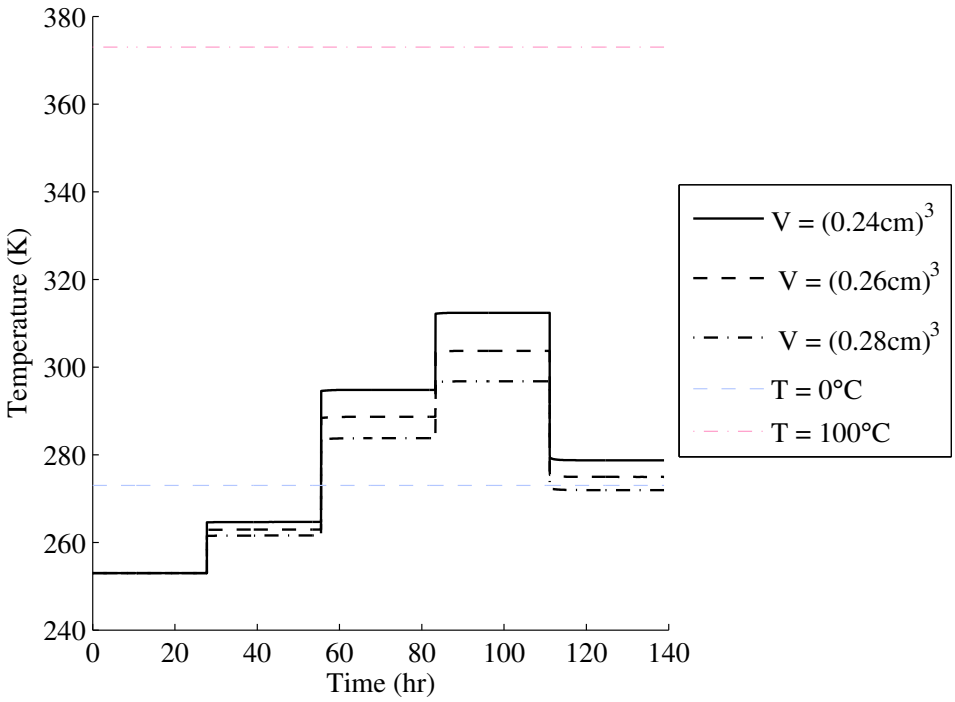

Figure 3.12 – Effect of Changing Enclosure Size on Enclosure Temperature

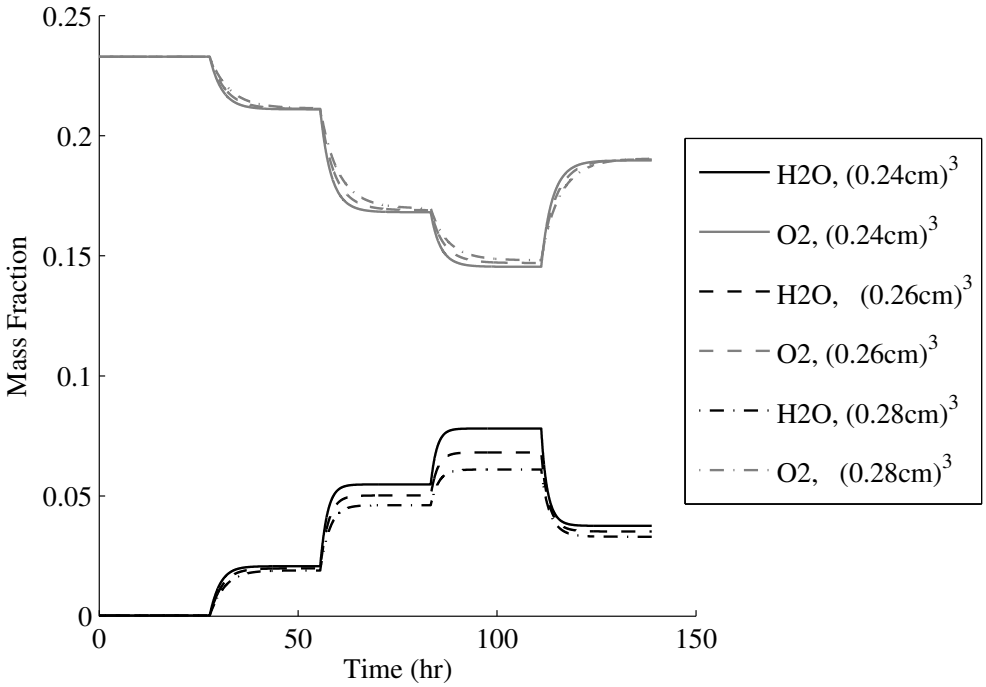

Figure 3.13 – Effect of Changing Enclosure Size on Enclosure Gas Composition

equilibrium. This is particularly evidenced by the change in the time required for the oxygen concentration to reach steady state, shown in Figure 3.13.

It is also observed that the mass fraction of water vapour decreases with a decrease in temperature. This occurs because the enclosure is at 100% relative humidity and condensation is occuring, therefore the water vapour mass fraction is decreasing because the saturation pressure decreases with decreasing temperature.

When designing an enclosure, the enclosure walls have a significant impact on the temperature within the enclosure. An increase in the thermal resistance of the walls leads to a higher temperature inside the enclosure, and an increase in the enclosure size decreases the temperature in the enclosure. Therefore, by varying the insulation and the size of the enclosure, it is possible to optimize the enclosure for a given set of operating conditions.

3.5.2 Enclosure Mass Flow

Inlet Mass Flow Rate

The mass flow into the enclosure is controlled by a fan with a prescribed flow rate which is set based on a stoichiometric ratio of the consumption of oxygen by the fuel cell stack. Flow rates corresponding to stoichiometric ratios of $\lambda = 2$, $\lambda = 4$, $\lambda = 124$, and $\lambda = 4.0 \times 10^4$ at 1A are tested. The low flow rates are selected to show the sensitivity of the enclosure with very low flow rates. The flow rate at $\lambda = 124$ is set during testing of the enclosure in Chapter 5, and the flow rate at $\lambda = 4.0 \times 10^4$ was selected to show the temperature dependency at very high flow rates.

Figure 3.14 shows the effect of the flow rate on the enclosure temperature. The ambient air flowing into the enclosure should help cool the stack, but as shown in Figure 3.14, an increase in the ambient flow rate actually has very little effect on the temperature of the air in the enclosure. This occurs because the quantity of heat transferred out of the enclosure with the air is 4 orders of magnitude smaller than the quantity of heat lost through the enclosure walls. At very high flow rates, such as $\lambda = 4.0 \times 10^4$, the flow rate is high enough to see a temperature change as it is now the same magnitude as the wall losses.

Figure 3.15 shows the change in gas composition with a change in the inlet flow rate. At low flow rate, most of the oxygen is consumed by the fuel cell stack. Therefore, the mass fraction of oxygen drops significantly, especially at high current. In a coupled model, the reduced oxygen concentration will limit

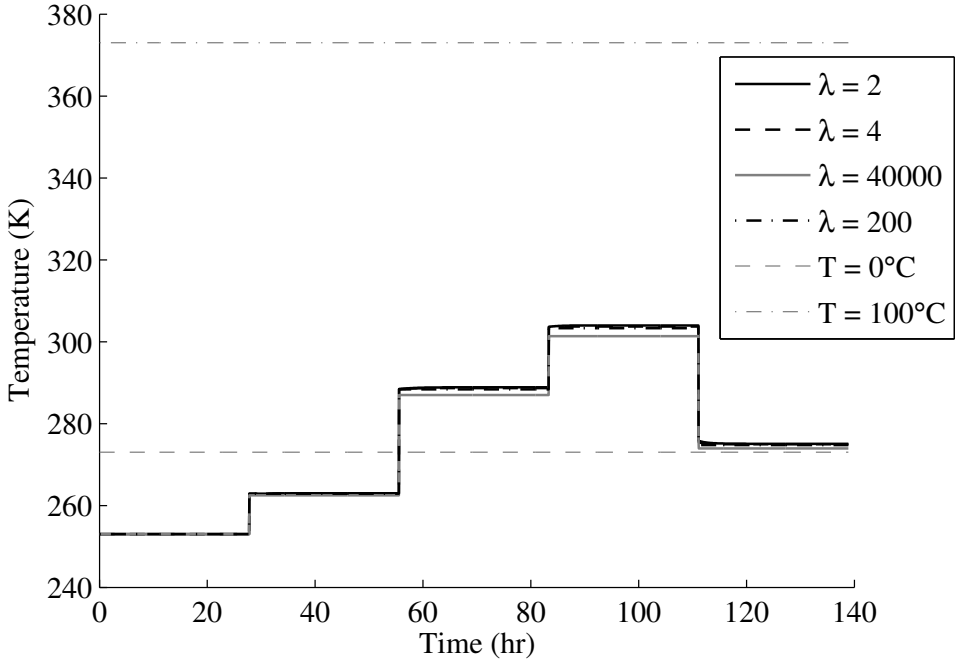

Figure 3.14 – Effect of Inlet Mass Flow Rate on Enclosure Temperature

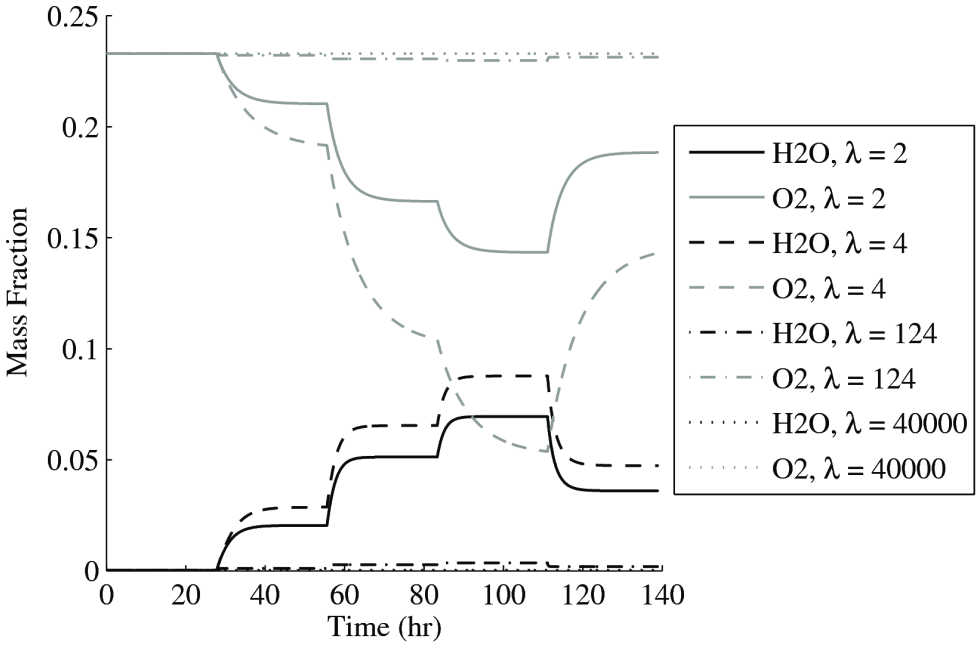

Figure 3.15 – Effect of Inlet Mass Flow Rate on Enclosure Gas Composition

the performance of the fuel cell stack. The mass fraction of water increases because it is produced by the stack. The changes in the gas composition are also affected by phase change.

3.5.3 Ambient Conditions

Ambient Temperature

The environment in which the enclosure will be installed can experience widely fluctuating temperatures through out the year. This will affect the heat transfer between the enclosure and the environment and therefore the temperature inside the enclosure. At colder temperatures, there is an increase in heat transfer between the enclosure and the ambient environment which can lead to the temperature inside the enclosure dropping below acceptable operating temperature. Figure 3.16 also shows that at low ambient temperatures, this enclosure design is not capable of heating sufficiently at low current and will freeze as the temperature inside reaches values below acceptable operating condition for the stack. The change in temperature affects the other variables as explained in the preceeding sections.

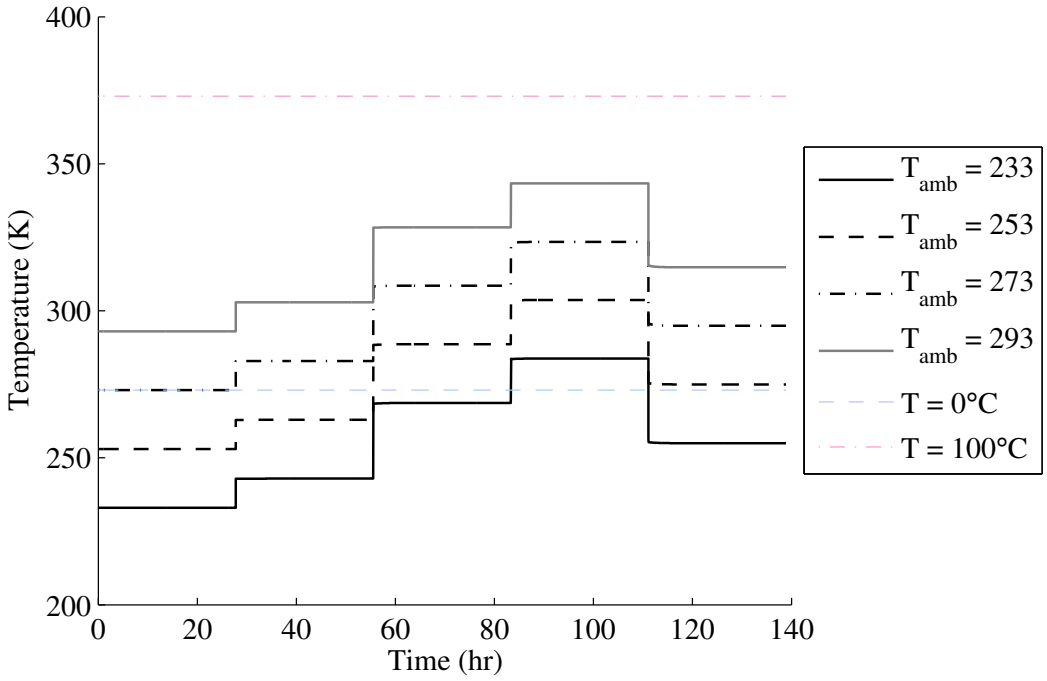

Figure 3.16 – Effect of Changing Ambient Temperature on Enclosure Temperature

Ambient Relative Humidity

At temperatures below 0℃ the saturation pressure is very low. Therefore, regardless of the relative humidity, air contains very little water. A change in the relative humidity at low ambient temperature has very little effect on the relative humidity of the enclosure, therefore the effect of changing the relative humidity of the ambient air was tested for an ambient air temperature of 293K. Figure 3.17 shows the relative humidity of the enclosure increases with increasing ambient relative humidity.

The relative humidity inside the enclosure is only slightly affected by the ambient relative humidity when the stack is operating. The relative humidity in the enclosure is only affected by the ambient relative humidity when the stack is not operating.

The enclosure temperature is not affected by a change in the relative humidity of the enclosure, unless considerable condensation or evaporation occurs because the energy released during condensation in this parametric study is two orders of magnitude less than the wall losses.

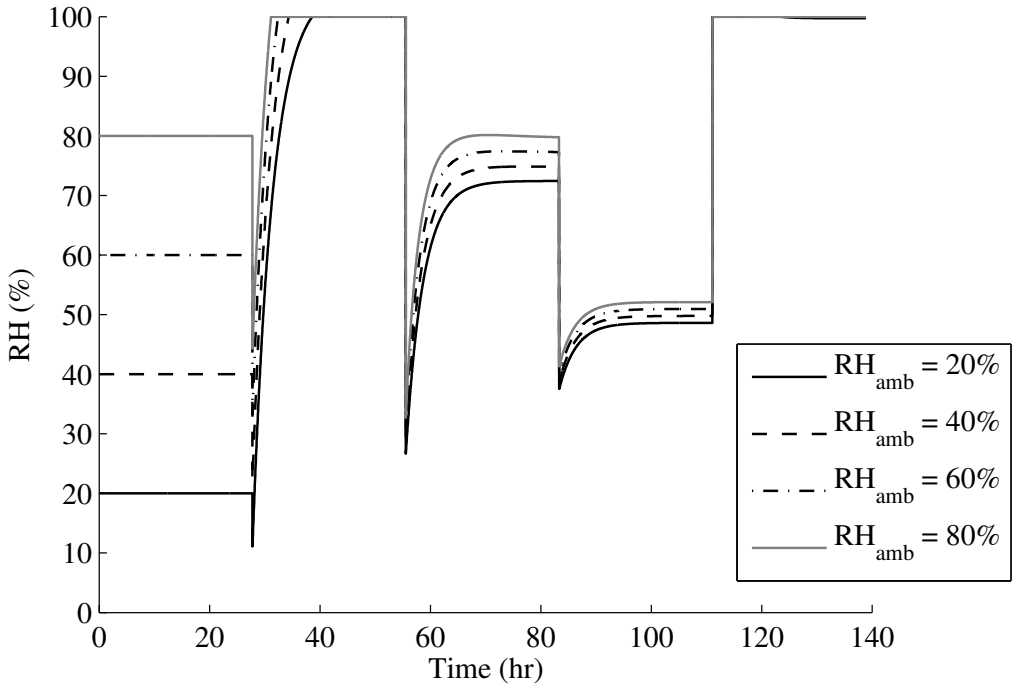

Figure 3.17 – Effect of Changing Ambient Relative Humidity on Enclosure Relative Humidity with T_{amb} = 293K

Chapter 4

Experimental Setup

To characterize the Horizon H-12 Fuel Cell Stack, several experiments were completed. This chapter describes the experimental setup and methods used to characterize the fan in the fuel cell stack and in the enclosure, and the experimental setup and methods used to characterize the fuel cell stack and the enclosure. The equipment and sensors used for the tests are detailed and the setups are illustrated.

4.1 Experimental Setup for Fan Air Speed

The open-cathode fuel cell stack uses a fan to pull air through the cathode channels to deliver oxygen to the cathode catalyst layer and cool the stack. To properly characterize a fuel cell stack, it is necessary to know the flow rate of air through the cathode channels. Therefore, the fan (SNOWFAN: YY4010H5), shown in Figure 4.1, is tested to determine its flow speed for varying voltage input conditions. With this information, it is possible to calculate the flow rate of air through the cathode channels and set the flow rate during fuel cell operation at a given stoichiometry.

The same type of fan is also used to circulate air within the enclosure to control the gas composition within the enclosure. This gas composition will affect the performance of the fuel cell stack as the enclosure air is delivered to the cathode channels of the fuel cell stack. Therefore, the air speed of the fan at the enclosure inlet is also characterized.

A test set up to characterize the fuel cell stack fan is developed based on the Standard Test Method for Average Velocity in a Duct Using a Thermal Anemometer, ASTM D3464-96(2007). A square duct with the same height and width as the fan diameter is fitted to capture the down stream flow from

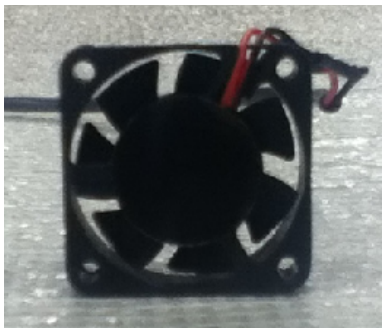

Figure 4.1 – Fan in the Fuel Cell Stack and Enclosure

the fan. The fan remained installed in the fuel cell stack to ensure that the effect of the fuel cell stack bulk and geometry would be characterized in the fan flow rate. As the fan must draw air through the small fuel cell channels, this the fuel cell geometry affects the outlet flow rate of the fan. The experimental setup is modified to characterize the fan installed in the enclosure by installing it upstream of the same square duct, and installing a length of tube in front of the fan to mitigate entrance effects.

The duct is constructed of lengths of cardboard folded into square tube with dimensions of 1 9/16“ (39.7mm) and connected at joints to reach a length of 2.7m. Per ASTM D3464-96(2007), which is applicable for standard air between 0℃ and 65℃, flow measurements are to be taken at least eight equivalent diameters downstream of the fan. Flow measurements were taken at 3cm (67 equivalent diameters) from the end of the square tube. Flow measurements are to be taken at several points in the cross-sectional area of the duct to determine the average flow velocity of the air in the duct. Flow measurements were taken at the centre of the tube, across the width at increments of 3/16” (4.8mm), to characterize the flow profile through the channel.

The fan in Horizon H-12 Fuel Cell Stack is electrically connected to the fuel cell stack so that during operation of the stack it will operate by drawing current from the power produced by the stack. In order to control the fan, it is disconnected from the fuel cell stack and connected to an external electrical circuit with a variable voltage controller. A multimeter is used to measure the voltage set by the variable voltage controller.

The voltage of the fan is controlled using a variable voltage regulator and a multimeter. By changing the voltage, the fan speed changes. A multimeter (Amprobe, model:DM9C) is used to measure the voltage. It has a range of 0V - 600V with an accuracy of ± (0.8% rdg + 3 dgts).

The air speed in the duct is measured using a hot wire anemometer (VelociCheck, model: 8330) with a flow range of 0 - 20m/s. The accuracy of the hot wire anemometer is the greater of ±5.0% of the reading or ±0.025m/s. The hot wire anemometer determines the flow rate of the air in relation to the change in the resistance of the wire due to the temperature change of the wire caused by the air flow. The anemometer has two measurement settings: fast and slow. The fast measurements displays the average air speed of the previous 3 seconds, and the slow measurement displays the average air speed of the previous 12 seconds.

This hotwire anemometer is also used to measuring the ambient temperature of the room, with a range of -18 to 93℃ and an accuracy of ±1℃.

To correct for actual velocity from standard velocity for the hotwire anemometer, the actual temperature and pressure are used in a density correction factor. The standard conditions for the VelociCheck hot wire anemometer are 21.1℃ and 101.4kPa. The velocity correction is:

$$v_{act} = v_{std} \left(\frac{273 + T}{273 + 21.1} \right) \frac{101.4}{P} \tag{4.1}$$

where v_{act} is the actual velocity, v_{std} is the velocity at standard conditions, T is the actual temperature in ℃ and P is the actual pressure in kPa.

Figure 4.2 shows the experimental set up for characterizing the fan when installed in the fuel cell stack.

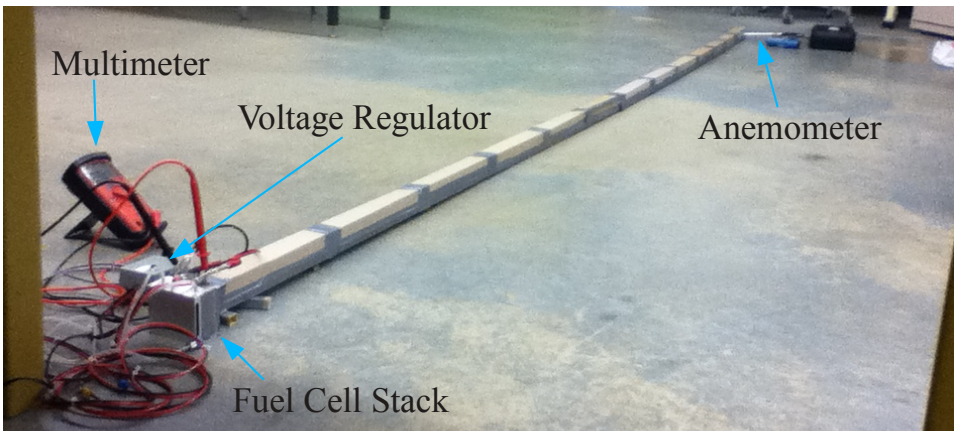

Figure 4.2 – Experimental Setup for Fan in the Fuel Cell Stack

4.1.1 Experimental Procedure

For the case of the fan in the fuel cell stack, the long, square cardboard tube is affixed to the fan front of the fuel cell stack where the fan downstream flow occurs. For the case of the fan for the enclosure, the fan is placed facing downstream into the square cardboard tube, and a 25cm length of tube is installed upstream of the fan.

The variable voltage controller is turned on and set, using the multimeter, to the desired voltage. The fan is connected to the voltage controller. The hotwire anemometer is turned on and the ambient temperature is recorded. The ambient pressure is assumed to be the ambient pressure for Edmonton for the date and time of testing, as reported by Environment Canada [77]. The hotwire anemometer is inserted into the tube with the wire perpendicular to the air flow. The room temperature, pressure and anemometer installation location are controlled variables and maintained constant.

The variable voltage controller is used to modify the voltage through the fan in steps of between 0.3-0.4V. Therefore, the voltage input is the manipulated variable. The fast measurement method, where the air speed displayed is the average of the previous 3 seconds, is used because it showed the rapid fluctuations in the air speed. The air speed measurement is the responding variable, and is recorded when the fast measurement reached steady-state. At high voltage and air speed, the air speed fluctuates significantly, often through a range of $\pm$ 0.6m/s. An time weighted average value of the air speeds reported over 1 minute of operation is recorded for the cases with highly fluctuating air speeds.

4.1.2 Post Processing

Air delivered to the fuel cell stack provides oxygen to the cathode channels to produce power through an electrochemical reaction. When studying the fuel cell stack, the mass flow rate is required to determine the stoichiometric ratio of oxygen supplied to the stack to ensure that the stack is receiving sufficient oxygen for the reaction. Additionally, to study the mass transport and energy transfer within the stack, the mass flow rate of air into the channels is an important input parameter. The mass flow rate of air in the channels is necessary to determine the stoichiometric ratio of oxygen available to the fuel cell stack for the electrochemical reaction which produces power.

To determine the mass flow rate of air in a channel of the fuel cell stack,

the measured maximum air speed output by the fan needs to be converted to the cathode channel speed. As the flow has been assumed to be laminar, the average velocity can be defined as [41]:

$$u_{avg} = \frac{1}{2} u_{max} \tag{4.2}$$

It is assumed that the flow output from the fan is the sum of the flow through all the cathode channels in the stack. This relationship is expressed in equation (4.3)

$$u_{ca} = \frac{u_{avg} A_{fan}}{A_{ca} n_{chan} n_{cell}} \tag{4.3}$$

where u_{ca} is the flow speed in a channel in m/s, u_{avg} is the average fan speed in m/s computed from equation (4.2), A_{fan} is the cross-sectional area of the fan in m^2, A_{ca} is the cross-sectional area of a channel in m^2, n_{chan} is the number of channels per cell, and n_{cell} is the number of cells in the stack.

The mass flow rate of air in a channel, $\dot{m}_{air,in}$, in the fuel cell stack can be calculated for a given voltage by (4.4):

$$\dot{m_{air,in}} = \rho_{air} u_{ca} A_{ca} \tag{4.4}$$

where ρ_{air} is the air density in kg/m^3, which is obtained using the room temperature and pressure conditions.

Error Analysis

The total error reported for the air speed measurements taken by the hotwire anemometer consists of the uncertainty due to the accuracy of the hotwire anemometer and a 95% confidence student's t-test for the deviation of the measurements, as in equation (4.5):

$$\omega_u = \left(\omega_a^2 + \omega_d^2\right)^{1/2} \tag{4.5}$$

where ω_u is the total error in the air speed measurement, ω_a is the accuracy uncertainty and ω_d is the uncertainty in the deviation of the measurements with 95% confidence as defined by the student's t-test. The 95% confidence interval is calculated by the student's t-test as [78]:

$$\omega_d = t_{\alpha,\nu} S_x \tag{4.6}$$

where S_x is the standard deviation of the measurements for the variable x, and $t_{\alpha,\nu}$ is the student's probability t as a function of α, which represents the 95% confidence level, and ν which is the number of degrees of freedom which is calculated as one less than the number of measurements taken, $\nu = n - 1$.

4.2 Experimental Setup for Stack Testing

Two sets of experiments will be conducted to characterize the open-cathode fuel cell stack and the enclosure. First the fuel cell stack will be tested without the enclosure to fully define the fuel cell stack characteristics. Then, the fuel cell stack will be tested inside the enclosure to develop a detailed model of the enclosure and stack system. The specifications for all the equipment mentioned in this section are detailed in the System Components and Equipment Section 4.2.1 or in the preceeding Experimental Setup for Fan Air Speed Section 4.1

The open-cathode fuel cell stack performance depends on the ambient conditions in which it operates. Therefore, an experimental set up is developed to test the performance of the fuel cell stack in a variety of ambient conditions ranging from -20℃ to 30℃, and 30% to 90% relative humidity. The fuel cell stack is installed in an environmental chamber which supplied the varying operating conditions. The effect of changing the air inlet flow rate to the fuel cell stack is also tested by varying the air speed of the fan in the fuel cell stack which draws air through the cathode channels. Depending on the desired study, one of: the temperature, relative humidity, and fan inlet flow rate, is manipulated while the others are controlled at constant conditions.

A prescribed current is applied to the fuel cell stack in steps for a given time. The same prescribed current steps are applied for each test. Therefore, when comparing the results from one step to the next for a given test, the current is a manipulated variable. When comparing results between two tests for the same current step, the current is a controlled variable. The anode inlet conditions: hydrogen temperature, flow rate and relative humidity, are all controlled. The measured responding variables are: stack voltage, stack temperature, cathode outlet temperature and cathode outlet relative humidity.

Figure 4.3 is a diagram of the instrumentation installed during a stack test, and Figure 4.4 shows a photo of the full installation. Figure 4.5 shows a photo detailing the fuel cell stack instrumentation installation. The solid flow lines in the diagram (orange insulated lines in the photos) carry hydrogen from the compressed hydrogen bottle to the test station which controls the flow to the stack. Any unreacted hydrogen is carried out of the stack and vented. The dashed load lines (red and black cables in the photos) draw a prescribed current from the stack. The fan on the fuel cell stack is controlled by the voltage controller. There are also voltage sense cables which transmit the voltage of the stack to the test station. A T-type thermocouple is sealed

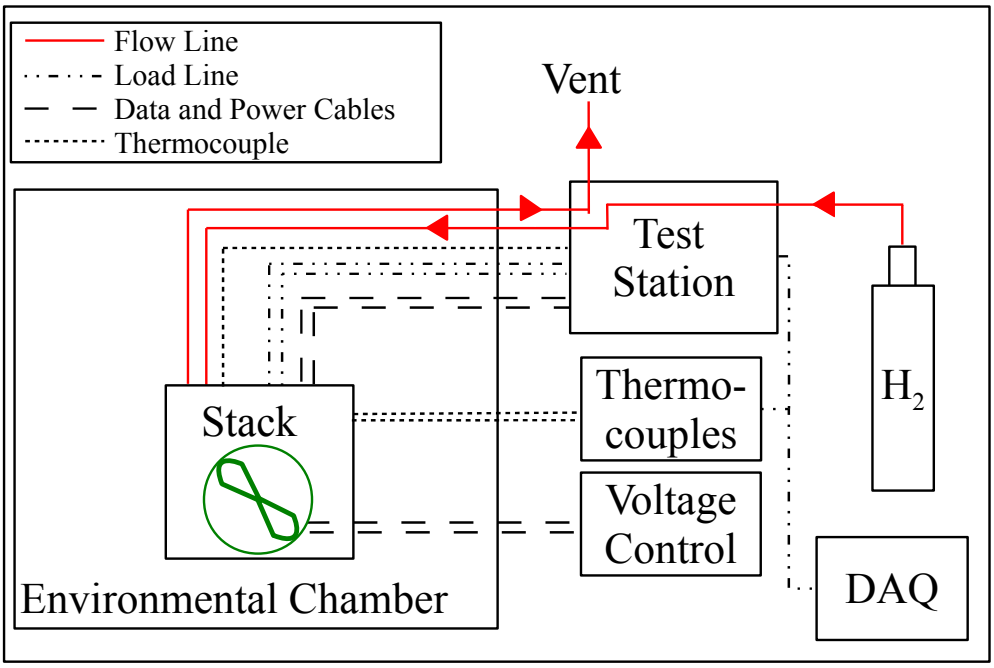

Figure 4.3 – Stack Testing Instrumentation

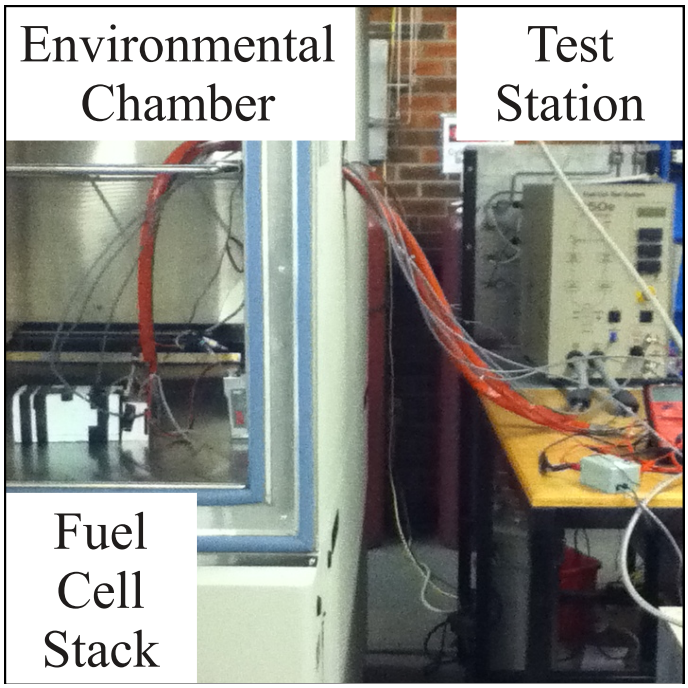

Figure 4.4 – Experimental Setup for Fuel Cell Stack

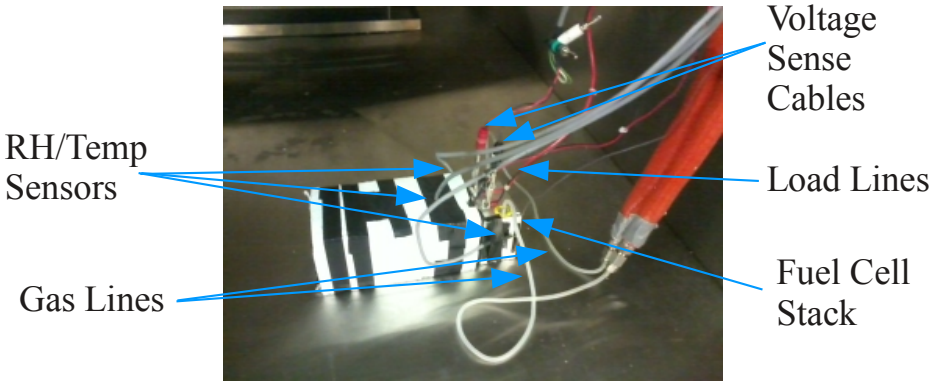

Figure 4.5 – Fuel Cell Stack Temperature/RH Sensor Setup

into one of the cathode channels and transmits the temperature of the stack, T_{stack} to the test station.

For the fuel cell stack tests, two Sensirion relative humidity sensors are installed at the inlets to the fuel cell stack, as shown in Figure 4.5. The data from these two sensors is averaged to determine the temperature, T_{in}, and relative humidity, RH_{in} of the ambient air that enters the fuel cell stack cathode channels and surrounds the fuel cell stack. A third sensor is used to measure the temperature, T_{out}, and relative humidity, RH_{out}, of the outlet air from the fuel cell stack. It is therefore placed inside an insulated tube which is attached to the outlet of the fuel cell stack to capture the outlet flow from the fuel cell stack, as shown in Figure 4.5

4.2.1 System Components and Equipment

Environmental Chamber

For testing in variable environment conditions, the fuel cell stack is installed in a Cincinnati Sub-Zero ZP-Series Environmental Chamber (model: ZPH-32-1.5-H/AC) [79]. This environmental chamber is able to regulate the temperature and relative humidity in its interior to provide varying surrounding and input conditions to the fuel cell stack. It has an operating range of -34℃ to +190℃, with a humidity range of 10% to 98% for 10℃ and warmer. Humidity cannot be actively controlled below 10℃.

Fuel Cell Test Station

The fuel cell stack is connected to a Fuel Cell Test System (FCTS), (Scribner Associates, Model 850C Compact Fuel Cell Test System) [80]. The open-cathode fuel cell stack testing makes use of the following capabilities of the FCTS: imposed fuel cell load, and anode gas mass flow, relative humidity, and temperature control. The software program supplied by Scribner Associates for the FCTS is used to test the fuel cell stack by controlling the conditions and recording the results.

As the stack has an open-cathode design, only the hydrogen supply is controlled by the FCTS. A mass flow controller in the FCTS is used to set the flow rate of hydrogen, from a compressed gas cylinder, to the fuel cell stack. For these experiments, the flow stoichiometry is set constant, so the flow rate changes with a change in current, and for a given current the flow rate will be constant. The FCTS also has the ability to control the temperature and humidity of the inlet gas to the anode. For these experiments, the fuel cell stack is run with dry hydrogen, so no water vapour is added to the hydrogen. The ability of the FCTS to control the temperature of the anode inlet gas is limited, however, as it only has a heater. Therefore, the inlet gas cannot be supplied at temperatures lower than room temperature, and is often supplied at temperatures above room temperature due to heat generated by the system.

The fuel cell load control is used to specify a load current for the stack to obtain, and the performance at varying load conditions is studied.

The software for the FCTS records these input conditions to the fuel cell stack, as well as the following performance output conditions: cell and stack voltage, cell and stack power, and cell/stack temperature. The fuel cell stack temperature is measured via a T-type thermocouple which is sealed into one of the open-cathode channels. The FCTS is also capable of measuring the stack resistance using the current interrupt method. However, the current interrupt method requires short cable lines to prevent noise [81], and this experimental set up required long cables to reach into the environmental chamber. Therefore, the stack resistance reported by the FCTS is not used for validation due concerns about its validity.

Temperature and Relative Humidity Sensors

The temperature and relative humidity of air in various locations is measured using Sensirion digital humidity sensors. The Sensirion SHT71 is a capacita-

tive, pin-type relative humidity and temperature sensor which has a relative humidity operating range of 0 to 100% and an accuracy of ± 3% between 20 - 80 % relative humidity and up to ± 5% for 80 - 100 % [82]. It has a temperature operating range of -40 to 125 ℃, with a minimum accuracy of ± 1.8 ℃ for the temperature range that the fuel cell stack will be tested [82].

Oxygen Sensor

In order to ensure that the fuel cell stack is obtaining sufficient oxygen when it is installed in the enclosure, it is necessary to monitor the oxygen concentration of the gas in the enclosure. For the fuel cell stack in enclosure tests, an Ocean Optics oxygen sensor is installed in the enclosure to measure the response of the oxygen concentration in the enclosure to the changing conditions.

The Ocean Optics FOXY-R is a fiber optic oxygen sensor that determines the oxygen concentration based on how much the oxygen quenches the fluorescent top of the blue LED probe [83]. The sensor has a range of 0-100% in a temperature range of -50 to +80℃, and an accuracy of 5% of the reading.

4.2.2 Fuel Cell Stack

A Horizon H-12 Fuel Cell Stack is tested to provide data for characterization and validation of the fuel cell stack and enclosure/stack models. This PEM fuel cell stack is open-cathode (air-breathing) and air-cooled via a fan, and its only source of humidification is the water vapour in the ambient air [70]. The

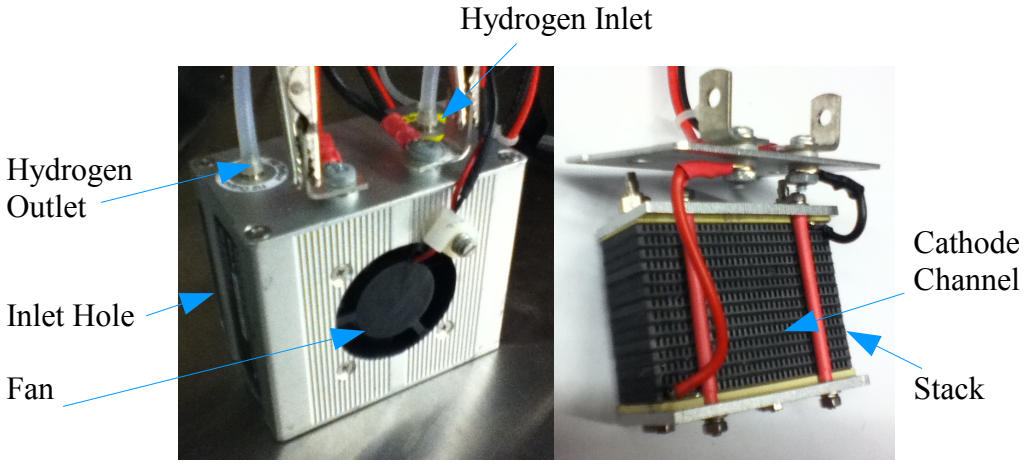

Figure 4.6 – Enclosure

stack consists of 13 cells and has a power rating of 12W, at a rated performance of 7.8V at 1.5A [70]. The size of the stack is 75x47x70mm and it weighs 275g [70]. The optimal operating conditions for the stack are between 5 to 30℃, with a maximum stack operating temperature of 55℃[70]. Figure 4.6 shows a picture of the PEM system and the stack inside.

4.2.3 Enclosure

To protect the fuel cell stack from cold temperatures which are outside of its ideal operating conditions, the fuel cell stack is placed into an enclosure. Two cubic enclosures were built out of Plastispan© extruded polystyrene (EPS) rigid insulation board [75]. Figure 4.7 shows the two enclosures; one an 11" × 11" × 12" (28cm × 28cm × 30.5cm) cuboid with 1" (2.5cm) thick walls and an RSI value of $1.0 W/m^2K$, the second a 13.5" × 13.5" × 13.5" (34cm × 34cm × 34cm) cuboid with 2" (5.1cm) thick walls and an RSI value of $1.42 W/m^2K$.

Each enclosure had a cutout where the enclosure inlet fan is installed, a cutout for the enclosure outlet, and a cutout through which all the tubing and wires for the fuel cell stack is passed. The inlet fan for the enclosure (SNOWFAN: YY4010H5S) is characterized during the fan speed tests and has an operational temperature range of -10℃ to +50℃ [84].

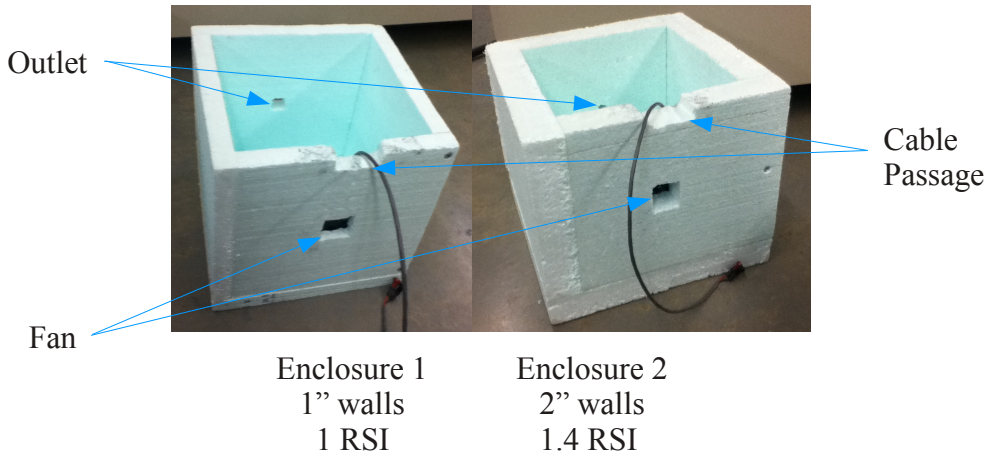

Figure 4.7 – Enclosure

4.3 Experimental Setup for Enclosure/ Stack Testing

For the enclosure/stack tests, the fuel cell stack is installed in the enclosure with the instrumentation also passing into the enclosure. Figure 4.8 shows a photo of the fuel cell stack installed in Enclosure 1, and Figure 4.9 is a diagram of all the instrumentation installed during the enclosure/stack tests. All the lines and cables required to run and collect data for the fuel cell stack, as detailed in Section 4.2, were required. Additionally, two Sensirison humidity sensors were installed inside the enclosure at different location, as shown in Figure 4.10, and their data is averaged to determine the average temperature and relative humidity inside the enclosure. The enclosure conditions are responding to changes in input conditions. A third sensor is placed at the inlet to the enclosure to measure the temperature and relative humidity of the air entering the enclosure, which are controlled variables. An oxygen sensor is also installed in the enclosure to measure the response of the oxygen concentration in the enclosure to condition changes.

Figure 4.8 – Photo of Enclosure/Stack Installation During Testing

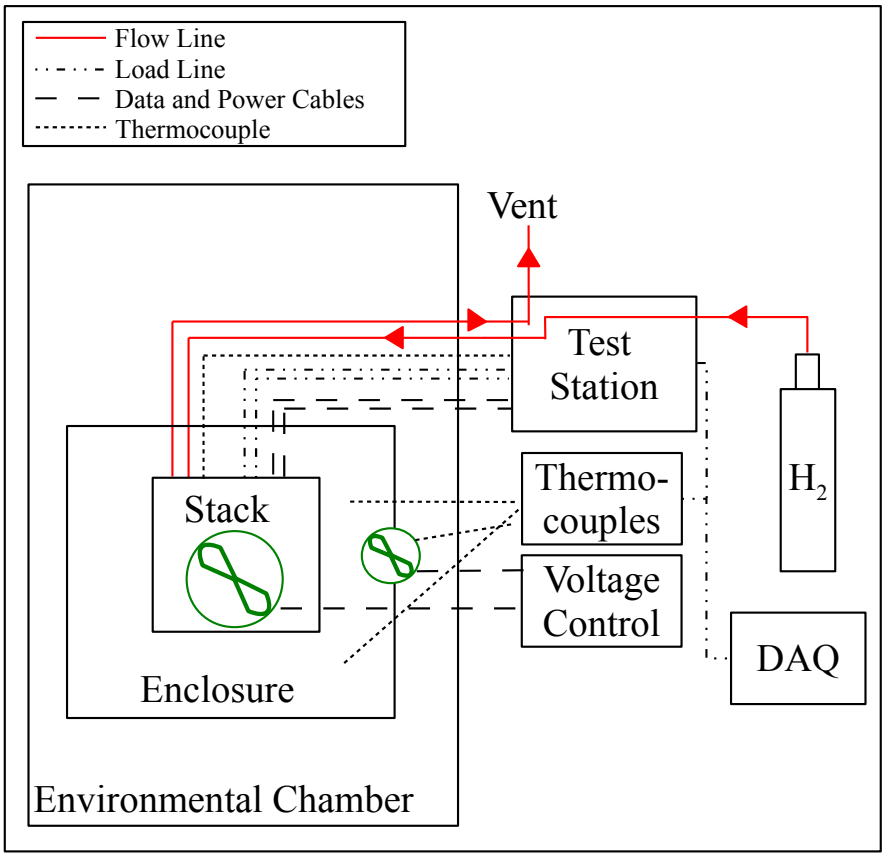

Figure 4.9 – Enclosure/Stack Instrumentation

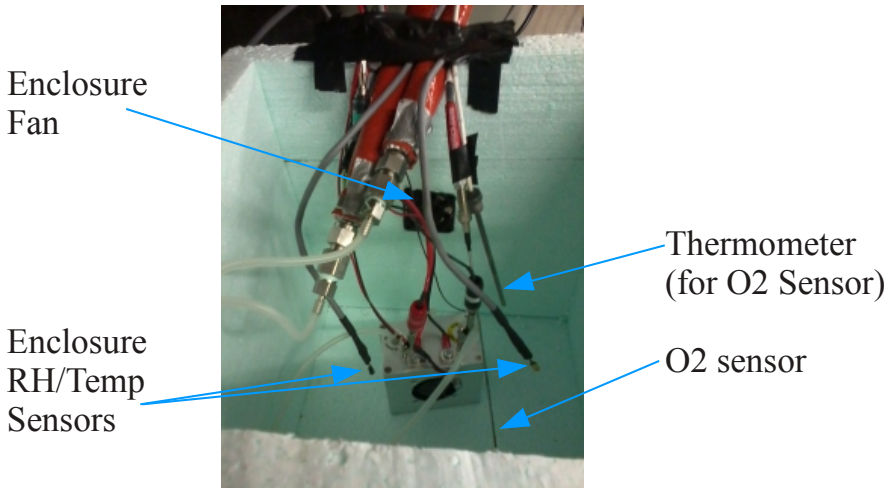

Figure 4.10 – Photo of Temperature/RH Sensor Installation in Enclosure

Chapter 5

Results and Discussion

The stack and enclosure were tested using the experimental setup and procedure outlined in Chapter 4. This chapter presents the experimental results for the characterization of three aspects of this thesis: the fan in the fuel cell stack and enclosure, the fuel cell stack, and the fuel cell stack in the enclosure. The first part of this chapter details the characterization of the fan which was used to supply air to the fuel cell stack and to the enclosure. The second part presents the results of the stack characterization experiments and parametric fitting of the Horizon H-12 Fuel Cell Stack using the mathematical model developed in Chapter 2. The third part of this chapter presents the results of experiments with the fuel cell stack installed in the enclosure. These experimental results are compared with the results predicted by a coupled fuel cell stack (Chapter 2) and enclosure (Chapter 3) mathematical model.

5.1 Fan Characterization

To characterize the fan (SNOWFAN: YY4010H5) used in the fuel cell stack and in the enclosure, the fan was tested following the experimental procedure outlined in Chapter 4. The purpose of characterizing the fan is to determine the relationship between the input voltage to the fan and the mass flow rate of air through the fan into the fuel cell stack or enclosure. The mass flow rate of air flowing through the fuel cell stack cathode channels is critical for both reactant delivery and cooling the fuel cell stack. The air flow into the enclosure is important for adequate oxygen availability in the enclosure and to cool the air in the enclosure.

5.1.1 Fuel Cell Stack Fan

When the fan is installed in the fuel cell stack, the air is drawn through the channels of the fuel cell stack by the fan. The presence of the fuel cell stack creates a large pressure drop which affects the flow rate through the fan. Thus the fan is installed in the fuel cell stack to characterize this case.

To ensure the validity of the measurements taken, a test of the effect of location on the flow velocity was completed. The test showed that the flow velocity varies along the width of the tube, as expected for a fully developed flow profile. In Figure 5.1, the measured flow profile is compared to a parabolic flow profile which is the expected profile for the laminar flow observed in this case. The measured profile closely approximates the laminar parabolic flow profile, therefore the flow in the channel can be assumed laminar, fully developed and this method of measurement of the flow rate of the fan is acceptable. The vertical error bars in Figure 5.1 indicate a 95% confidence interval using the student's t-test for the 10 readings taken at each location and the hotwire anemometer accuracy. The horizontal error bars in Figure 5.1 represent the non-dimensionalized equivalent of ±1mm, which accounts for human variability when using a standard ruler to set the location of the anemometer probe

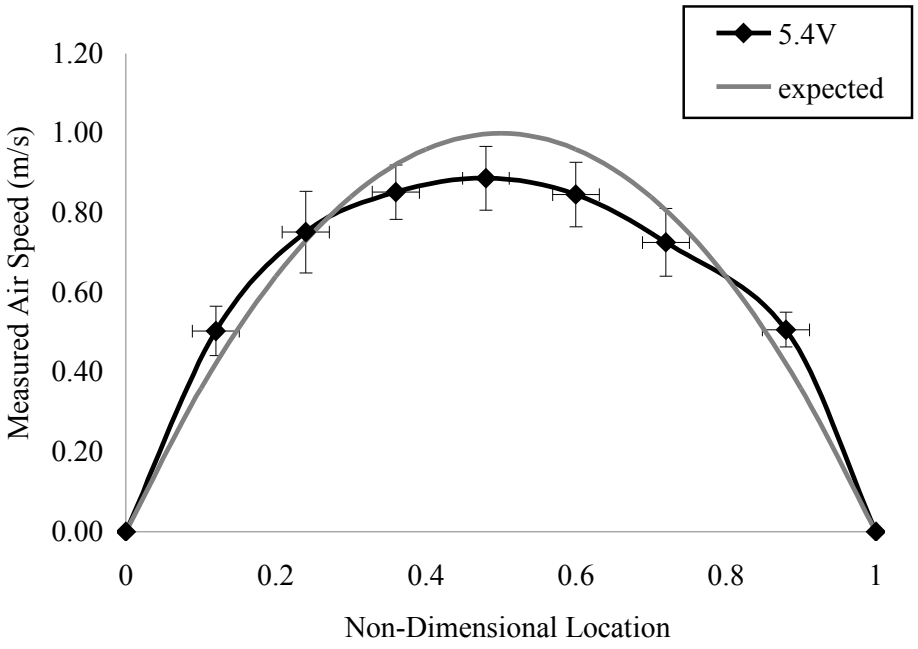

Figure 5.1 – Flow Profile of Tube Cross-Section for Fan in Fuel Cell Stack

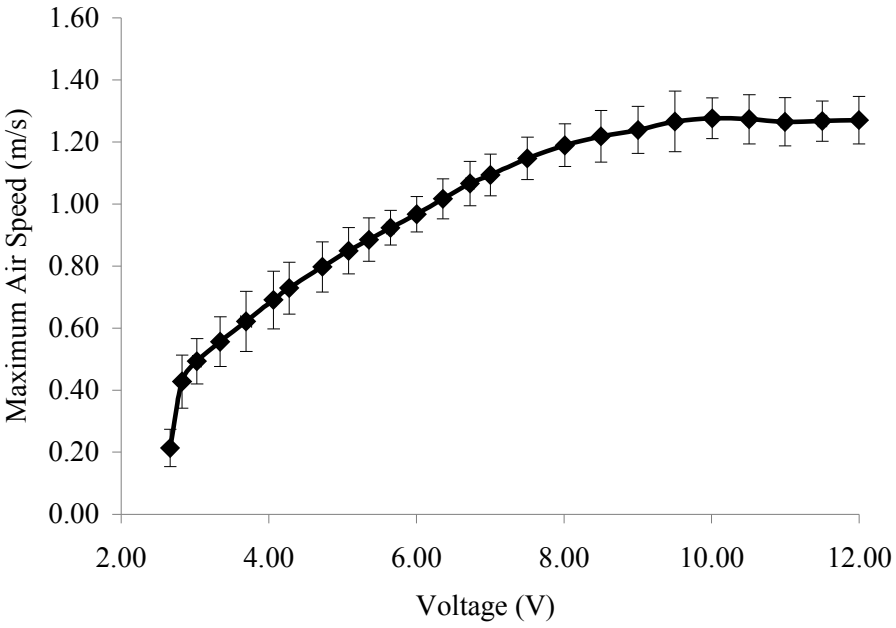

Figure 5.2 – Average Fan Air Speed

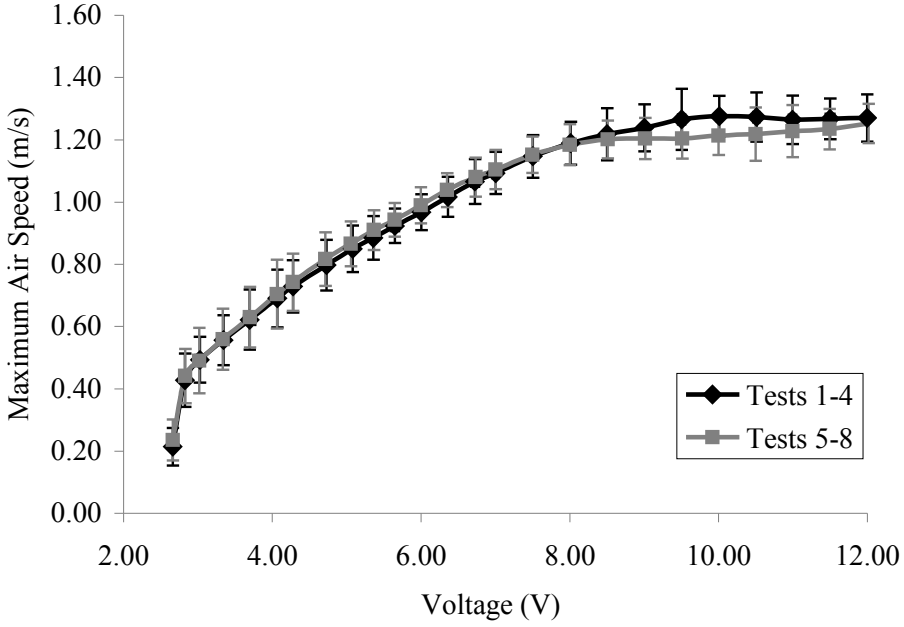

Figure 5.3 – Fan Air Speed Repeatability Study

inside the tube.

Figure 5.2 shows the maximum air speed in the tube averaged from four different voltage sweeps obtained by placing the hotwire anemometer into the centre of the tube. The maximum air speed in the tube was measured at several voltages while sweeping from 2.66V (the minimum voltage where the fan would operate) up to 12.0V. The error bars represent a 95% confidence interval for the readings calculated by the student's t-test and the accuracy of the hotwire anemometer, as computed by equation (4.5). To ensure the results were not influenced by the experimental setup, the test was repeated with four additional sweeps, and the results of the two tests are compared in Figure 5.3.

From this characterization of maximum flow through the fuel cell stack fan, the average flow rate can be determined using equation (4.2). The mass flow rate of the air through the fuel cell stack channels at a given fan voltage can be determined using equation (4.4). Table 5.1 shows the mass flow rate in a cathode channel and the stoichiometric ratio with respect to selected voltages for the fuel cell stack fan, as reported in Figure 5.2. The stoichiometric ratio is determined per channel and is a function of the maximum current, 2A, at which the Horizon H-12 Fuel Cell Stack will be tested.

Table 5.1 – Mass Flow Rate through Fuel Cell Cathode Channels at Selected Fan Voltages

Voltage (V)	*Average Air Speed (m/s)*	*Cathode Channel Mass Flow Rate (kg/s)*	*Reaction Stoichiometry*
2.7	0.18±40.06	0.7×10^{-6}	33
3.3	0.28±40.08	1.1×10^{-6}	51
3.7	0.31±40.10	1.2×10^{-6}	57
4.3	0.37±40.08	1.4×10^{-6}	67
4.7	0.40±40.08	1.6×10^{-6}	74
5.7	0.46±40.06	1.8×10^{-6}	85

5.1.2 Fan in Enclosure

A fan (SNOWFAN: YY4010H5) is installed in the enclosure to provide air from the environment to the enclosure. This will help to maintain the oxygen concentration in the enclosure at an acceptable level for good stack performance. It may also help cool the enclosure for cases when the external temperature is lower than the enclosure temperature if the fan speed is fast enough.

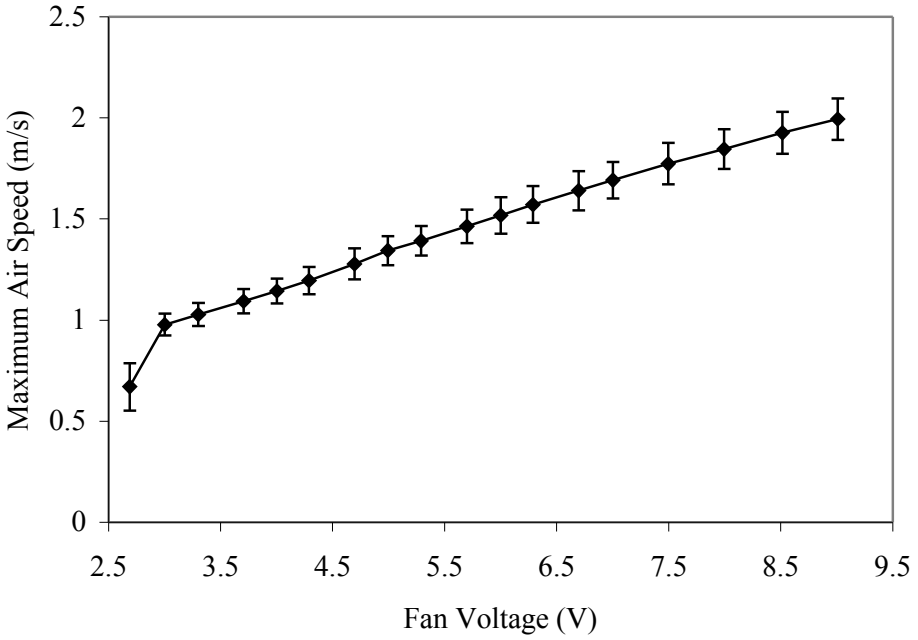

Figure 5.4 – Fan Air Speed When Installed in Enclosure

The pressure drop the fan must overcome is different than for the fan that is installed in the stack. The pressure drop from friction in the tube, which is installed around the fan, is calculated and determined to be negligible. To test the fan for the enclosure case, a length of tube was placed in front of the inlet to the fan to minimize the entrance effects. The maximum air speed was measured at the tube outlet using a hotwire anemometer, following the procedure outlined in Chapter 4.

Figure 5.4 shows the relationship between the fan voltage and the maximum air speed at the fan outlet, where the data presented is the average of 5 tests. The error bars are computed using equation (4.5) and include a 95% confidence interval using the student's t-test for the 5 readings and the hotwire anemometer accuracy. The flow in the channel from the fan is assumed to be laminar and fully developed with a parabolic profile, as it was in the case with the fuel cell stack installed. Therefore, the average flow velocity is one half of the maximum, as expressed in equation (4.2). In comparison with the case with the fan installed in the fuel cell stack, when the fan is installed in the enclosure its flow speed is approximately doubled. Some selected average fan speeds relative to the input voltage are shown in Table 5.2

Table 5.2 – Mass Flow Rate Through Enclosure Fan at Selected Voltages

Voltage (V)	*Measured Air Speed (m/s)*	*Enclosure Inlet Mass Flow Rate (kg/s)*
2.7	0.36±0.11	6.5×10^{-4}
3.3	0.56±0.06	1.0×10^{-3}
4.0	0.61±0.07	1.1×10^{-3}
4.7	0.70±0.08	1.2×10^{-3}
5.7	0.80±0.09	1.4×10^{-3}

5.2 Fuel Cell Stack Experiments

A Horizon H-12 Fuel Cell Stack was tested at varying prescribed currents in a range of operating conditions including different temperatures, relative humidity, and fuel cell stack fan speed. The experimental set up and procedure described in Chapter 4 was used to complete these experiments. The performance of the fuel cell stack in the different conditions was monitored and compared to determine the effect of the operating conditions.

With the exception of the repeatability test, which is an average of 8 tests, the remaining test results presented herein consist of only one test. The limited performance of the environmental chamber used to provide varying environmental conditions surrounding the stack reduced the quantity of data which could reasonably be obtained. Although many tests were taken at the varying conditions, the majority contained severe fluctuations in the performance of the environmental chamber, and averaging these tests did not help to reduce the severity of the fluctuations. Therefore, the tests with the best performance of the environmental chamber are presented here and this is why some fluctuations in the inlet conditions, caused by poor performance of the environmental chamber, are observed in the experimental results in some cases.

5.2.1 Repeatability Test

The repeatability of the fuel cell stack tests was determined by comparing 8 tests of the Horizon H-12 Fuel Cell Stack at the same operating conditions (room conditions, approximately 22℃ and 20%RH, fan speed 0.28m/s). The stack was tested in ascending current steps of 0.4A, with each step lasting 5 minutes, ascending from 0A to 2A and then descending from 2A to 0A in current steps of 0.4A each lasting 8 minutes.

The length of the time steps was selected to be long enough for the stack

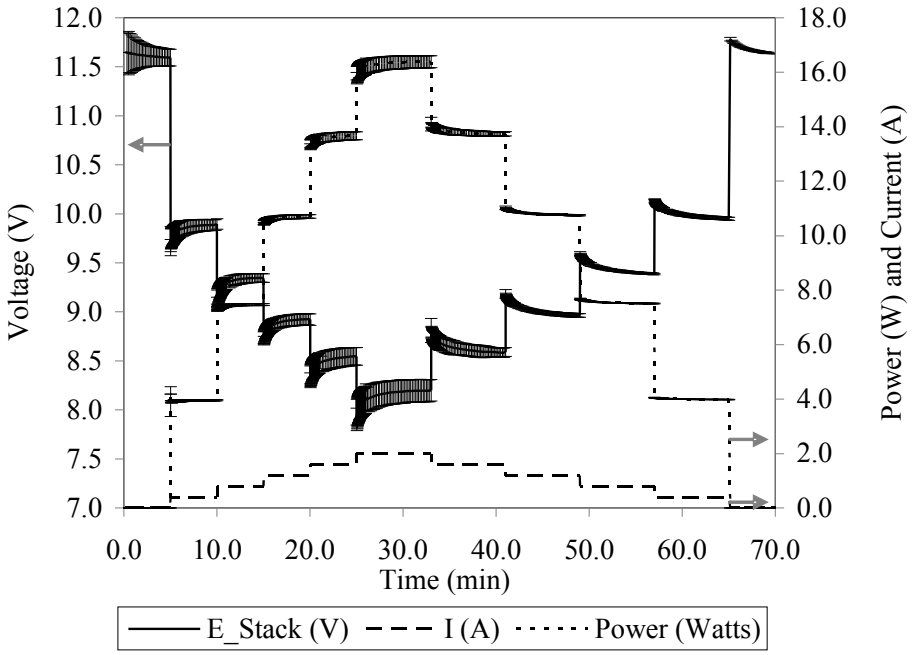

Figure 5.5 – Repeatability of Fuel Cell Stack Performance

voltage and temperature are able to reach steady state. The step gap of 0.4A was selected because it is the maximum current step the stack would reliably achieve. The overarching goal when setting these conditions was to minimize the test time to mitigate the effects of poor environmental chamber performance during long tests.

During the fuel cell stack experiments, the stack voltage and temperature are recorded every second for the first minute of the current step and every 10 seconds for the remaining step time. This sampling rate was selected to obtain good characterization of the transient section. The cathode outlet temperature and relative humidity; and inlet air temperature and relative humidity, are recorded every 10 seconds.

Figure 5.5 shows the average performance of the fuel cell stack and the 95% confidence level obtained from 8 tests using the student's t-test, shown in equation (4.6). The average confidence interval is ±0.06V.

Figures 5.6, 5.7, and 5.8 show the average stack temperature, cathode outlet temperature and relative humidity during operation of the stack at a 95% confidence level for 8 tests using the student's t-test. The confidence interval for each variable varies slightly, but it is approximately ±1.5℃, ±1.5℃, and ±2.4% respectively.

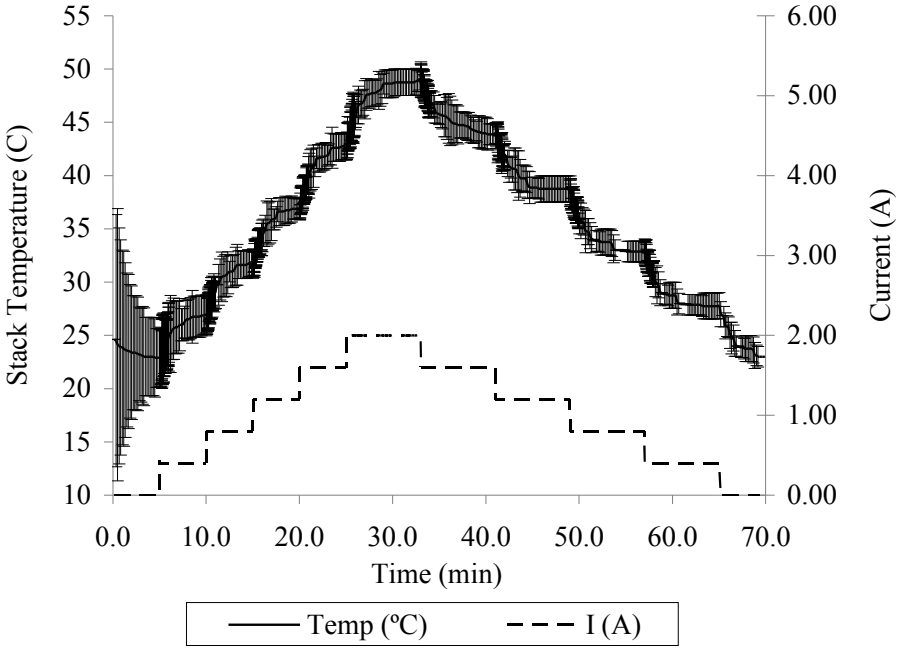

Figure 5.6 – Repeatability of Fuel Cell Stack Temperature

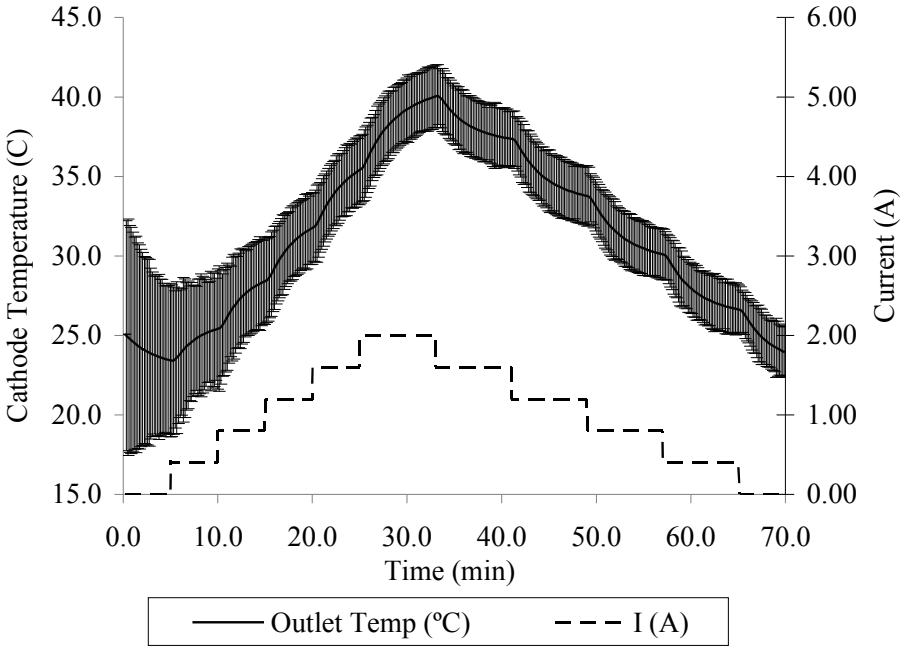

Figure 5.7 – Repeatability of Cathode Outlet Temperature

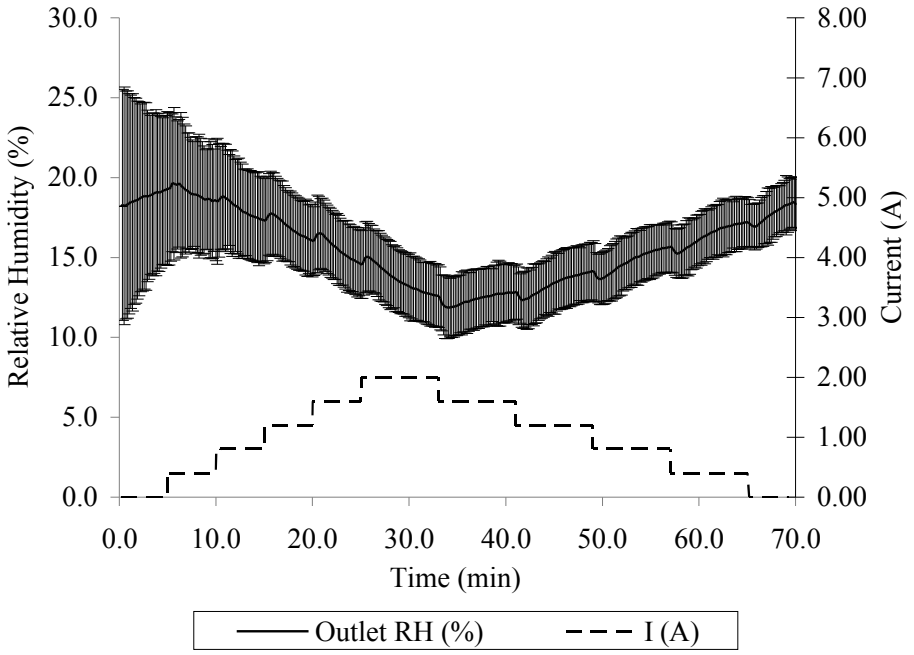

Figure 5.8 – Repeatability of Cathode Outlet RH

These tests show that for a given set of operating conditions, the results from the fuel cell stack experiments are repeatable. Therefore, the results from further tests, taken only once, can be accepted as reasonably accurate.

5.2.2 Effect of Temperature

The fuel cell stack was tested at several operating temperatures: 20℃, 10℃, and 0℃, in the environmental chamber. The same current steps of 0.4A, for 5 minutes, increasing from 0A to 2A, and decreasing in steps of 0.4A, for 8 minutes,from 2A to 0A, as in the repeatability test, were applied. The fan speed was constant at 0.28m/s, and the relative humidity was not set as it is difficult to control at low temperatures.

Figures 5.9 and 5.10 show the temperature and relative humidity inlet conditions for the three tests. It is observed that while the environmental chamber was set at 20℃, 10℃, and 0℃, that thermocouples placed at the inlets to the fuel cell stack consistently read temperatures 2-3℃ higher which is likely caused temperature gradients in the chamber at the specific location where the fuel cell stack and thermocouples were installed. The anode inlet temperature is set at 30℃ because the FCTS is not able to cool the anode

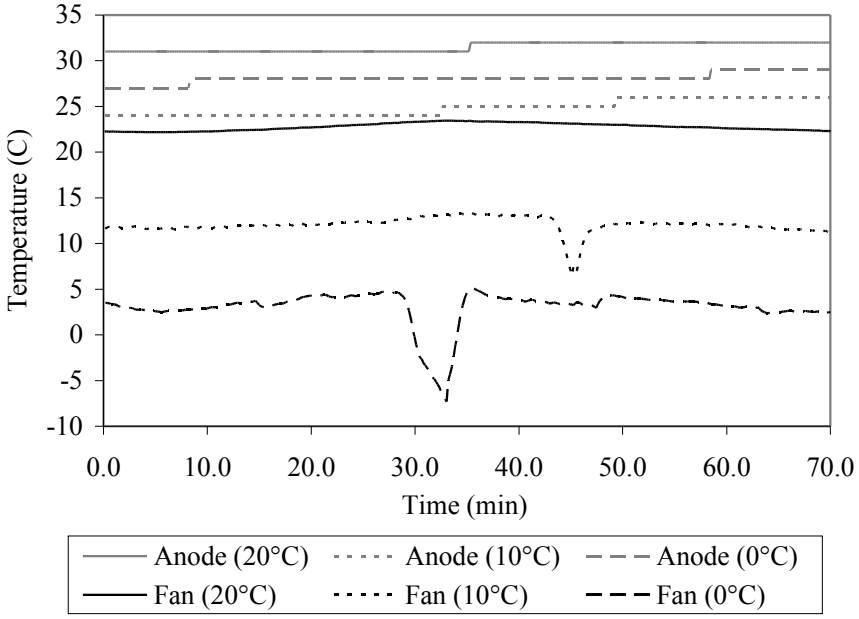

Figure 5.9 – Cathode/Ambient Inlet Temperature During Operation at Varying Ambient Temperatures

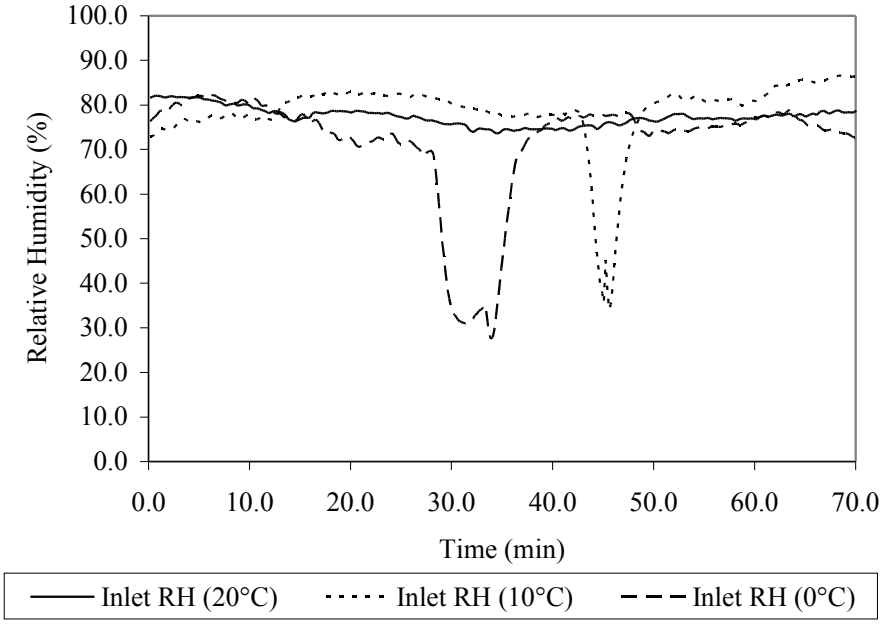

Figure 5.10 – Cathode/Ambient Inlet Relative Humidity During Operation at Varying Ambient Temperatures

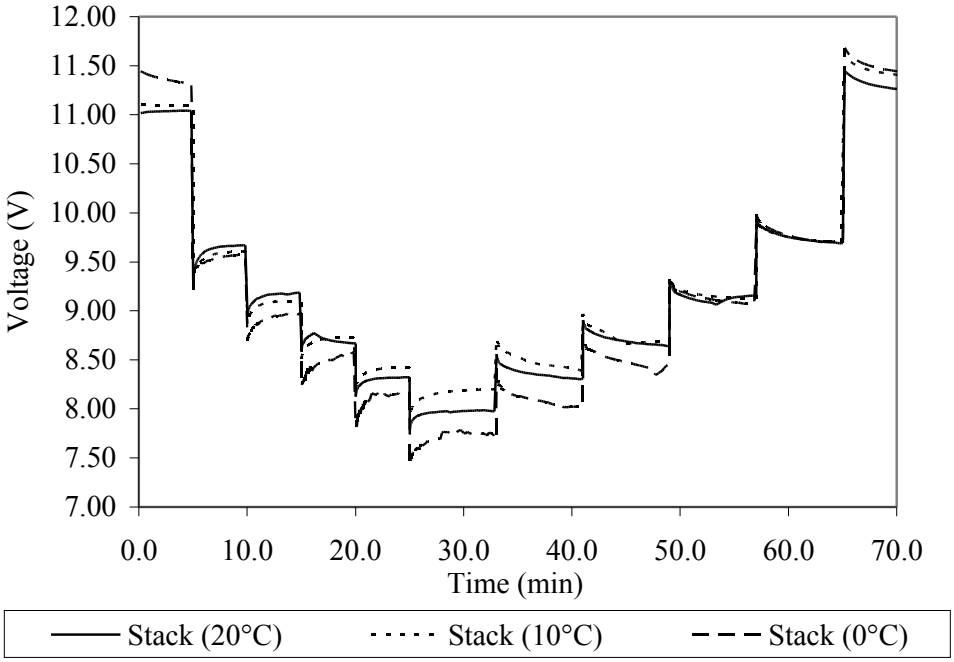

Figure 5.11 – Performance of Fuel Cell Stack at Varying Ambient Temperatures

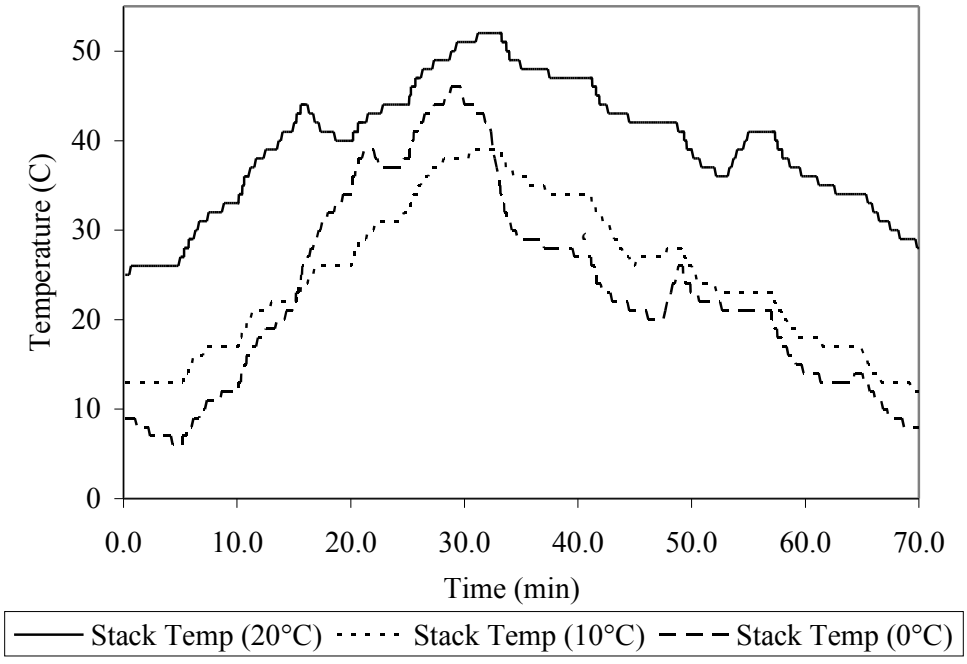

Figure 5.12 – Stack Temperatures During Operation at Varying Ambient Temperatures

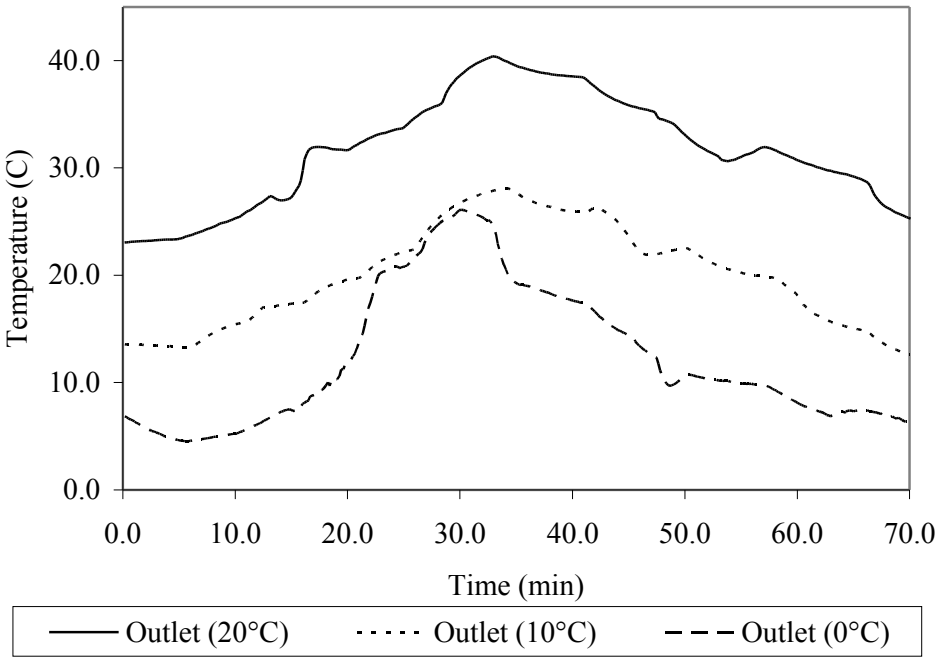

Figure 5.13 – Cathode Outlet Temperatures During Operation at Varying Ambient Temperatures

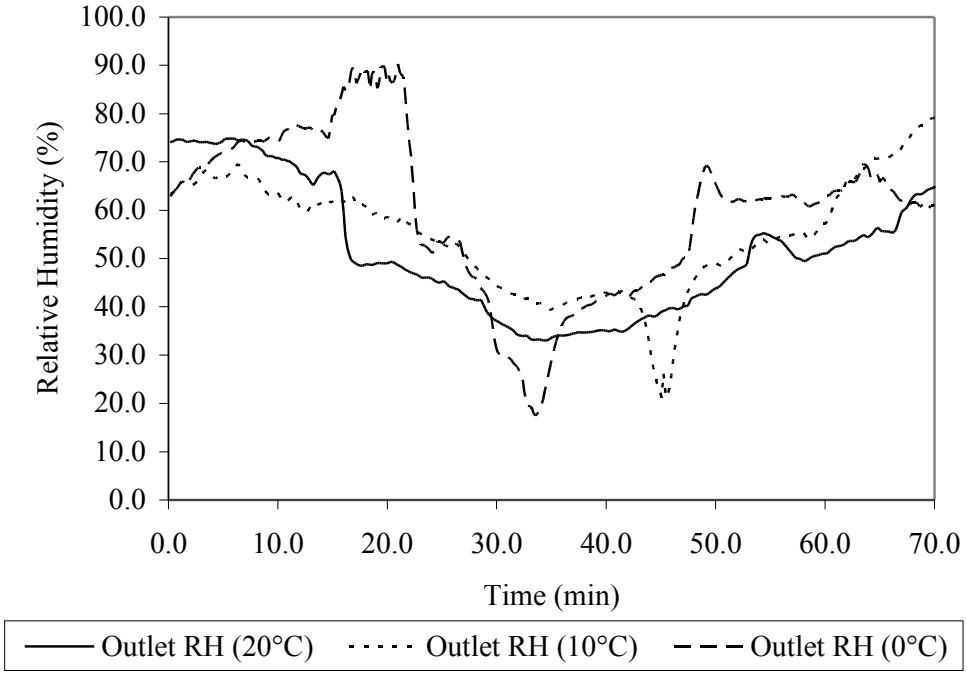

Figure 5.14 – Cathode Outlet Relative Humidity During Operation at Varying Ambient Temperatures

gases and if set at ambient temperature, the anode gas temperature will rise slightly over time.

Figures 5.11, 5.12, 5.13 and 5.14 show the performance of the fuel cell stack, the stack temperature, cathode channel outlet temperature, and cathode channel outlet relative humidity respectively for the three temperature case. Fluctuations in the temperature and relative humidity in the environmental chamber are observed at 30-35min for the 0℃ case and at 45min for the 10℃ case. The effects of these fluctuations are reflected by the fluctations in the temperature and relative humidity of the cathode channel outlet gas, as well as the stack temperature.

An abnormal fluctuation of the stack temperature is observed in Figure 5.12 for the 0℃ case from 15 - 33 minutes. This is reflected in cathode gas outlet temperature in Figure 5.13 as well. The probable cause for this fluctuation is in evidence in Figure 5.14, where it is observed starting at about 13 minutes that the relative humidity of the cathode outlet gases is fluctuating about 90%. This suggests that condensation is occuring in the cathode channels, which would release energy and raise the stack temperature.

5.2.3 Effect of Relative Humidity

It is expected that the relative humidity will affect the stack performance because it controls the hydration of the membrane. To study this effect, the fuel cell stack was tested at 20℃ and constant fan speed of 0.28m/s for a range of relative humidities: 30%, 50% and 70%. During the experiment, the stack voltage, stack temperature, cathode outlet temperature, cathode outlet relative and cathode inlet relative humidity were recorded and are shown in Figures 5.15, 5.16, 5.17, respectively.

Figure 5.15 shows that the performance of the stack at high relative humidity (70%) is better than for the cases with lower relative humidity. The temperature of the stack during operation is similar for all the cases, as shown in Figure 5.16. The temperature of the cathode outlet gases is also similar for all three cases as the changes fall within the confidence interval for the measurements.

Figure 5.17 shows that the relative humidity of the cathode outlet gases drops as the current draw for the stack increases. An increase in the ambient relative humidity leads to an increase in the cathode outlet relative humidity. It also shows that with increasing current, there is an increase in the cathode

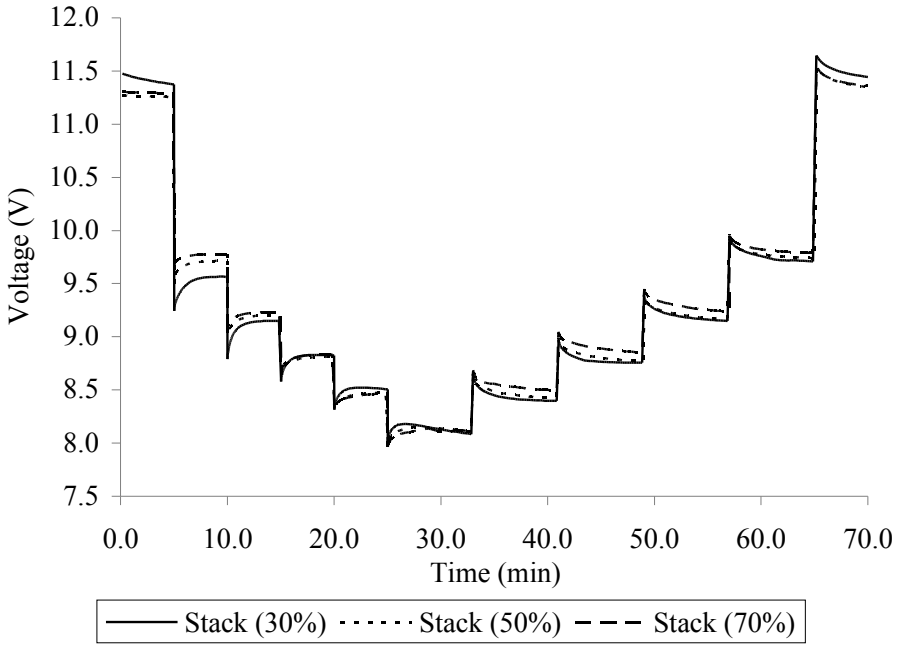

Figure 5.15 – Performance of Fuel Cell Stack at Varying Ambient Relative Humidity

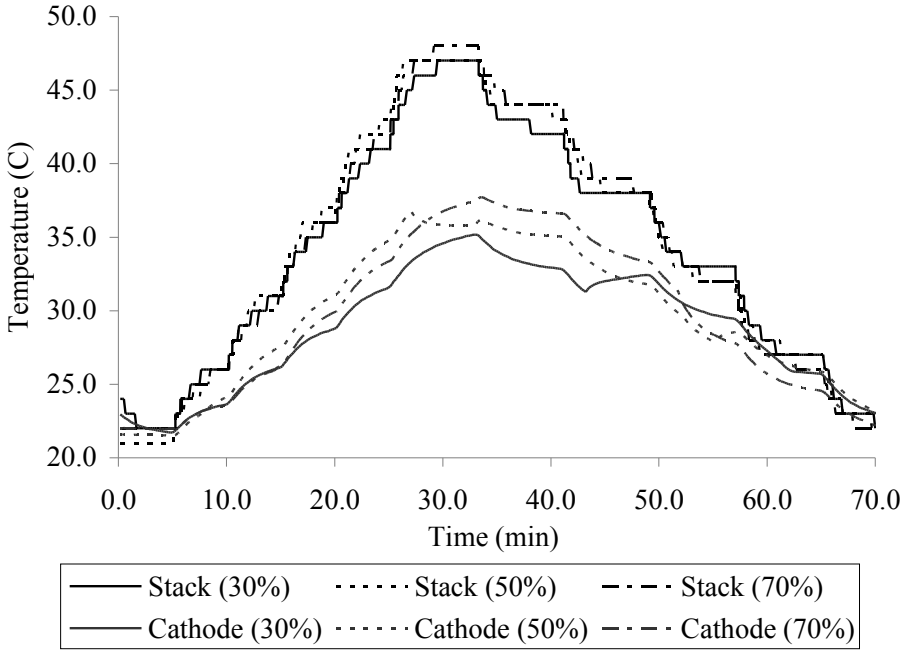

Figure 5.16 – Stack and Cathode Temperatures During Operation at Varying Ambient Relative Humidity

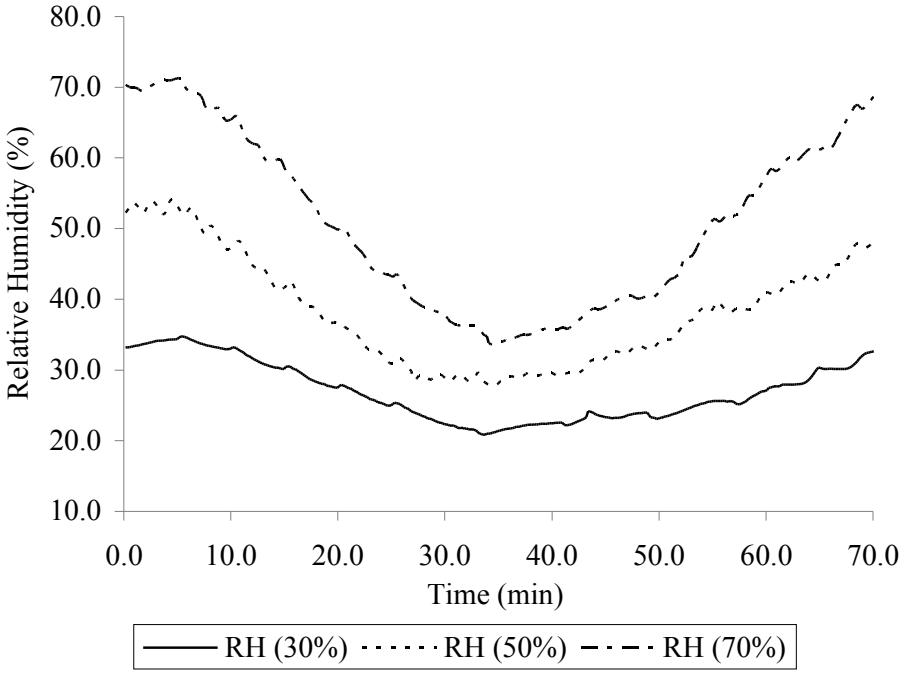

Figure 5.17 – Cathode Relative Humidity during operation at Varying Ambient Relative Humidity

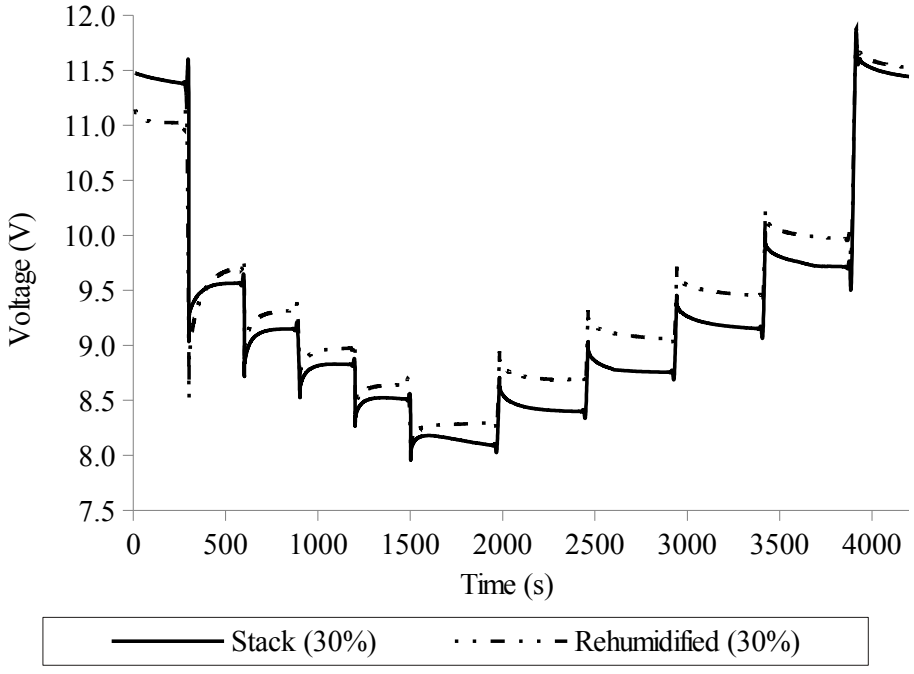

Figure 5.18 – Effect of Rehumidification of Stack on Performance

outlet temperature and therefore a drop in the cathode outlet relative humidity. This suggests that at high current, the increased temperature has a more significant effect on the relative humidity in the cathode outlet channel than the increase in water produced by the reaction.

The performance of the stack also depends on whether the stack has recently been rehumidified. Figure 5.18 shows a comparison of the performance of the stack before and after a rehumidification procedure was applied. Experiments and models by Onishi et al. [85] report that vapour equilibrating a membrane to a new condition takes time on the order of several weeks (3 weeks to 2.5 months observed), particularly at low temperatures. For the tests in this research, the stack was placed in the relative humidity conditions at which it would be tested for at least 5 hours prior to beginning a test at the specified conditions.

5.2.4 Effect of Fan Speed

The performance of the fuel cell stack is affected by the flow rate of air through the cathode channels. The fuel cell stack is air cooled, therefore the primary cooling mechanism is the cathode air flow. Additionally, the air flow through

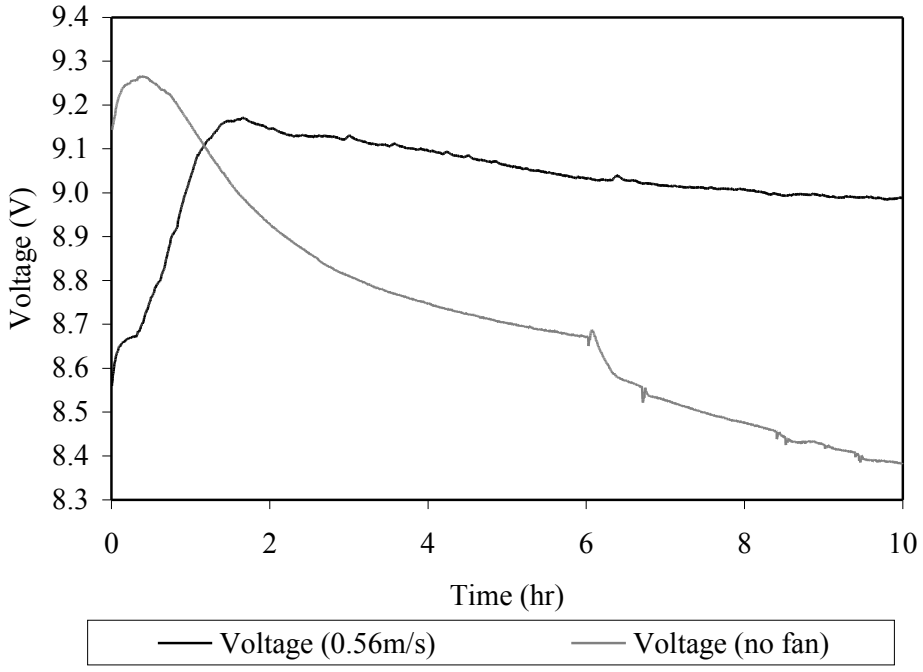

Figure 5.19 – Performance of Fuel Cell Stack at Varying Input Fan Speeds

the cathode delivers oxygen to be reacted. The fan that is installed in the fuel cell stack is tested at three fan speeds: 0.25m/s (3.0V), 0.28m/s (3.3V) and 0.40m/s (4.7V) and at room conditions of approximately 22℃ and 20% RH . These fan speeds correspond to stoichiometric ratios at 2A of approximately 42, 51, and 74 respectively, therefore it is expected that the effect of the change in the rate of stack cooling will dominate over the effect of the change in cathode reactant delivery rate.

The stack performance is shown in Figure 5.19, the temperatures of the stack and cathode outlet gases are reported in Figure 5.20, and the cathode outlet air temperature and relative humidity, which changes relative to the stack temperature, is shown in Figure 5.21.

Figure 5.19 shows that the performance of the stack at the highest fan speed of 0.40m/s has consistently lower performance than the case wiht a fan speed of 0.28m/s. This might be a result of a) the lower stack temperature and b) the lower relative humidity in the stack due to rapid removal of water produced, as shown in Figure 5.21.

The stack is not able to produce power at high imposed current during the

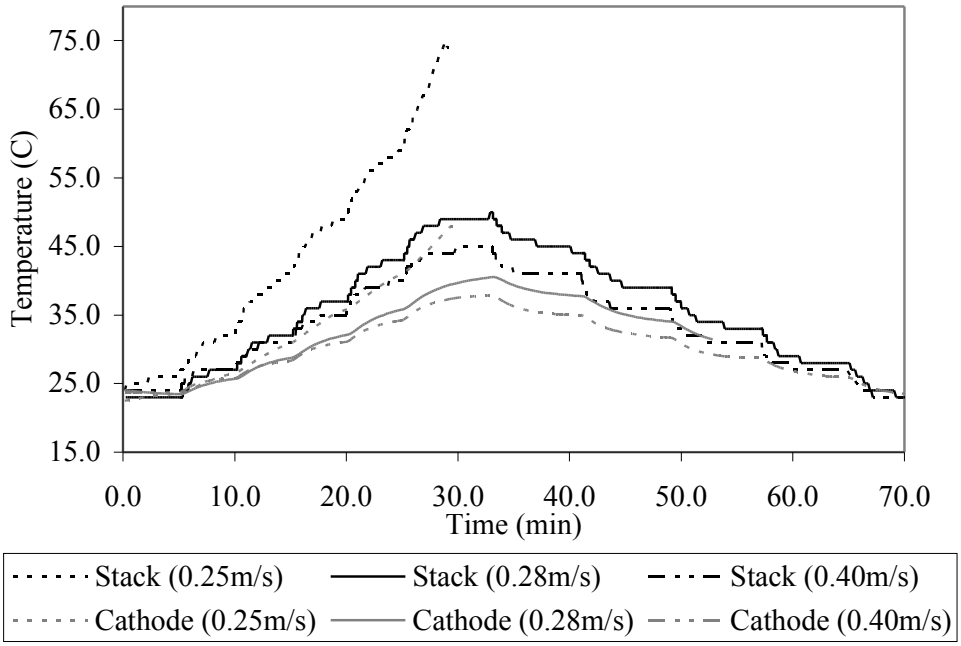

Figure 5.20 – Stack and Cathode Temperatures During Operation at Varying Input Fan Speeds

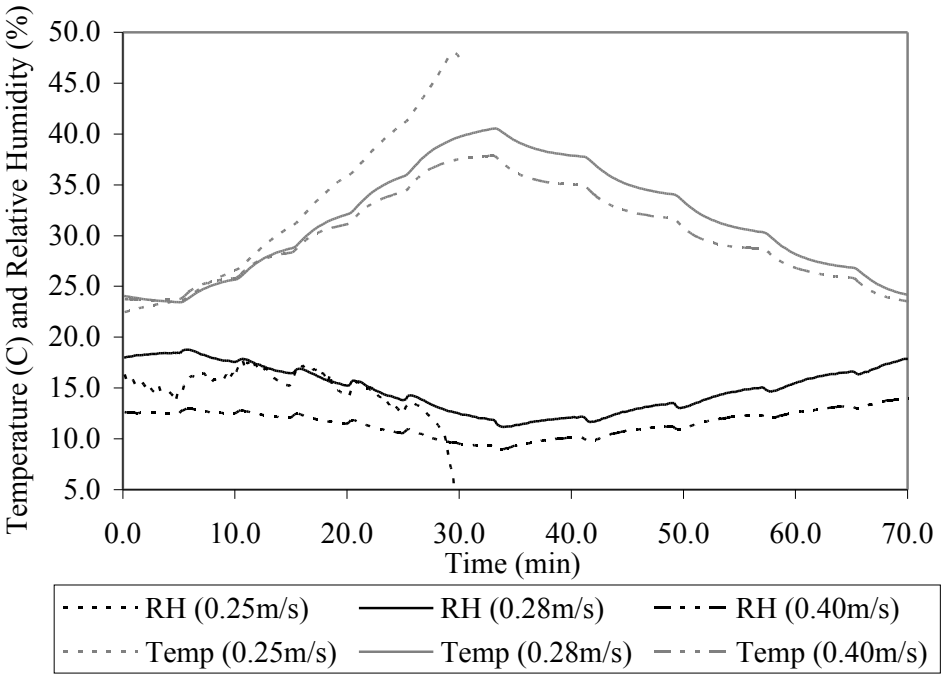

Figure 5.21 – Cathode Outlet Temperature and Relative Humidity During Operation at Varying Input Fan Speeds

case with a fan speed of 0.25m/s, as shown in Figure 5.19. When the stack does not have adequate air supply, this can lead to overheating, membrane dry out and poor stack performance. If the stack does not obtain enough oxygen for the reaction to draw the required current, the performance will drop as shown in Figure 5.19. The stack will overheat as there is insufficient cooling, shown in Figure 5.20. Finally, the coupled effects of the low relative humidity in the inlet air and the overheating stack leads to a drop in the relative humidity and membrane dry out, shown in Figure 5.21

5.3 Fuel Cell Stack Modelling

5.3.1 Parameter Estimation

The fuel cell stack model developed in Chapter 2 is fitted to the experimental results obtained from a Horizon H-12 Fuel Cell Stack. The data from the repeatability test is used for parameter estimation. The parameters for the Horizon H-12 Fuel Cell Stack are listed in Tables 2.4 and 2.5. The parameters which cannot be measured and are therefore manually fitted to the

Table 5.3 – Estimated Parameters for Horizon H-12 Fuel Cell Stack

Stack Properties	*Value*
Anode Channel Heat Transfer Coefficient and Area, $(hA)_{an}$	0.002 W/K
Cathode Channel Heat Transfer Coefficient and Area, $(hA)_{ca}$	0.003 W/K
Ambient Heat Transfer Coefficient and Area, $(hA)_{amb}$	0.2 W/K
Mass and Specific Heat Capacity of Stack, $m_s c_{p,s}$	90 W/K
Evaporation Rate Coefficient, k_v	$10\left(\frac{cm^2 LV}{(cm^2 ch)kPa*s}\right)$
Condensation Rate Coefficient, k_c	$10\left(\frac{cm^2 LV}{(cm^2 ch)s}\right)$
Electrochemical Properties	
Limiting Current Density, j_L	0.16 A/cm^2 ($\sim$ 2A for H-12 stack)
Component Resistance, R_{comps}	0.02 Ω

experimental results are listed in Table 5.3.

The fitted parameters for the electrochemical model of the fuel cell stack are the limiting current density j_L, and the resistance of the components R_{comps}. These values were varied to fit the voltage of the fuel cell stack determined by the mathematical model for the specified test conditions to the experimental voltage at these same conditions, as shown in Figure 5.22.

Testing of the Horizon H-12 Fuel Cell Stack showed that membrane dry out was the limiting factor in the performance of the fuel cell stack, particularly as the majority of tests were run at low relative humidity. Although the stack was able to reach up to a current of 4A, this current draw could not be maintained for longer than 5 minutes, during which the performance of the stack dropped rapidly. The highest current observed which could be maintained for a reasonable length of time (40 minutes) without significiant performance drop was 2A. Therefore, the limiting current was set at $0.16\text{A}/cm^2$, which is just slightly larger than $2\text{A}/13.1cm^2$, where $13.1cm^2$ is the active area of one cell. The component resistance was estimated as 0.017Ω based on scaling the component resistance reported by O'Hayre et al. [42] of 0.012Ω for an active area of $9cm^2$ to the active area of $13.1cm^2$ for this stack. It is fitted to 0.02Ω based on the experimental results.

Figure 5.22 shows a comparison between the performance of the stack during experimental testing at room conditions, as reported in the repeatability study in Figure 5.5, and the predicted performance by the model at these same

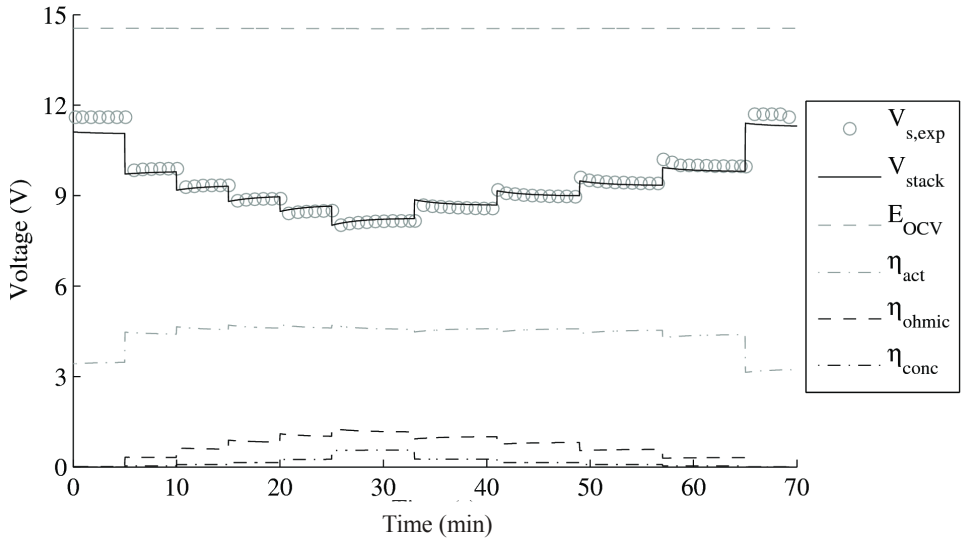

Figure 5.22 – Performance of Fuel Cell Stack

conditions. With the fitted parameters, the model predicts the stack voltage well. In exception are the first and last current steps, which were measured at a stack voltage of 0A, and are compared to the mathematical model computed at at stack voltage of 0.01A due to modelling limitations.

The stack properties that were fitted for the energy balance of the fuel cell stack are the anode and cathode channel heat transfer coefficient and areas hA_{an} and hA_{ca}, the ambient heat transfer coefficient and area hA_{amb}, the mass and specific heat capacity of the stack $m_s c_{p,s}$, and the evaporation and condensation time constants for the channels k_v and k_c. Figure 5.23 shows a comparison of the model prediction of stack and cathode temperatures and the experimental results at room conditions.

The heat transfer coefficient and area terms are combined for the anode channel, cathode channel and stack to ambient air, as it is not possible to directly measure the heat transfer area, nor the heat transfer coefficient. For the same reason, the mass and specific heat capacity of the stack was combined into one term.

The heat transfer coefficient and area for the anode and cathode channels were estimated to be on the order of 0.006W/K from internal pipe heat convection theory. These estimations were computed assuming that the flow is laminar, hydrodynamically developed and thermally developing, based on the channel length and flow velocity [71]. The heat transfer coefficient was

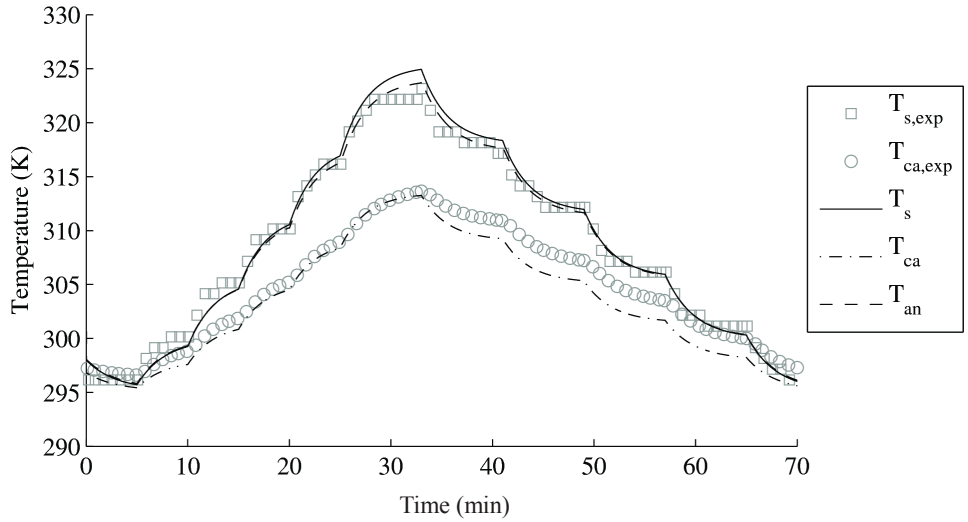

Figure 5.23 – Stack and Cathode Temperatures

determined from the Nusselt number for these specific conditions, and the assumed heat transfer area is the surface area of the channel. The fitted values of 0.002W/K for the anode channel and 0.003W/K for the cathode channel are of the same order. Finally, the natural convective heat transfer coefficient and area for the stack to ambient air was fitted as 0.2W/K. It is expected that the fitted value for the stack to ambient heat transfer coefficient and area will be significantly greater than the heat transfer coefficient and area for the gas channels because the surface area of the stack greatly exceeds that of one gas channel. The mass and specific heat capacity could be estimated as the mass and specific heat capacity of a graphite block with the same volume as the of the bipolar plates. This gives a value of approximately 100W/K, which is close to the fitted 90W/K for the mathematical model.

Figure 5.23 shows that the temperatures computed by the mathematical model follow the expected trends well. The computed cathode temperature drops more rapidly during the first decreasing current step than for the experimental set up; however, the difference is within the confidence interval of the repeatability study.

As experimental conditions where condensation and evaporation of water in the channels were not able to be obtained, the evaporation and condensation constants, k_v and k_c respectively, were arbitrarily set to $10kPa^{-1}s^{-1}$ and $10s^{-1}$ for good model convergence in the gas channels. Typically only the condensation rate constant is reported, with values ranging from $1s^{-1}$

[36, 64] to $100s^{-1}$ [49, 52]. He et al. reported an evaporation rate constant of $100atm^{-1}s^{-1}$ [52]. Based on these values reported in the literature, the phase change rate constants were arbitrarily selected for good convergence.

5.3.2 Mathematical Model Parametric Studies

The mathematical model was tested to determine its ability to accurately characterize changes in the fuel cell stack operation based on different operating parameters. These simulations are compared to the experimental data measured for the same operating conditions, as reported in Section 5.2. The operating conditions that are studied are the ambient temperature, the ambient relative humidity and the speed of the fuel cell stack fan.

Effect of Temperature

The ability of the mathematical model to predict changes in the performance of the fuel cell stack with changes in the ambient temperature is compared to experimental data from tests at 0℃, 10℃ and 20℃. Figure 5.24 illustrates the predicted effect of ambient temperature on the performance of the fuel cell stack by the mathematical model and the experimental results for the same conditions. Figures 5.25 and 5.26 compare the predicted and experimentally

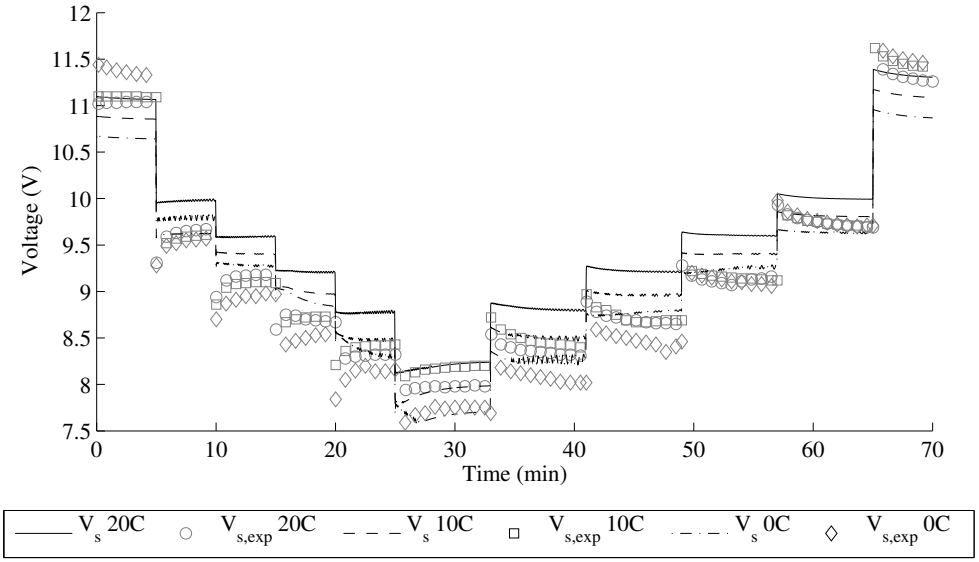

Figure 5.24 – Performance of Fuel Cell Stack During Operation at Varying Ambient Temperatures

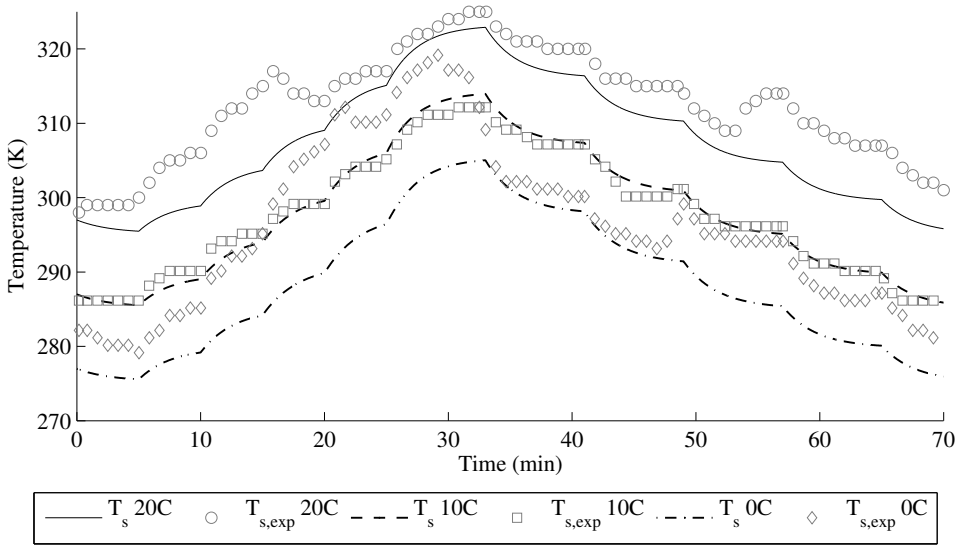

Figure 5.25 – Stack Temperature During Operation at Varying Ambient Temperatures

measured stack temperature and cathode channel outlet temperature respectively.

The mathematical model shows the trend of decreasing performance with decreasing ambient temperature well, although it overpredicts the specific stack performance values for most of the current steps. As discussed in Section 5.2.3, the stack membranes are affected by their humidification history.

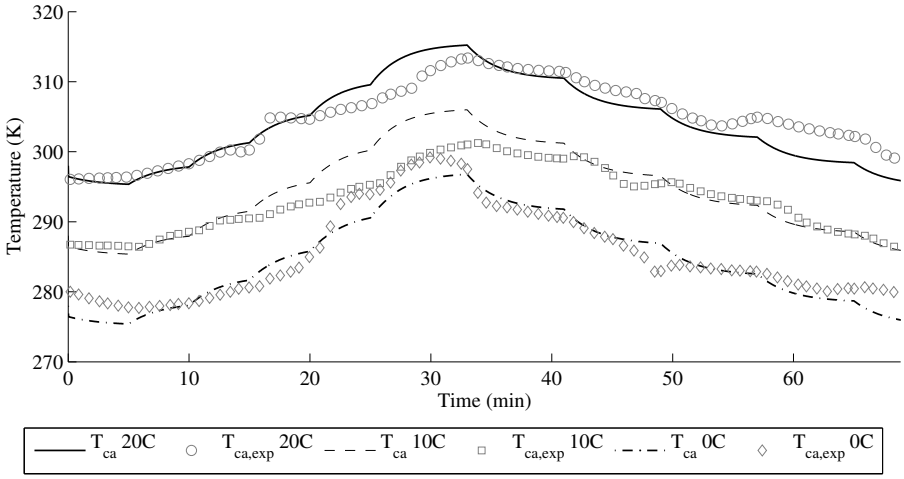

Figure 5.26 – Cathode Temperature During Operation at Varying Ambient Temperatures

Although the stack was subjected to the high humidity condition for several hours prior to the tests, it is observed that the mathematical model, which was fitted to a test at 20%RH, is more sensitive to changes in the supplied relative humidity for these tests at 80%RH than is observed during the experiments. This will be further explored in the next section, Effect of Relative Humidity.

The mathematical model closely predicts the stack performance, stack temperature and cathode temperature during the 10℃ and 0℃ tests. There is some overshoot of the stack and cathode temperatures during the higher current steps (1.2A-2A). It was previously observed in Figures 5.12 and 5.13 that the experimental temperatures for the 0℃ case were unexpectedly high from 10 mins - 33 mins. This is caused by two separate events. First, from 14 to 23 mins, a high and fluctuating relative humidity observed in the cathode outlet channel 5.14 which suggests that condensation, and possibly freezing, are occuring in the channels. Condensation releases energy into the channel, raising the temperature. Second, at 28 - 37 minutes, a significant drop in the relative humidity of the air input to the stack is observed, as shown in Figure 5.10. The drop in relative humidity increases the stack membrane resistance, leading to an increase in the stack temperature.

5.3.3 Effect of Relative Humidity

The fuel cell stack was modelled and experimentally tested at 20℃ and constant fan speed of (3.3V) for a range of relative humidities: 30%, 50% and 70%. Figure 5.27 shows the performance of the fuel cell stack as computed by the mathematical model in comparison with the experimental results from testing the fuel cell stack. In all cases, it is again observed that the mathematical model over predicts the performance of the fuel cell stack. The trends, however, are correct and the gaps between the different cases are similar to the gaps observed in the experimental model. Note that the model was fitted using data at approximately 22℃ and 15% RH, so the model shows a good ability to predict performance changes with changing temperature and relative humidity.

The stack and cathode temperatures computed by the mathematical model are shown in comparison with the experimentally measured temperatures in Figures 5.28 and 5.29 respectively. The mathematical model returns almost identical temperatures for all cases, which fall within the range of temperatures measured during the experiments in all cases. The model over predicts the

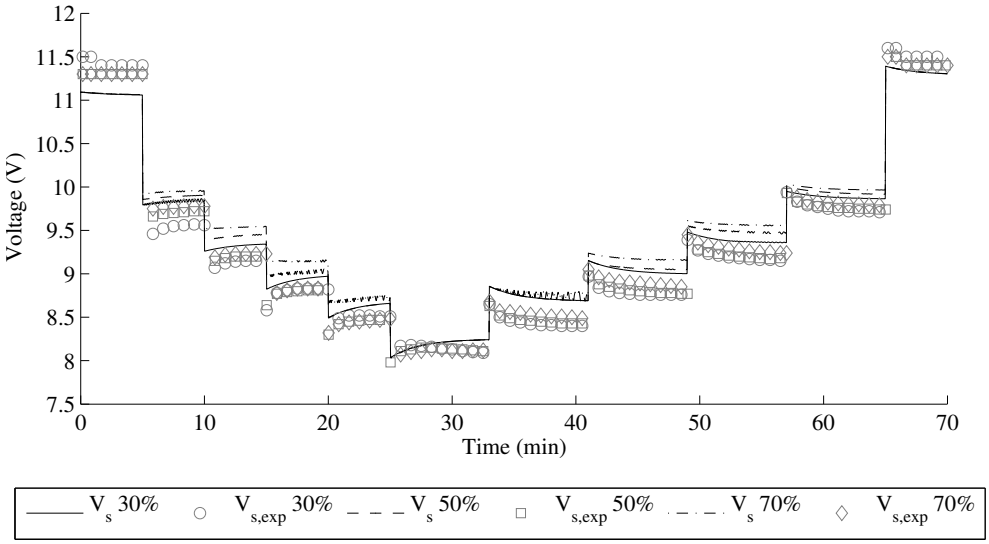

Figure 5.27 – Performance of Fuel Cell Stack During Operation at Varying Ambient Relative Humidity

temperature in the highest current case at 2A.

Figure 5.30 shows the expected and numerical cathode outlet relative humidity. The mathematical model closely approximates the relative humidities measured in the cathode channel during the experiments. At the highest cur-

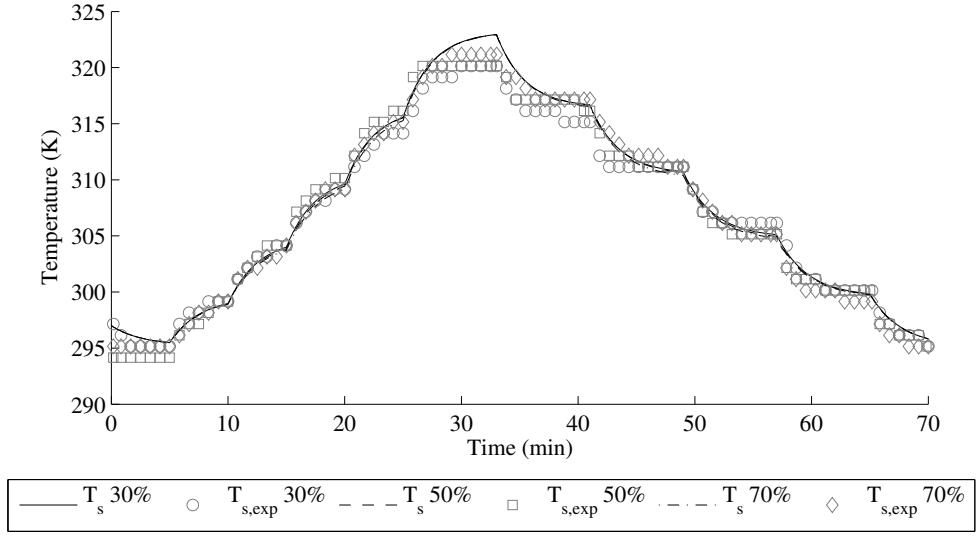

Figure 5.28 – Stack Temperature During Operation at Varying Ambient Relative Humidity

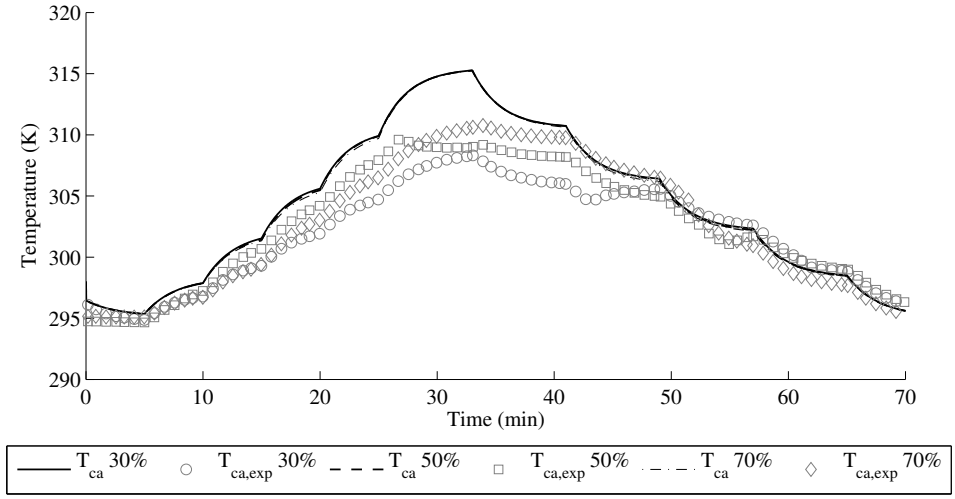

Figure 5.29 – Cathode Temperature During Operation at Varying Ambient Relative Humidity

rent case, 2A, the relative humidity is under predicted, which is caused by the over prediction of the temperature of the cathode in these cases. This occurs despite the addition of product water to the cathode outlet gases, as the increase in gas temperature increases the saturation pressure for the outlet gas. Therefore, the effect of the change in temperature during operation, shown in Figure 5.16 is more significant than the effect of additional product water added to the cathode channel on the relative humidity of the cathode.

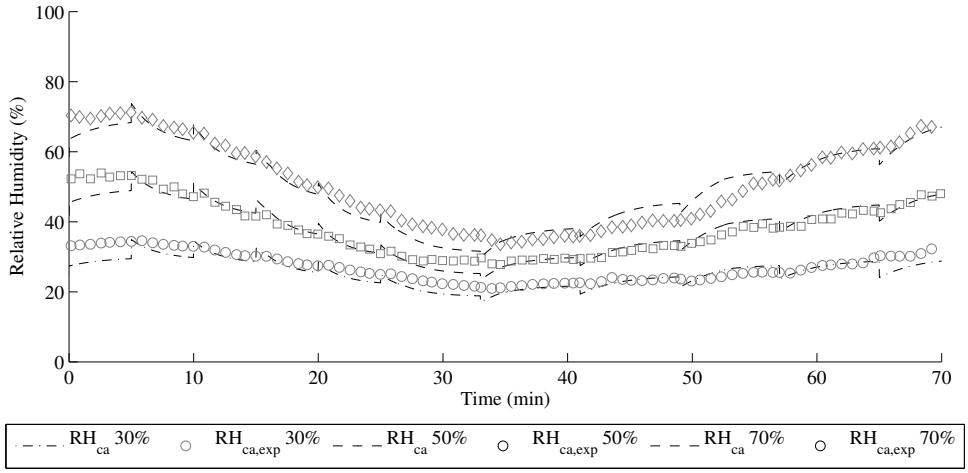

Figure 5.30 – Cathode Relative Humidity During Operation at Varying Ambient Relative Humidity

5.3.4 Effect of Fan Speed

The effect of the speed of the fan, which determines the speed of reactant delivery to the cathode channels and stack cooling, was modelled and compared to experimental tests at room conditions of approximately 22℃ and 20% relative humidity for three fan speeds (input voltage): 0.18m/s, 0.28m/s and 0.40m/s.

Figure 5.31 compares the performance of the stack during the experiments with the predictions of the mathematical model. It shows that the mathematical model predicts trends of change in performance well. When the flow rate increases, the performance decreases because of additional cooling. It does not, however, have a good prediction of the measured values and is unable to predict the inability of the stack to meet the high current demanded for the 0.25m/s inlet flow rate case.

The stack temperature is shown in Figure 5.32. During the lower current portion of the tests, the initial stack temperature shows different temperatures because it is difficult to control, and therefore only data after 5 minutes should be studied. Results show that the model predicts the stack temperature well for all current steps after 5 minutes. It follows the general trends for a change in current well.

The experiments at 0.25m/s showed in Figure 5.32, that the measured stack temperature was much greater than predicted, which is coupled with stack being unable to reach the desired performance during this test. The

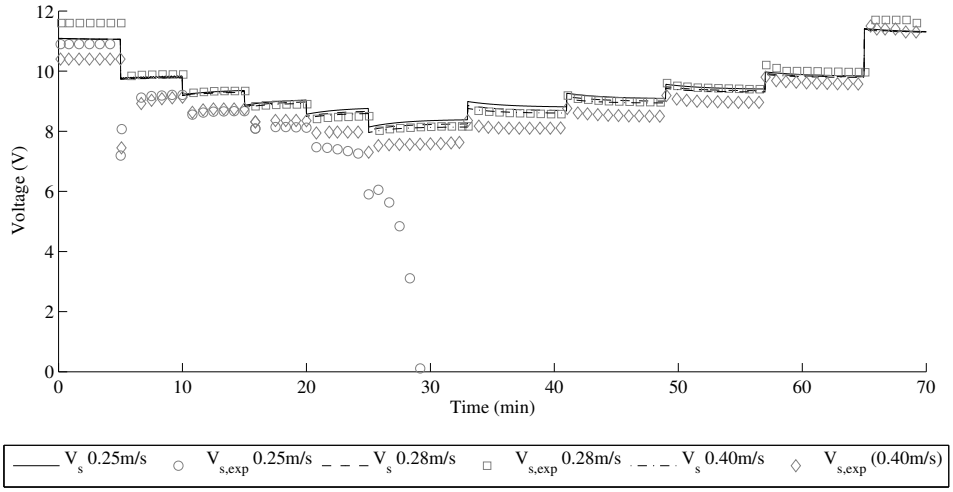

Figure 5.31 – Performance of Fuel Cell Stack During Operation at Varying Input Fan Speeds

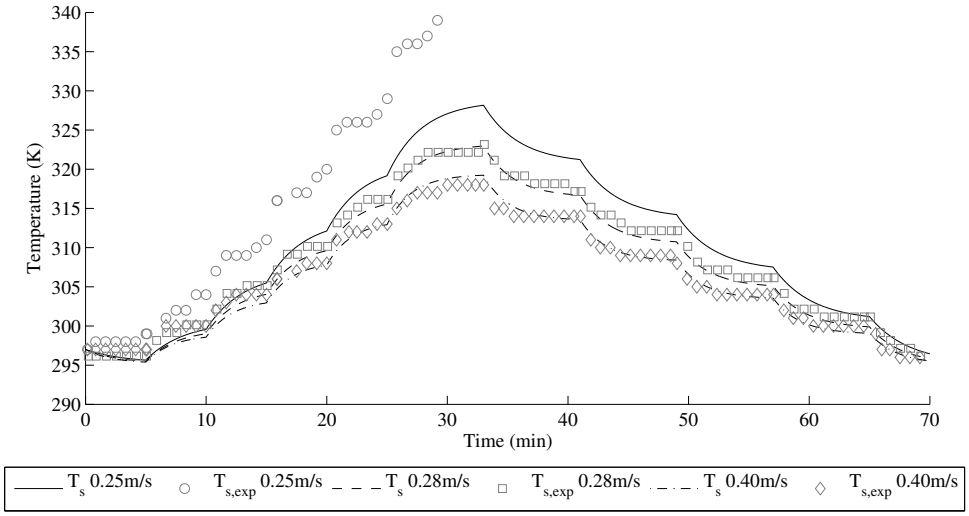

Figure 5.32 – Stack and Cathode Temperature During Operation at Varying Input Fan Speeds

experiments at 0.40m/s showed a good prediction of stack temperature.

Figure 5.33 shows that the temperature of the cathode outlet gases is well predicted for the three cases. As the mathematical model does not predict that the stack will not operate at high current, the model predictions for the entire simulation are included.

The fitted model of the Horizon H-12 Fuel Cell Stack proved capable of

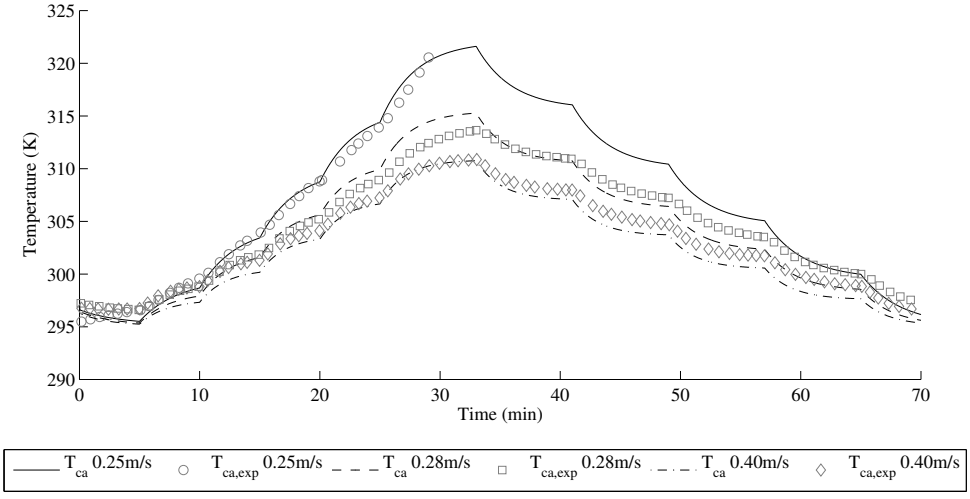

Figure 5.33 – Cathode Outlet Temperature and Relative Humidity During Operation at Varying Input Fan Speeds

predicting the expected trends of the fuel cell stack performance, temperature and cathode conditions. It is able to approximate the performance of the fuel cell stack during operation at varying ambient conditions, and can therefore be used to study the performance of the stack in an enclosure.

5.4 Enclosure/Fuel Cell Stack System Experiments

The effect of an enclosure on the performance of the fuel cell stack model was tested by installing the fuel cell stack model in an insulated enclosure. Two enclosure designs were tested, as well as the effects of ambient temperature and enclosure inlet fan flow rate. The experimental set up and procedure for the enclosure tests, as detailed in Chapter 4, was used to effectuate these studies.

5.4.1 Ambient Temperature Effects

The effect of the ambient temperature on the performance of the fuel cell stack was examined by changing the ambient temperature from 20℃ to -20℃ by decrementing steps of 10℃. The 20℃ step was held for 30 minutes, and all

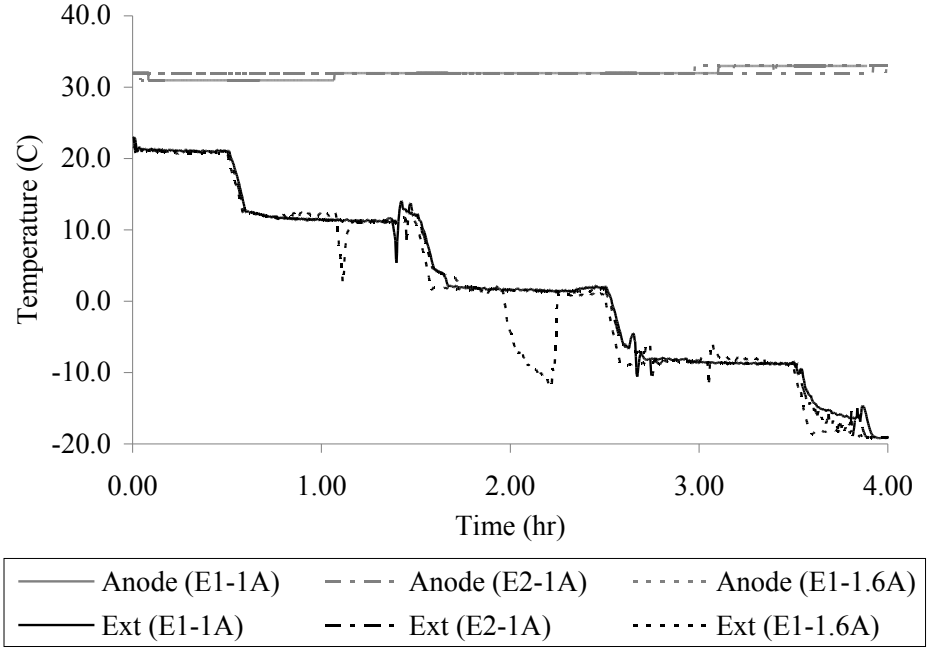

Figure 5.34 – Variation of Ambient Temperature

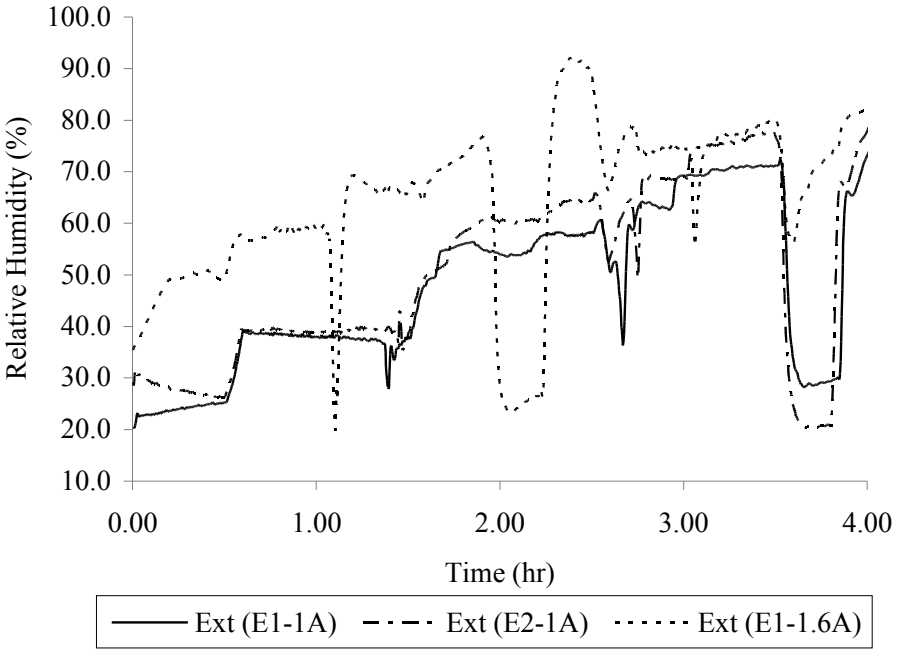

Figure 5.35 – Variation of Ambient Relative Humidity

subsequent temperature steps were held for one hour. The inlet temperature of the anode hydrogen gas was set at 30℃ and dry conditions. Figure 5.34 shows the inlet temperature of the anode and cathode gases. The environmental chamber caused some variability in the ambient temperature, notably during the test at 1.6A in Enclosure 1 at one hour and 10℃, and from 2 to 2.2 hours at 0℃. Figure 5.35 shows the inlet relative humidity conditions. The environmental chamber cannot control the relative humidity at temperatures below 10℃, therefore it was not controlled during any of the tests.

The test procedure for the enclosure cases consisted of stabilizing the stack in the enclosure for 30 minutes at 20℃ prior to beginning the test. The purpose of doing this was to avoid analyzing start up data for the stack as this research is focusing on observing the transient performance of the stack and enclosure during operation. The procedure was also followed because it reduced the effect of the stack start up on the enclosure temperature measured during the tests.

Three tests were performed for this varying temperature test: the stack at 1A in Enclosure 1, the stack at 1A in Enclosure 2, and the stack at 1.6A in Enclosure 1. Figure 5.36 shows the performance of the fuel cell stacks in the enclosures. The temperature of the enclosure during operation of the stack

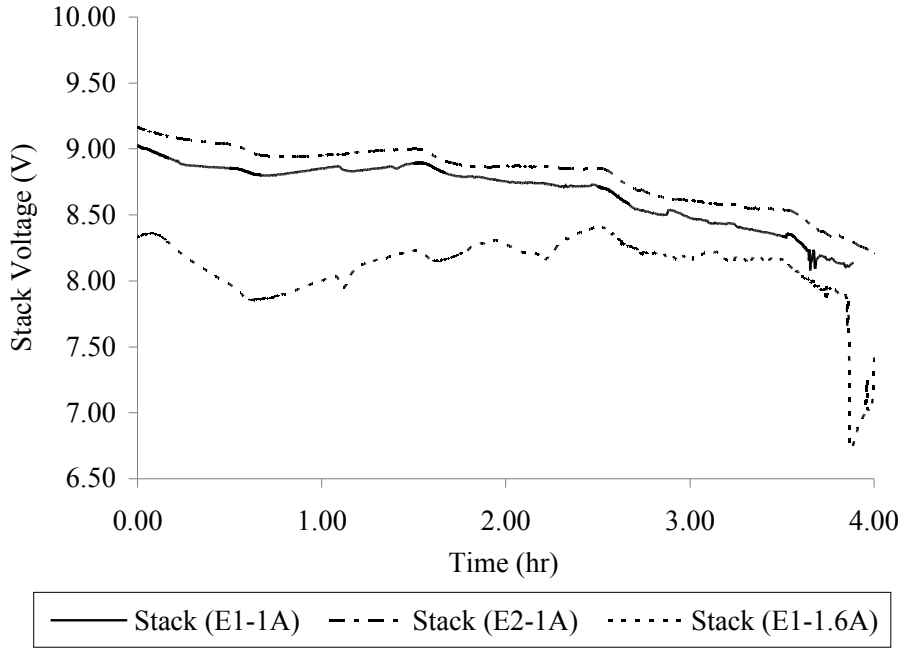

Figure 5.36 – Performance of Stack in Enclosure with Varying Ambient Temperature

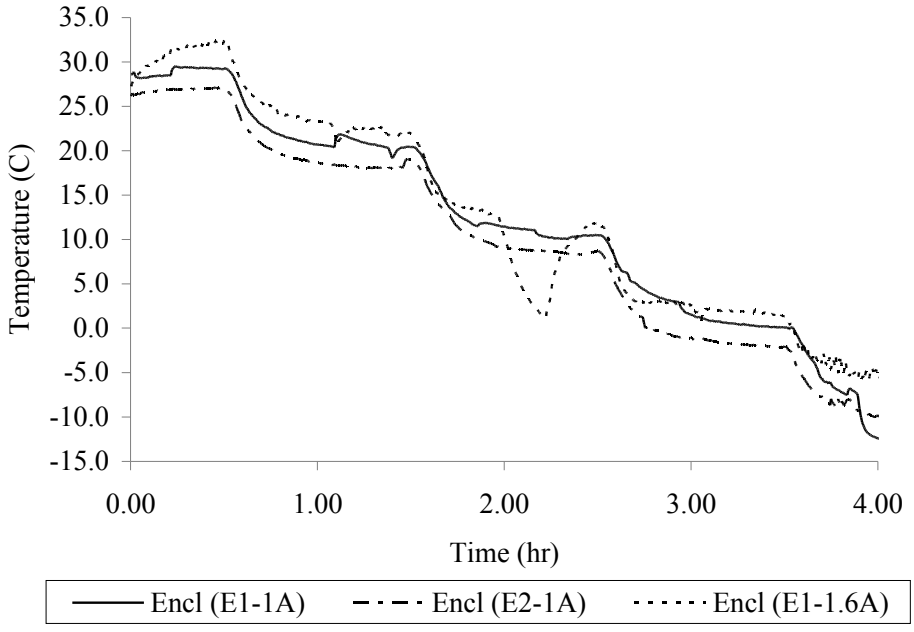

Figure 5.37 – Performance of Fuel Cell Stack at Varying Ambient Temperature

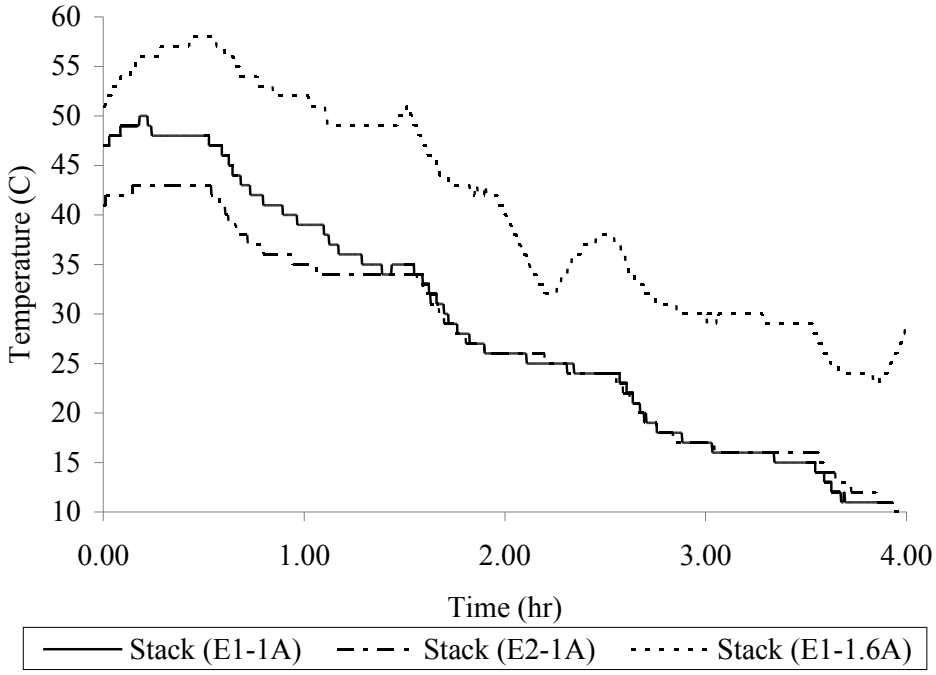

Figure 5.38 – Cathode Relative Humidity During Operation at Varying Ambient Temperature

at changing ambient temperatures is shown in Figure 5.37. Figure 5.38 shows the temperature of the stack during the varying temperature tests.

The stack voltage at 1A for the two enclosures is similar, and as expected the voltage of the stack at the higher current of 1.6A is reduced. Each test also shows some variation in the stack voltage which occurs as a result of the temperature changes. In the 1A cases, each change in the ambient temperature leads to a drop in the stack voltage. Note that even after an hour, the cell voltage has not stabilized to a steady value. In all cases, the stack performance drops off after 4 hours because, as shown in Figure 5.37, the enclosure temperature reached less than 0℃, which caused freezing in the anode outlet line.

For each 10℃ drop in the ambient air temperature, the temperature in each of the enclosures drops by approximately 10℃ as well. The temperature converges to a steady state temperature in about one hour. The primary difference between the three cases is the steady state temperature reached by the enclosure during the initial temperature step at 20℃. Of particular interest is that despite a higher insulation factor, Enclosure 2 is at a lower temperature

than Enclosure 1 for the 1A cases.

The enclosure temperature, shown in Figure 5.37 follows the same trends as the stack temperature, shown in Figure 5.38, with a fairly constant temperature gap.

The stack temperature during the test at 1.6A is greater than for the 1A tests because more heat energy is produced.

5.4.2 Effect of Enclosure Fan

The effect of the forced flow from the fan in the enclosure was tested by comparing a test with the fan at 0.56m/s and a test with the fan at 0m/s. When fan is at 0m/s, only diffusive flux transport occurs between the enclosure and the environment. These tests were carried out at room conditions of approximately 22℃ and 20% relative humidity in Enclosure 1 with the stack at 1A and the stack fan at 0.28m/s for 10 hours. The anode gas was set dry at 30℃. The stack was stabilized at 1A outside of the enclosure and then the test was started when the stack was installed in the enclosure to show the transient effect of the enclosure on the stack performance.

Figure 5.39 shows the performance of the stack when the enclosure fan is

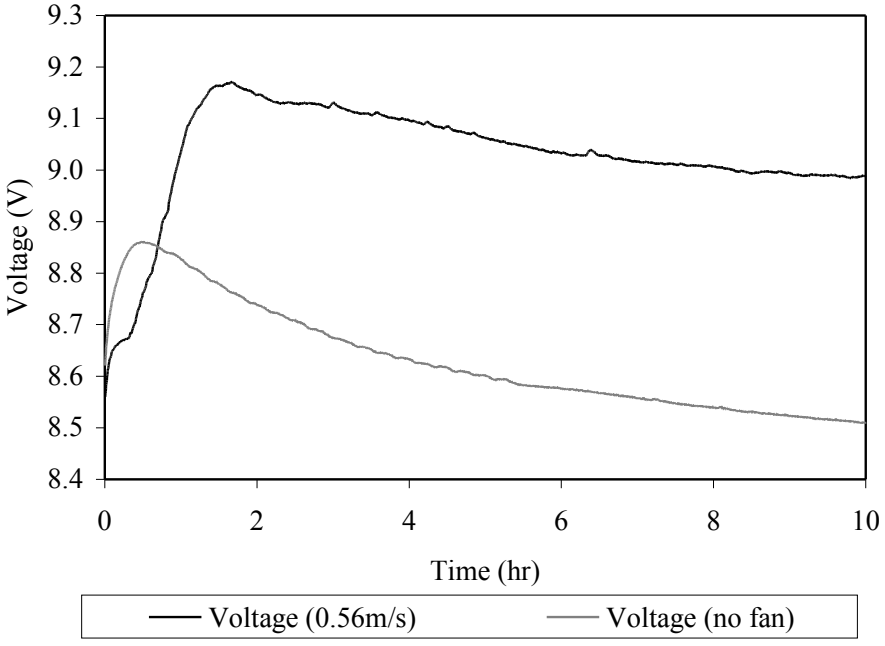

Figure 5.39 – Effect of Enclosure Fan on Stack Performance

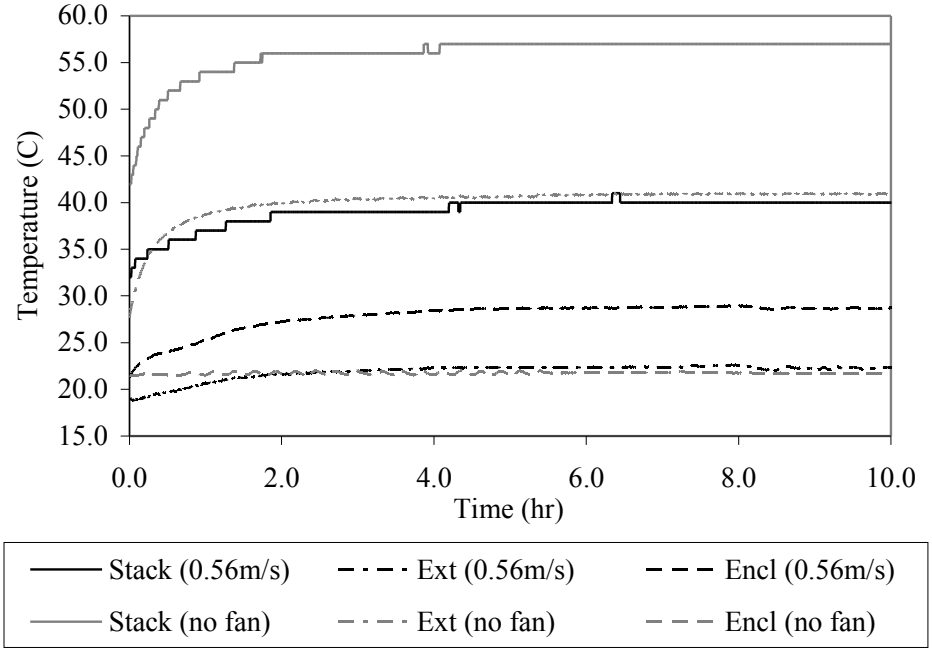

Figure 5.40 – Effect of Enclosure Fan on Enclosure Temperature

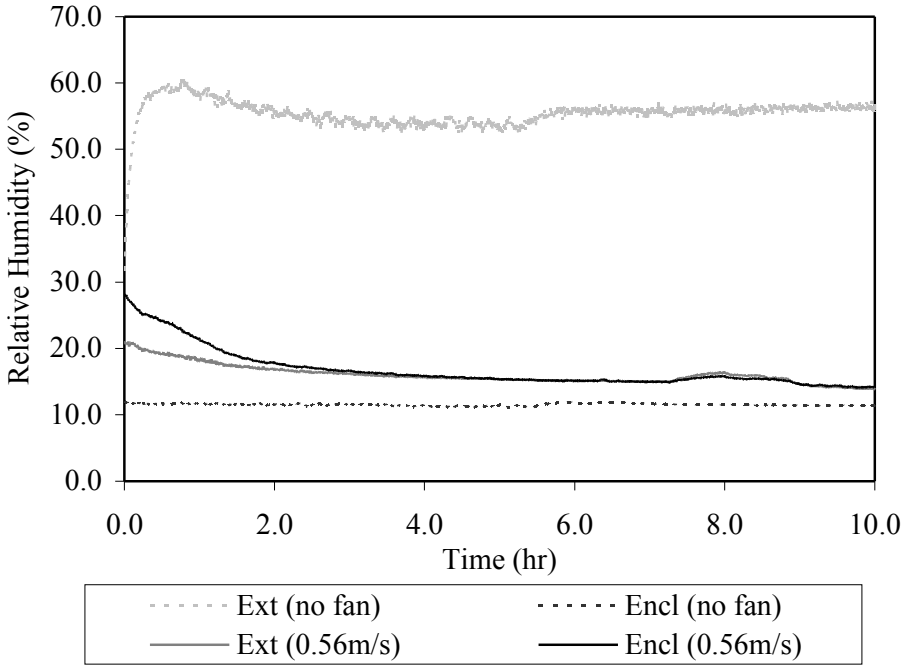

Figure 5.41 – Effect of Enclosure Fan on Enclosure Relative Humidity

set at 0.56m/s and 0m/s. It is observed that the performance of the stack changes with changes in the enclosure temperature during the first 2 hours for both cases. Then the performance drops; more rapidly for the case when the enclosure fan is off (0m/s). For the case with the enclosure fan off, the flow of oxygen into the enclosure is diminished and therefore the enclosure oxygen concentration is depleted and the performance of the stack suffers.

Figure 5.40 shows the stack temperature (solid line), enclosure temperature (dashed line) and ambient temperature (dash-dot line) during tests with the fan at 0.56m/s and with the fan off. The test when the fan is off shows that the enclosure and stack temperature rise to 40℃ and 56℃, in comparison with 28℃ and 40℃ when the fan is running at 0.56m/s. This occurs because the stack performance drops as the oxygen in the enclosure is depleated, shown in Figure 5.39, and the stack is producing less power and more heat.

Figure 5.41 shows the ambient relative humidity for the the two cases is fairly constant at 17% for the fan at 0.56m/s test and 12% for the fan off test. The relative humidity in the enclosure is also shown in Figure 5.41. The relative humidity for the fan at 0.56m/s case remains very close to the ambient relative humidity once stabilizes. The air flow rate in this case was high enough to remove product water from the enclosure and prevent accumulation. The relative humidity in the case with the fan off increases to approximately 55% and fluctuates around this point for the rest of the test because the product vapour was able to build up inside the enclosure.

5.5 Coupled Enclosure/Stack Model

A mathematical model of the fuel cell stack was developed in Chapter 2 and a mathematical model of the enclosure was developed in Chapter 3. The enclosure conditions are affected by the fuel cell stack which is installed within the enclosure. Therefore, the stack model will be coupled with the enclosure model to ensure an accurate representation of the conditions within the enclosure. Due to the nature of the system, the output of the fuel cell stack affects the enclosure conditions and consequently the input conditions to the stack.

The mass transport in the coupled enclosure/stack model is illustrated in Figure 5.42. The mass transported into and out of the fuel cell stack will affect the gas composition within the enclosure volume, so it will be coupled into the gas composition model of the enclosure. The effect of the fuel cell stack, which takes air from the enclosure into the cathode, uses oxygen during the reaction,

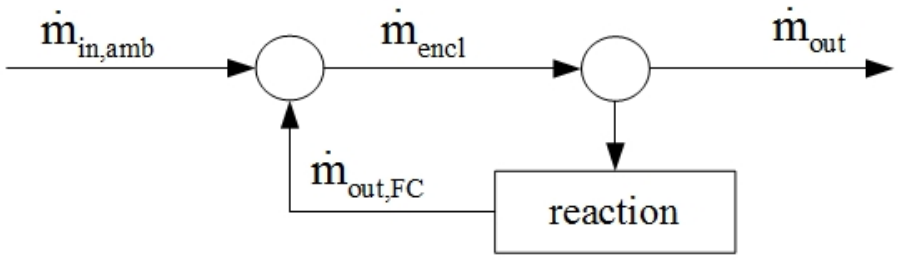

Figure 5.42 – Mass Transport Diagram

and produces water, will be examined through the coupled model.

The heat transfer in the coupled enclosure/stack model is illustrated in Figure 5.43. The heat generated by the fuel cell stack will be emitted into the enclosure space and heat the air in the enclosure. This heat energy will also be coupled into the enclosure mathematical model to study its effect on the enclosure temperature.

For this transient problem, the changes in fuel cell stack performance over time will significantly affect the enclosure conditions. The change in enclosure conditions will then in turn affect the fuel cell stack performance, as the performance of the stack is dependent on the enclosure air temperature, oxygen partial pressure and relative humidity. Therefore, the coupling of these two systems is essential to have a complete understanding of the change in the

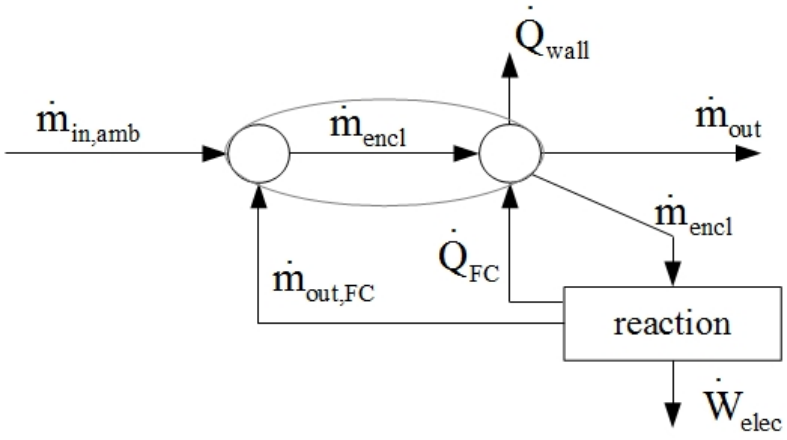

Figure 5.43 – Heat Transfer Diagram

operating conditions over time and its effect on the performance of the fuel cell stack.

In summary, the coupled enclosure/stack model solves for 15 unknowns characterized by 15 governing ODES, which are outlined in Tables 2.1 and 3.1.

5.5.1 Enclosure Modelling

The coupled fuel cell stack and enclosure model combines the fuel cell stack model developed in Chapter 2 and fitted in Section 5.3 with the enclosure model developed in Chapter 3 to predict the performance of the fuel cell stack in the enclosure and the conditions within the enclosure during operation at varying ambient and inlet conditions. The enclosure model developed in Chapter 3 is fitted to the experimental results obtained from a Horizon H-12 Fuel Cell Stack installed in Enclosure 1 during a varying temperature test. The parameters for the two Enclosures tested are listed in Tables 5.4. The parameters which cannot be measured and are manually fitted to the experimental results are listed in Table 5.5.

Enclosures 1 and 2, shown in Figure 4.7, have outer dimensions of 30.5cm × 28cm × 28cm, built with 2.5cm thick EPS (1 RSI) and 34cm × 34cm × 34cm, built with 5.1cm thick EPS (1.4 RSI) respectively. The enclosure dimensions are selected for modelling the enclosure height, width, and length are the mid dimensions based on the wall thickness, i.e. a wall with an outer length of 28cm and an inner length of 23cm, due to conjoining walls of 2.5cm thickness,

Table 5.4 – Enclosure Parameters

Parameter	*Enclosure 1*	*Enclosure 2*
Enclosure outer height (m)	0.31	0.34
Enclosure outer width (m)	0.28	0.34
Enclosure outer length (m)	0.28	0.34
Enclosure volume (m^3)	0.0133	0.0139
Outlet cross-sectional area (m^2)	0.0004	0.0001
Ambient Pressure (kPa)	93	93
Enclosure wall thickness (m)	1	2
Reported wall heat transfer coefficient (W/m^2K)	1	1.4
Plastispan density (kg/m^3)	22 [75]	22 [75]
Plastispan specific heat capacity (J/kgK)	1500 [76]	1500 [76]
Fuel cell - Enclosure contact area (m^2)	0.0035	0.0035

Table 5.5 – Estimated Parameters for Enclosure

Parameter	*Enclosure 1*	*Enclosure 2*
Effective wall resistance (m^2K/W)	1.2	1.6
Effective fan speed (m/s)	0.31	0.31
Evaporation Rate Coefficient, $\left(\frac{cm^2_{LV}}{(cm^2_{wall})kPa*s}\right)$	10	10
Condensation Rate Coefficient, $\left(\frac{cm^2_{LV}}{(cm^2_{wall})s}\right)$	10	10

is modelled with a length of 25cm. The enclosure gas volume is the volume inside the enclosure.

Experimental data for the case with the stack operating at 1A in Enclosure 1 during temperature steps from 20℃ to -20℃ was used to estimate the unknown enclosure parameters by fitting the model to the experimental data. Figure 5.44 shows the temperature of the fuel cell stack and the enclosure as predicted by the mathematical model in comparison with the experimentally measured data. To confirm the fit, the predicted enclosure relative humidity is compared with the measured enclosure relative humidity in Figure 5.45.

The wall resistance is based on the reported EPS heat transfer coefficient and fitted to account for the increase in the coefficient due to air films around the enclosure. For Enclosure 1, which has a wall resistance of $1m^2K/W$, the effective wall resistance was estimated as $1.2m^2K/W$. This falls within the

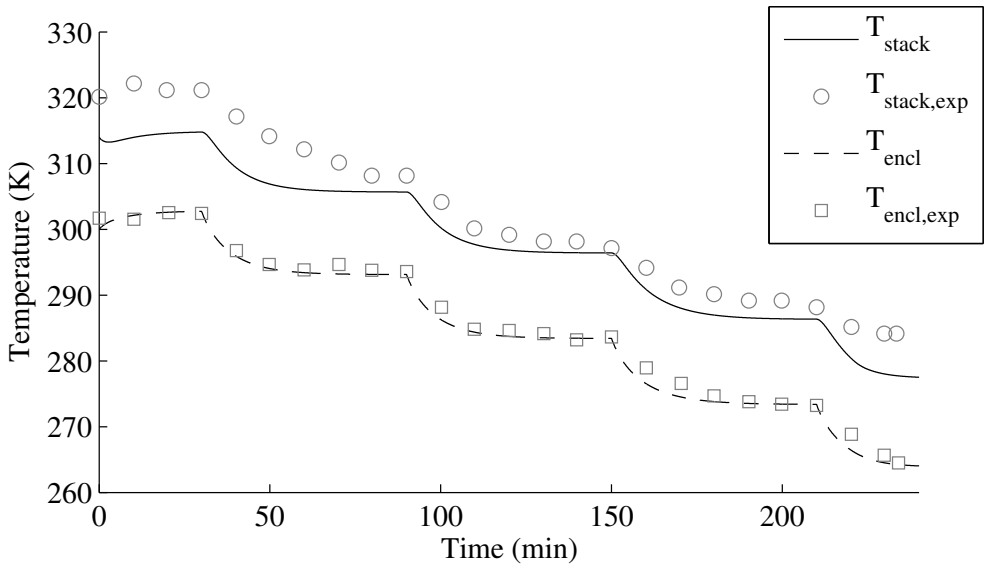

Figure 5.44 – Stack and Enclosure Temperature with Enclosure Model Parameter Estimation

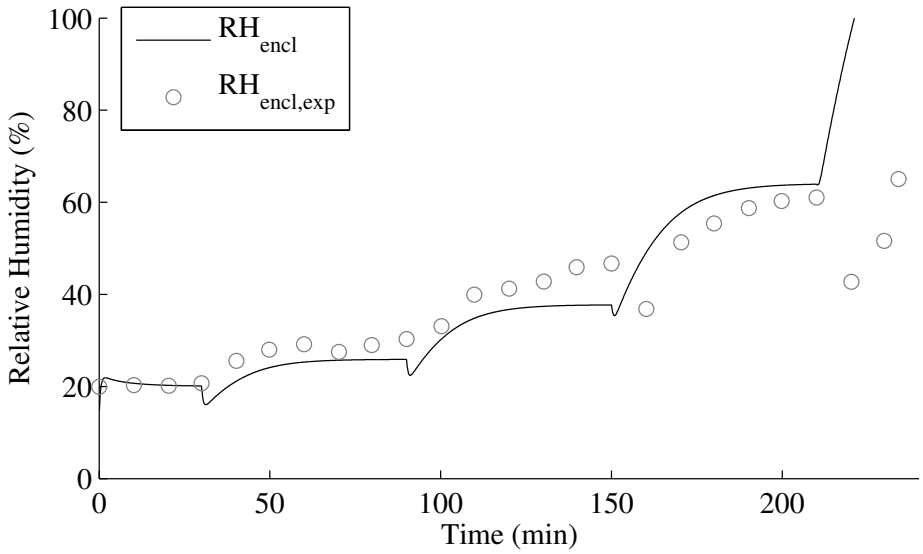

Figure 5.45 – Enclosure Relative Humidity with Enclosure Model Parameter Estimation

expected range of $0.2m^2K/W$ to $0.5m^2K/W$ for additional resistance caused by air films around the enclosure [74]. Since the enclosures have similar surface area and flow characteristics, this estimated air film resistance of $0.2m^2K/W$ was also applied to Enclosure 2, thus with a wall resistance of $1.4m^2K/W$, the effective wall resistance was estimated as $1.6m^2K/W$.

The speed of the air entering the enclosure was fitted to account for the pressure build up in the enclosure. The speed reported in Section 5.1.2 of 0.56m/s was not used as it was determined that the experimental set up used to measure the fan speed was not capable of adequately representing the conditions experienced by the fan in the enclosure. The effective fan speed for the enclosure tests was estimated as 0.34m/s to ensure a good prediction of the temperature in the enclosure, shown in Figure 5.44.

The evaporation and condensation rate coefficients were arbitrarily selected as $10\frac{cm^2_{LV}}{(cm^2_{wall})kPa*s}$ and $10\frac{cm^2_{LV}}{(cm^2_{wall})s}$ respectively for good model convergence as the enclosure model was unable to achieve conditions where phase changed occurred. No literature reporting values for phase change rate coefficients for this type of application was found.

5.5.2 Ambient Temperature Effects

The model with estimated parameters was then used to predict the stack and enclosure performance for a case where the stack was at 1.6A in Enclosure 1 and a case at 1A in Enclosure 2 over the same varying operating temperatures as the case used for parameter fitting. The performance predicted by the mathematical model is compared to the experimental results measured.

Figure 5.46 shows the predicted performance of the stack for the three tests in comparison with the experimental results for these same tests. Figure 5.47 shows the temperature of the stack and Figure 5.48 shows the temperature in the enclosure, as predicted by the mathematical model and as measured during the experiments. Figure 5.49 compares the predicted relative humidity in the enclosure to the measured value for the three tests.

The performance of the stack, shown in Figure 5.46, is predicted by the stack model from Section 5.3. The model is able to predict the performance of the stack within ±0.5V for the tests at 1A between 20℃ and -10℃. At -20℃, the performance of the stack drops due to freezing in the hydrogen outlet line and poor performance of the enclosure fan caused by the cold temperature. The mathematical model is not developed to account for these effects of cold

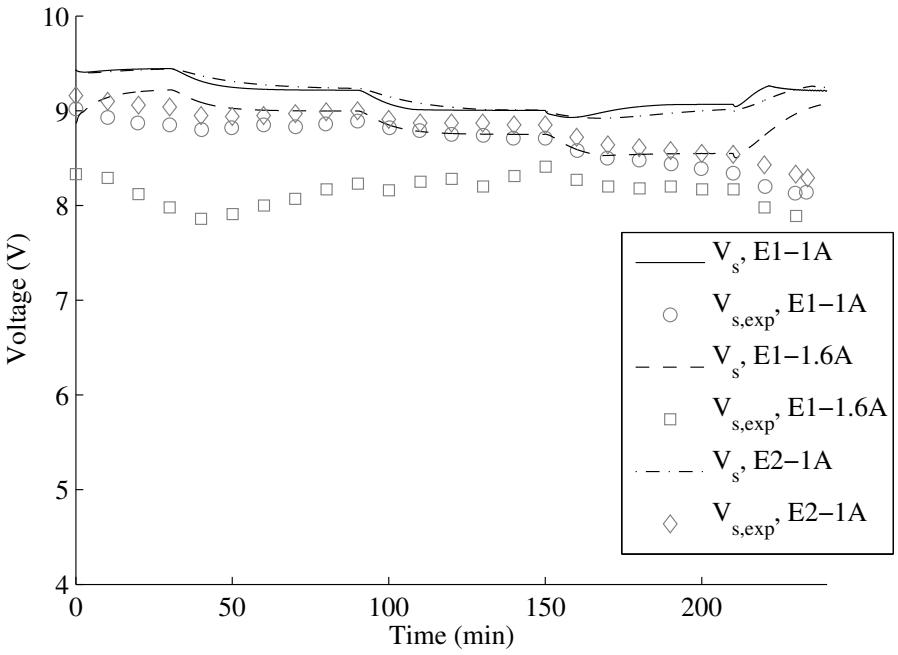

Figure 5.46 – Performance of Stack in Enclosure at Varying Temperatures

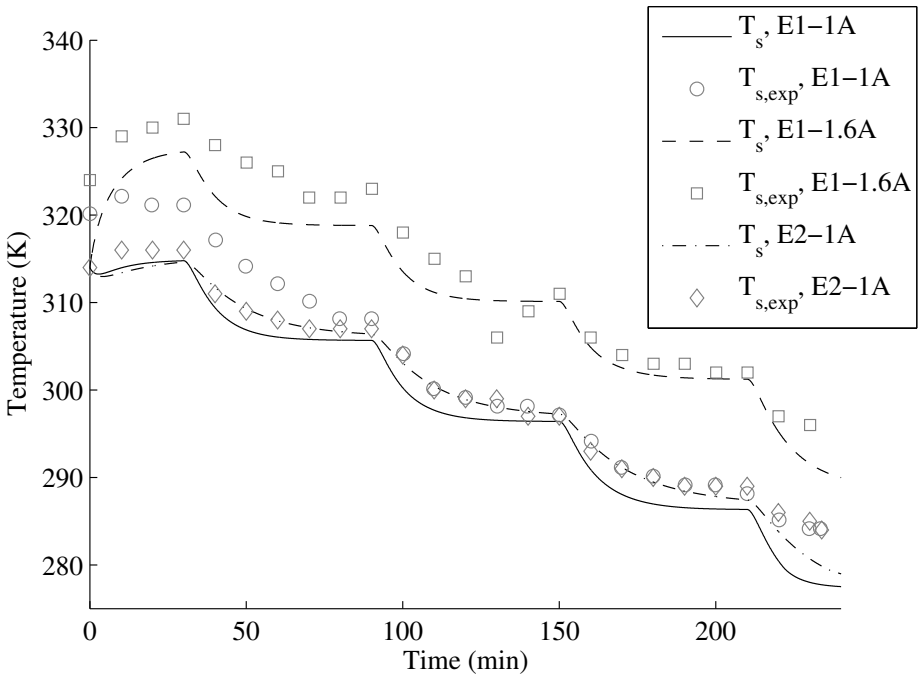

Figure 5.47 – Temperature of Stack in Enclosure During Temperature Steps

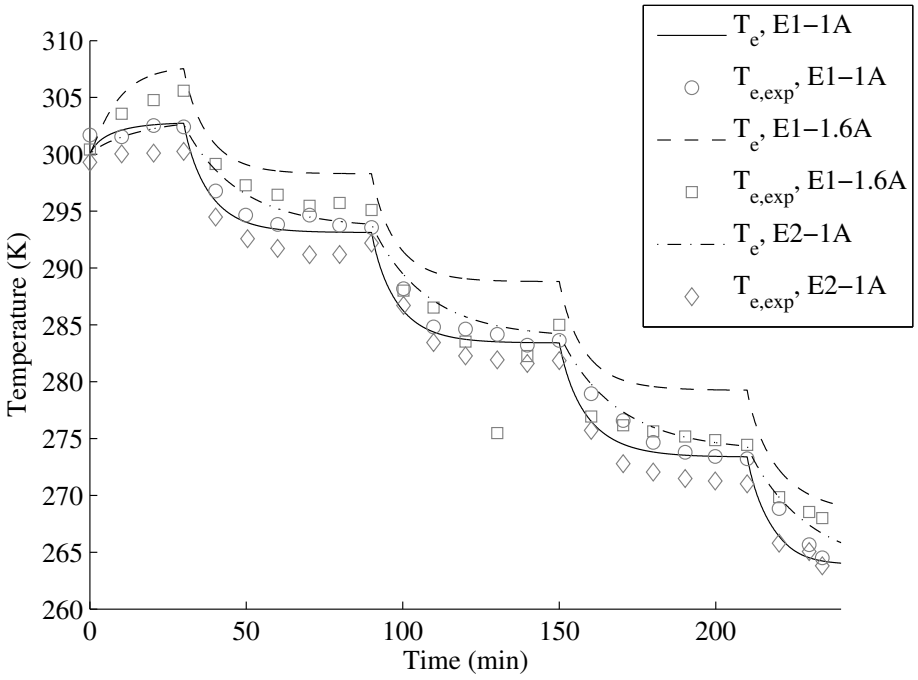

Figure 5.48 – Temperature of Enclosure During Temperature Steps

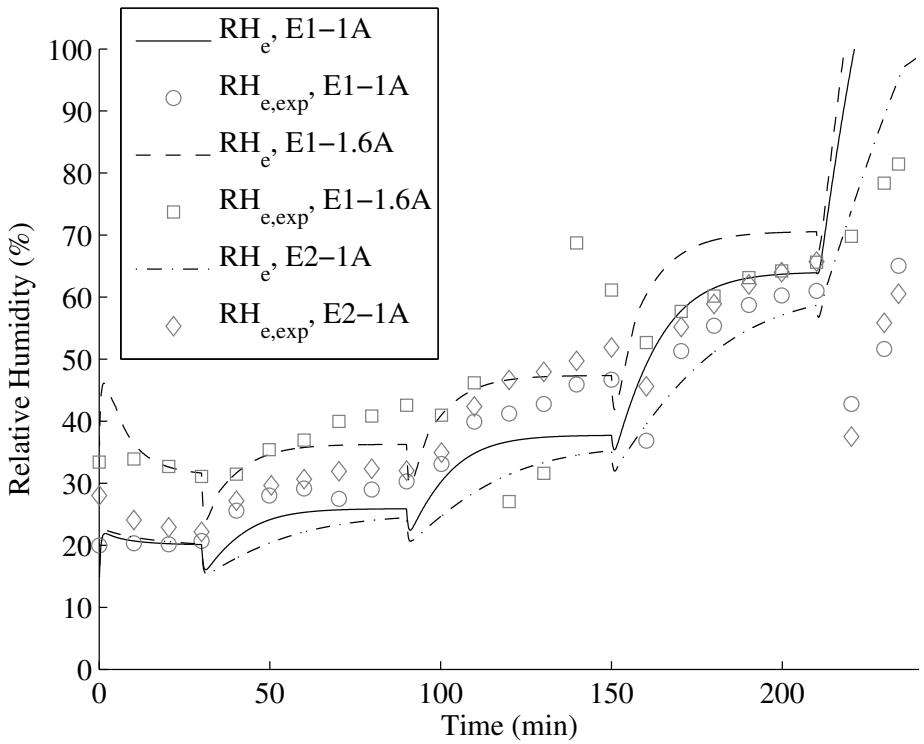

Figure 5.49 – Relative Humidity in Enclosure During Temperature Steps

temperature and therefore is not expected to fit. The performance of the stack for the 1.6A case is not well predicted for the first 3 temperature steps. Comparing to the stack tests run at 1.6A in Figures 5.5 and 5.19, it is observed that the performance of the stack during these steps is less than expected.

In Figures 5.47 and 5.48, is it observed that the temperature of the stack and enclosure during the two tests at 1A in Enclosure 1 and Enclosure 2 are approximately the same. This occurs because although Enclosure 2 has thicker insulation, it also has a larger size, and the effect of increasing the size of the wall through which heat is lost is sufficient to cancel out the improved insulating value. The case with Enclosure 2 at 1A shows that the model can predict the stack and enclosure temperatures well. The Enclosure 1 at 1.6A case shows a good prediction of the stack temperature, but overshoots the enclosure temperature during the low temperature cases.

The relative humidity of the enclosure is well fitted for Enclosure 1 and 2 at 1A, shown in Figure 5.49, although it underpredicts during the third temperature step. It is expected that the last temperature step will not fit due to freezing in the system. It is a function of the enclosure temperature

and the quantity of water vapour in the enclosure.

5.5.3 Effect of Enclosure Fan

The performance of the fuel cell stack in the enclosure with varying fan speeds was tested in Section 5.4.2. The purpose of this test was to examine the effect of the enclosure fan with respect to oxygen delivery and enclosure cooling. Figure 5.50 shows the performance of the fuel cell stack during these tests as well as the predicted performance. Figures 5.51 and 5.52 show the predicted temperature of the stack and enclosure in comparison with the experimentally obtained data. Figure 5.53 compares the measured relative humidity with the predicted value.

For the case when the fan is on, it is at the same speed as was used to fit the enclosure model and determine the effective fan speed of 0.34m/s. Therefore, a good prediction of the performance of the stack is expected. The mathematical model is able to predict the stack performance withing ±0.5V, stack temperature within ±7K, enclosure temperature within ±7K and relative humidity within ±5% for the test with the fan running at and effective fitted velocity of 0.34m/s, as shown in Figures 5.50, 5.51, 5.52 and 5.53. The

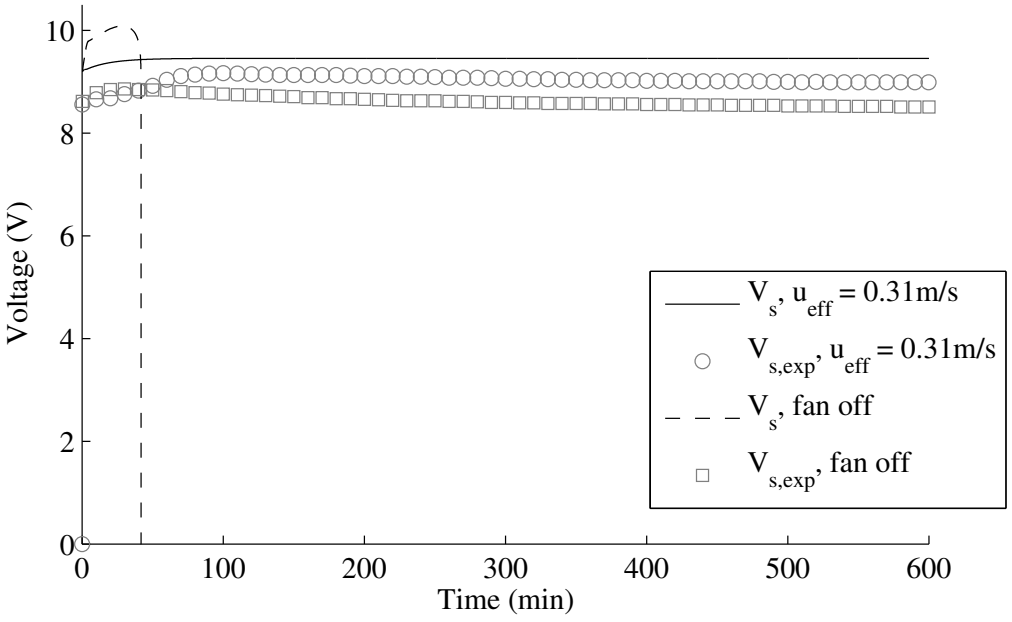

Figure 5.50 – Stack Performance in Enclosure during Fan Test

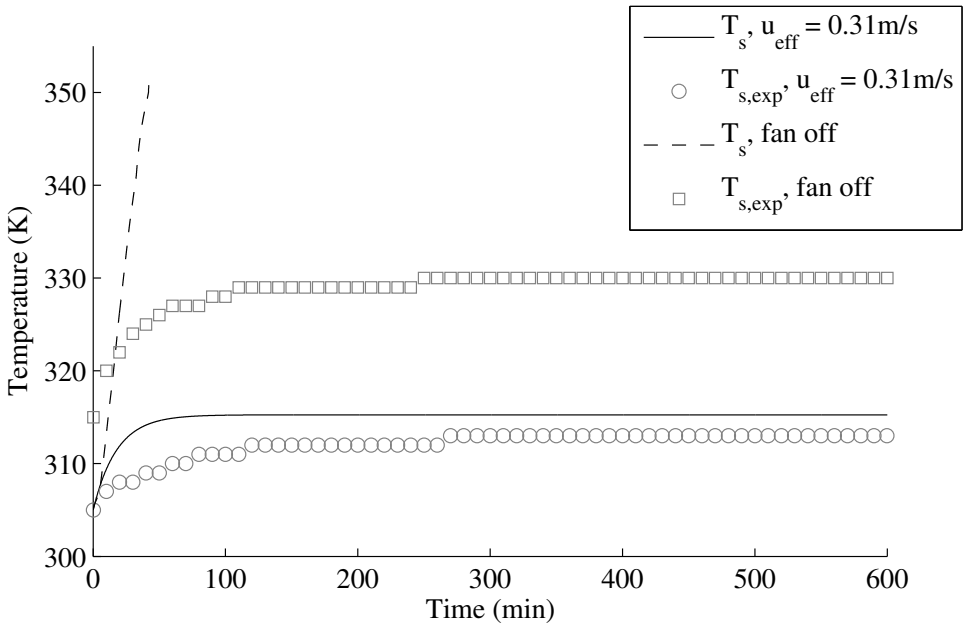

Figure 5.51 – Temperature of Stack During Enclosure Fan Test

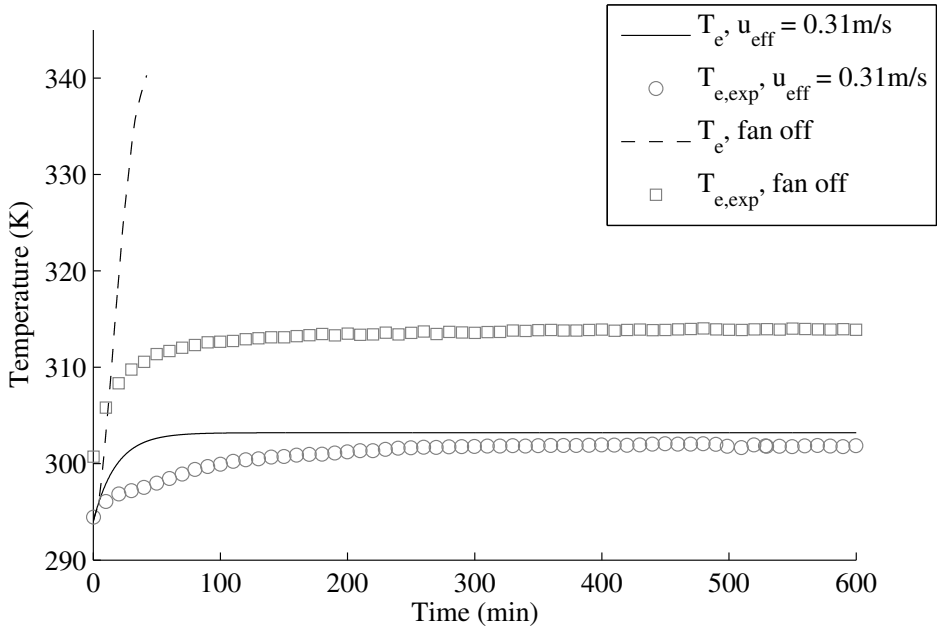

Figure 5.52 – Temperature of Enclosure During Enclosure Fan Test

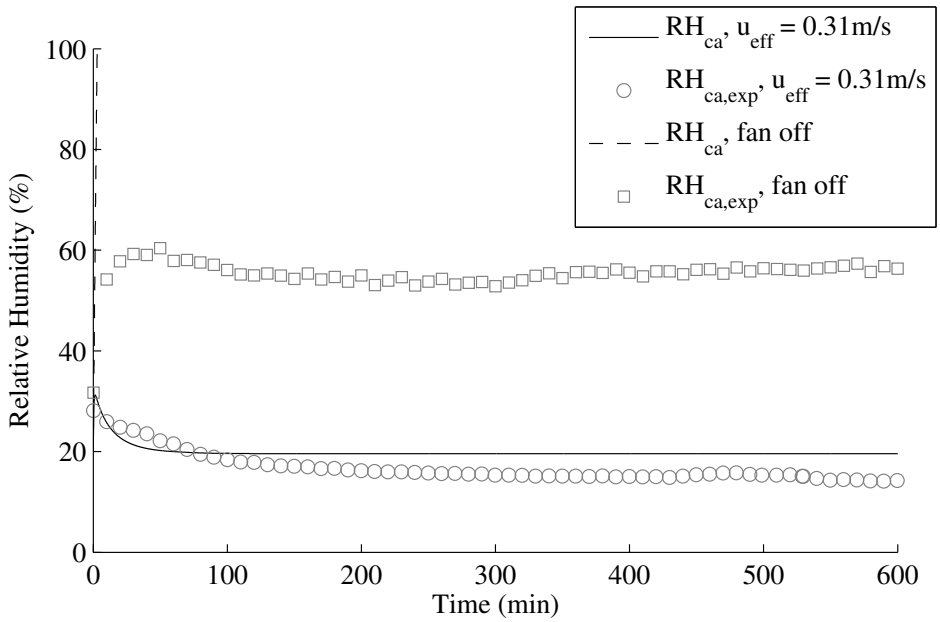

Figure 5.53 – Relative Humidity in Enclosure During Fan Test

mathematical model predicts a shorter time to equilibrium than is observed experimentally. However, the time to equilibrium for the temperature step test is well predicted. Therefore, the time to equilibrium during the 10 hour fan test at constant conditions is observed to be much longer than the time to equilibrium observed during the temperature step test.

For the case when the fan is off, the mathematical model shows that the stack shuts off after approximately 42 minutes in Figure 5.50. The experimental results for this test, however, show a trend of dropping performance over the 10 hours of operation. In comparison, a very short period of performance drop is observed prior to stack shut down for the mathematical model. This suggests that the mathematical model could be improved for this particular limiting case with reduced oxygen available for reaction. It also suggests that the flow inside the enclosure when the fan is off requires further characterization. An oxygen sensor installed in the enclosure would help to characterize the conditions to examine why the stack operates well with limited air flow into the enclosure.

When the stack operates at a low oxygen condition, which causes poor performance, the stack generates more heat leading to the temperature increase in the enclosure, as shown in Figure 5.52. The mathematical model predicts a temperature increase as well, which is affected by the performance of the

stack, leading to a large overshoot of the measured temperature.

The results in Sections 5.51, 5.5.2, and 5.5.3 show that the coupled model is able to predict the performance of the stack in the enclosure and the conditions within the enclosure during operation at varying ambient temperature, relative humidity and inlet flow conditions. This coupled mathematical model of the fuel cell stack and enclosure can therefore be used to investigate the design of an enclosure which will allow the stack to achieve good performance at varying operating conditions.

5.5.4 Enclosure Design Considerations

The enclosure design has a significant impact on the performance of the fuel cell stack, particularly when it experiences varying operating and environmental conditions. The important design criteria for the fuel cell stack are that the enclosure needs to provide an acceptable environmental temperature regardless of the ambient temperature, supply sufficient oxygen to the cathode, and maintain the relative humidity high enough to prevent the stack membrane from drying out.

For good stack performance, its temperature needs to be between 0℃ and 100℃, therefore, the enclosure is required to have gas temperatures which keep the stack temperature in this range. The parametric studies completed in Chapter 3 showed that the enclosure insulation and size both significantly influence the enclosure temperature. When the insulating property of the enclosure is increased, the temperature in the enclosure also increases. When the enclosure size is increased, the enclosure temperature decreases because the wall heat loss has increased. The two enclosures which were tested showed approximately the same performance because while Enclosure 2 had a higher insulating value, it was larger and the effect of increasing the insulation on the enclosure gas temperature was negated by the effect of increasing the enclosure size. This demonstrates how sensitive the design of the enclosure is to changing the enclosure size and insulating properties.

The experimental studies showed that the inlet air flow rate has an effect on the stack performance. If the stack does not have sufficient oxygen, its performance will degrade which leads to additional waste heat being generated. Therefore, the temperature of the stack and enclosure will rise. Managing the air flow rate to ensure that there is sufficient oxygen supply to the cathode will ensure good stack performance.

The experiments at varying ambient temperatures showed that the enclosure designs tested increase the operating range of the stack to include lower ambient temperatures. Stack tests at -10℃ are unstable, but when in an enclosure, the stack test does not become unstable until -20℃. However, it is important to note that in Chapter 3, it is observed that one enclosure design is not able to satisfy the range of operating temperatures from -40℃ to 20℃ and for a power range of 0W to 13W.

The oxygen concentration in the enclosure is important to ensure sufficient oxygen is supplied to the cathode. Parametric studies in Chapter 3 showed that an inlet flow rate greater than approximately 15 times the stoichiometric ratio at the maximum applied power showed negligible change in the oxygen concentration in the enclosure

Finally, the relative humidity of the gas in the enclosure is also important for good humidification of the fuel cell stack membranes. The experimental tests showed that decreasing the fan speed allowed water vapour to accumulate in the enclosure, however this caused the temperature in the enclosure to increase and caused a depletion of oxygen. The tests with changing temperature showed that when the temperature decreases that the enclosure humidity increases, which is expected as the saturation pressure will decrease. However, the stack performance also drops when the stack temperature drops, so the enclosure needs to be designed to maintain an optimal temperature and relative humidity.

The three important parameters for good operation of the fuel cell stack are the stack temperature, concentration of oxygen available to the stack cathode, and the relative humidity of the cathode gases. A good enclosure design will account for these factors and how the enclosure size, insulation and inlet flow rate will affect the enclosure conditions ensure the stack is provided with appropriate operating conditions regardless of the ambient conditions.

Chapter 6

Conclusion and Future Work

6.1 Conclusion

The goal of this research work was to develop a coupled mathematical model of an enclosure and fuel cell stack which could be used to predict the performance of the fuel cell stack during operation in varying ambient conditions. To realize this goal, a transient, non-isothermal, lumped parameter mathematical model of an open-cathode fuel cell stack was developed and coupled with a transient, non-isothermal mathematical model of an insulated enclosure. A Horizon H-12 Fuel Cell Stack and two enclosure designs were tested and characterized by fitting model parameters to experimental results.

The mathematical model of the open-cathode fuel cell stack was developed using a control volume approach, considering the anode gas channel, the cathode gas channel and the remaining cell volume. The mass transport, heat transfer, and fuel cell electrochemistry were modelled. The mathematical model was validated by comparison with experimental data presented by Philipps and Ziegler [25]. Using the parameters reported by Philipps and Ziegler, the mathematical model was able to predict the performance and temperature of the fuel cell stack for several current steps which was measured experimentally by Philipps and Ziegler. This model was then used to predict the performance of a H-12 Horizon Fuel Cell Stack.

Further to the development of the mathematical model, experiments were completed to obtain data for a Horizon H-12 Fuel Cell Stack. Using estimated parameters, the fuel cell stack mathematical model was fitted to the experimental data sets used for a repeatability test for the stack and then compared to data sets from different operating conditions. The fitted Horizon H-12 Fuel Cell Stack model can predict the performance of the stack for ambient temper-

ature, ambient relative humidity and fan inlet condition changes. The fuel cell stack was tested at varying ambient temperatures, ambient relative humidity and inlet flow rates and compared to the mathematical model predictions. The mathematical model was able to predict changes in the fuel cell stack performance, stack temperature and cathode outlet conditions well.

During the fuel cell stack experiments at varying conditions, it was observed that a decrease in ambient temperature led to a decrease in stack performance and that a decrease in ambient relative humidity led to a decrease in stack performance. The performance of the stack with varying inlet flow rates depends on the oxygen delivery to the stack, and the cooling effects of the stack. At low flow rates, the performance drops because the stack receives insufficient oxygen, and at high flow rates the performance drops because the stack is cooler and less humidified.

The mathematical model of the Horizon H-12 Fuel Cell Stack with estimated parameters was able to predict the changes in the fuel cell stack performance, stack temperature and cathode outlet conditions for varying condition tests well. In comparison with the experimental data obtained for the varying condition tests, the mathematical model of the fuel cell stack predicts the trends observed. The mathematical model predictions generally fall within the 95% confidence interval computed based on the repeatability test as applied to the experimental results for all varying condition tests. Therefore, the mathematical model of the Horizon H-12 Fuel Cell Stack is recommended for use in the coupled fuel cell stack/enclosure model that is developed.

A transient mathematical model of an insulated enclosure was also developed considering mass transport and heat transfer. For good operation of the fuel cell stack, it is necessary to maintain an acceptable stack temperature, ensure sufficient oxygen is supplied to the cathode, and keep the stack membranes well humidified. Therefore, a parametric study examining the effect of enclosure design (size and insulating properties), inlet air flow and ambient conditions was completed to ascertain the importance of these parameters when designing the enclosure.

For good stack performance, the stack temperature must be kept between 0℃ and 100℃. As the stack transfers heat to the enclosure, the enclosure temperature needs to be controlled to keep the stack temperature within the desired temperature range. Parametric studies examining the effect of the enclosure wall design showed that increasing the wall insulation resistance decreased the heat loss through the enclosure walls, and that increasing the

enclosure size increased heat loss through the enclosure walls. A study of the inlet air flow rate showed that the inlet air flow has a negligible effect on the enclosure temperature, unless it is 4 orders of magnitude greater than stoichiometry at 1A. Changes in the ambient relative humidity also have negligible effect on the temperature in the enclosure. A parametric study testing the effect of changing the ambient temperature outside of the enclosure revealed that the enclosure temperature increases as the ambient temperature increases.

These studies showed that for one enclosure design, the enclosure temperature is particularly sensitive to changes in ambient temperature and stack power produced. Therefore, when designing an enclosure for a specific application, the expected operating range of the stack and the expected environmental conditions will be most critical for ensuring an appropriate temperature inside the enclosure. In particular, it was observed that for the Horizon H-12 Fuel Cell Stack, a single enclosure design cannot provide acceptable enclosure temperature conditions for an ambient temperature range of -40℃ to 20℃ for a power range of 0W to 13W.

The other important criteria for enclosure design are the oxygen concentration and relative humidity in the enclosure during stack operation. The composition of the gas in the enclosure must have sufficiently high oxygen concentration as the enclosure gas in the cathode gas is supplied to the fuel cell stack cathode. Parametric studies examining the effects of various enclosure design parameters revealed that the most critical factor for maintaining high oxygen concentration in the enclosure is the inlet flow rate. An inlet flow rate greater than approximately 15 times the stoichiometric ratio at the maximum applied power showed negligible change in the oxygen concentration in the enclosure

The relative humidity of the gas in the enclosure is also important as the fuel cell stack membranes need to be well humidified. The relative humidity of the gases from the enclosure, which flow through the channels, will affect the fuel cell stack membranes humidification. The enclosure parametric studies showed that the temperature of the gases in the enclosure is the most significant factor pertaining to the relative humidity of enclosure gases. An increase in the enclosure temperature means an increase in the saturation pressure and for a constant quantity of water in the enclosure, this leads to a decrease in the relative humidity. Therefore, to ensure a well humidified stack, the temperature of the enclosure must be carefully controlled.

Using the results from the enclosure parametric studies, two enclosure designs were built and experimentally tested with the fuel cell stack installed, over a range of temperatures and with different inlet flow rates. It was observed that the particular enclosure designs selected were able to insulate the stack enough to operate well down to -10℃, and for approximately 30 minutes at -20℃. It was observed that reducing the inlet flow rate has a significant effect on the performance of the fuel cell stack. The reduction in the stack performance leads to an increase in waste heat generated and increases the stack and enclosure temperature. The enclosure model was fitted to the experimental data for a test at 1A during decreasing temperature steps in a 30.5cm by 28cm by 28cm enclosure with 2.5cm thick, 1 RSI walls. The model can be used to predict the stack temperature and performance, and enclosure temperature and relative humidity for varying enclosure designs and ambient conditions.

With this coupled fuel cell stack/enclosure mathematical model, the performance of the Horizon H-12 Fuel Cell Stack for varying enclosure designs and operating conditions can be predicted. Experiments were completed for a higher loading condition (1.6A) and for a second enclosure design and the mathematical model was able to predict the stack performance and temperature, and enclosure temperature and relative humidity well. Additionally, the mathematical model was able to predict the trends of an inlet air flow rate study. Therefore, the mathematical model developed in this work can be used to determine the appropriate design for operation in those, and other, conditions.

In summary, a transient, non-isothermal, lumped parameter model of an open-cathode fuel cell stack was developed and coupled with a transient, non-isothermal enclosure model. The fuel cell stack model was validated and the mathematical model of a Horizon H-12 Fuel Cell Stack was characterized and fitted to experimental data. The effect of the enclosure was studied and it was also characterized and fitted using experimental data. This produced a mathematical model capable of predicting the performance of a Horizon H-12 Fuel Cell Stack in varying enclosure designs and at varying operating conditions. The coupled fuel cell stack/enclosure mathematical model was shown to be able to predict the effect of enclosure design changes and changes in ambient inlet conditions. Therefore, the developed models can be used for enclosure optimization and for control of a fuel cell system.

6.2 Future Work

The research work presented herein has limited experimental data presented due to limitations with the performance of the environmental chamber. With a better performing method of supplying varying ambient conditions to the fuel cell stack and enclosure, additional testing of the fuel cell stack and enclosure could be completed. Some additional studies could include: the effect of changing the gas pressure in the anode and the effect of a forced enclosure outlet flow rate.

The oxygen concentration in the enclosure is important to ensure that the stack has sufficient reactant available. The oxygen concentration in the enclosure was measured during these experiments, however calibration difficulties with the oxygen sensor for the temperature range experienced by the system led to the omission of its data. Future work will include proper calibration of the oxygen sensor to examine the oxygen concentration in the enclosure.

Data obtained from the oxygen sensor can be used to study the effect of cases with limited oxygen on the performance of the fuel cell stack. The mathematical model of the fuel cell stack was not able to predict the performance of the fuel cell stack well during a limiting case with decreased oxygen available to the stack. Additional development of the mathematical model of the fuel cell stack may improve its ability to predict low oxygen concentration performance.

This work was limited to two water phases, but at low temperatures, an ice model could also be implemented to study the performance and operation of the stack at freezing conditions. This would allow further development of the fuel cell stack model, particularly for low temperature operation.

The performance of the stack during a cold start in an enclosure can also be studied. Operating protocols could be developed to create favourable start up conditions in the enclosure prior to stack start up, or as previously indicated, the freeze start can be examined.

The mathematical model developed in this work can also be used to determine an optimal enclosure design to achieve good performance of the fuel cell stack for a set of operating conditions.

References

[1] Larminie J and Dicks A. *Fuel Cell Systems Explained*. John Wiley & Sons, West Sussex, UK, 2003.

[2] Secanell M. *Computational modeling and optimization of proton exchange membrane fuel cells*. PhD thesis, University of Victoria, November 2007.

[3] Rosa D. S, Pinto D, Silva V, Silva R, and Rangel C. High performance PEMFC stack with open-cathode at ambient pressure and temperature conditions. *International Journal of Hydrogen Energy*, 2007.

[4] Wu J, Galli S, Lagana I, Pozio A, Yuan X, Martin J, and Wang H. An air-cooled proton exchange membrane fuel cell with combined oxidant and coolant flow. *Journal of Power Sources*, 2009.

[5] Sasmito A, Lum K, Birgersson E, and Mujumdar A. Computational study of forced air-convection in open-cathode polymer electrolyte fuel cell stacks. *Journal of Power Sources*, 195:5550–5563, 2010.

[6] Sasmito A, Birgersson E, and Mujumdar A. Numerical evaluation of various thermal management strategies for polymer electrolyte fuel cell stacks. *International Journal of Hydrogen Energy*, 2011.

[7] Sasmito A, Birgersson E, Lum K, and Mujumdar A. Fan selection and stack design for open-cathode polymer electrolyte fuel cell stacks. *Renewable Energy*, 2012.

[8] Gavello G, Zeng J, Francia C, Icardi U, Graizzaro A, and Specchia S. Experimental studies on Nafion®112 single PEM-FCs exposed to freezing conditions. *International Journal of Hydrogen Energy*, pages 8070–8081, 2011.

[9] Chu D, Jiang R, Gardner K, Jacobs R, Schmidt J, Quakenbush T, and Stephens J. Polymer electrolyte membrane fuel cells for communication applications. *Journal of Power Sources*, pages 174–178, 2001.

[10] Dantherm Power. Available from: `http://www.dantherm-power.com`, c2012. [Online; accessed July 2012].

[11] Ballard Power Systems. Available from: `http://www.ballard.com`, c2012. [Online; accessed July 2012].

[12] SFC Energy. Available from: `http://www.sfc.com/en`, c2012. [Online; accessed July 2012].

[13] Ensol Systems. Available from: `http://www.ensolsystems.com`, c2012. [Online; accessed July 2012].

[14] Energy For You. Available from: `http://www.efoy.ca/en`, c2012. [Online; accessed July 2012].

[15] Ward C, Stanga D, Pataki L, and Venter R. Design for the cold start-up of a man-portable fuel cell and hydrogen storage system. *Journal of Power Sources*, 41(3):335–352, 1993.

[16] Oszcipok M, Zedda M, Hesselmann J, Huppmann M, Wodrich M, Junghardt M, and Hebling C. Portable proton exchange membrane fuel-cell systems for outdoor applications. *Journal of Power Sources*, 157(2):666–673, 2006.

[17] Yan Q, Toghiani H, Lee Y.-W, Liang K, and Causey H. Effects of sub-freezing temperatures on a PEM fuel cell performance, startup and fuel cell components. *Journal of Power Sources*, 160:1242–1250, 2006.

[18] Jiao K and Li X. Effects of various operating and initial conditions on cold start performance of polymer electrolyte membrane fuel cells. *International Journal of Hydrogen Energy*, 34:8171–8184, 2009.

[19] Rock J and Plant L. United States Patent 6,358,638, March 19, 2002.

[20] Assarabowski R, Unkert W, Bach L, Grasso A, and Olsommer B. United States Patent 6,797,421 B2, September 28, 2004.

[21] Newbold A, Benson P, and Reisch T. International Patent WO 2008/038032 A2, April 3, 2008.

[22] Giddey S, Ciacchi F, and Badwal S. Design, assembly and operation of polymer electrolyte membrane fuel cell stacks to 1 kWe capacity. *Journal of Power Sources*, 125:155–165, 2004.

[23] Chang H.-P, Chou C.-L, Chen Y.-S, Hou T.-I, and Weng B.-J. The design and cost analysis of a portable pemfc ups system. *International Journal of Hydrogen Energy*, 2007.

[24] Ishizawa M, Kimata K, Kuwata Y, Takeuchi M, and Ogata T. Portable Fuel Cell Systems. *Electronics and Communcations in Japan*, 1999.

[25] Philipps and Ziegler . Computationally efficient modeling of the dynamic behaviour of a portable PEM fuel cell stack. *Journal of Power Sources*, 180:309–321, 2008.

[26] Xue X and Tang J. PEM Fuel Cell Dynamic Model with Phase Change Effect. *Transactions of the ASME: Journal of Fuel Cell Science and Technology*, 2:274–283, 2005.

[27] Xue X, Tang J, Smirnova A, England R, and Sammes N. System level lumped parameter dynamic modeling of PEM fuel cell. *Journal of Power Sources*, 133:188–204, 2004.

[28] Pukrushpan J, Peng H, and Stephanopoulou A. Control-Oriented Modeling and Analysis for Automotive Fuel Cell Systems. *Transactions of the ASME*, pages 14–25, 2004.

[29] Pathapati P, Xue X, and Tang J. A new dynamic model for predicitng transient phenomena in a PEM fuel cell system. *Renewable Energy*, 30: 1–22, 2005.

[30] Chu K, Ryu J, and Sunwoo M. A lumped parameter model of the polymer electrolyte fuel cell. *Journal of Power Sources*, 171:412–423, 2007.

[31] Litster S and Djilali N. Mathematical modelling of ambient air-breathing fuel cells for portable devices. *Electrochimica Acta*, 52(11):3849–3862, 2007.

[32] Amphlett J, Baumert R, Mann R, Peppley B, Roberge P, and Rodrigues A. Parametric modelling of the performance of a 5-kW proton-exchange membrane fuel cell stack. *Journal of Power Sources*, 49:349–356, 1994.

[33] Amphlett J, Baumert R, Mann R, Peppley B, and Roberge P. Performance Modeling of the Ballard Mark IV Solid Polymer Electrolyte Fuel Cell. I. Mechanistic Model Development. *Journal of the Electrochemical Society*, 142(1):1–8, 1995.

[34] Bernardi D. M and Verbrugge M. W. Mathematical model of the solid-polymer-electrolyte fuel cell. *Journal of the Electrochemical Society*, 139 (9):2477–2491, 1992.

[35] Springer T, Zawodzinski T, and Gottesfeld S. Polymer electrolyte fuel cell model. *Journal of the Electrochemical Society*, 138(8):2334–2342, 1991.

[36] Ngyuen T and White R. A Water and Heat Management Model for Proton-Exchange-Membrane Fuel Cells. *Journal of the Electrochemical Society*, 140:2178–2186, 1993.

[37] Rowe A and Li X. Mathematical modeling of proton exchange membrane fuel cells. *Journal of Power Sources*, 102:82–96, 2001.

[38] Wishart J, Dong Z, and Secanell M. Optimization of a PEM fuel cell system based on empirical data and a generalized electrochemical semi-empirical model. *Journal of Power Sources*, pages 1041–1055, 2006.

[39] Secanell M, Carnes B, Suleman A, and Djilali N. Numerical optimization of proton exchange membrane fuel cell cathodes. *Electrochimica Acta*, 52 (7):2668–2682, 2007.

[40] Amphlett J, R.M.Baumert , R.F.Mann , B.A.Peppley , and P.R.Roberge . Performance Modeling of the Ballard Mark IV Solid Polymer Electrolyte Fuel Cell. II. Empirical Model Development. *Journal of the Electrochemical Society*, 142(1):9–15, 1995.

[41] Çengel Y. A and Cimbala J. M. *Fluid Mechanics: Fundamentals and Applications*. McGraw-Hill, New York, NY, First edition, 2006.

[42] O'Hayre R, Fabian T, Litster S, Prinz F, and Santiago J. Engineering model of a passive planar air breathing fuel cell cathode. *Journal of Power Sources*, 167:118–129, 2007.

[43] Yalcinoz T and Alam M. Dynamic modeling and simulation of air-breathing proton exchange membrane fuel cell. *Journal of Power Sources*, 182(1):168–174, 2008.

[44] Hussain M, Baschuk J, Li X, and Dincer I. Thermodynamic analysis of a PEM fuel cell power system. *International Journal of Thermal Sciences*, 44:903–911, 2005.

[45] Yu X, Zhou B, and Sobiesiak A. Water and thermal management for Ballard PEM fuel cell stack. *Journal of Power Sources*, 147:184–195, 2005.

[46] Amphlett J, Mann R, Peppley B, Roberge P, and Rodrigues A. A model predicting transient responses of proton exchange membrane fuel cells. *Journal of Power Sources*, 61:183–188, 1996.

[47] Weber A. Z and Newman J. Transport in Polymer-Electrolyte Membranes: II. Mathematical Model. *Journal of the Electrochemical Society*, 151(2):A311–A325, 2004.

[48] Weber A. Z and Newman J. Transport in Polymer-Electrolyte Membranes: I. Physical Model. *Journal of the Electrochemical Society*, 150(7): A1008–A1015, 2003.

[49] Golbert J and Lewin D. Model-based control of fuel cells: (1) Regulatory control. *Journal of Power Sources*, pages 135–151, 2004.

[50] Sone Y, Ekdunge P, and Simonsson D. Proton Conductivity of Nafion 117 as Measured by a Four-Electrode AC Impedance Method. *Journal of Electrochemical Society*, 143:1254–1259, 1996.

[51] Asl S. S, Rowshanzamir S, and Eikani M. Modelling and simulation of the steady-state and dynamic behaviour of a PEM fuel cell. *Energy*, 35: 1633–1646, 2010.

[52] He W, Yi J, and Nguyen T. Two-phase flow model of the cathode of PEM Fuel Cells using interdigitated flow fields. *AIChE Journal*, 46:2053–2064, 2000.

[53] Sundaresan M and Moore R. Polymer electrolyte fuel cell stack thermal model to evaluate sub-freezing start up. *Journal of Power Sources*, 145: 534–545, 2005.

[54] Kolodziej J. Thermal Dynamic Modeling and Nonlinear Control of a Proton Exchange Membrane Fuel Cell Stack. *Journal of Fuel Cell Science and Technology*, 4:255–260, 2007.

[55] Datta B, Velayutham G, and Goud A. P. Fuel cell power source for a cold region. *Journal of Power Sources*, 106(2):370–376, 2002.

[56] Mangold M, Piewek S, Klein O, and Kienle A. A Model for the Freeze Start Behavior of a PEM Fuel Cell Stack. *Journal of Fuel Cell Science and Technology*, 2011.

[57] Oszcipok M, Zedda M, Riemann D, and Geckeler D. Low temperature operation and influence parameters on the cold start ability of portable PEMFCs. *Journal of Power Sources*, 164:404–411, 2006.

[58] Yoshizawa K, Hyama A, Higashi S, and Hagans P. International Patent Application WO 03/073547 A2, February 27, 2002.

[59] Clingerman B and Mowery K. United States Patent 6,413,661 B1, July 2, 2002.

[60] Hobmeyr D. W. R. United States Patent 7,368,196 B2, May 6, 2008.

[61] Kandlikar S and Lu Z. Thermal management issues in a PEMFC stack A brief review of current status. *Applied Thermal Engineering*, 29:1276–1280, 2009.

[62] Koh J.-H, Hsu A, Akay H, and Liou M. Analysis of overall heat balance in self-heated proton-exchange-membrane fuel cells for temperature predictions. *Journal of Power Sources*, 144:122–128, 2005.

[63] Li X and Sabir I. Review of bipolar plates in pem fuel cells: Flow-field designs. *International Journal of Hygrogen Energy*, 30:359–371, 2005.

[64] Weber A. Z and Newman J. Transport in Polymer-Electrolyte Membranes: III. Model Validation in a Simple Fuel-Cell Model. *Journal of the Electrochemical Society*, 151(2):A326–A339, 2004.

[65] Pukrushpan J, Peng H, and Stephanopoulou A. Simulation and Analysis of Transient Fuel Cell System Performance based on a Dynamic Reactant Flow Model. pages 1–12, November 17-22 2002.

[66] O'Hayre R, Cha S.-W, Colella W, and Prinz F. *Fuel Cell Fundamentals*. John Wiley and Sons, Hoboken, New Jersey, First edition, 2006.

[67] Paquin M and Fréchette L. Understanding cathode flooding and dry-out for water management in air breathing PEM fuel cells. *Journal of Power Sources*, 180:440–451, 2008.

[68] Çengel Y. A. *Heat and Mass Transfer: A Practical Approach*. McGraw-Hill, New York, NY, Third edition, 2007.

[69] Zhang Y, Mawardi A, and Pitchumani R. Numerical studies on an air-breathing proton exchange membrane (PEM) fuel cell stack. *Journal of Power Sources*, 173(1):264–276, 2007.

[70] Horizon Fuel Cell Technologies. H-Series: PEM Fuel Cell Systems. Available from: `http://www.horizonfuelcell.com/file/H-Series.pdf`, c2012. [Online; accessed February 2012].

[71] Jiji L. *Heat Convection*. Springer-Verlag Berlin Heidelberg, New York, NY, First edition, 2006.

[72] Çengel Y. A and Boles M. A. *Thermodynamics: An Engineering Approach*. McGraw-Hill, Boston, Massachusetts, Fifth edition, 2007.

[73] Bird R. B, Stewart W. E, and Lightfoot E. *Transport Phenomena*. J. Wiley and Sons, 2nd edition, 2002.

[74] McQuiston F, Parker J, and Spitler J. *Heating, Ventilation, and Air Conditioning: Analysis and Design*. John Wiley and Sons, Inc, New York, NY, Sixth edition, 2005.

[75] Product Information Bulletin: PlastiSpan HD EFS Insulation Material Properties. Available from: `http://www.plastifab.com/dealers/downloads/products/plastispan.pdf`, c2011. [Online; accessed November 2012].

[76] Winterling H and Sonntag N. Rigid Polystyrene Foam. *Kunststoffe International*, 2011.

[77] Environment Canada. National Climate Data and Information Archive. Available from: `http://www.climate.weatheroffice.gc.ca/climateData/canada_e.html`, c2010. [Online; accessed July 2010].

[78] Wheeler A and Ganji A. *Introduction to Engineering Experimention*. Prentice Hall, Upper Saddle River, NJ, Third edition, 2010.

[79] Cincinnati Sub-Zero. Z-Plus Test Chambers and Temperature Humidity Chambers [Internet]. Available from: `http://www.cszindustrial.com`, c2011. [Online; accessed May 2012].

[80] Scribner Associates Inc. 850/840 Series - Turn-Key Fuel Cell Test Stations. Available from: `http://www.scribner.com`, c2012. [Online; accessed November 2012].

[81] Cooper K and Smith M. Electrical test methods for on-line fuel cell ohmic resistance measurement. *Journal of Power Sources*, 2006.

[82] Sensirion SHT71 - Digital Humidity Sensor. Available from: `http://www.sensirion.com/en/products/humidity-temperature/humidity-sensor-sht71/`, c2011. [Online; accessed October 2012].

[83] Ocean Optics Oxygen Sensing Technologies. Available from: `http://www.oceanopticssensors.com/products/oxygen.htm`, c1989-2012. [Online; accessed October 2012].

[84] SNOWFAN. Available from: `http://www.snowfan.com.cn/products_info.asp?pid=84`, c2008-2009. [Online; accessed April 2012].

[85] Onishi L, Prausnitz J, and Newman J. Water-Nafion Equilibrian. Absence of Schroeder's Paradox. *Journal of Physical Chemistry*, 2007.

Appendix A

Enclosure Model Verification

A.1 Enclosure Model Verification

In Chapter 3.3, the transient enclosure model is validated by comparing its results to the results of the steady state model. For selected currents, the steady state enclosure model gives the temperatures listed in Table A.1 which are the

Table A.1 – Comparison of Steady-State and Transient Model Temperatures

Current (A)	*Ambient Temp (K)*	*Steady State Model Temp (K)*	*Transient Model Temp (K)*
0	233	233	233
0.4	233	249.2	249.2
0.8	233	268.6	268.6
1.2	233	290.9	290.9
1.6	233	315.3	315.3
0	253	253	253
0.4	253	269.2	269.2
0.8	253	288.6	288.6
1.2	253	310.9	310.9
1.6	253	335.3	335.3
0	273	273	273
0.4	273	289.2	289.2
0.8	273	308.6	308.6
1.2	273	330.9	330.9
1.6	273	355.3	355.3
0	293	293	293
0.4	293	309.2	309.2
0.8	293	328.6	328.6
1.2	293	350.9	350.9
1.6	293	375.3	375.3

same as the temperatures reported as the steady operating temperatures given by the transient enclosure model at the same currents.

As shown in Table A.1, the temperature of the steady state model at a given fuel cell stack current output and ambient temperature is identical to that of the transient model once steady conditions have been achieved for the same operating conditions. This indicates that the transient model has been developed correctly, and also that the effect of the transient gas composition on the temperature of the enclosure is negligible.

Appendix B

MATLAB code structure

B.1 Stack Model

The mathematical model of the fuel cell stack developed in MATLAB is solved using the code structure listed in Table B.1.

Table B.1 – Stack mathematical model in MATLAB

File Name	*File Purpose*
main.m	- gets initial conditions - sets up and calls the ode solver for stack.m - post processes the results and plots figures
stack.m	- ode function to be solved for 10 variables - sets up variables and conditions - calls mass.m, cellvoltage.m and temperature.m
mass.m	- 7 odes are solved for anode and cathode channel density, species mass fractions, liquid water mass - calls inlet_properties.m and mass_flow.m
cellvoltage.m	- computes cell voltage, open circuit voltage, losses
temperature.m	- 3 odes are solved for anode and cathode channel temperature and stack temperature - calls inlet_properties.m and mass_flow.m
inlet_properties.m	- computes inlet conditions: species mass flow rate, species mass fraction, and density for channels
mass_flow.m	- contains 2 functions: 1. computes channel outlet flow rates, mass phase change, and liquid water mass in channels, 2. computers reactions flow rates

The following files listed in Table B.2 contain parameters or compute properties and are common for both the stack and coupled model:

Table B.2 – Parameters and Properties files

File Name	*File Purpose*
constants.m	- constants class
parameters.m	- Horizon H-12 stack specific parameters class
water_saturation.m	- computes saturation pressure $P_{sat}(T)$
dynamic_viscosity.m	- computes dynamic viscosity $\mu_i(T)$
water_density.m	- computes liquid water density $\rho_l(T)$
entropy.m	- computes entropy of reactants
LennardJones.m	- computes Lennard Jones parameters for O_2 in N_2

B.2 Coupled Enclosure/Stack Model

The coupled mathematical model of the fuel cell stack and enclosure developed in MATLAB is solved using the code structure listed in Table B.3, and the parameter and properties files listed in Table B.2.

Table B.3 – Stack mathematical model in MATLAB

File Name	*File Purpose*
mainE.m	- gets initial conditions - sets up and calls the ode solver for stack.m - post processes the results and plots figures
stackE.m	- ode function to be solved for 15 variables - sets up variables and conditions - calls enclosure.m mass.m, cellvoltage.m and temperature.m
enclosure.m	- 5 odes are solved for enclosure temperature, gas species mass fractions, density and liquid water - calls inletE.m, inlet_stack.m and mass_flow.m
massE.m	- 7 odes are solved for anode and cathode channel density, species mass fractions, liquid water mass - calls inlet_properties.m and mass_flow.m
cellvoltageE.m	- computes cell voltage, open circuit voltage, losses
temperatureE.m	- 3 odes are solved for anode and cathode channel temperature and stack temperature - calls inlet_properties.m and mass_flow.m
inletE.m	- computes enclosure inlet conditions: species mass flow rate, species mass fraction and density
inlet_stack.m	- computes stack inlet conditions: species mass flow rate species mass fraction and density for channels
mass_flow.m	- contains 2 functions: 1. computes channel outlet flow rates, mass phase change, and liquid water mass in channels, 2. computers reactions flow rates